Molecular analysis of antimalarial therapies: from drug development to mode of action

PhD Dissertation

Jerzy Michal Dziekan

2018

School of Biological Sciences

“Molecular analysis of antimalarial therapies: from drug development to mode of action”

Jerzy Michal Dziekan

School of Biological Sciences

A thesis submitted to the Nanyang Technological University
in partial fulfilment of the requirement for the degree of
Doctor of Philosophy

2018

Statement of Originality

I hereby certify that the work embodied in this thesis is the result of original research, is free of plagiarised materials, and has not been submitted for a higher degree to any other University or Institution.

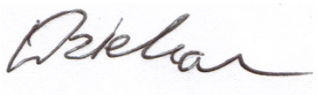

17 January 2019 Jerzy Michal Dziekan

Supervisor Declaration Statement

I have reviewed the content and presentation style of this thesis and declare it is free of plagiarism and of sufficient grammatical clarity to be examined. To the best of my knowledge, the research and writing are those of the candidate except as acknowledged in the Author Attribution Statement. I confirm that the investigations were conducted in accord with the ethics policies and integrity standards of Nanyang Technological University and that the research data are presented honestly and without prejudice.

17 January 2019 Prof. Zbynek Bozdech

Authorship Attribution Statement

This thesis contains material from one paper published in the following peer-reviewed journal where I was the first author.

Chapter 3 and 4 feature information published as J. M. Dziekan, H. Yu, D. Chen, L. Dai, G. Wirjanata, A. Larsson, N. Prabhu, R. M. Sobota, Z. Bozdech, P. Nordlund, Identifying purine nucleoside phosphorylase as the target of quinine using cellular thermal shift assay, *Science Translational Medicine* **11**, eaau3174 (2019).

The contributions of the co-authors are as follows:

- I prepared the manuscript drafts. The manuscript was revised by Dr Bozdech, Dr. Prabhu and Dr. Nordlund.
- I co-designed the study with Prof. Bozdech and Prof. Nordlund and performed the laboratory work at School of Biological Sciences, NTU and Agency for Science Technology and Research (A*STAR) Proteos.
- Dr. Yu assisted in processing CETSA samples.
- Protein expression, co-crystallization and ITC experiments were conducted in collaboration with Dr. Chen from the Protein Production Platform, NTU. Data analysis was conducted by the author.
- Dr. Dai designed CETSA data analysis software (mineCETSA).
- Drug-synergy assays were conducted by Dr. Wirjanata.
- SPR experiments were conducted in collaboration with Dr. Larsson at the Biomolecular Interactions Platform, SBS, NTU.
- Dr. Sobota designed Mass Spectrometry sample analysis workflow.

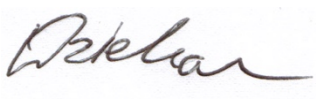

17 January 2019 Jerzy Michal Dziekan

Acknowledgements

I would first and foremost like to thank Professor Zbynek Bozdech, whose guidance, support and advice have been leading my scientific training for the past four years. I am thankful for the opportunity I was offered by him to move to Singapore to pursue to my scientific interests with creative freedom on how to approach encountered challenges. I owe deep gratitude to my co-supervisor Professor Roderick Wayland Bates for his guidance and tireless efforts in training a biologist in intricacies of organic and analytical chemistry. I also want to thank Professor Par Nordlund for his guidance and feedback during optimisation of CETSA for malaria. I would like to thank all members of the ZB lab for their help and support throughout the past 4 years, all members of Rod Bates' group for their patience and positive attitude whilst explaining chemistry to me, as well as members of Par Nordlund's group for the training, valuable discussions, technical and experimental assistance they offered, both with CETSA sample processing and Mass Spectrometry. I want to acknowledge and thank everyone who has contributed to the work presented here: including Ka Diam and Dr. Yan ting Lim for the training in CETSA, Dr. Dai Lingyun for his help optimising statistical data analysis algorithm, Dr. Yu Han for her help in CETSA sample processing, Dr. Chen Dan for her assistance with protein expression, crystallisation and ITC, Dr. Grennady Wirjanata for his help with drug assays, Dr. Andreas Larsson for his SPR contribution, Dr. Nayana Prabhu, Dr. Sachel Mok, Dr. Frances Rocamora and Dr. Radoslaw Sobota for valuable discussions. And last, but not least, I would like to thank my parents who enabled me to start the path which eventually led me here and all my friends and family for their continuous emotional support and encouragement throughout the graduate school with all its difficult moments.

Table of contents

Summary

Mechanisms of action (MoA) have been elusive for most antimalarial drugs in clinical use. Decreasing responsiveness to antimalarial treatments stresses the need of a more resolved understanding of their MoA and associated resistance mechanisms. In the present work we have implemented the Cellular Thermal Shift Assay (CETSA) for drug target deconvolution in *Plasmodium falciparum*. We used the CETSA assay to characterise the thermal unfolding patterns of the *P. falciparum* proteome. Subsequently, we validated the efficacy of CETSA for antimalarial drug-target identification using pyrimethamine, a drug with well-known MoA relying on inhibition of folic acid synthesis pathway and E64d, a broad-spectrum cysteine proteinase inhibitor. As a next step, we applied CETSA to quinine and mefloquine, two important anti-malarial drugs with poorly characterised MoA. Combining studies in parasite lysate and intact *P. falciparum*-infected red blood cells, we discovered *P. falciparum* Purine Nucleoside Phosphorylase (PfPNP) as a common putative target for these two quinoline drugs. The interactions were confirmed using biophysical and activity studies on recombinant proteins and crystal structures revealed binding of the two compounds in the enzyme's active site. Our results suggest that PfPNP inhibition is likely contributing to the therapeutic effect of aryl aminoquinolines. Additionally, we coupled the CETSA assay with an in-house-developed natural products drug discovery pipeline from Traditional Chinese Medicine to demonstrate assay's efficacy for drug discovery efforts. We isolated and identified skullcapflavone-II and wogonin, two previously uncharacterised molecules with antimalarial properties from *Scutellaria baicalensis* plant extract and used CETSA to determine the candidate molecular targets for skullcapflavone-II, the more potent of the two substances. This work demonstrates that implementation of CETSA for *P. falciparum* constitutes a new promising strategy to establish MoA for existing and candidate antimalarial drugs.

List of figures

Supplementary Figures

List of tables

List of abbreviations

ACT	Artemisinin-based Combination Therapy
ATM	Arthemeter
AUC	Area Under the Curve
AY	Ai Ye (*艾叶*)
BCA	Bicinchoninic acid
BJ	Bie Jia (鳖甲)
BL	Bing Lang (槟榔)
BLVRB	Flavin reductase
CE	Cang Erzi (苍耳子)
CETSA	Cellular Thermal Shift Assay
CG	Cao Guo (草果)
CH	Chai Hu (柴胡)
CNV	Copy Number Variation
COSY	Homonuclear Correlation Spectroscopy
CQ	Chloroquine
CX	Chuan Xiong (川芎)
CZ	Cang Zhu (苍术)
DARTS	Drug Affinity Responsive Target Stability
DCM	Dichloromethane
DGP	Di Gu Pi (地骨皮)
DHA	Dihydroartemisinin
DHFR-TS	Dihydrofolate Reductase – Thymidylate Synthase
DHPS	Dihydropteroate Synthetase
DNA	Deoxyribonucleic acid
DSF	Differential Scanning Fluorimetry
DUBs	De-ubiquitinating enzymes
EA	Ethyl Acetate
ESG	Extended similarity group Gene Ontology prediction
FC	Fold Change
FDR	False Discovery Rate
Fe(III)PPIX	Iron(III) protoporphyrin IX
FIC_{50}	Fractional Inhibitory concentration 50
GADHP	Glyceraldehyde−3−phosphate dehydrogenase
Hex	Hexane
HMBC	Heteronuclear Multiple Bond Correlation
HQ	Huang Qin (黄芩)
HSQC	Heteronuclear Single Quantum Coherence
HSW	He Shou Wu (何首乌)
$IC_{50\ /\ 90\ /\ 99}$	Inhibitory Concentration required for 50/90/99% growth inhibition
IDC	Intraerythrocytic Developmental Cycle
IMAC	Immobilised Metal Affinity Chromatography
ImmH	Immucillin H
iRBC	Infected Red Blood Cells

ITC	Isothermal Titration Calorimetry
ITDR	IsoThermal Dose Response
IVART	In Vitro Analysis and Reporting Tool
JH	Ju Hua (菊花)
KASbeta	Karyopherin beta
K_D	Equilibrium constant
KLP8	kinesin−13
Km	Michaelis constant
LDC	Long Dan Cao (龙胆草)
LM	Lumefantrine
MAD	Median Absolute Deviation (*here: of AUC)
MCM	Malaria Culture Medium
MeOH	Methanol
MFQ	Mefloquine
MMV	Medicines for Malaria Venture
MoA	Mechanism of action
MS	Mass Spectrometry
NMR	Nuclear Magnetic Resonance
PBS	Phosphate Buffered Saline
PM	Pyrimethamine
PNP	Purine Nucleoside Phosphorylase
PPQ	Piperaquine
PQ	Primaquine
PSM	Peptide Spectrum Matches
QD	Quinidine
QN	Quinine
RBC	Red Blood Cell
RNA	Ribonucleic Acid
ROS	Reactive Oxygen Species
SEA	South-East Asia
SERCaP	Single exposure, radical cure and prophylaxis
SKF-II	Skullcapflavone-II
SNP	Single Nucleotide Polymorphism
SPR	Surface Plasmon Resonance
TACT	Triple Artemisinin-based Combination Therapy
TCM	Traditional Chinese Medicine
TLC	Thin Layer Chromatography
Tm	Melting temperature
TRAC	Tracking Resistance to Artemisinin Collaboration II
TSA	Thermal Shift Assay
UV	Ultraviolet Light
WHO	World Health Organisation
WWARN	Worldwide Antimalarial Resistance Network
XHC	Xian He Cao (仙鹤草)
XXC	Xi Xian Cao (豨莶草)

CHAPTER 1

Introduction

1.1 Malaria burden and pathogenesis

Malaria is a vector-borne neglected tropical disease caused by five protozoa species: *Plasmodium falciparum, Plasmodium vivax, Plasmodium ovale, Plasmodium malariae* and *Plasmodium knowlesi*. Prevalent in over 100 countries, malaria remains a substantial health problem threatening an estimated 3.3 billion people living in tropical and subtropical regions *(1)*. In 2016 alone, 216 million new malaria cases were recorded with estimated 445,000 malaria-related deaths worldwide *(2)*. *P. falciparum,* causing the most severe symptoms, accounts for approximately 90% of global malaria cases and over 91% of deaths caused by malaria sub-Saharan Africa. *(2)*. Children under the age of 5 are most vulnerable and the most severely affected group accounting for over 70% of deaths in regions of high malaria transmission *(2)*. Amongst over 400 species of *Anopheles* mosquitos, 34 act as major vectors for this parasite and their prevalence is one of the main factors determining local intensity of transmission *(3)*. The hallmark malaria symptoms include periodic high fever, chills, sweating and nausea. However the disease might also lead to severe complications, such as renal failure, hypoglycaemia, respiratory failure and severe anaemia *(4)*. The rupture of red blood cells (RBCs) and release of daughter merozoites during parasite's intraerythrocytic developmental cycle (IDC) is the direct causative factor of the malaria pathophysiology, initiating a cytokine cascade and inducing clinical symptoms onset *(4)*.

The highly complex and multistage life cycle of *Plasmodium* (Fig. 1.1) allows the parasite to survive in intra- and extra- cellular environments both in vertebrate and invertebrate hosts, invading diverse cell types and evading host immune response. The parasite is transmitted to the human host via mosquito saliva during biting, after which it travels in the bloodstream and develops in human liver, and is released into the bloodstream entering the asexual life cycle. From there, it can be picked up by another mosquito to complete its sexual life cycle before moving onto another host.

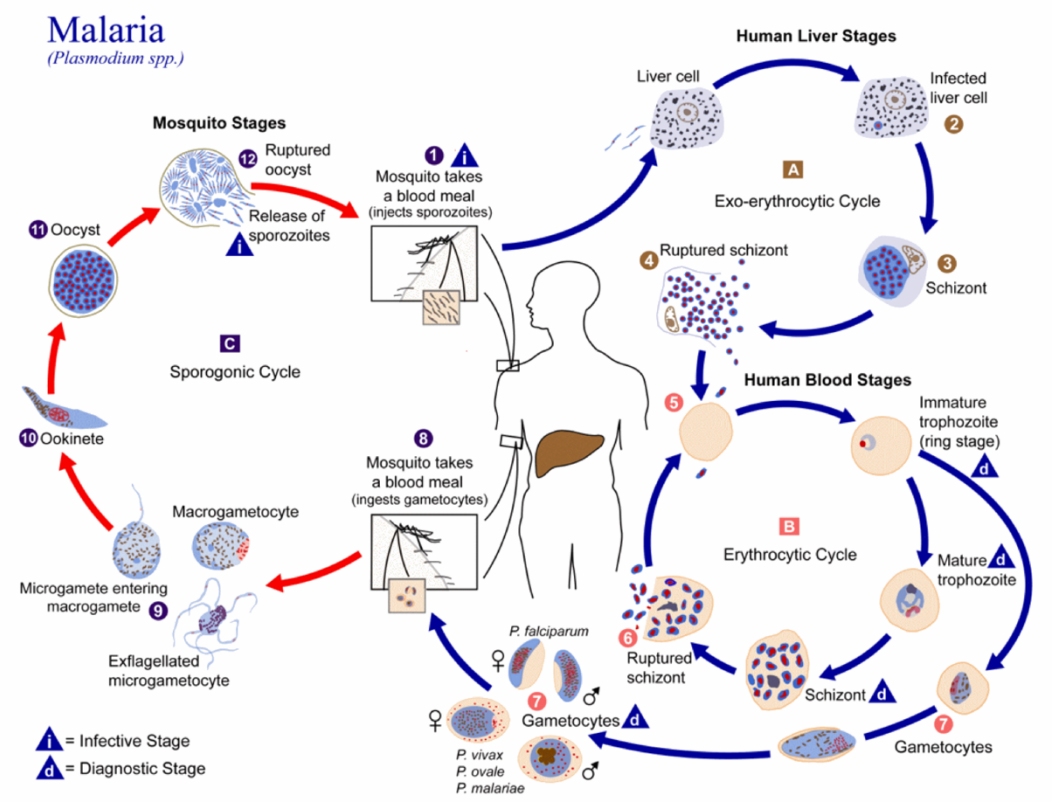

Figure 1.1 – *Plasmodium falciparum* life cycle *(adapted from http://www.cdc.gov/malaria)*

1.2 Antimalarial drugs

1.2.1 History and chemical diversity

Quinine – the first widely used antimalarial drug and a major alkaloid in the bark of *cinchona* tree was first isolated by Pierre Pelletier et Joseph Caventou in 1820 *(5)*. However, its first recorded use for malaria treatment extends back to 1630s in Peru, where a Jesuit Juan Lopez was reportedly cured of malaria by powdered bark from this tree *(5)*. Quinine has been used as the only effective antimalarial treatment until the 1940s when its more active derivatives, including chloroquine, were synthesised *(6)*. Over the years, a range of quinine derivatives were introduced into clinical use, giving a raise to the most historically crucial family of antimalarial compounds.

Three more naturally occurring cinchonia alkaloids are found in the bark of *cinchona* tree beside quinine: quinidine, cinchonin and cinchonidine. However, despite their parasiticidal activity, their use for malaria treatment has been limited. The first synthetic analogues of quinine shared a similar fate: pamaquine and quinacrine synthesised in 1932 and 1933 in Germany exhibited significant toxicity *(7)*. Ironically, chloroquine, which was also synthesised during those early studies was initially considered too toxic for human use *(8)*. Only after a decade, additional studies were conducted in the USA, chloroquine, amodiaquine and primaquine were introduced into clinical use in the late 1940s. The low production cost of chloroquine, its limited toxicity relative to other quinoline derivatives and its efficacy both as a therapeutic drug, as well as a chemoprophylaxis agent resulted in it becoming the principal antimalarial agent for nearly five decades *(7)*. Continuing efforts to identify new antimalarial drugs have led to synthesis of various other quinoline derivatives over the years. However, three main categories can be discerned among all quinoline derivatives based on the chemical structure: 4- or 8- substituted aminoquinolones, as well as the arylamino alcohols (Fig. 1.2).

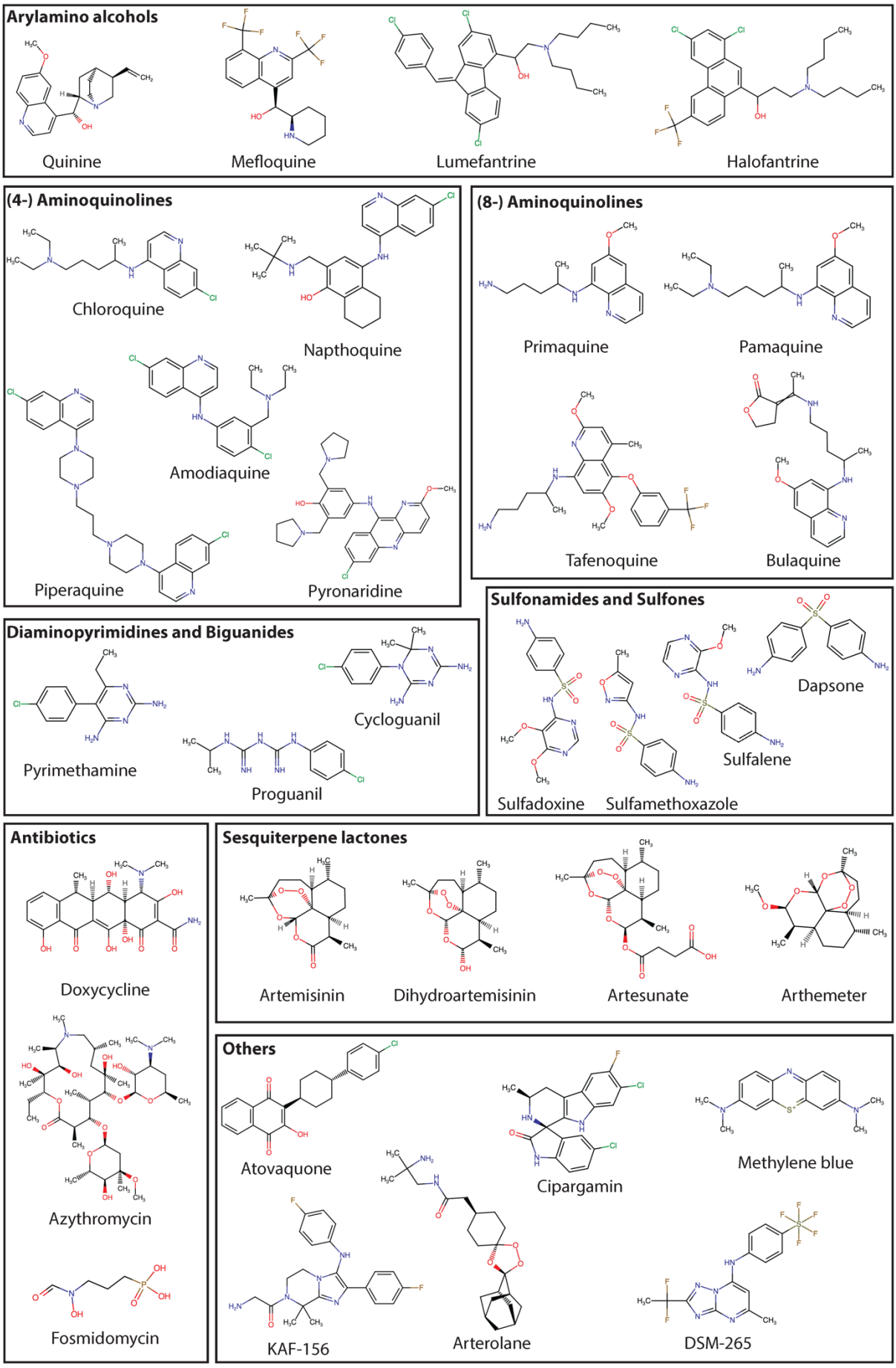

Figure 1.2 – Structural diversity of antimalarial compounds

The emergence of chloroquine resistance provoked introduction of the second generation antimalarial drugs as a first-line of treatment *(9)*. These drugs included two principal types of antifolates targeting two distinct enzymes in the folate synthesis pathway of *P. falciparum*. The type 1 antifolates included inhibitors of the dihydrofolate reductase-thymidylate synthase (DHFR-TS) enzyme. Its principal representatives are a 2,4-diaminopyrimidine developed in 1949: pyrimethamine and biguanides discovered in 1951: proguanil and its bioactive metabolite cycloguanil *(9)*. The type 2 antifolates target the dihydropteroate synthetase (DHPS) enzyme and consist of various sulfonamides and sulfones antibiotics, including sulphadoxine and dapsone (Fig. 1.2). The clinical usefulness of antifolates in monotherapy has proven to be limited. Therefore, combination therapies, exploiting the synergistic effect of type 1 and type 2 antifolate drugs, have been in use since their introduction in 1964. The most successful combinations of this type include sulphadoxine-pyrimethamine and Chlorproguanil-Dapsone *(9, 10)*.

Among successful antimalarials developed during and after the Vietnam War, was a potent synthetic analogue of quinine: mefloquine discovered by the Walter Reed Army Research Institute in 1984. Subsequently, it was developed as a major antimalarial drug by the collaboration of US Army, WHO and Roche Pharmaceuticals *(7)*. In the Maoist China, four other compounds were identified in the 1980s under a nation-wide initiative called 'Taskforce 523', launched by the government in response to communist Vietnam's request to protect its soldiers from malaria *(11)*. Those included three synthetic quinoline derivatives: lumefantrine, naphoquine and pyronaridine, as well as one natural product: artemisinin, which is the most potent antimalarial drug currently available on the market. The Taskforce 523 combined the expertise of TCM practitioners, pharmacologists, doctors, chemists and biologists to find new drugs against malaria *(12)*. They synthesised new antimalarial compounds,

as well as investigated over 2,000 traditional Chinese herbal preparations and tested them for possible antimalarial activity. Artemisinin was isolated from an extract of sweet wormwood (*Artemisia annua*), a plant that has been used in Chinese medicinal teas for over 2000 years, to treat malaria like symptoms *(11, 12)*. This first-in-class sesquiterpene lactone endoperoxide has given rise to several potent derivatives, which represent the forefront of antimalarial therapies today.

Diverse compounds with proven activity against malaria were identified over the years, some of which have become highly successful and widely used as drugs. However, none has dominated the malaria clinical treatment landscape in the same manner as quinine, chloroquine, pyrimethamine or artemisinin did once upon a time. Multiple members of the naphthoquinone compound family were investigated in the 1940s for their antimalarial activity during sizeable collaborative effort of industry and academia to replace quinine, leading to discovery of atovaquone *(13)*. The drug is not recommended for monotherapy due to significant risks of resistance emergence, but it has been available in combination with synergistic proguanil since 1999 as 'Malarone' *(14)*. Tetracycline antibiotics, including doxycycline have been successfully used for malaria treatment and prophylaxis ever since identification of their potent antimalarial properties in the 1950s *(12, 13)(15)*. In areas of high quinine resistance, they have been used as partner drugs in combinations with quinine to improve the cure rates *(16)*. Several promising compounds representing novel structural classes are currently under development and clinical testing, including artelolane, methylene blue and cipargamin *(17, 18)*.

1.2.2 Antimalarial drug resistance

One of the crucial factors contributing to malaria's morbidity is the efficacy of antimalarial treatment or the lack thereof. Recent success in malaria control can be attributed to effective vector-control strategies, as well as the mass implementation of Artemisinin-based Combination Therapies (ACTs). However, an escalation in mosquito resistance to commonly used insecticides *(19)*, as well as decreased responsiveness to standard ACTs *(20, 21)* threaten to escalate malaria incidence significantly.

Class		Example	First used in therapy	Resistance observed
Cinchona alkaloids		quinine	c.1630	1907
(4-)Aminoquinolines		chloroquine	1945	1957
(8-)Aminoquinolines		primaquine	1951	1959
Methanolquinolines		mefloquine	1975	1982
Phenanthrenes		lumefantrine	1992 (combination)	2011 (combination)
Naphthoquinones		atovaquone	1996	1996
Sesquiterpene lactones		artemisinin	1980s	2008
Antifolates	Type 1	sulfadoxine	1964 (combination)	1967 (combination)
	Type 2	pyrimethamine	1952	1952

Table 1.1 – Emergence of antimalarial drug resistance *(16, 22–26)*

In the past, the emergence of resistance to all classes of clinically used antimalarial drugs has been observed, rendering them obsolete in affected areas *(22)* (Table 1.1). The first incidence of drug resistance in malaria patients was recorded in Rio de Janeiro in 1907 in response to quinine treatment, marking the beginning of a new era. Chloroquine, introduced in 1945 quickly shared the fate of its predecessor. In the 1950s the first cases of chloroquine resistant *P. falciparum* were documented

and in 1989 resistance emerged in *P. vivax (16, 27)*. Nowadays, high resistance to chloroquine is widespread, but the drug is continuously being administered and misused in many endemic countries *(22)*. The principal mechanism of chloroquine resistance was linked to point mutations in the *Pfcrt* gene, encoding a food vacuole membrane transporter *(25)*. Single Nucleotide Polymorphisms (SNPs) in this gene were shown to affect parasite's susceptibility to other 4-aminoquinolines, arylamino quinolines and artemisinin *(25)*. Polymorphisms in *Pfcrt* increase chloroquine's (and likely other 4-aminoquinolines) efflux from the food vacuole, but the molecular basis of gene's involvement in modulating parasite's susceptibility to other drug classes remain poorly understood *(28)*. Chloroquine and quinine resistance also appears to be associated with polymorphisms of the *Pfnhe1* gene, which encodes a NA+/H+ transporter and involved in the regulation of the cytosolic pH *(25)*.

Mefloquine was first clinically tested in 1975 in the USA, but decreased efficacy of the drug was first recorded already in 1982 in Thailand *(23, 24)*. By 1995 substantial resistance to mefloquine was already well established in many endemic regions *(23, 24)*. Parasite's resistance to mefloquine is mediated through *Pfmdr1* (multidrug resistance protein 1) gene copy number amplification and increased expression of its product: the PGH1 protein, yet another food vacuole membrane transporter *(29)*. There is substantial evidence that increased expression of the *Pfmdr1* gene, induced by mefloquine pressure renders parasites less susceptible to remaining arylamino alcohol antimalarials: halofantrine, lumefantrine and quinine *(29, 30)*.

The resistance of *P. falciparum* to sulfadoxine-pyrimethamine (SP) combination developed within a year of its introduction in Thailand as a first-line drug in 1967, spreading rapidly across the entire South-East Asia *(31)*. By late 1990s high levels of SP resistance were present worldwide and this drug combination is no longer recommended clinically *(32)*. The resistance trait was unambiguously linked to point

mutations in the active sites of the two specific molecular targets of those drugs: the DHFR-TS *(33–36)* and DHPS *(37–40)*. The introduction of atovaquone monotherapy for malaria treatment in 1996 resulted in a rapid rise of resistance, observable within one year *(13)*. A sharp decrease in the susceptibility to atovaquone was associated with a single point mutation in the *Pfcytb* gene, encoding its direct target the mitochondrial cytochrome bc1 complex *(25)*.

ACTs, first recommended by the WHO as a first-line treatment against *P. falciparum* malaria nearly two decades ago, remain on the forefront of today's battle against this disease. However, ever since the decreased responsiveness to artemisinin-based therapies was first reported in 2008, the resistance traits have been strengthening and spreading throughout the SEA region *(20, 21)*. Recent reports of increased treatment failure rates of artesunate-amodiaquine in western Cambodia *(41)* are particularly worrisome, considering it is already the fifth ACT failing in that region *(21, 42–48)*. The mechanism of resistance to artemisinin is not fully understood. However, several phenotypic and genetic traits strongly associated with decreased responsiveness to artemisinin or related compounds have been reported. Transcriptional and morphological studies have demonstrated that 'resistant' parasites exhibited delayed IDC progression and strong upregulation in transcription of genes associated with the unfolded protein response *(49–51)*. The polymorphism of *Pfk13* (Kelch 13) gene is the most-reliable biomarker of artemisinin resistance, identified both in *in vitro* and *in vivo* samples, but it remains unknown exactly how it mediates decreased responsiveness to artemisinin *(52)*. Additional evidence from *in vitro* and clinical studies show the involvement of other genetic traits in artemisinin resistance has also been presented, including copy number variation and/or SNPs in *Pfmdr1, PfPrp22, Pfmrp, PfG7* and *Pffp2a (53)*. Overall, the basis of mechanisms of artemisinin resistance remain not fully understood and resistance phenotypes unrelated to *Pfk13* mutations have also been reported *(54)*.

The issue of drug resistance in malaria infections is further complicated by the occurrence of cross-resistance, in which mutations resulting from the selective pressure by a given drug can confer resistance to another compound via a similar mechanism *(29, 37, 55–58)*. Further spread of multidrug-resistant *P. falciparum* threatens to undermine substantial gains achieved in the global fight against malaria over the past two decades. Therefore, there is a pressing need to develop new antimalarial therapies based on new and diverse chemotypes, which would be unaffected by the resistance traits existing in the field *(17, 25)*.

1.2.3 Mechanism of action

The mechanism of action (MoA) of the majority of antimalarial drugs remains poorly understood. Only few clinically used compounds, such as antifolates and atovaquone, possess clearly defined molecular targets. However, their useful therapeutic lives have proven limited, particularly in monotherapy, due to rapid and rampant resistance development. Contrarily, the MoA of some of the most successful antimalarial drugs such as quinine, chloroquine, mefloquine and artemisinin remains ambiguous. Furthermore, based on available evidence, polypharmacology appears to be one of the key features of successful antimalarial drugs.

1.2.3.1 (4)-aminoquinolines

Among all available antimalarial drugs, on the side of artemisinins, quinolines represent the largest and undoubtedly the most clinically important group. Despite decades of research, the MoA has not been fully characterised for either one of those compounds. The understanding of the MoA of 4-aminoquinolines is based primarily on mechanistic studies of the most clinically relevant compound from that group: chloroquine. Since all 4-aminoquinolines are weak bases, they tend to selectively accumulate to high concentrations in acidic intracellular compartments, most notably the parasite's digestive vacuole *(59)*. The importance of the intravacuolar drug

accumulation for the MoA is supported by the morphological changes observed in treated parasites: digestive vacuole swelling and malaria pigment clumping *(60)*. The leading hypothesis, first proposed by Slater et Cerami in 1992 *(61)*, is that chloroquine disrupts the process of haemozoin formation, which takes place in the digestive vacuole. Consequently, the parasites are unable to detoxify soluble haem derived from the haemoglobin digestion process and to deposit it in insoluble haemozoin crystals, as a result dying from general toxicity of free haem. An extensive body of evidence supporting this MoA has been accumulated to date *(7)*. Most notably, 4-aminoquinolines have been shown to form complexes with haem precursor: iron(III) protoporphyrin IX [Fe(III)PPIX] and with the synthetic haemozoin: β-haematin, inhibit haematin crystal growth *in vitro*, as well as associate with the haemozoin *in vivo (62–65)*. Subsequent evidence of the central role of the haemoglobin digestion process to the antimalarial activity of chloroquine has been demonstrated with support of cysteine proteases inhibitors and their strong antagonistic effects for the activity of chloroquine *(66)*. Other potential MoA have also been suggested based on the *in vitro* evidence, including binding to DNA *(67)*, inhibition of protein synthesis *(68)* and inhibition of polyamine metabolism *(69)*, although based on the available evidence they likely play a minor role if any. Findings from studies investigating other 4-aminoquinoline compounds seem to suggest MoAs related to haem detoxification similarly to chloroquine *(5, 7, 66, 70–72)*, but the basis of differences in activity between independent compounds remain poorly understood.

1.2.3.2 Arylamino alcohols

Quinine and its close derivative: mefloquine have also been shown to display activity characteristics similar to chloroquine suggesting that they likely have an overlapping MoA with 4-aminoquinolines, at least to a certain degree *(7)*. Similarly to

chloroquine, both drugs have been reported to interact with Fe(III)PPIX and β-haematin *in vitro* interfering with haemozoin crystallisation *(73–75)*. Morphological changes to the digestive vacuole were also observed upon treatment with both quinoline methanols *(60, 76)*. However, they are non-identical to chloroquine. Overall, the evidence suggests that haemoglobin digestion process is also crucial to the antimalarial action of quinoline methanols *(66)*, but distinct differences are present between them and 4-aminoquinolines. For instance, it has been shown that unlike 4-aminoquinolines, mefloquine and quinine treatment do not lead to accumulation of the undigested haemoglobin in the parasite *(77)*.

Furthermore, parasite co-treatment with mefloquine was found to inhibit chloroquine-induced morphological changes and haemoglobin accumulation *(77)*. Authors suggested that mefloquine might inhibit haemoglobin ingestion, rather than digestion, although these conclusions need to be further substantiated and other targets of aryl aminoquinolines likely remain unidentified *(77)*. Resistance to quinine and mefloquine was reported in SEA in the 1980's and it was associated with the increased copy number of *pfmdr1* gene *(78, 79)*. *Pfmdr1* encodes a transmembrane transporter PfPGH1 that is believed to mediate drug efflux from cytoplasm to the digestive vacuole *(80)*. This suggests that the molecular target(s) of both drugs is present in the cytosol and thus the MoA of both drugs is (at least partially) distinct from that of chloroquine. Consistent with this, recent findings suggest that mefloquine inhibits translation through 80S ribosome binding, although polypharmacology involving other unidentified target(s) is expected *(81)*. Evidence has been presented linking mefloquine and quinine antiplasmodial activity with interference of membrane-system/endocytosis of the host cytosol *(77)*, DNA&RNA synthesis *(82)* and haemoglobin metabolism *(66, 75, 83)*, but no direct protein targets have been identified for these effects. Overall, no specific targets of quinine have been discovered to date. Similarly, the MoAs of the two structurally related phenanthrenes: halofantrine

and lumefantrine remain unknown. Limited *in vitro* evidence has been provided demonstrating Halofantrine's interaction with haematin *(75)* and Plasmepsin II *(84)*, but the relevance of these findings for its MoA remains undetermined.

1.2.3.3 (8-)aminoquinolines

The bioactivity profile of 8-aminoquinolines suggests that their MoA is fundamentally different to those of 4-aminoquinolines or arylamino alcohols. Firstly, unlike other quinoline drugs, the 8-aminoquinolines are effective against liver stages of the parasite life cycle. The absence of haemoglobin in liver cells precludes its involvement in the antimalarial activity of these compounds against local parasite forms *(7)*. The most relevant representatives of this compound family: primaquine and tafenoquine are both prodrugs, and the majority of their antimalarial activity is attributed to their hepatic metabolites *(85, 86)*. The 8-aminoquinolines retain activity against blood stages of the malaria parasite, however, only some exhibit the capacity to inhibit haem polymerisation (e.g. tafenoquine) *(87)*, while others lack it (e.g. primaquine) *(74, 88)*. While no molecular targets have been identified to date for these compounds; the oxidative stress generation *(89, 90)*, interference with parasite's DNA structure and negatively affecting mitochondrial membrane integrity *(91)* have been suggested as their possible MoAs.

1.2.3.4 Antifolates

The two main types of antifolate drugs represent the most well-characterised groups of antimalarials. Unlike some of the aforementioned quinoline compounds, antifolates do not exhibit an apparent polypharmacology and their antimalarial MoA depends on the inhibition of a specific enzyme. Pyrimethamine is a well characterised competitive inhibitor of the DHFR-TS enzyme *(33, 92)*. Similarly, cycloguanil, the active metabolite of proguanil has been shown to bind the active site of the enzyme

inhibiting its enzymatic activity *(93)*. Mutations in the active site of DHFR-TS have been shown to specifically drive parasite resistance to both compounds, both in the *in vitro* conditions, as well as in the clinical setting *(33, 93, 34–36)*. Sulfones and sulfonamides, such as sulfadoxine and dapsone were introduced as partner drugs to DHFR-TS inhibitors, due to their capacity to inhibit the DHPS enzyme. Similarly, sulfadoxine and dapsone were shown to inhibit the DHPS enzyme and that mutations in its active site drive the resistance to both compounds *(37–40)*. The inhibition of DHFR and/or DHPS disrupts parasite's folate synthesis pathway, resulting in significant impairment of nucleic and amino acid synthesis *(94)*

1.2.3.5 Naphthoquinones

The MoA of atovaquone was validated in 1992, demonstrating that it is an inhibitor of parasite's mitochondrial electron transport chain, consistent with the hypothesis that this class of compounds acts as ubiquinone antagonists *(95)*. This mode of action was later on validated through observation that drug-pressure induced SNP in the gene coding for cytochrome B leads to 1000 times lower parasite sensitivity to the drug *(25)*.

1.2.3.6 Sesquiterpene lactones

The MoA of artemisinin and related compounds remains to be fully characterised. Several diverse plausible mechanisms of action and molecular targets have been suggested and are currently the subject of scientific debate*(54, 96, 97)*. The antimalarial bioactivity of this class of compounds is known to be dependent on the presence of an endoperoxide bridge in compounds' structure *(98)*. Its opening is believed to result in reactive oxygen species (ROS) generation, which induces more or less targeted damage to the parasite. However, the mechanism of ROS generation and their primary target(s) relevant for the antimalarial activity of artemisinin is yet to

be discerned *(53)*. The very high potency of artemisinin-like drugs and their fast-acting nature suggests that they do possess specific targets, rather than inducing non-specific global damage *(97)*. Several large-scale proteomic studies attempting to identify sesquiterpene lactones' molecular targets indicate a large number of potential interactions. However, they were not validated nor was their relevance for the MoA demonstrated *(96, 99)*. To date, several candidate targets of artemisinin (or related compounds) have been suggested including: sarco/endoplasmic reticulum membrane calcium ATPase (SERCA), phosphatidylinositol-3- kinase (Pfpi3k) enzyme, a translationally controlled tumour protein homolog (PfTCTP), however there is no consensus in the scientific community regarding their relevance *(53, 97)*. Overall, further studies on the subject are required and it is likely that other targets of this class of drugs remain unidentified.

1.2.3.7 Others

None of the remaining clinically used antimalarial drugs possess a clearly defined mode of action. However, the antimalarial drug discovery efforts ongoing for the past two decades have led to the identification of various novel compounds with antimalarial properties along with their respective molecular target. Some of them have progressed into successful drug candidates and are currently under development, including drug- target pairs such as spirindolones (e.g. Cipargamin) targeting PfATP4 (Plasma membrane P-type cation translocating ATPase), imidazolpiperazines (e.g. KAF-156) targeting yet-to-be identified target, triazolpyrimidines (e.g. DSM-265) targeting PfDHODH (Dihydroorotate dehydrogenase) and Immucillins targeting PfPNP (Purine Nucleoside Phosphorylase) *(17, 18, 100)***.** Nevertheless, the drug-target identification efforts have not been successful for many other antimalarial candidate compounds, and their MoA remain poorly understood *(17, 18)*.

1.3 Antimalarial drug discovery

1.3.1 Identification of new antimalarial drug candidates

An ideal new antimalarial drug would satisfy a series of requirements *(17, 18, 101, 102)*. Firstly, it would be active against all parasite developmental stages, including liver and blood stages and block parasite transmission. In order to overcome the issue of patient compliance, it would be potent enough to provide a curative effect in a single dose. The desired characteristics of novel antimalarial drugs were initially formulated as SERCaP (Single exposure, radical cure and prophylaxis) treatment *(101)* Furthermore, inexpensive production cost ($\leq$ 0.15 USD/dose) is necessary to ensure that the drug is accessible to all affected, many of whom live in extreme poverty. Considering substantial levels of resistance to existing drugs in affected areas, the new compound would represent a radically new chemotype with a distinct mode of action to existing drugs. Synergistic antimalarial effect of the new drug, when administered together with existing artemisinin, derivatives would provide an additional benefit, allowing deployment of novel ACTs and reducing the risk of rapid emergence of resistance.

Diverse approaches have been undertaken to develop new antimalarial drugs. Synthetic chemistry-based strategies, relying on chemical diversification and building upon structural scaffolds of existing drugs have proven successful in the past, particularly regarding the quinoline drug family *(7, 71)*. However, many of these compounds appear to exhibit similar MoA and are affected by the same mechanisms of resistance *(7, 21)*. Therefore, despite their efficacy in clearing the infection, they do not represent ideal replacements for existing therapies. An alternative approach for identifying new antimalarial drugs relies on high-throughput screens of compound libraries, derived from synthetic chemical synthesis efforts or representing assembles of natural products isolated from plants, animals, fungi and bacteria *(18)*. Such

chemical library screens were deployed in two principal manners: to identify novel inhibitors to previously selected targets in specific biochemical assays or to identify molecules which inhibit parasite growth *in vitro* in the 'whole-cell' / 'phenotypic' screening *(18, 103)*.

Target-based drug discovery approaches are reliant on the identification of potent inhibitors to a druggable protein, the inhibition of which results in cell death. Such targets are typically selected based on chemical validation data (the protein is a target of another molecule) or genetic validation data (the protein is essential for parasite survival) *(18)*. Following target selection, a given protein is typically recombinantly expressed and included in high-throughput biochemical screens of chemical or fragment libraries to identify new molecules with desired affinity characteristics. Such approaches have been moderately successful in the pursuit of novel antimalarial drugs, leading to the identification of P218 as a new PfDHFR inhibitor, as well as DSM-265 targeting PfDHODH *(104, 105)*. Both compounds are currently undergoing clinical testing *(100)*.

Nevertheless, the majority of antimalarial compounds have been identified through the phenotypic screening approaches. This strategy offers several advantages over the target-based strategies, as it allows identifying compounds of diverse chemotypes with potent activity against the malaria parasite without the need of a prior selection of a target and expression of the target protein *(18, 103)*. As a consequence, drug candidates with novel targets can be identified, but the downside of this approach is the necessity of the MoA characterisation following identification of bioactive molecules. Diverse phenotypic screens have been developed to identify drugs against hepatic, IDC or sexual parasite stages *(18, 103)*. Additionally, the approach allows identification of compounds with specific properties, such as parasite transmission blocking.

1.3.2 Traditional medicine as a source of new antimalarial drugs

The vast majority of pharmaceuticals currently in use are either natural products themselves, their derivatives or substances inspired by natural products *(106)*. Natural products possess multiple advantages over synthetic drugs, primarily the complexity and nearly unlimited structural diversity they can achieve while still retaining their function due to millions of years of evolution *(107)*. Despite the time and effort required to identify such active substances, many of the most successful drugs have been developed through the sourcing of nature's arsenal. The phenomenon of characterising, isolating and using pure bioactive constituents of medicinal plants for the treatment of different ailments had not begun until the 19th century *(108)*. Until then, we had been relying on treating diseases with medicinal plants and various preparations thereof, according to traditional recipes. This is also the case when it comes to antimalarial compounds. Beside quinine, isolated in 1820 *(5)* and artemisinin characterised more recently, a range of very potent antimalarial compounds has been isolated over the years from plants traditionally used for the treatment of this disease *(109–111)*. Authors of a recent review reported over 480 compounds with antimalarial properties isolated from plants and published within 2005-2008 period *(112)*. Even if only a small proportion of this group exhibited antimalarial activity within the desired nanomolar range, it demonstrates the potential of the natural product research for the identification of new antimalarial lead compounds. The rationale behind identification and isolation of antimalarial compounds from plants traditionally used for the treatment of this disease, relies on their historically proven efficacy thus a higher likelihood of identifying potent bioactive compounds.

Traditional Chinese Medicine (TCM) represents one of the largest and oldest compendia of knowledge about the medicinal application of plants and animal products. A recent review estimated that TCM encompasses 11,146 species of plants belonging to 2,309 genera and 383 families, together with 1,581 species of animals and 80 minerals *(113, 114)*. The most extensive exploration of TCM for compounds with antimalarial properties, conducted within the 'Taskforce 523' has identified, on a side of artemisinin, several highly potent and chemically diverse antimalarial compounds *(11, 12)*. However, none of them has progressed past the clinical trials, as they induced undesired side effects (e.g. excessive vomiting) or exhibited insufficient curative profile in human trials. An alternative approach for exploiting TCM as a source of new treatments, involves the use of herbal extracts instead of identifying a singular bioactive constituent. The reasoning behind using multi-component botanical extracts is based on the fundamental belief of TCM that the therapeutic effect of traditional herbal preparations is achieved through the cross-talk between multiple ingredients they include *(114)*. Several of such plant extracts are currently undergoing clinical trials or pending FDA approval for treatment of malaria and other ailments *(18, 114)*. Nevertheless, the identification of the MoA of such multicomponent mixtures is highly challenging and rarely attempted. Thus, their therapeutic use introduces additional risks including the potential for drug interactions and undesired side effects, which might be difficult to predict. Overall, the TCM represents an attractive source of novel antimalarial compounds, but their identification and determination of their respective MoA still represent a challenge.

1.3.3 Characterisation of the mechanism of action of antimalarial drugs

Collaborative efforts of academic, non-profit and industrial partners to identify new molecules with antimalarial properties could be considered one of the largest breakthroughs of the past decade in the field of antimalarial drug discovery. High-throughput phenotypic screens conducted by Medicine for Malaria Venture (MMV), Gate's foundation, Novartis, GSK and various academic bodies tested millions of compounds yielding tens of thousands of molecules with <1μM activity against different developmental stages of *P. falciparum (115–124)*. One of the main remaining challenges is identification of intrinsic molecular targets for the most potent compounds while prioritising radically new chemotypes.

The most well-established and historically successful approach for the characterisation of the antimalarial compound MoA is the 'resistance-screening' *(125, 126)*. This strategy relies on continuous parasite exposure to sub-lethal drug concentrations *in vitro*, aimed at provoking parasite's evolutionary adaptation to withstand the drug pressure *(126)*. Subsequent omics' analysis of resistant parasites allows characterisation of molecular basis of increased drug tolerance, absent from the wild-type parasites. Such analyses can be of genomic, proteomic, transcriptomic and metabolomic nature and allow identification of SNPs, CNVs, altered gene/protein expression levels or metabolic profiles associated with the resistance phenotype and often will directly reveal the drug target candidate *(54, 127–129)*. A similar approach can also be used for clinical isolates exhibiting drug resistance profiles, but automatically it is limited to clinically used drugs and not available for candidate compounds *(49, 78, 130, 131)*. Other methods historically used to support the antimalarial drug-target identification studies include diverse chemo-proteomics affinity-chromatography based approaches, which allow isolation of proteins exhibiting

in vitro affinity to the small molecule drug upon incubation with the cellular lysate and their subsequent identification through mass spectrometry *(132–134)*.

Several new technologies developed for *P. falciparum* over the past few years have greatly enhanced our capacity to identify and validate candidate drug targets. Notably, CRISPR/Cas9-based genome editing *(135)*, chemogenomic profiling *(136, 137)*, target prediction via transcriptional profiling *(138)*, click-chemistry proteomics *(96, 99, 139)* and drug affinity responsive target stability (DARTS) techniques *(140)* have been recently optimised for studying *P. falciparum* and offer new alternative means to approach the problem of antimalarial drug-target identification. Nevertheless, the unusual biology of this protozoa and the absence of a genetic point of reference due to its phylogenetical diversity from all other model organisms renders it difficult to study *(141)*. Consequently, many research tools developed and used to elucidate drug's MoA in other pathogenic organisms have been applied to studying protozoa with limited success *(141)*. The available techniques for the *P. falciparum* research, although valuable, have limited scope of application, as illustrated by the fact that after decades of research the MoA of many clinically used antimalarial drugs remains uncharacterised. Therefore, despite the recent advances and expansion of the arsenal of tools available to assist the antimalarial drug MoA deconvolution, there still remains the need for further development in that field.

1.3.4 Cellular Thermal Shift Assay (CETSA)

Cellular Thermal Shift Assay (CETSA) is the first broadly applicable label-free method to study drug-target engagement in intact cells, originally developed to assist anti-cancer drug target discovery *(142–144)*. The technique is based on the discovery that heat-induced unfolded proteins precipitate rapidly in cells, allowing melting curves to be measured by monitoring the remaining soluble protein after a heat challenge *(143)*. As for classical Thermal Shift Assay (TSA) using purified proteins *(145, 146)* ligand binding typically leads to protein stabilisation and a positive shift in melting curves (Fig. 1.3A). Coupling CETSA with multiplexed quantitative Mass Spectrometry (MS-CETSA), allows simultaneous monitoring of the entire proteome for changes in protein stability under drug treatment *(147)*. As a result, binding protein-targets can be identified in CETSA without any prior knowledge on the mechanism or site of drug's action.

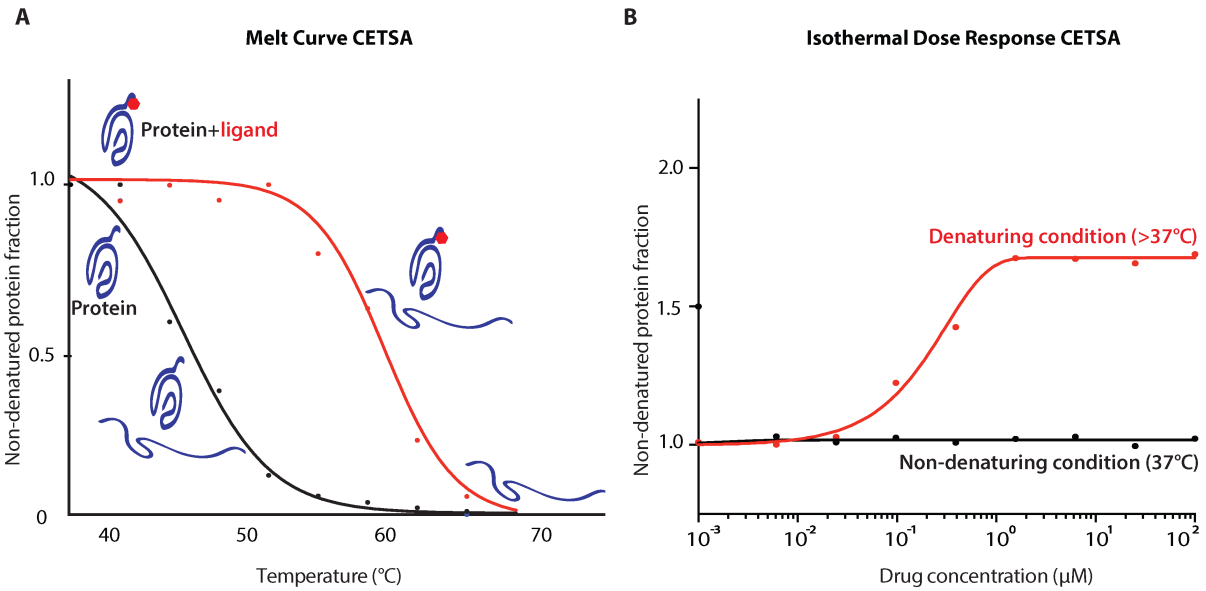

Figure 1.3 – The principle of the two CETSA variants

The two existing variants of the CETSA protocol are based on the common principle: ligand-induced protein stabilisation *(i.)* the melt curve CETSA approach in which protein precipitation is monitored at 10 distinct temperatures in drug's presence

or absence (Fig. 1.3A); *(ii.)* the Isothermal Dose Response CETSA (ITDR) in which protein stabilisation is monitored at multiple drug concentrations at a single temperature *(147)* (Fig. 1.3B). While the melt curve CETSA is used to assess the variance in protein melting curves between drug-treated and vehicle control samples, the ITDR experiments monitor the change in protein stability under thermal denaturation conditions across drug concentration gradient. In both experimental variants, the proteins which are not engaged by the ligand are expected to behave in an identical manner disregarding of the presence or absence of the drug and/or denaturing vs non-denaturing condition. Both, the melt curve and ITDR experiments can be conducted in the context of drug-target interactions within an intact cell or in the cell lysate

CETSA offers several advantages over existing tools for antimalarial drug-target identification. Technique's capacity to monitor the entire parasite proteome simultaneously makes it suitable for identification of drug-targets of compounds with previously undetermined modes of action. Furthermore, it selectively identifies direct drug targets, rather than approximating them based on parasite's response to the treatment. Chemical tagging of drug molecules and genetic modifications of parasite strains, required by some techniques, can be expensive, time-consuming and could introduce undesired effects altering molecule's binding properties or parasite's response to the treatment *(148)*. The label-free principle that CETSA is based on - monitoring of intrinsic thermodynamic protein properties, allows its usage with the parasite strain of choice and standard unmodified compounds. It is our belief that the development of MS-CETSA for *P. falciparum* can complement existing tools, facilitating antimalarial drug target discovery efforts and serve to deepen our understanding of the parasite biology further.

1.4 Aims and experimental approach

In this work we attempted to address some of the principal challenges present in the antimalarial drug discovery research field. For that purpose, we aimed to adapt the MS-CETSA method for the malaria research and explore its application for stringent identification of antimalarial drug targets in the *P. falciparum* proteome. However, considering that the CETSA method has never before been used to study organisms other than cancer cells (and since this year bacteria), extensive modifications of the sample preparation protocol were necessary to accommodate an intracellular protozoa, such as *P. falciparum*. Overall, in the time-course of the project, we aimed to address five principal objectives:

- Develop a robust protocol for MS-CETSA analysis of the *P. falciparum* proteome in the lysate and intact-cell protocol variants
- Characterise the thermal denaturation behaviour of the *P. falciparum* proteome through melt curve MS-CETSA in lysate and intact-cell settings
- Provide a proof-of-principle for the antimalarial drug-target discovery through MS-CETSA
- Utilise MS-CETSA to uncover previously unknown drug-targets for clinically used antimalarials: quinine and mefloquine
- Develop a fully functional pipeline for the antimalarial drug discovery from TCM

In order to adapt the CETSA protocol for the malaria parasite, it was necessary to address the principal challenge of the proteomic analysis of human RBCs – the high haemoglobin content. We explored diverse method variants and evaluated their performance regarding the extent of haemoglobin depletion they provide, proteome coverage they attain and the sample quality and reproducibility they deliver. The approaches evaluated were based on three main strategies: haemoglobin depletion,

infected cell enrichment, host-cell removal. The latter approach was chosen for lysate CETSA experiments and we demonstrated its high performance. However, the infected cell-enrichment strategy has proven the best protocol variant for the intact-cell application. Both best performing methods were used for the melt curve CETSA characterisation of the melting behaviour of the *P. falciparum* proteome. Protein unfolding patterns were recorded in the lysate and the intact-cell settings, compared in between each other and contrasted with the melting behaviour of the reference and the host cell. Subsequently, we aimed to evaluate the performance of MS-CETSA for the identification of direct drug-targets and provide the proof-of-principle for the technique. For that purpose, we have selected two compounds with known molecular targets in the *P. falciparum* proteome: pyrimethamine and E64d and demonstrated that our designed protocol unambiguously identifies their known interacting proteins.

The rudimentary understanding of the MoA of the majority of antimalarial drugs, resulting from the ambiguity concerning their specific molecular targets, substantially hinders the implementation of successful counter-measures to clinical drug failure. Having validated the CETSA approach for drug-target identification with pyrimethamine and E64d, we applied the CETSA protocol to uncover the molecular targets of two clinically important and structurally related antimalarial drugs with poorly defined modes of action: quinine and mefloquine. The target-binding predisposition of both compounds was evaluated in the lysate and intact-cell setting. The interaction of both compounds with their newly identified common molecular target: *P. falciparum* Purine Nucleoside Phosphorylase was subsequently validated through biophysical and cellular assays.

Understanding how existing antimalarial drugs exert their parasiticidal action, while crucial, remains only a stepping stone for the design of more effective future treatments. The need for new therapeutics becomes particularly urgent in the light of

emerging artemisinin resistance. Therefore, as an additional objective, we aimed to address the second principal challenge of the antimalarial drug discovery field: the need for the new antimalarial treatments. In an attempt at identifying new potent drug candidates with antimalarial properties, we set out to establish a functional drug-discovery pipeline sourcing the TCM. Our desired experimental setup would allow isolation and identification of bioactive molecules from plants historically used to treat malaria. A combination of that pipeline with an optimised CETSA protocol has the potential to identify new drug candidate molecules along with their respective molecular targets in the malaria proteome. The approach was successfully used to identify wogonin and skulcapflavone-II, as novel antimalarial compounds from a TCM herb: *Scutellaria baicalensis,* along with the candidate antimalarial targets of the latter.

CHAPTER 2

Materials & Methods

2.1 *P. falciparum in vitro* culture conditions

Plasmodium falciparum T996 and 3D7 strain parasites were maintained in human red blood cells culture *in vitro* in accordance with the following guidelines. Briefly, cultures were grown in complete Malaria Culture Media (MCM) (RPMI 1640 powder 16.2g/L (GIBCO), Hypoxanthine 0.1mM (SIGMA), NaOH 1mM (SIGMA), $NaHCO_3$ 23.8mM (SIGMA), Gentamicin 10mg/L (GIBCO) and Albumax II 2.5g/L (GIBCO)) under hypoxic conditions (5% O_2 5% CO_2 90% N_2) maintaining 2% haematocrit. Parasites were synchronised with 5% Sorbitol *(149)* at early ring and late ring stages, at least once one life cycle prior to drug activity testing or CETSA sample preparation.

2.2 Smear preparation, assessment of parasitaemia and staging.

Thin blood films from cultures were air-dried, fixed with MeOH and stained for 3-4min with 5% Giemsa stain in Sorenson's buffer pH7.2. The assessment of the parasite stage development and parasitaemia was carried out using light microscopy under oil immersion 100x objective following the criteria from Silamut et al. (1999) *(150)*.

2.3 Percoll gradient iRBC enrichment

Percoll gradient enrichment of parasitised cells was conducted in accordance with previously described *(151)*. In brief, 2mL of washed 10% parasitised 10% haematocrit RBC were deposited in a 15mL falcon, followed by addition of 2.5mL ice-

cold 60% Percoll and centrifugation (1.500g, 4°C, 15min). Interphases containing mature stages were collected and washed with MCM.

2.4 Haemodepletion intact-cell CETSA sample preparation method

Mid-trophozoite stage synchronised (28±4hpi) *P. falciparum* 3D7 culture at ~10% parasitaemia, 2% hematocrit was used for all candidate workflow variants. In case of haemoglobin depletion protocols, the cells were pelleted down (2500rpm, 5min), washed with PBS and the cell density was quantified with haematocytometer. Then cells were resuspended in 100μL of PBS and heated for 3min at 37°C and 3min at 4°C, followed by addition of 2x lysis buffer to the final concentration of 50mM HEPES pH 7.5, 5mM beta-glycerophosphate, 0.1mM Na_3VO_4, 10mM $MgCl_2$, 2mM TCEP and cocktail EDTA-free protease inhibitors (Sigma). Then cells were lysed by 3x flash freezing-thawing cycles, followed by mechanical sheering. Obtained lysate was centrifuged (20.000g, 20min, RT), the supernatant was isolated and subjected to the haemodepletion protocol variants with Hemoglobind (2.92mg protein), HemoVoid (2.92mg protein) or NuGel (2.24mg protein) commercial kits (Biotech Support Group) in a technical triplicate following the manufacturer's guidelines. Protein concentration prior and post haemodepletion was quantified via Bicinchoninic acid (BCA) assay (Pierce). In order to remove undesired buffer from resulting post-haemodepletion samples, elution samples from all three variants were purified via the 'In-gel digestion' or the 'Acetone precipitation' protocols. Following this, samples were processed as described in section 2.9 with the exception of TMT10 labelling, which was not performed, as all samples were derived from one temperature only. Additionally, instead of ÄKTAmicro system-driven peptide separation, a manual separation was conducted. Briefly, peptides were solubilised in 10mM ammonium formate pH10.0 and loaded onto C18 beads Oasis HLB 30 μm (Waters)-packed tip, washed with 10mM ammonium formate pH10.0 and ten fractions were eluted increasing concentration of

ACN by 10% (v/v) for every subsequent fraction, until reaching 100% ACN. Subsequently, samples were dried in speed vac and analysed as described in section 2.10.

2.5 In-gel protein digestion

The in-gel digestion protein samples were incubated with 55mM CAA for 20min at RT, mixed with 2x Laemmli sample buffer (Biorad) and samples were boiled for 5min at 95°C prior to loading on 8% SDS gel for separation. Following separation, the gel was stained with Coomassie Blue and the entire 'gel-line' containing protein was cut into small tubes ~1-2mm in diameter and de-stained in 50% Ethanol/50mM Ammonium Bicarbonate on a shaker at 25°C. Distaining step was repeated 5 times and afterwards the gel was washed with 100% Ethanol (5min, RT), repeating the step twice. Following gel drying in a speed-vac, trypsin solution (12.5µg/mL) in 50mM Ammonium Bicarbonate was added to cover the cubes and incubated over night at 37°C on a shaker. The liquid was collected and the gel cubes were washed twice with extraction solution (3%TFA 30% ACN) on a shaker at 37°C for 10min. Subsequently sample was washed twice with 100% ACN. All liquids were combined with the initial digestion liquid, dried in a speed-vac, followed by protein desalting step as described below.

2.6 Acetone protein precipitation

Eluted protein samples were diluted with acetone (sample 1 : 4 acetone ratio) and stored at -20°C O/N to induce protein precipitation. The following day, samples were centrifugated (20.000g, 20min, 4°C), supernatant was discarded and the pellet was dried in a speed-vac. The step was followed by desalting step as described below.

2.7 Melt curve CETSA and ITDR sample preparation method

Mid-trophozoite stage synchronised (28±4hpi) *P. falciparum* 3D7 culture at ~10% parasitaemia, 2% hematocrit was used for all CETSA preparations. In case of 'Lysate CETSA', parasite culture was centrifuged (2500rpm, 5min), the pellet was washed with PBS and incubated with 10x volume of fresh 0.1% Saponin in PBS pH 7.2 for 5min. Following centrifugation (2500g, 5min) the supernatant containing RBC cytosol and vacuolar content was removed, whilst intact parasite pellet was washed 3x with 50mL of ice cold PBS. Parasite pellet was then resuspended in 1mL of lysis buffer composed of 50mM HEPES pH 7.5, 5mM beta-glycerophosphate, 0.1mM Na_3VO_4, 10mM $MgCl_2$, 2mM TCEP and cocktail EDTA-free protease inhibitors (Sigma) and lysed by 3x flash freezing-thawing cycles, followed by mechanical sheering. Samples were centrifuged (20,000g, 20min, 4°C) and supernatant containing soluble parasite proteins was isolated. Remaining pellet was resuspended in 1mL of lysis buffer and the procedure was repeated. The protein concentration in lysate was quantified by BCA assay (Pierce). Ten aliquots of protein (100µg each) were added to serially diluted drug, incubated for 3min at RT in order to minimise metabolism *in vitro* and heated at respective temperature for 3min (ITDR experiments – one temperature, 'Melt curve' experiments temperature gradient: 37-73°C with 4°C intervals) in a 96-well thermocycler, followed by 3min incubation at 4°C. The post-heating lysates were centrifuged (20,000g, 20min, 4°C) and the supernatant was transferred to a fresh eppendorf tube. The protein concentration of the post-heating lysate (no-drug control in ITDR experiment or 37°C condition in the melt curve experiments) was measured by the BCA assay. See 'peptides preparation and labelling' section for the following steps. K562 lysate melt curve CETSA samples were prepared analogously, following the method previously described in *(152)*.

In case of 'Whole Cell CETSA', 1mL of ~10% infected packed blood was loaded on MACS CS column (Miltenyi Biotech), washed and eluted according to

manufacturer's instructions. Enriched infected Red Blood Cells (iRBC) (to the level of 75-96% parasitaemia) were incubated for 1h in excess of MCM at 37°C with agitation, subsequently ~25-30 million per concentration point were added to 2mL of MCM containing the drug or an equivalent volume of DMSO at final concentration 0.4% (v/v) and incubated (1h at 37°C under agitation). Cells were pelleted by centrifugation (2,500rpm, 5min), washed with PBS, resuspended in 1.1mL of PBS and transferred in 100μL aliquots onto 10 wells each on a 96 well microtiter plate, subsequently subjected to thermal challenge for 3min, followed by 3min at 4°C. Samples were then lysed by flash freezing/thawing 3x, followed by mechanical sheering. Soluble fractions were isolated by centrifugation (20,000g, 20min, 4°C) and protein concentration was quantified by the BCA assay in the same manner as previously described for the lysate assay. K562 intact-cell melt curve CETSA samples were prepared analogously, following the method previously described in *(152)*.

2.8 CETSA Drug treatment

Pyrimethamine (PM), quinine (QN) and mefloquine (MFQ) were purchased from Sigma and E64d from ApexBio and Immucillin H (ImmH) from Pharmablock Sciences (Nanjing) Inc., whilst Skulcapflavone II (SKF-II) was isolated from *Scutellaria baicalensis* root DCM extract in house. All drug stock solutions were prepared in DMSO. Highest drug dose used in all Lysate ITDR experiments with conventional drugs was 100μM, except QN (10 μM), whilst for SKF-II enriched fraction it was 100μg/mL. In intact-cell ITDR experiments, the doses were as follows 10μM for QN and MFQ, 125μM for E64d and 250μM for PM. All ITDR drug treatments were performed with four-fold serial dilution except the intact-cell-QN-ITDR, where five-fold serial dilution was applied, with last concentration point being a drug-free control. PM melt curve CETSA experiments were carried out with 100μM PM or drug free control

in both lysate and intact-cell conditions. All the above treatments were performed in the presence of 0.4% (v/v) DMSO in intact-cell experiments and 1% (v/v) in lysate.

2.9 Peptides preparation and labeling

One hundred µg of total soluble protein isolated after thermal challenge per experimental point was aliquoted and reduced with 20mM TCEP, 0.05% (w/v) RapiGest (55°C, 20min). Subsequently samples were alkylated with 55mM CAA (RT, 30min), followed by digestion with LysC (0.05µg of LysC per 1µg of protein) for 4h at 37°C and then trypsin digestion for 18h at 37°C. Digestion was halted by addition of TFA to 1% final concentration and incubation for 45 min at 37°C to hydrolyse the remaining RapiGest, which was pelleted by centrifugation at 20,000g for 15 min. The soluble fractions were collected and dried in a speed vac, solubilised in 200mM TEAB to a final concentration of 1µg/µl. Labelling was carried out according to the manufacturer's instruction. Briefly, 10µg of the digested protein was labelled for at least 1h with TMT10plex™ Isobaric Label Reagent Set (Pierce) at pH>6 and then quenched with 1M Tris, pH 7.4. The labelled samples were subsequently combined and desalted using a C18 Sep-Pak (Waters) cartridge, followed by vacuum drying. Samples were resuspended in 10mM Ammonia Formate pH 10.5, 5% ACN and separated using high pH reverse phase Zorbax 300 extend C-18 4.6mm x250mmcolumn (Agilent) and liquid chromatography ÄKTAmicro system (GE). Overall, 96 fractions were collected and combined into 20 fractions ensuring peptide diversity in each fraction. Samples were then vacuum dried and washed again with 60% ACN, 0.1% Formic Acid followed by another vacuum drying step. See 'LC-MS analysis' for subsequent steps.

2.10 LC-MS analysis

Twenty peptide fractions produced for each experimental sample-set were subjected to LC-MS analysis. Following injection, the separation of the peptides was conducted via reverse phase liquid chromatography (RP-LC) Dionex 3000 UHPLC system, equipped with a 50cm x 0.75mm Easy Spray column (Thermo Scientific) retaining a flow rate of 300nl min^{-1} for 70min gradient. The gradient was composed of mobile phase A (0.1% formic acid) and mobile phase B (99.9% acetonitrile, 0.1% formic acid), with pre-programmed mixing of mobile phase B to the following gradient/concentrations over time:1-55min (2-25%) 55-57min (25-50%), 57-58min (50-85%), 58-63min (85%), 63-70min (2%). MS analysis was performed using a Q Exactive instrumentation (Thermo Scientific) and the following acquisition parameters were applied: Data Dependent Acquisition (DDA) with MS scan of 70.000 and AGC target of 3e6; top12 MS/MS 35,000 and AGC target of 1e5; isolation window 1.2 m/z. Subsequently, the peak list was generated with the Proteome Discoverer 2.1 software (Thermo Scientific) and the spectra matching with the database was conducted with Mascot 2.6.1 (Matrix Science) using combined Sanger institute *P. falciparum* 3D7 Coding Sequences database (accessed October 2015) and Uniprot database for human proteins. The search parameters used were as follows: MS precursor mass tolerance 30ppm; MS/MS 0.06Da; 3 missed cleavages; static modifications: carboamidomethyl (C); variable modifications: oxidation (M), deamidated (NQ), acetyl N-terminal protein; forward/decoy searches were used for false discovery rate (FDR) estimation. Peptide and PSMs with high = FDR 1% and medium =FDR 5% levels were accepted.

2.11 Protein quantification and CETSA data processing

Only unique peptides were used for quantification of associated protein abundance, and only proteins quantified by at least three peptide spectrum matches

(PSMs) were trusted and kept for downstream analysis. The relative abundances of proteins under different compound concentrations were derived by dividing against the abundance value from the lowest compound concentration. Protein groups with quantification information were exported and fed into an in-house developed CETSA data processing R script ("mineCETSA") for data extraction, clean-up, normalisation, QC, curve fitting and plotting. Ligand-induced protein stabilisation curve typically follows standard sigmoidal curve *(143)*. Hence each protein stabilisation profile was evaluated for the dose-response curve best-fitting quality (expressed as R^2), the level of stabilisation relative to non-denaturing conditions at 37^{o}C calculated as the difference in Area Under the Curve (ΔAUC) and fold change in the protein level relative drug free condition. The criteria used for hit selection is characterised by $R^2 \geq 0.8$, ∆AUC surpassing three times the baseline Median Absolute Deviation (MAD*3) and 3-fold change (FC) ≥1.3 in the protein level under drug treatment relative to DMSO treated sample.

2.12 Western blotting

Western blots were performed with help of Dr. Yu Han. Western blots were prepared using the post-heating lysates generated from the corresponding lysate/intact-cell ITDR experiments as samples. Sample (10µg) for each treatment condition was run on NuPAGE 4-12% Bis-Tris Gel and transferred to nitrocellulose membrane using iBlot Dry Blotting system (Invitrogen). Primary anti-PfPNP mouse polyclonal antibodies *(153)* and secondary anti-mouse HRP-conjugated antibodies (Pierce) were diluted (1:5000) in 5% nonfat milk in TBST. Blots were visualised with Clarity Western ECL system (Biorad) with image analysis being performed in ImageQuant™ LAS 4000 (GE Healthcare).

2.13 PfPNP molecular cloning and expression

The initial clone of PfPNP *(154)* was a generous gift from Dr. Kami Kim. The following re-cloning and protein expression were done in collaboration with the Protein Production Facility at NTU SBS. The sequence encoding PfPNP was sub-cloned into pNIC-CH vector using ligand-independent cloning *(155)*. The constructs were heterogously expressed in the Rosetta BL21-DE3 *Escherichia coli* (Novagen). Bacterial culture was sustained in the Terrific Broth media with addition of kanamycin (50µg/ml) and Chloramphenicol (34µg/ml) at 37°C under agitation. When culture density OD_{600} reached ~2.0, protein expression was induced with isopropyl-β-D-1-thiogalactopyranoside (IPTG) (0.5mM) at 18°C O/N. Cells were pelleted by centrifugation (4,500*g* ,15min, 15°C) and re- suspended in lysis buffer (NaCl 500mM, HEPES 100mM, imidazole 10mM, TCEP 1mM and glycerol 10% (v/v) pH 8.0) supplemented with EDTA-free protease inhibitor cocktail (1µl/ml) (Calbiochem) and Benzonase (125U/ml) (Merck). Cell lysis was carried out by sonication at 70% amplitude, 3s on/off for 3min at 4°C. Following centrifugation (47,000*g,* 25min, 4°C) the supernatant was filtered (1.2µm) and stored at -80°C.

2.14 PfPNP Recombinant protein purification

Original *(154)* and in-house modified PfPNP constructs were purified using immobilised metal affinity chromatography (IMAC) followed by gel filtration chromatography on ÄKTAxpress system (GE Healthcare). Briefly, the cellular lysate supernatant was loaded on HisTrap™ HP column (GE Healthcare) pre-equilibrated with sample buffer. Following sample loading the column was washed with IMAC wash buffer 1 (NaCl 500mM, HEPES 20mM, imidazole 10mM, TCEP 1mM and glycerol 10% (v/v) pH7.5) and wash buffer 2 (NaCl 500mM, imidazole 25mM, HEPES 20mM, TCEP 1mM and glycerol 10% (v/v) pH7.5). Following elution with NaCl 500mM, imidazole 500mM, HEPES 20mM, TCEP 1mM and glycerol 10% (v/v) pH7.5, the protein was

loaded onto a HiLoad 16/60 Superdex-200 column (GE Healthcare) pre- equilibrated in KH_2PO_4 50mM, TCEP 0.5mM and glycerol 10% (v/v) pH7.4. Pure protein fractions were pooled and concentrated based on Nu-PAGE gel profile.

2.15 PfPNP Protein co-crystallisation

Co-crystal preparation was conducted by Dr Chen Dan. The PfPNP protein solution (37mg/ml) was incubated with 1mM MFQ or QN on ice for 15min prior to the co-crystallisation setup. Both compounds were co-crystallised with PfPNP using sitting drop vapour diffusion method, retaining 20°C temperature during the process. The PfPNP-MFQ co-crystals were grown in the presence of 2µl of drug-protein solution and 1µl of 0.2M magnesium formate buffer. The PfPNP-QN co-crystals were produced from 1µl of drug-protein solution and 2µl of 0.1M sodium citrate tribasic, 1.0M ammonium phosphate monobasic buffer pH5.6.

2.16 Wogonin Crystallisation

High purity fraction F13' obtained from chromatography fractionation of the *Scutellaria baicalensis* (HQ) DCM extract was dissolved in DCM with traces of chloroform in an NMR tube and allowed to crystalise at room temperature over the period of 1 week. Obtained crystals were subsequently analysed by X-ray diffraction to resolve compounds' structure.

2.17 X-ray diffraction data collection and structure determination

PfPNP co-crystal structures X-ray diffraction data were collected at Synchrotron (Australia) on the beamline MX1 and subsequently indexed and processed with XDS by Dr. Chen Dan *(156)*. Phaser was used for molecular replacement mediated structure solving *(157)* with PDB 1SQ6 as the selected search model. REFMAC5 was used for building the model refining the structure *(158)* with final manual improvements being added in Coot *(159)*. Structure was validated with the use of Ramachandran

plot *(160)*. Phenix.eLBOW was used to generate ligand structures *(161)*. Wogonin crystal structure X-ray diffraction data were collected on the Bruker X8 CCD Diffractometer in the X-ray crystallography facility in SPMS NTU by Dr. Rakesh Ganguly.

2.18 Differential Scanning Fluorimetry

ImmH, QN, MFQ, CQ, PMQ, LUM were serially diluted at 0-100μM gradient and added to mixture of recombinant PfPNP (in-house prepared construct) (0.2mg/mL) in PBS pH7.2, 5x SYPRO™ Orange Protein Gel Stain (Invitrogen) to the final volume 25μL and DMSO concentration 1% (v/v). Samples were sequentially heated for 10sec on a 96 well plate in IQ^{TM}5 Real Time PCR (Biorad) across 25-95°C temperature gradient with 1°C intervals, monitoring fluorescence emission with $\lambda_{excitation}$ = 492 nm and $\lambda_{emission}$ = 610nm after each heating step. Data analysis was performed using software package XLfit (ID Business Solutions) and non-linear regression fitting was done with GraphPad Prism, determining the Tm of PfPNP at each drug concentration.

2.19 Enzymatic activity inhibition Assays

Enzymatic activity assays *(162)* were conducted in triplicate in 200μL of assay mixture containing 50mM potassium phosphate pH7.5, 60mU/mL (i.e. 32.6nM) of Xanthine Oxidase (Sigma), 10-400μM Inosine (Sigma) and varying concentration of the inhibitor: QN 50-0μM or MFQ 250-0μM. Reaction was started by addition of 10ng of recombinant PfPNP (in-house prepared construct). Formation of Uric acid from coupled reaction was measured at λ_{293nm} using Tecan infinite m200 plate reader at 1min iterations over 3h at 30°C. Initial rate of reaction [Absorbance/time] was based on the linear part of the curve in each experimental variant. Non-linear regression fitting and data analysis was performed in GraphPad Prism.

2.20 Surface Plasmon Resonance

SPR experiments were performed in collaboration with the Biomolecular Interactions Platform at NTU SBS. Experiments were run on a Biacore T200 instrument (GE Healthcare) at 25 °C. Anti-histidine tag antibody modified CM5-S chip was prepared via EDC/NHS (0.1M, 7 min at 10μl/min) anti-histidine antibody (50ug/ml, 7min) in the immobilisation buffer (His Capture Kit; GE Healthcare). Recombinant His-PfPNP *(154)* was captured to approximately 1100RU, and the characterisation of compound interactions were conducted in in PBS (137mM NaCl, 2.7mM KCl, 8mM Na_2HPO_4, 2mMKH_2PO_4), 1mMDTT, 0.05% Tween-20 and 3% DMSO buffer. Ligands were injected in increasing concentration with for 30-120s at a flow rate of 30μl/min in either multi or single cycle mode, and dissociation was monitored for 50s (MFQ), 2000s (QN) and 4500s (ImmH). Between each cycle, the chip surface was regenerated by 15mM HCl for 30s. Data analysis was performed using Biacore evaluation software V3.0, where sensorgrams were double referenced (reference surface, blanks) prior to a global analysis using a simple 1:1 binding model kinetic or steady state model.

2.21 Isothermal Titration Calorimetry

ITC experiments were conducted by Dr. Chen Dan. Protein was buffer-exchanged to a buffer containing 50mM KH2PO4 at pH7.4. The protein was injected into the iTC200 (Microcal) cell with a titration syringe filled up with solution containing assayed compound diluted in the assay buffer, retaining constant buffer conditions and DMSO concentration between the two. Sample titrations were commenced with 0.5μl injection, followed by 16-20 larger injections of increasing volume, retaining 25°C temperature and 700rpm stirring speed throughout the experiment. The heat peaks integration and non-linear regression analysis were performed with the Origin software (Microcal) with binding-model fitting (QN- one site, MFQ- two sets of sites) to

determine the stoichiometry parameters: N, K_D and ΔH.

2.22 Cytotoxic drug complementarity assessment

Assays performed with assistance of Dr. Grennady Wirjanata. Drug assays were performed in 200µL volume in triplicate with *P. falciparum* 3D7 strain at 1% haematocrit and 1% parasitaemia in purine free media in a (96 well) microtiter plate format. Prior to beginning of the assay, parasites were washed 3 times with purine free media to remove residual hypoxanthine. The top concentration of compounds used in was 480nM ImmH, 20µM E64d, 3.2µM QN and 320nM MFQ followed by 2-fold serial dilution and a no-drug control. IC50 measurements were conducted for each drug alone and for combinations at fixed volumetric ratios [i.e. Drug A:Drug B ratio - 5:0, 4:1, 3:2, 2:3, 1:4, 0:5). Following 48h incubation, supernatant was removed, parasites were stained with 100µL of pre-warmed 8µM Hoechst 33342 in PBS pH7.2 for 20min and reaction was halted by addition of 200µL of ice-cold PBS. Results readout was performed with the LSR Fortessa X-20 Flow Cytometer (BD Biosciences) using UV laser (355nm) and results were analysed with FACS Diva Software (BD Biosciences). Linear regression analysis of dose-response curves and IC_{50} determination was subsequently performed in WWARN's In Vitro Analysis and Reporting Tool (IVART). ΣFIC_{50} were calculated using the following equation:

$$Sum\ FIC\ (\Sigma FIC) = \frac{IC50\ of\ A\ in\ mixture}{IC50\ of\ A\ alone} + \frac{IC50\ of\ B\ in\ mixture}{IC50\ of\ B\ alone}$$

2.23 Assessment of the antimalarial drug effect under differential purine-availability conditions

The drug assays were initiated on synchronised mid-ring stage parasites (10±4hpi) with final parasitaemia of 1%, hematocrit of 2% and total volume of 100µL on 96 well microtiter plates in technical duplicates. Prior to beginning of the assay, parasites were washed 3 times with purine free media to remove residual hypoxanthine. A serial dilution of QN, ImmH or MFQ was conducted with purine-free MCM or MCM supplemented with 10µM Hypoxanthine, 100µM Hypoxanthine, 10µM Inosine or 100µM Inosine. The top concentration used in was 500nM for all compounds, followed by 2-fold serial dilution and a no-drug control. Following 48h long incubation at 37°C the results readout was conducted as described in '*In vitro* antimalarial activity assessment of TCM extracts and fractions' section. Drug response curve plotting featuring all conditions was subsequently done in Sigma Plot.

2.24 TCM material selection and procurement

The antimalarial TCM candidate materials (Fig. 2.1) were selected based on their historical use in the Traditional Chinese Medicine for treatment of malaria-like symptoms, by the TCM students from the NTU TCM clinic during the course of previous projects *(163–165)*. The materials were then procured from the TCM Clinic (SBS, NTU, Singapore).

Figure 2.1 – Antimalarial Traditional Chinese Medicine candidates

2.25 Sequential Soxhlet extraction

TCM materials were pulverised into fine powder form with a blender or mortar in order to increase solvent accessible area and loaded into cellulose extraction timbles (Whatman). Sequential Soxhlet extraction *(166)* with three organic solvents in order of increasing polarity (Hexane, Dichloromethane and Methanol) for 48h each was used to isolate and pre-fractionate their phytochemical constituents. Following extraction each respective extract was dried on rotavap, then under vacuum for at least 10h and stored at 4°C.

2.26 Column Chromatography assisted fractionation of TCM extracts

Extracts/fractions of interest were separated by silica column chromatography with a step-wise gradient of increasing polarity, initially with Hexane (Hex) and Ethyl Acetate (EA) (from 100%/ 0% to 0%/100% of Hex/EA), followed by gradient of EA and Methanol (MeOH) up to 20%MeOH 80%EA. Eluting fractions were profiled using thin layer chromatography and pulled together based on the presence of common constituents.

2.27 Thin Layer Chromatography

TLC was performed using pre-coated silica gel 60 F_{254} plates 0.2mm thickness plates (Merck). Compound visualisation was performed under UV and through Cerium Molybdate and Potassium Permanganate staining.

2.28 NMR sample analysis

Vacuum dried TCM extract fractions were dissolved in deuterated chloroform and Nuclear Magnetic Resonance (NMR) spectra were obtained from Bruker Avance III 400Mhz UltraShield with auto-tunable BBFO probe (5mm). ^{1}H and ^{13}C NMR spectra analysis was performed with Bruker TopSpin software. Spectral assignment was assisted by COSY and (^{1}H - ^{13}C)-HSQC/HMBC experiments.

2.29 *In vitro* antimalarial activity assessment of TCM extracts and fractions

Drug assays were initiated on synchronised mid-ring stage parasites (10±4hpi) with final parasitaemia of 1%, hematocrit of 2% and total volume of 100µL on 96 well micro titer plates in technical duplicates. Each vacuum dried TCM extract/fraction/compound was initially dissolved in relevant volume of DMSO necessary completely solubilise it. Ten microliters of each soluble extract was then dissolved in 990µL of MCM and serially diluted with cMCM to obtain 11 consecutive twofold dilutions that were used in the assay. Each 96 well microtiter plate contained a series of controls in technical

duplicates including: non-infected control (pure RBCs), no drug control, death control (50nM artemisinin) and solvent control (DMSO 1%). Following 48h incubation at 37°C under hypoxic conditions media was removed and cells were incubated in the dark with 100µL of 8µM Hoechst H33342 (Sigma) in Phosphate Buffered Saline pH 7.4. Labelling was stopped after 20min with 200µL of ice-cold PBS. The level of dye incorporation was determined with the LSR II Flow Cytometer (BD Biosciences) using UV laser (355nm) and results were analysed with BD FACSDiva Software. Readings from technical duplicate data were averaged and analysed through non-linear regression using ICEstimator software *(167, 168)*. Based on plotted drug dose response curves, extract/fraction/compound concentrations required to inhibit 50%, 90% and 99% of parasite growth were determined and indicated as IC_{50}, IC_{90} and IC_{99}.

2.30 Small molecule GC-MS analysis

Mass spectrometry analysis of purified TCM fractions, as well as pure compounds was carried out using GC-MS ThermoScientific Finnigan LCQ Deca XP setup. Fractions/compounds solubilised in DCM were further diluted in Methanol prior to injection into MS. Sample (10µL) was injected into the system and separated with 50% Methanol, 50% H2O, 0.1% Formic Acid buffer prior to reaching the analyser. Data was collected for 2min per sample. Data analysis and visualisation was conducted in Xcalibur 2.2 SP1.48 (Thermo Scientific)

CHAPTER 3

Adaptation of the MS-CETSA protocol for *Plasmodium falciparum*

Poor understanding of the MoA of the vast majority of antimalarial drugs is likely a result of a combination of multiple challenges. Protozoan parasites possess unique biology which combines both animal- and plant-like features and thus remain much less well understood compared to other eukaryotic systems. Consequently, many research tools developed and used to elucidate drug's MoA in other pathogenic organisms have been applied to studying protozoa with limited success *(141)*. In this work we aimed to adapt MS-CETSA protocol for the *P. falciparum* research with its future application for the drug-target identification in mind. However, the malaria CETSA sample preparation method required for the subsequent MS-based analysis had to be re-developed, due to distinct differences between cancer cells, the method has been designed for, and *P. falciparum*.

High haemoglobin abundance, equivalent to ~98% of its cytosolic protein content of RBC, is an established challenge in the analysis of its proteome *(169, 170)*. Expectedly, the malaria research community experiences the same challenges and the proteomic analysis of *P. falciparum*-infected RBCs has rarely been performed *(171)*. Instead, the majority of proteomic studies of malaria parasites resort to saponin-mediated host-cell removal and release of free parasites prior to their lysis and MS analysis *(171, 172)*. Considering that this is the most established and reliable method for generating high-quality *P. falciparum* protein lysate sample, this approach was adopted for the malaria lysate CETSA protocol (Fig. 3.1).

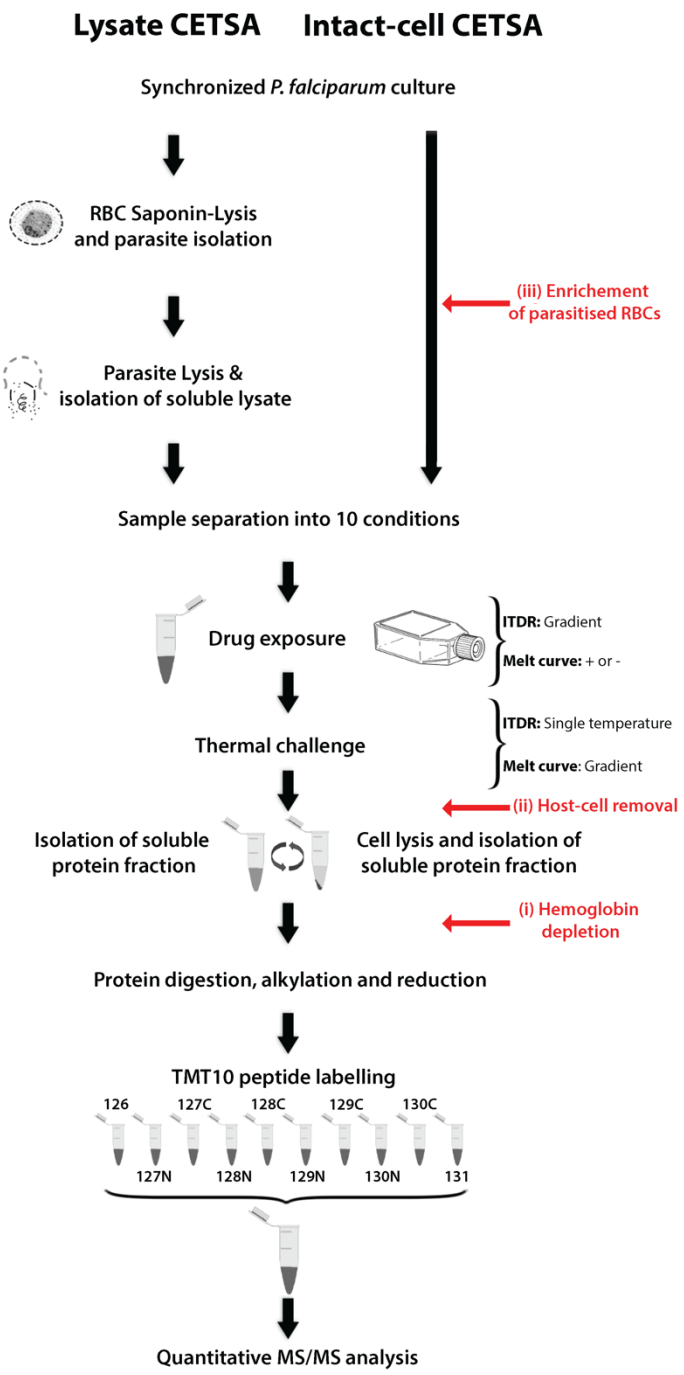

Figure 3.1 – MS-CETSA Method Overview

Lysate and Intact-cell CETSA experiments are conducted using soluble parasite protein lysate or infected Red Blood Cells (iRBCs), respectively. In both scenarios, the samples are separated into 10 identical fractions, subjected to drug treatment and exposed to the thermal challenge to denature and irrevocably precipitate unstable proteins. Two alternative CETSA variants: ITDR or melt curve can be performed. ITDR involves treating samples with a drug concentration gradient and exposing them to a single temperature, while melt curve CETSA relies on presence or absence of the drug in corresponding samples, which are then heated to 10 distinct temperatures along 37-73°C thermal gradient. Soluble protein is isolated by centrifugation and in case of whole-cell approach preceded by cell lysis and

samples are reduced, alkylated, digested by LysC and Trypsin and then labelled with distinct TMT10 isobaric tags. Peptide levels across ten fractions are then quantified through multiplexed mass spectrometry and following mapping to plasmodium proteome database are translated to protein levels along thermal/drug gradient.

Unlike the lysate CETSA, which monitors drug-protein binding taking place in a standardised but artificial environment *in vitro*, the intact-cell CETSA protocol relies on drug-protein interactions occurring within a much more complex environment: the living cell. Therefore, the intact-cell CETSA allows for possible prerequisites for the interaction to occur, including drug-metabolism following cell entry, the presence of co-factors, compound accumulation at a specific subcellular site or an appropriate local environment. In order to maintain the intact-cell CETSA experimental conditions most closely related to the physiologically normal state and to retain all of the above advantages; the drug treatment needs to be conducted directly on the living intraerythrocytic *P. falciparum* culture *in vitro*. Furthermore, the 'thermal challenge' should be performed directly after the drug exposure in order to 'freeze' the biochemical makeup of the cell in the presence of the drug, limiting its dissociation from the target. However, the cellular lysate isolated from standard *P. falciparum in vitro* culture consists of a mixture of parasite and host proteins and contains high haemoglobin levels.

Diverse approaches for overcoming the haemoglobin abundance in the proteomic analysis of RBCs and intraerythrocytic *P. falciparum* parasite stages have been proposed in the literature. Some solutions, such as extensive chromatographic peptide fractionation or FASP *(143, 147)* offered no advantages over the existing CETSA protocol employed previously for the analysis of mammalian cells *(147)*. Others are unsuitable for CETSA because they: are unable to provide high-quality quantitative data on the protein abundance (e.g. peptide libraries *(173)* or N-

terminomics *(174)*), induce substantial losses in certain protein subsets (e.g. haemoglobin depletion through metal affinity chromatography *(169)*), are not easily scalable to mid-to-high throughput applications (e.g. Extensive gel fractionation *(175)*), or involve use of detergents and/or high temperatures to assist cell lysis *(176)*, which risks to interfere with the principle CETSA is based on. Therefore, three main alternative approaches aimed at increasing *P. falciparum* proteome coverage were explored (Fig. 3.1): (i) haemoglobin depletion from cellular lysates (ii) host-cell removal after the thermal challenge step and (iii) the enrichment of parasitised RBCs prior to the drug treatment. The first variant was aimed at targeted haemoglobin removal, the second at global depletion of host-cell proteins, while the third only at decreasing the ratio of host-to-parasite proteins in the analysed sample.

3.1 Optimisation of the *P. falciparum* Intact-cell CETSA sample processing method

Initially, aiming to establish the reference gold-standard for the qualitative protein detection in malaria samples, we determined the depth of proteome coverage in the lysate melt curve CETSA experiment. Similarly, the baseline level of protein detection in the intact-cell preparation was established through the melt curve CETSA analysis of a standard 10% *P. falciparum*-infected RBC culture. The lysate CETSA analysis provided qualitative detection of 2324 parasite and 1217 human proteins, while the unmodified intact-cell CETSA analysis yielded only 390 parasite and 801 human proteins detected (Fig. 3.2A). The relative haemoglobin abundance in analysed samples was quantified as the percentage of Peptide Spectrum Matches (PSMs) corresponding to Haemoglobin subunits α-ζ out of total recorded PSMs. The haemoglobin level in the lysate and intact-cell samples was found to be substantially different, with 3% and 66% of the total analysed PSMs matching haemoglobin,

respectively (Fig. 3.2B). The significantly lower *P. falciparum* proteome coverage attained in the intact-cell analysis can be attributed to very high haemoglobin abundance and demonstrates the need for protocol improvement. In order to evaluate the suitability of the three main intact-cell CETSA protocol modification variants (i.e. haemoglobin removal, host-cell removal or enrichment of parasitised cells), each of them was independently incorporated into the CETSA workflow and used for sample generation. The level of qualitative protein detection and the relative haemoglobin abundance in each sample processing variant was contrasted with those of the 'gold standard' and the 'baseline' sample analyses (Fig. 3.2A-B). To begin with, the three resin-based haemoglobin depletion methods: Hemoglobind™, HemoVoid™ and NuGel™ *(177–179)* were evaluated. Soluble protein lysate derived from *P. falciparum*-infected RBCs (10% parasitaemia) was subjected 37°C thermal challenge, followed by haemoglobin depletion by each of the kits in triplicate assays, monitoring the extent of the protein depletion they accomplish and its reproducibility (Table 3.1).

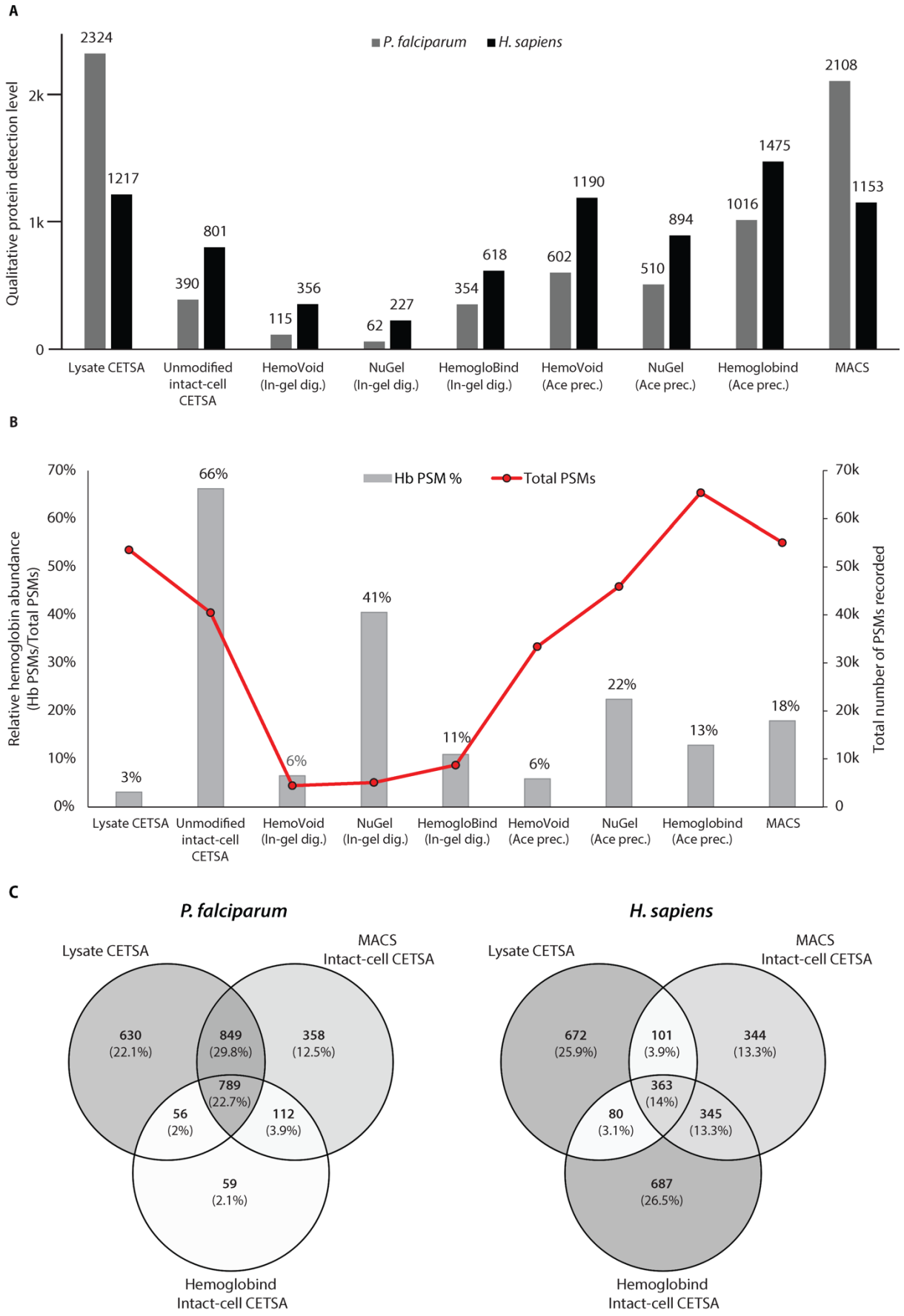

Figure 3.2 – Performance comparison of candidate Intact-cell CETSA method variants

Panel (**A)** represents the number of unique P. falciparum (grey) and human (black) proteins identified with evaluated variants of the intact-cell CETSA protocol (x-axis). The number of proteins represented

by each of the bar indicators is listed above. Panel (**B**) represents the total number of Peptide Spectrum Matches (PSMs) recorded for each of the evaluated protocol variants indicated as red line (right y axis). Additionally, the proportion of PSMs attributed to haemoglobin proteins out of all PSMs recorded in each of the datasets is presented as a bar chart, indicating the respective percentage values (left y axis). (**C**) Venn diagram comparison of the P. falciparum and human proteomes coverage by Lysate CETSA and the two most reliable Intact-cell CETSA protocol variants: Hemoglobind (Ace. Precipitation) and MACS. The overlap in the qualitative protein detection between each technique is indicated for each variant.

	Starting material	**Protein input**	**Post-depletion yield**	**Reproducibility**	**Depletion level**
Hemoglobind	200 x 10^6 cells	2.92mg	250ug	±0.01mg/mL	91.5%
NuGel	150 x 10^6 cells	2.24mg	150ug	±0.04mg/mL	93.3%
HemoVoid	200 x 10^6 cells	2.92mg	135ug	±0.01mg/mL	95.4%

Table 3.1 – Performance evaluation of haemoglobin-depletion kits

All three kits depleted over 90% of the original protein content, although small differences were present, with 4.6%, 6.7% and 8.5% of the initial protein load being recovered with HemoVoid, NuGel and Hemoglobind, respectively. Hemoglobind and HemoVoid have proven more reproducible than NuGel, with comparably low variability (i.e. 0.01mg/mL) in the protein concentration of post-depletion elution. NuGel on the other hand exhibited four times higher fluctuations in the resulting protein concentration. The polymers derived from the haemoglobin-binding resin and potentially present in analysed samples risked causing technical issues with the MS performance. Therefore, two diverse sample clean-up strategies: the in-gel protein digestion or the acetone protein precipitation *(180)* were employed to remove the polymers from haemoglobin depleted samples prior to the MS analysis. The striking

difference in the total number of PSMs recorded between the two clean-up protocol variants for each of the three sample types, suggests that the extent of peptide recovery from the in-gel digestion was limited (Fig. 3.2B). Consequently, the acetone precipitation was deemed better suited for CETSA analysis. Among the three haemodepletion protocols, Hemoglobind has provided the highest coverage of both the *P. falciparum* and the human proteomes with 1016 and 1475 detected proteins, respectively (Fig. 3.2A). The remaining two kits offered 40-50% lower levels of parasite protein identification, with a smaller decrease of 20-40% in the human proteome coverage. The HemoVoid kit provided most extensive haemoglobin depletion, as only 6% of total analysed PSMs mapped to haemoglobin, relative to 66% attained with the unmodified protocol (Fig. 3.2B). The Hemoglobind samples contained 11-13% haemoglobin-specific peptides, indicating satisfactory depletion level, whilst NuGel performed the worst retaining substantial haemoglobin levels in depleted samples.

The second intact-cell CETSA protocol modification variant (i.e. host-cell removal after the thermal gradient *(172)*) was deemed unsuitable because large quantities of precipitated protein derived from the host-cell were observed in the higher range of the thermal gradient (i.e. 63°C onwards). As a result, the parasite pellet could not be easily separated from the precipitated protein, what introduced the undesired variability between samples and affected accurate protein quantitation. The third remaining method variant: enrichment of infected-cells was performed via two established protocols: Percoll gradient *(151)* and MACS *(181)*, attempting to enrich and concentrated parasitised RBCs from a standard of 10% parasitaemia. The enrichment achieved with MACS was superior to Percoll gradient, reaching an average of 89% (±8 SD) and 64% (±13 SD) parasitaemia in triplicate assays, respectively. MACS has also proven to be more versatile, allowing purification of younger trophozoite stages (i.e ≥26hpi) as well as the schizont stages, while Percoll

gradient was limited to schizont stage only. Furthermore, MACS protocol was much more readily scalable, allowing large (i.e. up to 6mL of packed RBC) sample processing volume in a single preparation. Consequently, MACS sample preparation was deemed superior and MACS-enriched Intact-cell melt curve CETSA sample was subjected to MS analysis. Resulting sample allowed qualitative detection of 2108 parasite and 1153 human proteins.

Among all tested intact-cell sample preparation methods MACS and Hemoglobind followed by Acetone precipitation provided the highest quality samples and substantially improved the depth of the *P. falciparum* proteome analysis. The relative haemoglobin abundance was higher in the MACS-derived sample, which exhibited three times higher ratio of haemoglobin-specific PSMs than encountered in the lysate CETSA analysis (Fig. 3.2B). The Hemoglobind depleted sample exhibited two times higher ratio of haemoglobin PSMs than the lysate analysis. However, despite lower haemoglobin levels, Hemoglobind sample preparation favours identification of human over plasmodial proteins in a 3:2 ratio, likely due to relatively low parasite per cell density (i.e. 10%) in the original sample. As a consequence, MACS preparation provided 90% of the *P. falciparum* proteome coverage observed in the gold standard analysis, whilst Hemoglobind achieved only 44% of the proteome coverage seen in the Lysate CETSA. Hemoglobind protocol has proven superior only in the depth of the host-cell proteome analysis with nearly 700 unique RBC protein species identified (Fig. 3.2C). The core detectable parasite proteome identified by both MACS and Lysate CETSA analyses consisted of ~1600 proteins, but both sample sets show additional an 12.5% and 22.1% of uniquely detected proteins, respectively. Overall, the magnetic enrichment of *P. falciparum* infected RBC (i.e. MACS) was deemed sufficient and most practical for the generation of intact-cell CETSA data. The analysis of GO-localisation annotations of proteins detected across MACS intact-cell and Lysate CETSA datasets indicates comparable coverage of all major sub-cellular

components with an enrichment of the cytosolic fraction in both sample sets (Fig. S3.1B). This suggests that all cells have been appropriately lysed and no coverage bias is present between experimental variants despite differences in the analysis depth.

3.2 Characterisation of *P. falciparum* proteome melting dynamics in lysate and intact-cell setting

Proteome-wide survey of protein thermostability and unfolding patterns represents a novel tool for systematic comparative phenotypical characterisation of parasite biology. Here, we determined the global protein melting curve reference dataset for the *P. falciparum* 3D7 strain trophozoite stage. The data can be further exploited to provide insights into protein properties in drug-engagement, metabolic and *in vitro* protein studies, as well as to broaden our understanding of the parasite physiology. In order to assess the melting behaviour of the *P. falciparum* proteome in the lysate and intact-cell variants, we subjected DMSO-treated samples to CETSA melt curve analysis, monitoring protein denaturation levels along the 37-73°C temperature gradient. The melting curves obtained for independent proteins were used to generate the global proteome melting profile for both (i.e. lysate and intact-cell) variants (Fig. 3.3A) and to calculate the distribution of individual protein melting temperatures (Tm) equivalent to 50% protein denaturation, within each dataset (Fig. 3.3B). Overall, the melting curves were defined for 2488 proteins in the lysate and 1962 in the intact-cell variant. The proteins isolated from the lysate experiment exhibited apparent higher global thermo-stability (Fig. 3.3A) with 44% of them displaying <50% denaturation at the highest temperature tested. In contrast, only 6% of proteins in the intact-cell setting showed less than 50% decrease in abundance in the soluble fraction following thermal challenge. The “non-melting” proteins could

represent soluble protein-aggregates, an effect that could have been enhanced by the use of detergent for host-cell removal prior to sample generation. Consequently, for further analysis, we applied stringent filtering criteria including a ≥50% cut-off for the loss in protein abundance at the highest temperature and the Tm residing within the temperature range tested. As a result, Tms were determined for 1335 and 1439 proteins in lysate and intact-cell conditions, respectively (Fig. 3.3B). The functional enrichment analysis of both datasets demonstrates substantial overlap in the protein classes/categories in high abundance, with cytoplasmic/cytosolic proteins representing the most significantly enriched categories in both experimental variants (Fig. 3.3C). Contrastingly, the “non-melting” lysate CETSA protein subset, excluded from the Tm analysis, displays distinctly diverse constituents’ profile being significantly enriched in protein classes interacting with nucleic acid (Fig. 3.3C).

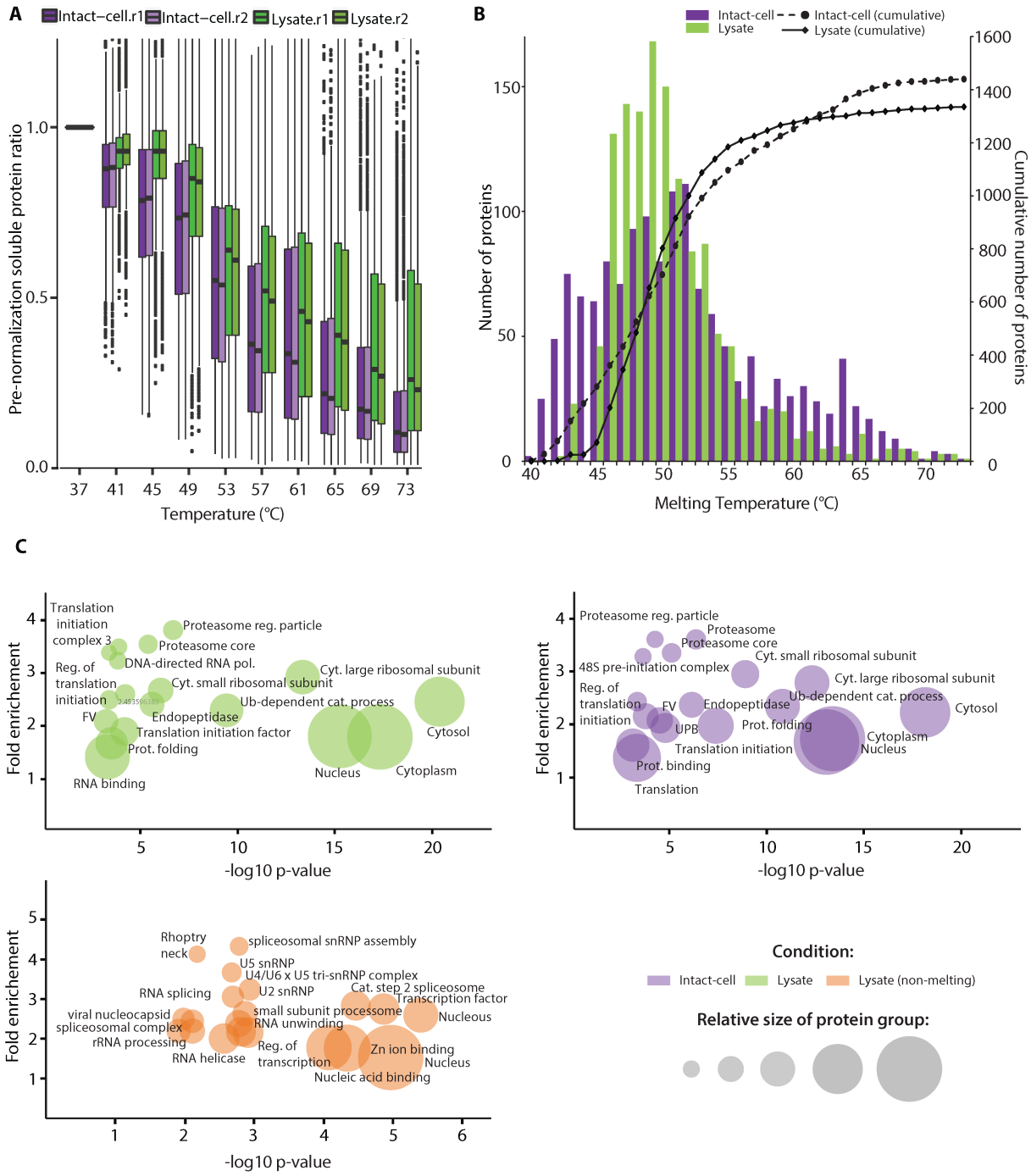

Figure 3.3 – Global *P. falciparum* proteome melting behaviour in lysate and intact-cell conditions

(A) Global protein melting behaviour in Lysate (green) and intact-cell (purple) melt curve CETSA in the absence of drugs. The box plot is drawn based on independent protein melting profiles within each dataset with remaining soluble protein relative to 37°C on y axis and Thermal challenge temperature gradient on x axis. Median (second quartile) protein levels are indicated with a black band, first and third quartiles with coloured boxes, while the lowest/highest datum within 1.5*IQR (interquartile range) of the lower/higher quartile is represented with whiskers. Data outliers not included within whiskers are plotted as dots. **(B)** Proteome-wide melting temperature (Tm) distribution in lysate (green) and intact-

cell (purple) experimental setting. Only proteins achieving >50% denaturation within the thermal gradient, detected at >3 PSM and with <5ºC Tm Standard Deviation between replicates were included in the analysis. The number of proteins (left y axis) exhibiting Tm at a given temperature (x axis) is plotted as a bar chart, while their cumulative number including proteins with lower Tm is indicated on the right y axis. (**C**) Functional enrichment analysis of proteins representing high quality melting profiles in lysate CETSA (green) and intact-cell CETSA (purple), as well as the non-melting protein subset removed from lysate CETSA analysis (orange). Each graph represents 20 most significantly enriched protein classes within each dataset, as indicated by the Gene Ontology (GO) annotations (see tables S3.1 - S3.3 for details). Fold enrichment of each protein class is plotted against the statistical significance. Circle size represents the relative size (i.e. protein count) of each protein class. Functional enrichment was performed using DAVID (https://david.ncifcrf.gov/).

The protein thermal unfolding assessment has proven highly reproducible between replicates in both experimental conditions (R^2=0.96), indicating the high accuracy of acquired data (Fig. 3.4A). When the Tm of 946 *P. falciparum* proteins present in both data sets is compared, slightly lower average stability of proteins in intact-cell setting can be observed (ΔTm = 0.3°C), but a very distinct melting profile becomes apparent for individual proteins (R^2=0.34) between the two conditions (Fig. 3.4A). Some proteins exhibit identical thermo-stability profile in both experimental variants [e.g. elongation factor 2 (PfEF2, PF3D7_1451100) and Pantothenate kinase (PF3D7_1437400)], while others tend to be more thermostable in the intact-cell setting [e.g. Purine nucleoside phosphorylase (PNP, PF3D7_0513300) and Glyceraldehyde−3−phosphate dehydrogenase (GADHP, PF3D7_1462800)] or the lysate setting [e.g. Karyopherin beta (KASbeta, PF3D7_0524000) and Protein disulfide isomerase (PDI8, PF3D7_0827900)] (Fig. 3.4B**)**. Notably, subunits of large multimeric molecular complexes tend to exhibit homogenous melting curves regardless of experimental variant, as demonstrated for the 40s and 60s Ribosome, the T-complex and Proteasome (Fig. 3.4C). Such correlated precipitation of many large protein complexes in CETSA data was recently described for the human proteins

in the K562 cells and the thermal proximity co-aggregation concept was introduced for this phenomenon *(152)*.

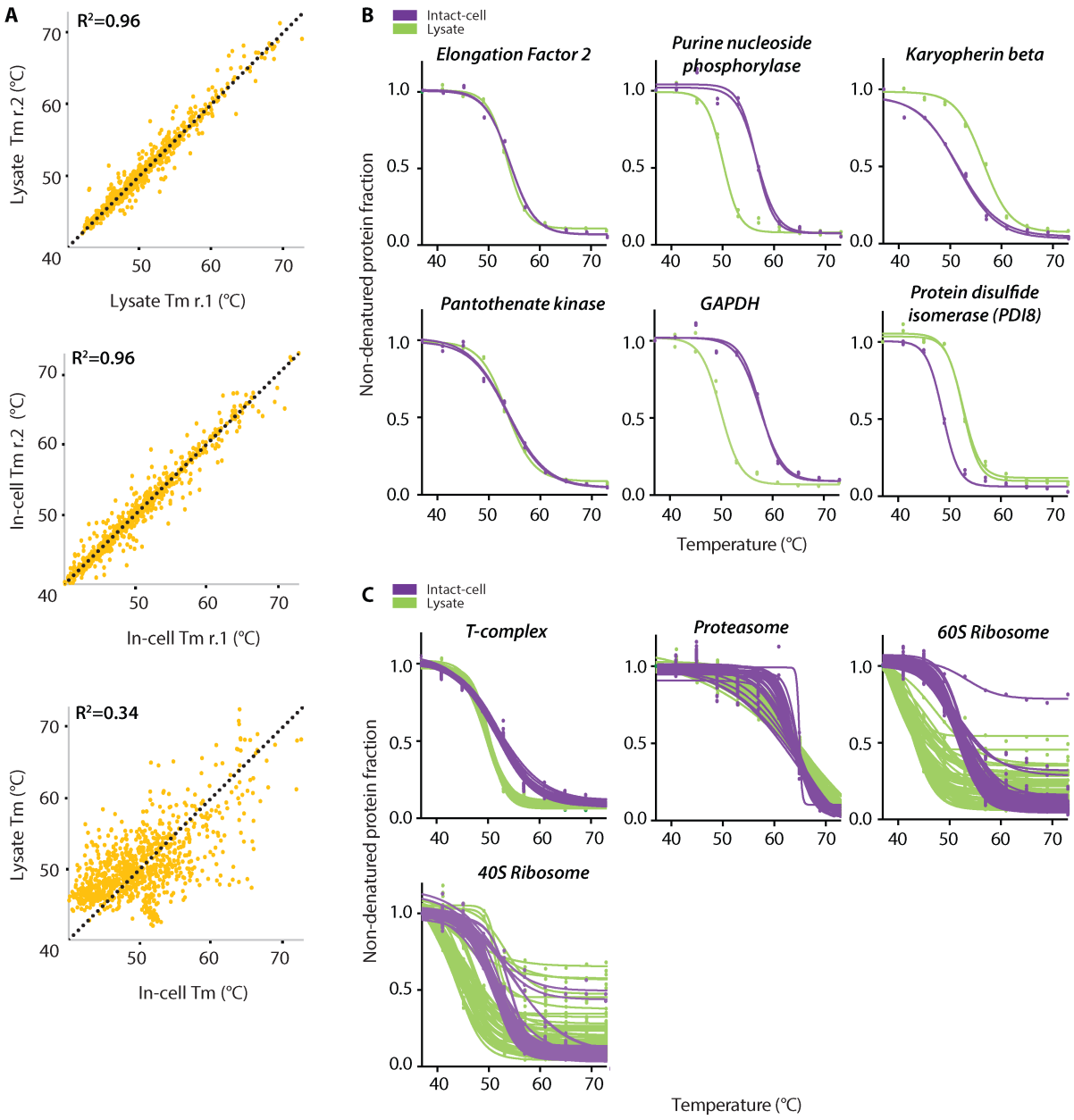

Figure 3.4 – Individual differences in protein melting between lysate and intact-cell conditions

(**A**) Tm comparison of 964 proteins identified in lysate and intact cell melt curve. The R^2 for two replicate measurements in each experimental variant is 0.96, while the R^2 in between the two conditions is only 0.34. Dashed black reference trend-line indicates perfect overlap of values in two conditions. (**B**) Exemplary melting curve profiles demonstrating unfolding profile of selected protein candidates in lysate (green) and intact-cell (purple) CETSA variants. The abundance of the soluble protein after the thermal challenge relative to the 37°C condition (y-axis) is plotted for all tested temperatures across the thermal

gradient (x-axis). (**C**) Unfolding behaviour of large molecular complexes. All detected subunits of the four complexes listed were plotted on each of the respective overlay melt curve plots.

3.3 Cell-wide analysis of protein thermal stability in *P. falciparum*, human K562 and RBC proteomes

In order to gain further insights into the dynamics of the parasite proteome, the global protein unfolding patterns in its proteome were contrasted with those of the proteomes of co-isolated host RBC and the reference K562 cell type (Table 3.2). Considering that this constitutes the first CETSA dataset on the erythrocyte proteome, the behaviour of human proteins across different cell types was also assessed. Both human cell lysate analyses contain significantly higher proportion of proteins that failed to meet the cut-off criteria for melting curve analysis (i.e. achieving >50% denaturation within the thermal gradient, detected at >3 PSM, with <5ºC Tm Standard Deviation between replicates and Tm<73ºC), than the corresponding Intact-cell CETSA experiments. However, unlike the *P. falciparum* dataset, the global 'non-melting' phenomenon was not observed in the RBC or K562 lysate experiments. The majority of filtered-out proteins in the RBC analysis failed to meet the PSM cut-off criteria, consistent with them being carry-over host-cell remnants derived from the RBC ghosts. Altogether, suggesting that the lysate experimental variant could be more prone to negatively affect the stability of some protein subsets, which is likely a direct result of its standardised *in vitro* environment.

Cell type	Variant	Identified in both replicates	Melting curve data	Average Tm (°C)	Median Tm (°C)
P. falciparum	Lysate	2488	1335	50.38	49.48
	Intact-cell	1962	1439	51.54	50.56
RBC	Lysate	2185	771	53.78	52.99
	Intact-cell	733	362	55.05	54.5
K562	Lysate	4419	2764	51.83	51.87
	Intact-cell	5449	4473	51.46	51.34

Table 3.2 – Protein thermal unfolding patterns across different cell types and conditions

Unexpectedly, upon a comparison of the average Tm of the six datasets the RBC proteome was found to exhibit the highest general thermal stability, while the *P. falciparum* proteome appears the least thermostable. The average Tm difference between the two proteomes is 3.4°C and 3.5°C in the lysate and intact-cell experimental variant, respectively (Table 3.2). Moreover, the broader general distribution of Tms in the intact-cell condition relative to the lysate, previously observed for the *P. falciparum* proteome (Fig. 3.3B), is not present in the proteome of either of the two human cell types (Fig. 3.5.A-B). Both, RBC and the K562 cells exhibit similar Tm distribution in both conditions. When the two human proteomes are compared, the higher global thermal stability of the RBC proteins is also apparent, although the average Tm difference is less striking with only 2°C in lysate and 3.5°C in the intact-cell setting. The comparison of the Tm distribution in the RBC and K562 proteomes suggests that both proteomes have a similar general melting profile, except for the population of highly thermostable proteins observed in the RBC setting (Fig. 3.5A-B). Consistently, the high correlation of Tm values between the replicate experiments in

the intact-cell CETSA (R^2=0.94) and lysate CETSA (R^2=0.87) experiments for both: the RBC and the K562 cells, suggests satisfactory experimental reproducibility, albeit somewhat lower in the lysate setting (Fig. 3.5C). The analysis confirms previously observed differences in the melting properties of individual proteins between lysate and intact-cell conditions in RBC (R^2=0.43) and the K562 cells (R^2=0.45). Interestingly, a similar degree of variability was observed in between the two human cell types for 268 proteins in the intact-cell setting (R^2=0.44), with proteins in erythrocyte displaying on average 1.7ºC higher Tm (Fig. 3.5D). The dissimilarity of the unfolding behaviour between RBC and K562 proteins was even greater in the lysate setting, based on the Tm of 153 common proteins (R^2=0.29). The measurement of CETSA data for the erythrocyte proteome can be in principle further explored to assess the interactions and downstream effects of the antimalarial drug exposure on host proteins. Overall, human proteins derived from infected RBC appear to possess different unfolding profile than their counterparts in the K562 cells. Similarly, the *P. falciparum* proteome appears to exhibit very distinct unfolding patterns to both human cell types analysed. Although, the relevance of these findings remains undetermined.

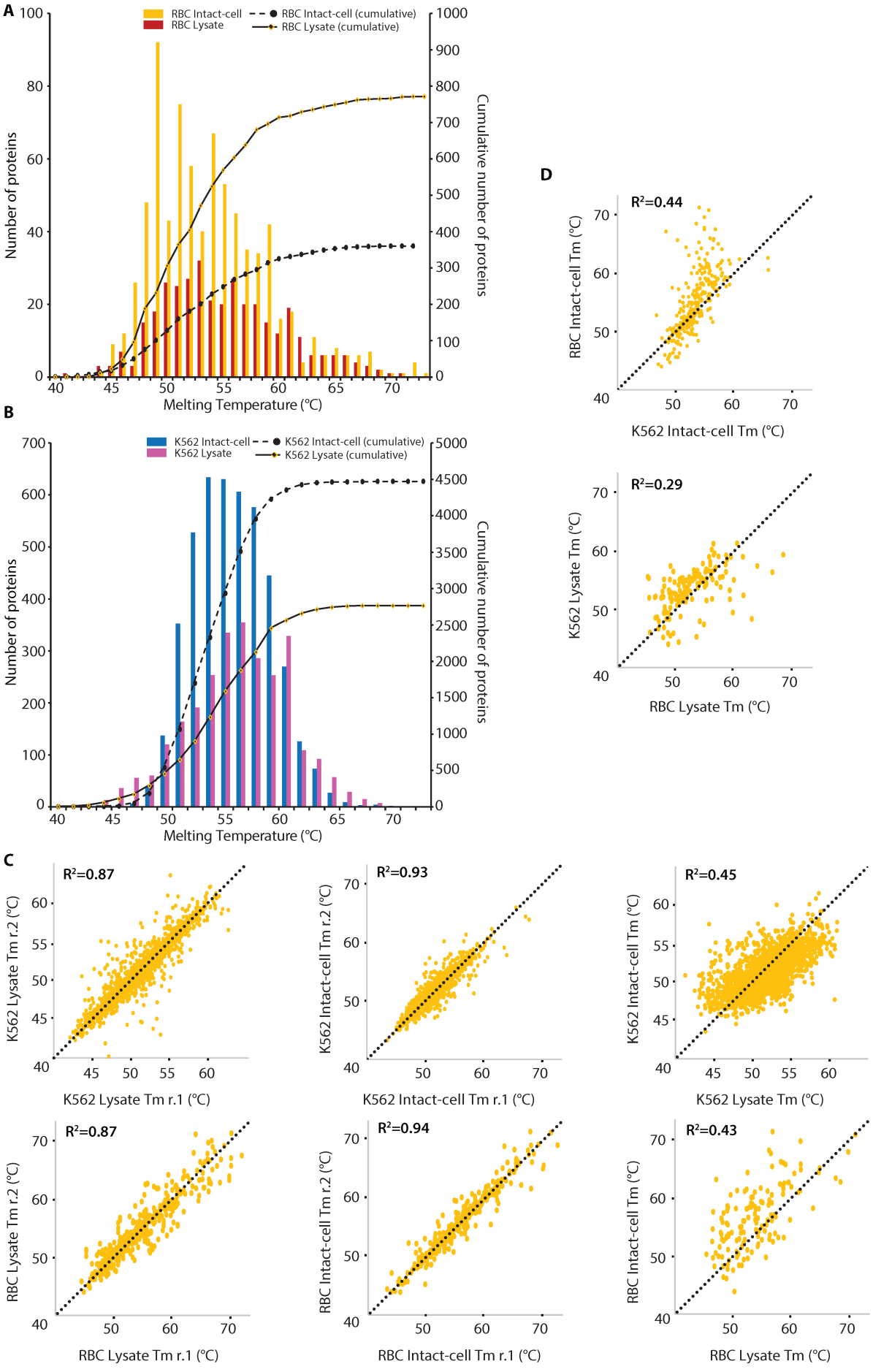

Figure 3.5 – Protein melting behaviour in proteomes of RBC and K562 cells

Proteome-wide melting temperature (Tm) distribution in melt curve CETSA lysate of the RBC (**A**) and K562 cells (**B**). The Tm distribution between lysate and intact-cell CETSA preparations is contrasted for each cell type. Only proteins achieving >50% denaturation within the thermal gradient, detected at >3 PSM and with <5ºC Tm Standard Deviation between replicates were included in the analysis. Number of proteins (left y axis) exhibiting Tm at a given temperature (x axis) is plotted as bar chart, while their cumulative number including proteins with lower Tm is indicated on the right y axis. (**C-D**) Human protein melting temperature (Tm) comparison between independent CETSA replicates or experimental conditions (i.e. lysate / intact-cell) and/or cell types (RBC/K562). Each of the yellow spots reflects an independent protein with two Tm measurement (x/y axis). The Tm assignment fidelity between the two conditions is represented as R^2 value. Black reference dashed line indicates perfect overlap of values between the two conditions (i.e. $R^2 = 1$).

3.4 The proof-of-concept studies of the MS-CETSA application for the identification of antimalarial drug targets.

The melt curve CETSA is a useful tool for studying proteome thermodynamics. However, the ITDR CETSA variant is more practical for accurate identification of drug-protein engagement. Therefore, for the identification of drug-target interactions in the *P. falciparum* proteome we leveraged the information gained from the melt curve CETSA experiments presented above, but primarily relied on the ITDR approach for hit selection. Target protein engagement in ITDR is recognised as gradual protein stabilisation in response to increasing drug concentration under thermal challenge at a single temperature and relative to the non-denaturing conditions (i.e. 37°C) and the no-drug control (see Fig. 3.1 and materials and methods). Ligand-induced protein stabilisation curve typically follows a sigmoidal curve *(143)*. Hence each protein stabilisation profile is evaluated for the dose-response curve best-fitting quality (expressed as R^2), the level of stabilisation relative to non-denaturing conditions at 37ºC calculated as the difference in Area Under the Curve (ΔAUC) and the fold change in the protein level relative drug-free condition. The

criteria used for hit selection is characterised by $R^2 \geq 0.8$, ΔAUC surpassing three times the baseline Median Absolute Deviation (MAD*3) and the fold change ≥1.3 in the protein level in the sample under drug treatment relative to DMSO treated sample (Fig. 3.6).

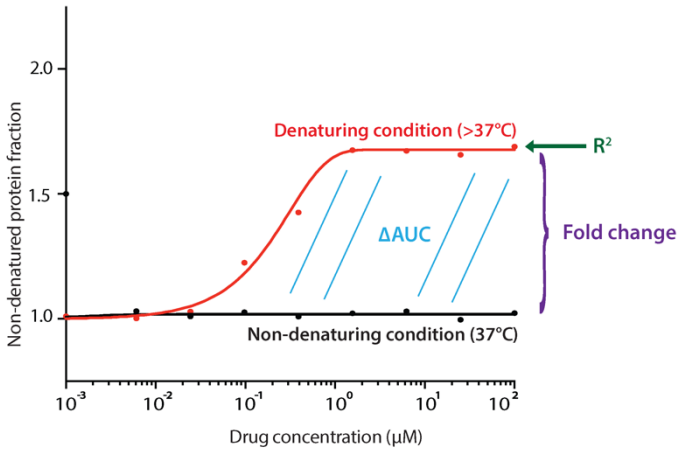

Figure 3.6 – The cut-off criteria for detection of significant protein stabilisation in ITDR

Plotted representation of an ITDR result demonstrating drug dose-dependent protein stabilisation under denaturing conditions (plotted in red). The non-denatured protein level remaining in the soluble fraction following the thermal challenge (y axis) is plotted relative to vesicle control sample (not shown) along an increasing drug concentration gradient (x axis). The three principal criteria determining the extent and significance of protein stabilisation is fold change of protein level between drug treated and vesicle control samples (in purple), the R^2 indicating the goodness of fit of expected dose-response stabilisation plot (in green), as well as the change in the Area Under the Curve (ΔAUC) (blue) of the protein stabilisation curve under denaturing conditions (red) relative non-denaturing control (black).

3.4.1 Pyrimethamine

We first carried out an ITDR experiment in lysate for pyrimethamine (PM), the well-characterised antimalarial drug known to inhibit *P. falciparum* dihydrofolate reductase-thymidylate synthase (PfDHFR-TS) *(33, 92)*. Due to the high melting temperature observed for PfDHFR-TS in the melt curve CETSA (Fig. S3.2A), the ITDR experiments were carried out at 59°C and 65°C. Among 2102 distinct proteins

detected only PfDHFR-TS (PF3D7_0417200) exhibited a significant dose-dependent stabilisation (Fig. 3.7A). Protein response was observed at both temperatures, although the stabilisation surpassed the significance threshold for hit selection only at 65°C (Fig. 3.7B). The Minimal Dose threshold (MDT) (i.e. the lowest drug concentration inducing significant protein stabilisation in ITDR assays) for DHFR-TS was ~14.7nM. This corresponds to the activity concentration range of PM previously reported for *P. falciparum in vitro* growth inhibition assays *(182, 183)* and *in vitro* kinetic studies with a purified enzyme *(184)*. As an additional validation, we conducted melt curve CETSA experiments in the presence and absence of the drug, demonstrating PM-dependent stabilisation of PfDHFR-TS (Fig. S3.2B). Stabilisation observed only at the high-temperature range of the melting curve likely reflects the dual-domain nature of this protein and corresponds to the temperatures where the DHFR domain unfolds. In the initial ITDR and melt curve experiments of PM in intact-cells, no stabilisation was observed for PfDHFR-TS (Fig. S3.2C-D). However, a small negative DHFR-TS shift was seen, which could be explained by the drug introducing a reorganisation of this two-domain protein, or alternatively, reflect the out-competition of another relatively high-affinity ligand such as folate.

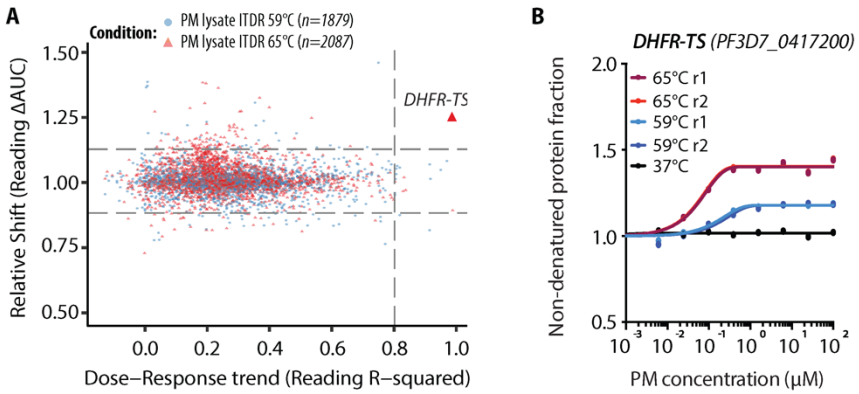

Figure 3.7 – Protein engagement by pyrimethamine in lysate ITDR

(A) Whole proteome analysis in Lysate ITDR experiments under 100-0μM pyrimethamine treatment with thermal challenges at 59°C (blue dots) or 65°C (red triangles). Distribution of protein stabilisation is plotted as function of R squared value (which quantifies the adherence of protein stabilisation profile to the dose-response trend) against ΔAUC (AUC of heat-challenged sample normalised against non-denaturing 37°C control). Three times the Median Absolute Deviation of AUC in each dataset (i.e. MAD*3) and R squared=0.8 cut-offs are indicated on the graph. Significantly stabilised protein - PfDHFR is highlighted in red. (**B)** Stabilisation curves of proteins identified in panel A. The extent of stabilisation under thermal denaturation conditions: 59°C (blue) or 65°C (red) is plotted relative to the no-drug control. Non-denaturing 37°C control condition is plotted in black.

3.4.2 E64d

As opposed to the PM-PfDHFR-TS interaction, for most drug-target identification experiments, the targets are unknown and hence no *a priori* knowledge exists about their Tm distribution. Therefore, the temperatures for the ITDR analysis should be selected such that the global proteome is sufficiently sampled. To that end, two temperatures were selected for ITDRs: 51°C, corresponding to average Tm for the *P. falciparum* proteome and an additional temperature, 57°C to account for the more thermostable portion of the proteome observed in intact-cell samples (Fig. 3.3B). To validate this drug-target identification strategy in the intact-cell CETSA, we investigated protein target engagement by the cysteine protease inhibitor E64d in two

ITDR experiments with the thermal challenge set to 51°C and 57°C, respectively. E64d is a broad-spectrum inhibitor known to interact with several targets in the *P. falciparum* proteome *(185–187)*. Accordingly, following the exposure of intact *P. falciparum*-infected RBCs to the drug, four proteins showed significant dose-dependent stabilisation in ITDR (57°C) experiment (Fig.3.8A-B). Three of the stabilised proteins: Falcipain 2A (FP2A, PF3D7_1115700), Falcipain 3 (FP3, PF3D7_1115400) and Dipeptidyl Aminopeptidase 1 (DPAP1, PF3D7_1113400) carry a cysteine protease domain that is expected to be the primary target of E64d. In contrast, the last identified protein DSK2 protein homologue (PF3D7_1113400) does not carry a signature cysteine protease activity site in its primary amino acid sequence. Interestingly, the MDTs observed for detected stabilisations were all within low nanomolar range (i.e. FP3 ~3nM; FP2A ~11nM, DSK2 ~9nM, DPAP1 ~11nM), which is significantly lower than the micromolar concentrations at which the compound inhibits parasite's growth *in vitro (188).* Taken together these results demonstrate that CETSA has the capacity to detect direct drug-target binding in the proteome of malaria parasites with a high degree of specificity.

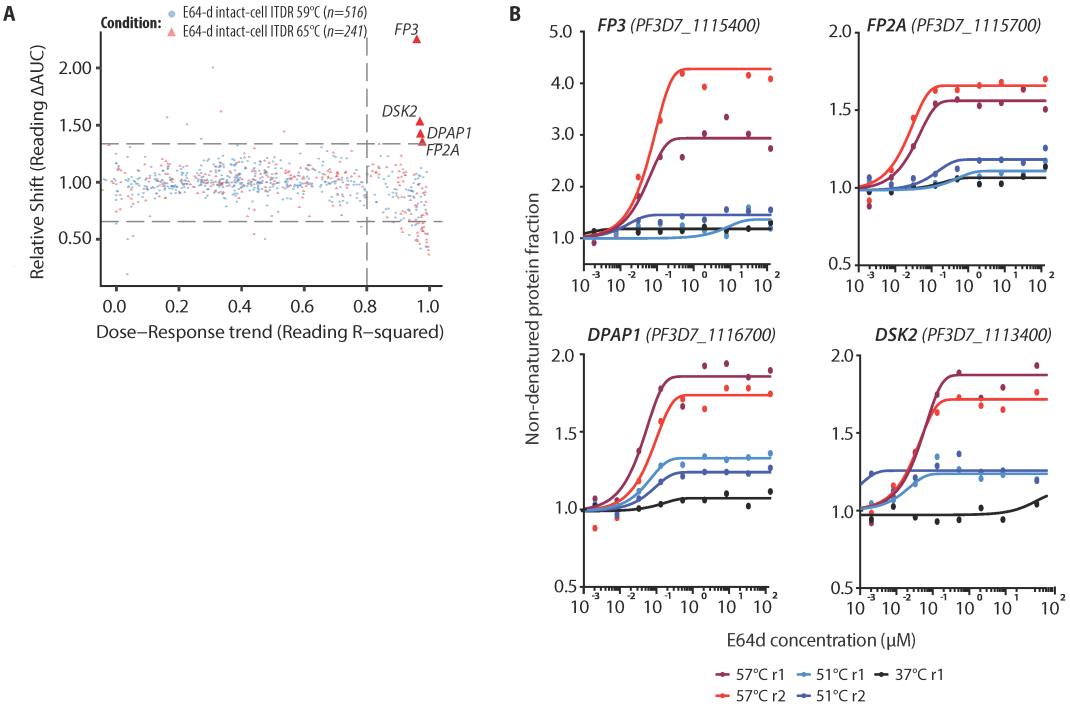

Figure 3.8 – Protein engagement by E64d in intact-cell ITDR

(A) Whole proteome analysis in Intact-cell ITDR experiments under 125-0μM E64d treatment with thermal challenges at 51°C (blue dots) or 57°C (red triangles) experiments under 100-0μM pyrimethamine treatment with thermal challenges at 59°C (blue dots) or 65°C (red triangles). Distribution of protein stabilisation is plotted as function of R squared value (which quantifies the adherence of protein stabilisation profile to the dose-response trend) against ΔAUC (AUC of heat-challenged sample normalised against non-denaturing 37°C control). Three times Median Absolute Deviation of AUC in each dataset (i.e. MAD*3) and R squared=0.8 cut-offs are indicated on the graph. Significantly stabilised proteins are highlighted. (**B)** Stabilisation curves of proteins identified in panel A. The extent of stabilisation under thermal denaturation conditions: 51°C (blue) and 57°C (red) for E64d is plotted relative to the no-drug control. Non-denaturing 37°C control condition is plotted in black.

3.5 Discussion

Omics technologies remain been the primary tools used for the untargeted comparative characterisation of malaria parasites. They have been successfully employed to characterise the differences in parasites' drug-response, mechanisms of resistance, pathogenicity and disease outcome *(49, 138, 189–195)*. The differential gene and protein expression profiling have provided invaluable insights into specific pathways and signalling cascades associated with drug resistance phenotypes and drug's MoA *(49, 54, 99)*. However, due to the indirect association between transcript/protein levels and given biological phenomenon the relevance of specific differentially expressed genes/proteins for the phenotype is often poorly understood and questioned *(196, 197)*. At the same time, the expression levels of proteins functionally relevant to studied phenotypes, might remain constant across the entire population. Other changes to parasite's proteins, such as mutations, post-translational modifications, their mis-localisation or misfolding could be more relevant for observed cellular phenotypes than their expression levels. Many of the above would affect protein's stability, which can be accurately quantified through MS-CETSA-mediated unfolding behaviour profiling *(143, 198–200)*. A functional MS-CETSA protocol for *P. falciparum* offers a chance to investigate these diverse parasite phenotypes from a novel and previously largely unexplored perspective. Our method provides a satisfactory level of *P. falciparum* proteome coverage, equal or surpassing previously achieved levels *(171)*, with an additional benefit of monitoring the unfolding behaviour of host proteins concomitantly present in analysed samples. We demonstrated that both adaptations of the CETSA protocol: melt curve and ITDR are highly functional with malaria samples, both in the lysate and in the intact-cell experimental variants.

3.5.1 Thermal proteome profiling

The comprehensive characterisation of *P. falciparum* trophozoite proteome melting behaviour provides an unprecedented body of knowledge on protein stability patterns, both in their native intracellular state and in the *in vitro* conditions. This information can be further exploited for studies exploring the effect of protein sequence motifs, domains and biological features on their thermal stability *(201)*, prediction of protein-protein interactions and components of protein complexes *(152)*, as well as serving as a reference for future malaria CETSA studies. Significant differences in protein thermal stability observed between intact-cell and lysate settings, consistent with studies in other systems *(202, 203)*, demonstrate how the environment can affect protein properties. Protein stability within a living cell is affected by multiple factors, including cross-talk with the intracellular environment, molecular crowding, the rate of translation, abundance of chaperones and co-factors are likely to strongly affect protein folding/unfolding behaviour *(201, 202, 204)*. However, even more basic environment properties, such as fluctuations in pH or the strength and nature of salts present etc. can affect protein stability. The differences in the melting curve in between the two conditions may suggest which proteins undergo conformational changes, lose or gain interactions with other proteins/ligands or are highly sensitive to fluctuation in the environmental conditions upon cell lysis and purification. Furthermore, detailed profiling on the ~1400 *P. falciparum* trophozoite proteins provides invaluable information for subsequent *in vitro* protein studies, optimisation of their experimental conditions, as well as troubleshooting and identifying plausible causative factors affecting protein stability.

The three characterised proteomes (i.e. *P. falciparum*, RBC and K562) exhibit distinct differences in their global melting behaviours and Tm distribution profiles, which could be a direct result of their distinct intracellular environments. It is not

surprising that different proteins isolated as different lysates from different cell types exhibit different melting behaviour. However, even the same proteins derived from RBC or K562 cells were found to present non-uniform unfolding behaviour. Those differences might be related to cell-type specific properties of the cellular matrix in the two cell types *(202, 203)*, but also be a result of isoform variability or differential patterns of post-translational modifications related to the inherent functions those proteins have in the two different cell types *(205–207)*. Alternatively, differential protein stability pattern in the RBC could be a result of the extensive parasite-induced erythrocyte remodelling that occurs during the asexual developmental cycle *(208–210)*. In future, CETSA-mediated comparison of protein thermodynamics in between *Plasmodium*-infected and uninfected RBCs would provide valuable information on the nature and extent of the changes this parasite evokes in the human proteome.

Distinct proteome melting behaviour presented by *P. falciparum* is challenging to interpret on its own. To our surprise the parasite proteome contains a large number of proteins exhibiting relatively low Tm in intact-cells, but also a similar number of highly thermostable proteins, which are significantly less abundant in human cells. Perhaps, some of those stability patterns represent essential evolutionary adaptations to survive in the host. Fever is an evolutionary defence mechanism in vertebrates, developed to combat infection using body temperature elevation to selectively injure pathogenic organisms *(211)*. Such thermal stress may have profound effect on proteins' conformational stability affecting their biological functions, as has been demonstrated for fever-induced inhibition of bacterial replication *(212)*. Periodic fever is also a clinical hallmark of malaria, although rapid parasite growth suggests it does not offer much therapeutic advantage *(213)*. Other organisms have been shown to undergo evolutionary adaptations to elevated temperatures mediated by preferential thermal stabilisation of physiologically important proteins *(201)*. It remains unknown if *P. falciparum* acquired similar evolutionary adaptations to withstand elevated

temperatures during fever periods. Although, this warrants additional studies and CETSA might help to address this question.

The majority of limitations encountered and expected in this study are intrinsic to the CETSA technique itself and the principle it's based on, regardless of the model it is applied to. Thus, the points raised and discussed in Jafari et al. 2014 are valid both in the cancer cell *(147)* and malaria CETSA (as presented in this work). In brief, those include low solubility of the membrane proteins and as a consequence limited coverage of the membrane proteome in CETSA. The limited depth of proteome coverage might be particularly relevant for the profiling of the RBC proteome, which relies on only 362 and 771 proteins in lysate and intact-cell conditions, respectively. Although those protein subsets likely encompass the most abundant proteins, their unfolding patterns might not correctly reflect the behaviour of the entire RBC proteome. Secondly, the protein melting curve assessment and Tm determination are based on two technical replicate measurements only in all three datasets. Despite the implementation of a cut-off for maximum variability between measurements, a certain degree of inaccuracy in Tm determination is expected, due to inadvertently introduced biological and technical variations unavoidable with only one biological replicate. An analysis of three independent biological replicate experiments would provide more reliable data for future experiments.

There remain however challenges specific to the malaria application of CETSA, including presence of high levels of hemoglobin in samples, which mask certain peptides derived from less abundant parasite proteins and as a consequence limit the analysis depth particularly in the intact-cell CETSA application. Further intact-cell protocol modifications might be required to remove remaining haemoglobin and increase sample quality for MS analysis. Combination of MACS approach with

Hemoglobind-mediated haemoglobin depletion in tandem would, in theory, combine the strengths of both techniques, providing haemoglobin-free sample enriched in parasite proteins. On the other hand, the sample preparation protocol for the lysate CETSA variant introduces yet another challenge through employment of saponin for host-cell removal and could potentially lead to formation of soluble aggregate species with certain proteins. Furthermore, higher denaturation temperature of malaria proteins (i.e. requirement of heating cell up to 73°C instead of 64°C in the melt curve analysis, which could affect the integrity of host cell membrane during the thermal challenge). Unlike the long thermal gradient used for *P. falciparum*-RBC sample analysis, the K562 experiments were carried out with standard (i.e. 37-64°C) gradient typically employed for analysis of this cell type. This could have affected the profiling accuracy of the highly thermostable proteins in K562 cells, particularly in relation to the same proteins in the RBC. Despite those potential issue, the malaria CETSA workflow is fully functional and serves the purpose it was designed for.

3.5.2 MS-CETSA as a tool to study drug-target engagement in *P. falciparum*

Decades of research on the two largest and most important groups of antimalarial drugs: quinolines and artemisinins yielded an only fragmentary understanding of their MoA, also owing to their pleiotropic effects *(99, 214, 215)*. Although some candidate targets for quinoline and artemisinin-related compounds have been proposed in the *Plasmodium* proteome, only limited evidence has been provided to support their relevance for the drug's MoA *(96, 99, 216, 217)*. Hence, development of novel tools for accurate and reliable drug-target identification in malaria is of high importance. CETSA has previously proven useful for identification of direct drug targets *(143, 147, 218)*, downstream effects *(142)*, drug resistance deconvolution *(219)* and compound libraries screening for novel inhibitors to target

proteins *(220)* in human cells. Here, we adapted CETSA as a tool for identification of antimalarial drug targets in the *P. falciparum* proteome.

In order to provide a proof-of-principle for the CETSA method, we demonstrated its capacity to unambiguously detect well-validated targets of PM and E64d in the lysate and intact-cell implementations, respectively. PfDHFR-TS remains the sole identified target of PM in *Plasmodium* and its inhibition has been directly linked to the parasiticidal effect of the drug *(33, 92)*. Multiple *in vitro* and clinical studies have provided further support for this interaction *(34–37, 57)*, making the MoA of PM one of the most well characterised among all antimalarial drugs. Consistently, in the present study, only PfDHFR-TS was identified as an interacting partner of PM. The stabilisation of PfDHFR-TS in response to PM, was also observed in the lysate melt curve experiment, albeit displaying a non-canonical stabilisation profile, responding only at the higher temperatures. It is likely a result of the independent unfolding of the two enzyme domains at different but overlapping temperature ranges. In intact-cell ITDR and melt curve experiments of PM, no stabilisation was observed for PfDHFR-TS. In spite of CETSA efficiently detecting the interaction of PfDHFR-TS in lysate, this illustrates that certain binding scenarios can mask CETSA shifts under specific conditions. Few other potential pitfalls exist for efficient identification of drug targets in *P. falciparum* using CETSA. While, *P. falciparum* trophozoite proteome coverage achieved in lysate CETSA exceeds those attained in most other studies *(171)*, the proteome coverage in intact-cell CETSA analyses remains much less extensive, likely due to remaining issues with high haemoglobin abundance. Therefore, all targets of tested drugs were not necessarily identified, either due to limited MS analysis depth, or lack of observable thermal stabilisation at temperatures chosen for ITDR experiments.

The E64d is a cell-permeable synthetic analogue of E64 – an epoxysuccinyl-based broad spectrum cysteine protease inhibitor *(221, 222)*. Following cell entry, E64d is hydrolysed by esterases to its active form, E64c, which covalently binds to a sulfhydryl group at the active site of the protease *(223, 224)*. Among predicted cysteine proteases in the *P. falciparum* genome *(225)*, only three proteins: Falcipain 1, 2 and 3 have been validated as direct targets of E64/E64d *(185–187)*. We successfully verified the interaction of the drug with two of these proteins: Falcipain 2 and 3. Falcipain 1 on the other hand, was not present among the detected proteins in the CETSA experiment. Among the additional two proteins which pass the cut-off criteria, DPAP1 is a cysteine protease and likely a new E64c/E64d target. This *P. falciparum* ortholog of mammalian Cathepsin C was previously implicated in haemoglobin catabolism critical for the parasite's asexual growth *(226)* and identified as a target of MMV029272 *(227)*. Although no evidence for the interaction of DPAP1 with E64/E64d has been previously presented, both E64/E64d and MMV029272 are known inhibitors of human Cathepsin C *(221, 228)*.

Together, the data provide strong support for DPAP1 as an additional target of E64d. In addition to revealing direct drug targets, the intact-cell CETSA experiments also have the potential to report on biochemical effects on proteins downstream of the drug interactions *(142)*. This can provide interesting mechanistic information, but also presents ambiguities for whether a CETSA shift observed in intact-cell experiment corresponds to a direct target or a downstream effect. PfDSK2 identified as a candidate target in the E64d experiment has been predicted to function as a shuttle protein for Ubiquitin-tagged proteins destined for proteasomal degradation *(229, 230)*. The observed stabilisation of PfDSK2, might be a result of direct binding of the E64d di-peptide. However, it could also represent a downstream effect of drug's action. De-ubiquitinating enzymes (DUBs), which remove ubiquitin chains from proteins prior to proteolysis are cysteine proteases in the vast majority *(231–233)*. If they were inhibited

by E64d, resulting accumulation of ubiquitinylated protein cargo bound to PfDSK2 could lead to its stabilisation.

Summarising, we demonstrated that the MS-CETSA protocol is capable of identifying antimalarial drug targets in *P. falciparum* proteome with a high degree of specificity, providing the first label-free drug-target discovery technique to monitor drug-protein engagement in lysates and intact cells. In its intact-cell implementation, CETSA has the ability to detect drug-target binding within a living organism, thus allowing for possible prerequisites for the interaction to occur including drug-metabolism following cell entry, the presence of co-factors, compound accumulation at a specific subcellular site or an appropriate local environment. Furthermore, intact-cell CETSA is also capable of identifying the potential downstream effects of the drug action. Considering the intracellular nature of malarial parasites, this technique can also be used to detect human-protein engagement by a drug, which is relevant for evaluating potential drug-induced adverse effects or for identifying synergistic targets within the RBC proteome. Nevertheless, there remain certain limitations to the technique *(147)* including the occurrence of false positives (though unlikely) or false negatives (i.e. non-detectable shift in in protein stability in an ITDR assay, derived from inappropriate ITDR temperature, insufficient time for drug penetration, weak or even no ligand-induced response or other processes masking the CETSA shift).

CHAPTER 4

De-orphanisation of antimalarial drugs through MS-CETSA

The increase in the frequency of clinical treatment failures encountered with standard ACTs is signalling phenotype reinforcement and spread of the multidrug-resistant *P. falciparum* (see chapter 1.2.2). As a result, new antimalarial "Triple Artemisinin-based Combination Therapies" (TACTs) were co-formulated and are currently undergoing phase 3 clinical trials within the TRACII (Tracking Resistance to Artemisinin Collaboration II) study *(234)*. The TACTs under evaluation include dihydroartemisinin-piperaquine-mefloquine (DHA-PPQ-MFQ) and arthemeter-piperaquine-lumefantrine (ATM-PPQ-LUM). In the absence of a clearly defined MoA for either of the five compounds used in TACTs, the combinations were formulated primarily based on drugs' pharmacokinetic/pharmacodynamic properties, combining fast-acting artemisinin-derivative with two long-acting partner compounds (personal communication with TRAC-II study coordinator Dr. Rob van der Pluijm). The clinical complementarity of each of the three drugs used in TACTs is unknown. Considering that no *in vitro* nor *in vivo* data supporting the effectiveness of chosen combinations has been produced, there remains a possibility of antagonistic effects between the three drugs. Such a conclusion was made in a 2004 clinical study in Burkina Faso, which evaluated the effectiveness of methylene blue – chloroquine combination in 435 young children with uncomplicated malaria *(235)*. Overall, they reported significant treatment failure rates resulting from antagonistic effects of both compounds. This illustrates the dire reality we are faced with and how limited our knowledge is on the

existing antimalarial drugs. There is a desperate need for the deconvolution of the MoA of the majority of existing antimalarial drugs. Identification of clinically relevant molecular targets and characterisation of the specific mechanisms in which different drugs kill the parasite is a prerequisite for the development of new more effective antimalarial therapies and better designed drug combinations. Additionally, characterisation of how the existing drugs work can help us better understand the biology of the malaria parasite.

Among all available antimalarial drugs, beside artemisinins, quinolines represent the largest and undoubtedly the most clinically important group. From these, quinine (QN), mefloquine (MFQ) and chloroquine (CQ) are amongst the most historically relevant drugs still in clinical use *(214)*. Whilst the antimalarial effect of CQ appears strongly associated with the inhibition of haem detoxification in the parasite's digestive vacuole (DV) *(64)*, the MoAs of remaining quinoline drugs remain largely elusive *(71, 215)*. QN, first isolated in 1820 from *cinchona* tree bark, became the first-in-class quinoline [for review see *(214)*]. Currently, it represents an essential alternative for treatment of severe malaria and remains the treatment of choice for uncomplicated malaria in pregnant women during the first trimester *(236)*. Over the years, a range of its derivatives was synthesised, including MFQ developed by the Walter Reed Army Institute of Research in 1984 *(237)*. Today, MFQ is a crucial partner drug within the ACT formulations, particularly those used in South-East Asia (SEA) and remains a vital chemoprophylaxis agent for malaria *(234, 238)*. Taken together, the broad knowledge gap remaining in our basic understating of the MoA of common antimalarial drugs substantially hinders implementation of effective counter-measures to clinical drug failure *(26)*.

4.1 Identification of molecular targets of quinine and mefloquine

Having validated CETSA as an effective method for identification of molecular targets for antimalarial drugs with PM and E64d, we applied the ITDR assays to discover protein targets of two arylamino alcohols: QN and MFQ. Applying the ITDR (51°C) protocol for lysate samples exposed to QN (10-0μM) or MFQ (100-0μM), we identified Purine Nucleoside Phosphorylase (PfPNP, PF3D7_0513300) as the most significantly drug-stabilised among 2157 and 2032 *P. falciparum* proteins detected in the two datasets (Fig. 4.1A-D). The MDT for PfPNP stabilisation was ~0.1μM for QN and ~0.6μM for MFQ. No other targets were detected over the significance cut-off selection in lysate ITDR for QN or MFQ. Crucially, a significant dose-dependent stabilisation of PfPNP was also observed upon QN treatment of parasite-infected RBCs in the intact-cell ITDR (57°C) with an MDT of ~2.5nM, accompanied by smaller observable shift at 51°C (Fig. 4.1E-F). Similarly to lysate, no other targets were identified for QN in the intact-cell experiments. No stabilisation of PfPNP was observed in the two-corresponding intact-cell ITDRs conducted with MFQ, but instead we detected a dose-dependent stabilisation of three other proteins (Fig. 4.1G). Pyruvate Kinase II (PfPyKII, (PF3D7_1037100) exhibited an early dose-dependent stabilisation (MDT ~19.5nM) in intact-cell ITDR (57°C), but this was concomitant with an increase of protein level at 37°C condition (Fig. 4H). The change in basal protein level in response to the drug suggests that observed 'stabilisation' at a higher temperature likely does not represent a direct binding event. Considering the importance of PyKII for parasite's metabolism *(239, 240)*, the shift in the reference protein levels is likely reflecting a downstream effect of drug binding, such as the cellular response to stress. Additionally, a stabilisation of two mitochondrial proteins was observed in the intact-cell ITDR (57°C): Heat shock protein 70 (Hsp70−3, PF3D7_1134000) and GrpE

protein homolog (Mge1, PF3D7_1124700) (Fig. 4H). A single point stabilisation observed for both proteins at the highest drug dose (10μM) makes them unlikely candidates as direct drug-targets, but rather suggests a downstream response to local drug-induced perturbations. Mge1 and Hsp70-3 were previously proposed to interact with each other, assisting protein transport through the mitochondrial membrane *(241)*. The stabilisation of PfPNP detected by the mass spectrometry approaches was further verified for both compounds using Western blot, reproducing observed change in protein stability (Fig. 4.2). Western blotting offers a direct visual validation of MS results, providing additional proof that the correct protein of the correct size was indeed identified and stabilized by the drug, as well as, that no-target degradation has taken place in the assay conditions. Taken together, the collective results from both lysate and intact-cell ITDRs suggest PfPNP as a new target of QN and to some degree MFQ. PfPNP has previously been demonstrated to be a promising antimalarial drug target, due to its key function in purine metabolism *(242, 243)* and thus it is conceivable that it plays a role in the MoA of the two drugs.

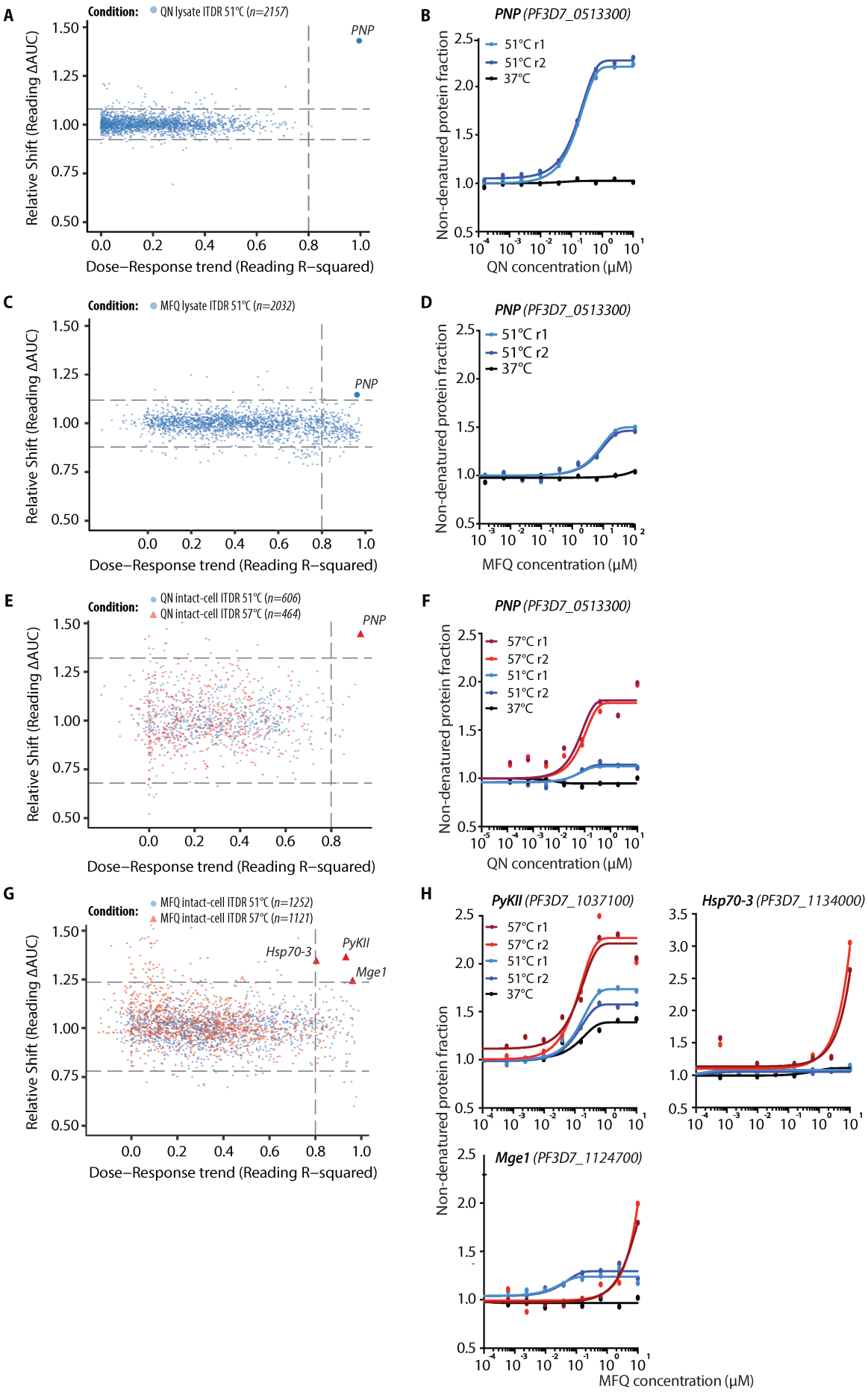

Figure 4.1 – Protein target engagement by QN and MFQ in lysate and intact-cells

Whole proteome ITDR analysis performed with QN 10-0μM in lysate (**A**) and intact-cells (**E**) and MFQ 100-0μM in lysate (**C**) and 10-0μM in intact-cells (**G**) with thermal challenges at 51°C (blue dots) or 57°C (red triangles). Distribution of protein stabilisation is plotted as function of R squared against ΔAUC. MAD*3 of ΔAUC and R squared=0.8 cut-offs are indicated on the graph. Significantly stabilised proteins are highlighted. **(B,D,F,H) -** Protein stabilisation curves of the candidate targets identified in the respective preceding panels, thus A->B etc. The extent of stabilisation, depicted as remaining soluble protein level after thermal challenge: 51°C (blue) and 57°C (red) relative to no-drug control is plotted along QN or MFQ gradients. Non-denaturing 37°C control condition is plotted in black.

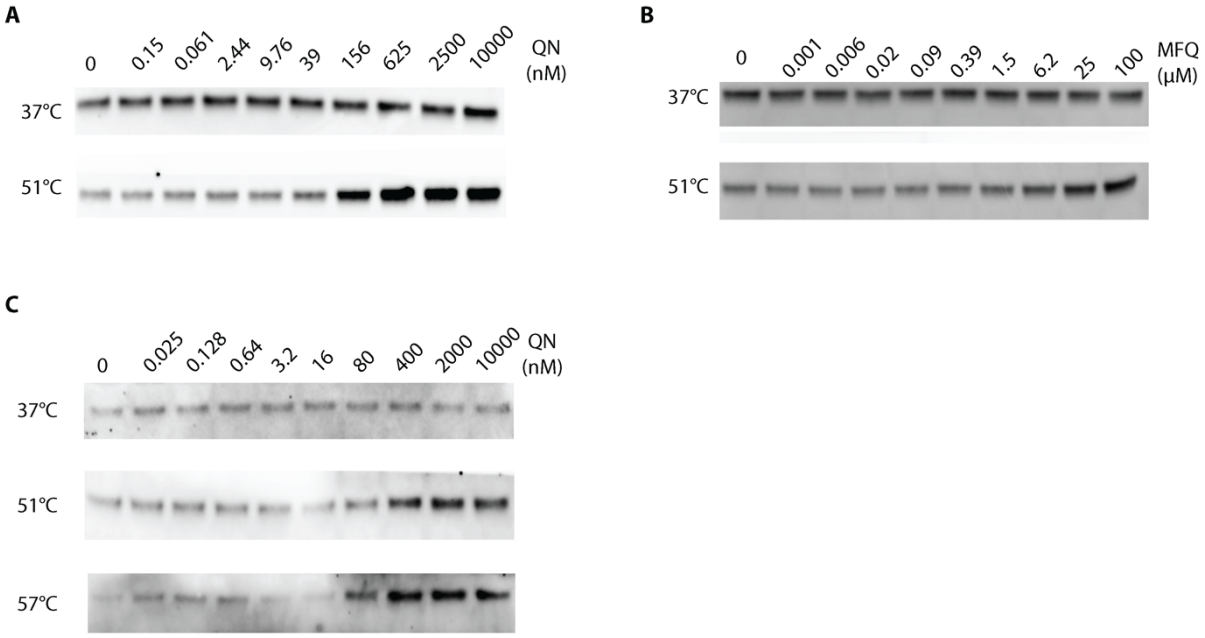

Figure 4.2 – Western Blot validation of PfPNP stabilisation by QN and MFQ in ITDR assays

Anti-PfPNP primary antibody was used for the protein detection in samples previously analysed by Mass Spectrometry (Fig. 4.1) for MFQ lysate ITDR (**A**) QN Lysate ITDR (**B**) and QN Intact-cell ITDR (**C**). Following visualisation, a single band was present in each sample lane at the same level corresponding to PfPNP molecular weight.

In order to maximise the information gained from ITDR experiments, we further examined QN and MFQ ITDR datasets for proteins, which exhibited apparent stabilising shifts but did not meet the high confidence cut-off criteria (Table 4.1). Interestingly, we observed stabilization of four ribosomal subunits and a putative subunit of the translation initiation factor 2 by MFQ in the lysate assay. The extent of detected stabilization was considerably lower for each subunit as compared to PfPNP, satisfying only two of the three cut-off criteria for high-confidence target identification (**Table 4.1**). Nevertheless, this finding is consistent with previous studies demonstrating MFQ interaction with the ribosomal complex *(81)*. Moreover, among the low-confidence drug-target candidates, only one additional protein was identified as a potential interacting partner of QN: Uncharacterised protein (PF3D7_1456300) (Fig. 4.3A). Its strong stabilisation was observed in lysate 51°C ITDR with an MDT and FC similar to PfPNP (i.e. 124nM and 1.73 respectively), but the protein was not detected in the 37°C reference condition. Interestingly, the same protein also exhibited a similar response in the lysate MFQ ITDR dataset, but with weaker stabilisation (MDT=350nM and FC=1.44) and similarly the lack of protein detection in the non-denaturing reference condition. Its apparent engagement by both compounds makes it a more reliable target lead, however without the data on protein behaviour in the reference control sample makes we are unable to determine if the stabilisation indeed occurs. When no antibodies were available for this protein, we have not been able to confirm the CETSA response with WB.

Condition	Gene id	Protein name	R^2	ΔAUC	FC	Sum PSMs	MDT (μM)
QN 51°C lysate	PF3D7_0513300	PfPNP	0.996	1.43	2.24	137	0.0973
	PF3D7_1456300	conserved *Plasmodium* protein, unknown function	0.931	1.34*	1.73	4.5	0.124
QN 57°C intact-cell	PF3D7_0513300	PfPNP	0.929	1.44	1.97	51.00	0.002
MFQ 51°C lysate	PF3D7_0513300	PfPNP	0.965	1.14	1.48	212	0.594
	PF3D7_1456300	conserved *Plasmodium* protein, unknown function	0.801	1.12*	1.44	3	0.35
	PF3D7_1234900	conserved *Plasmodium* protein, unknown function	0.870	1.10	1.27	14.5	0.157
	PF3D7_1013900	initiation factor 2 subunit family, putative	0.947	1.10	1.41	6.5	2.958
	PF3D7_1351400	60S ribosomal protein L17, putative	0.817	1.12	1.28	2.5	3.987
	PF3D7_1466200	conserved *Plasmodium* protein, unknown function	0.886	0.88	1.37	5.5	14.802
	PF3D7_0932800	conserved *Plasmodium* protein, unknown function	0.753	1.18	1.44	36.5	0.819
	PF3D7_1225900	conserved *Plasmodium* protein, unknown function	0.980	1.25*	2.49	6	2.289
	PF3D7_1130100	60S ribosomal protein L38 (RPL38)	0.927	1.04	1.35	2	14.714
	PF3D7_0210100.1	60S ribosomal protein L37ae, putative	0.792	1.12	1.43	2.5	0.018
	PF3D7_1124900	60S ribosomal protein L35, putative	0.824	1.10	1.37	4.5	0.105
MFQ 57°C intact-cell	PF3D7_1037100	PyKII	0.933	1.36	2.07	5	0.019
	PF3D7_1134000	HSP70-3	0.804	1.35	2.83	61.5	3.628
	PF3D7_1124700	MGE1	0.962	1.24	2.38	21.5	1.176
	PF3D7_1434800	mitochondrial acidic protein MAM33	0.927	1.23	2.76	8	1.721
	PF3D7_0602200	MYND finger protein, putativ	0.781	1.17	1.40	8	0.122
	PF3D7_1360800	falcilysin (FLN)	0.813	1.07	1.36	55.5	1.051
MFQ 51°C intact-cell	PF3D7_1037100	PyKII	0.987	1.09	1.65	12	0.038
	PF3D7_1124700	MGE1	0.818	1.20	1.20	28.5	0.005
	PF3D7_1222100	conserved *Plasmodium* protein, unknown function	0.920	1.14	1.38	13	0.045

Table 4.1 – High and low confidence protein stabilisations observed in QN/MFQ ITDR assays

The ITDR-mediated identification of drug-targets presented above is assisted by a stringent hit selection protocol involving 4 principal prerequisites: the presence of a reference 37°C dose-response curve, significant protein stabilisation under drug treatment in denaturing conditions relative to 37°C control (ΔAUC) and to the untreated sample (protein quantity fold change (FC)), as well as adherence of the stabilisation profile to the sigmoidal shape of the dose response curve (R^2). AUC cut-offs equivalent to 3*MAD for the dataset were as follows: 1.119 (MFQ lysate), 1.235 (MFQ intact cell), 1.083 (QN lysate)

and 1.321 (QN intact-cell). Fold change cut-off is 1.3 and R squared cut-off 0.8. Passing of cut-off criteria is coloured in green, not passing in orange. Asterix indicates that AUC has not been normalised against 37ºC control, due to the lack of protein detection in the reference dataset. The sum of peptide-to-spectrum matches (PSMs) is indicated for each protein along with the minimal dose threshold (MDT) of the respective drug required for its significant stabilisation.

In order to predict the potential role of the PF3D7_1456300 we carried out bioinformatic analysis of its sequence (i.e. the extended similarity group Gene Ontology prediction by iterative PSI-Blast search (ESG)) *(244)* (Table 4.2). The analysis suggested with high confidence that the PF3D7_1456300 protein has nucleotide/ATP binding propensity and possess both cytoplasmic and membrane features, as well as that it could be involved in transport. None of the remaining protein stabilisations observed for MFQ was present in both conditions (i.e. lysate and intact-cell), nor the protein exhibited response to both drugs. They theoretically could represent actual binding partners of MFQ, the downstream effectors of its MoA, or experimental artefacts, thus should be analysed with caution. Subsequently, we assessed the effect of QN and MFQ on the stability of RBC proteins concomitantly present in the intact-cell ITDR experiments and identified stabilisation of one human protein: mitochondrial 60kDa Heat Shock protein (HSPD1, P10809) in response to QN (MDT=0.15μM) (Fig. 4.3B-D).

Probability	Confidence level	Term	Description
54.1%	High	GO:0000166	nucleotide binding
54.1%	High	GO:0005524	ATP binding
52.6%	High	GO:0016020	membrane
50.3%	High	GO:0005737	cytoplasm
40.2%	High	GO:0005886	plasma membrane
32.3%	Moderate	GO:0006810	transport

Table 4.2 – ESG prediction model-based protein sequence analysis of PF3D7_1456300

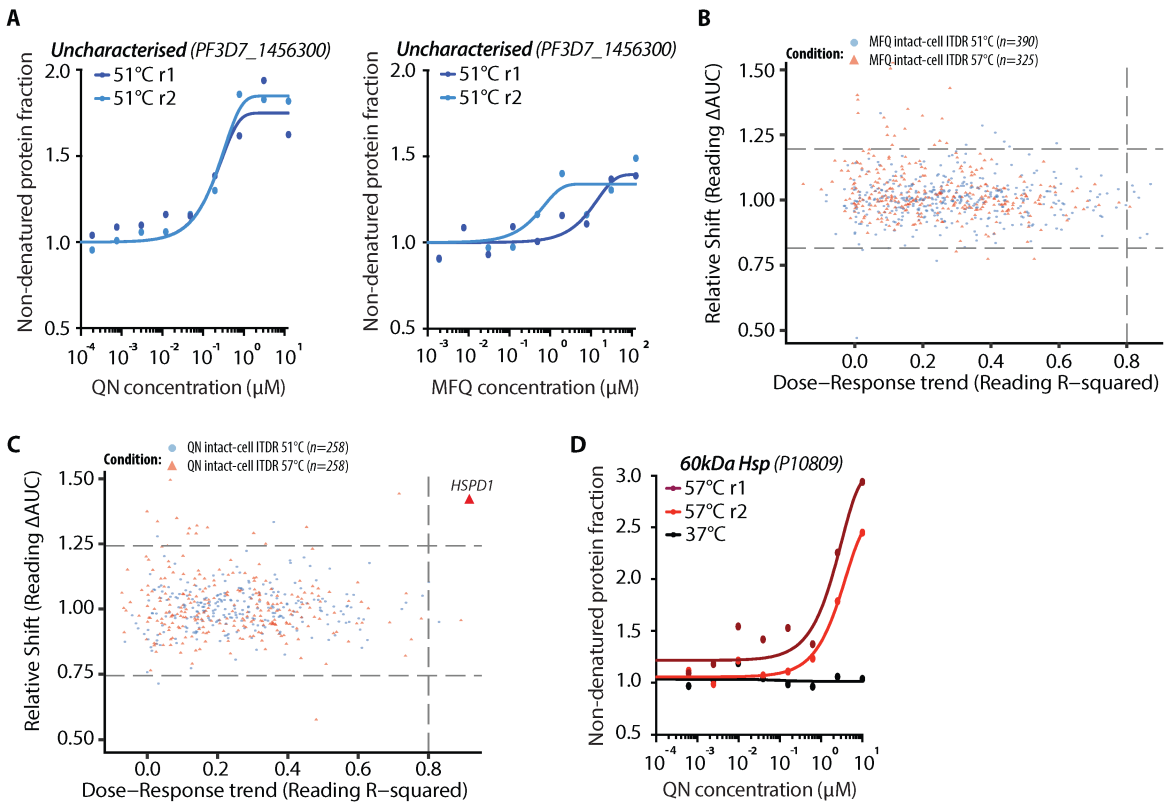

Figure 4.3 – PF3D7_1456300 and human protein engagement by QN and MFQ in intact-cell ITDR assays

(**A**) Protein stabilisation profile of PF3D7_1456300 under exposure to QN or MFQ in lysate ITDR assays. The extent of stabilisation, depicted as remaining soluble protein level after thermal challenge: 51°C (blue) relative to the no-drug control is plotted along QN or MFQ gradients. Non-denaturing 37°C control condition is plotted in black. (**B-C**) Whole proteome analysis of human proteins identified in Intact-cell ITDR experiments under (B) 10-0µM MFQ or (C) 10-0µM QN treatment with thermal challenges at 51°C (blue dots) or 57°C (red triangles). Distribution of protein stabilisation is plotted as function of R squared value against ΔAUC. MAD*3 AUC and R squared=0.8 cut-offs are indicated on the graph. Significantly stabilised proteins are highlighted. (**D**) Human protein stabilisation curve of the protein identified in panel B for QN Intact-cell ITDR experiments. The extent of stabilisation in replicate experiment, depicted as remaining soluble protein level after thermal challenge relative to no-drug control is plotted along drug gradient. Non-denaturing 37°C control condition is plotted in black.

4.2 Validation of PfPNP as a target of quinine and mefloquine

4.2.1 Biochemical validation of target engagement

To further investigate if PfPNP is a bona fide target of the two arylamino alcohols or a ubiquitous quinoline-binding protein, we heterologously expressed His-tagged recombinant PfPNP. The relative stabilising effects of the MFQ and QN interactions were quantified with differential scanning fluorimetry (DSF). DSF, similarly to CETSA allows assessment of ligand-mediated thermal stabilisation, but it quantifies protein unfolding via binding of a hydrophobic fluoro-probe, rather than monitoring the level of protein denaturation. The extent of thermal stabilisation of recombinant PfPNP was determined for 0-100μM concentration gradients of QN, MFQ, related quinoline compounds: quinidine (QD), chloroquine (CQ), lumefantrine (LM), primaquine (PQ), as well as Immucillin H (ImmH) a specific inhibitor of PNP proteins *(245)*. Beside Imm-H, only QN, MFQ and QD exerted gradual stabilising effect with a change in Tm of 25°C (ImmH), 17.3°C (QN), 11.2°C (MFQ) and 1.5°C (QD) at 100μM dose, relative to the no-drug control (Fig. 4.4A). No change in protein stability was detected in the presence of CQ, LM, or PQ at ≤100μM, suggesting no interaction. To complement the DSF analysis, we investigated the affinity and binding kinetics of QN and MFQ with the recombinant PfPNP using Surface Plasmon Resonance (SPR) (Fig. 4.4B-C). Association and dissociation rates of the three compounds were measured using single- and multi-cycle steady state or kinetic fit experiments (Table S4.2). As expected, ImmH displayed a tight binding and very slow dissociation rate to PfPNP with equilibrium constant (K_D) of approximately 250pM, similar to what has previously been reported (i.e. K_D=860pM) *(154)* (Fig. 4.4B). The quinolines have lower affinities to PfPNP with QN and MFQ exhibiting K_D around 30nM and 40μM, respectively (Fig. 4.4B-C). Finally, we validated the observed PfPNP engagement with QN and MFQ by Isothermal Titration Calorimetry (ITC). The ITC results were also in a good agreement

with the SPR results, showing similar binding affinities for QN, K_D = 65nM, and MFQ, K_D = 10μM (Fig. 4.4D-E, Table S4.3). Mixed exo- and endo-thermic enthalpy observed upon QN binding to PfPNP may suggest a secondary binding event with K_D an order of magnitude higher (i.e. ~534nM). However, the origin of such a secondary binding event remains uncertain. Next we employed an *in vitro* enzymatic assay, monitoring PfPNP-catalysed conversion of inosine to hypoxanthine *(245, 246)*, to investigate the inhibitory effect of QN and MFQ on PfPNP. Indeed, both drugs can block the PfPNP enzymatic activity with the inhibitory constants (Ki) of 138nM for QN and 5.9μM for MFQ (Fig. 4.4F, Table S4.4). This effect is somewhat weaker when compared to previously reported Ki of ImmH (i.e. Ki=29nM and slow onset Ki*=0.6nM) *(245)*. However, these values correlate with affinities from SPR and ITC showing that both QN and MFQ interact with PfPNP, albeit with lower affinities than for ImmH. PfPNP enzymatic inhibition experiments (Fig. 4.4F, Table S4.4) show that the maximal velocity (V_{max}) of the reaction does not change in the presence of QN or MFQ, while the Michaelis-Menten constant Km (substrate concentration at ½ Vmax) for the reaction increases proportionally to increasing drug dose. Such profile is suggestive of drugs competing with the substrate for binding to PfPNP, following competitive inhibition model *(247)*. This conclusion is also supported by the Lineweaver-Burk plot analysis generated through the regression fit of the reciprocal data for PfPNP enzymatic activity inhibition by each drug (Fig. S4.1). Furthermore, both drugs appear to exhibit reversible binding to PfPNP, as suggested by the aforementioned analyses *(247)* and demonstrated by successful regeneration of SPR chips in QN and MFQ experiments (Fig. 4.4B-C). Of the two antimalarial compounds, QN exhibits a consistently higher affinity to PfPNP and increased inhibitory activity, which is also reflected in the initial CETSA ITDR measurements (Fig. 4.1). It is therefore likely that inhibition of PfPNP is relevant for the MoA of QN and (possibly to a lesser degree) MFQ.

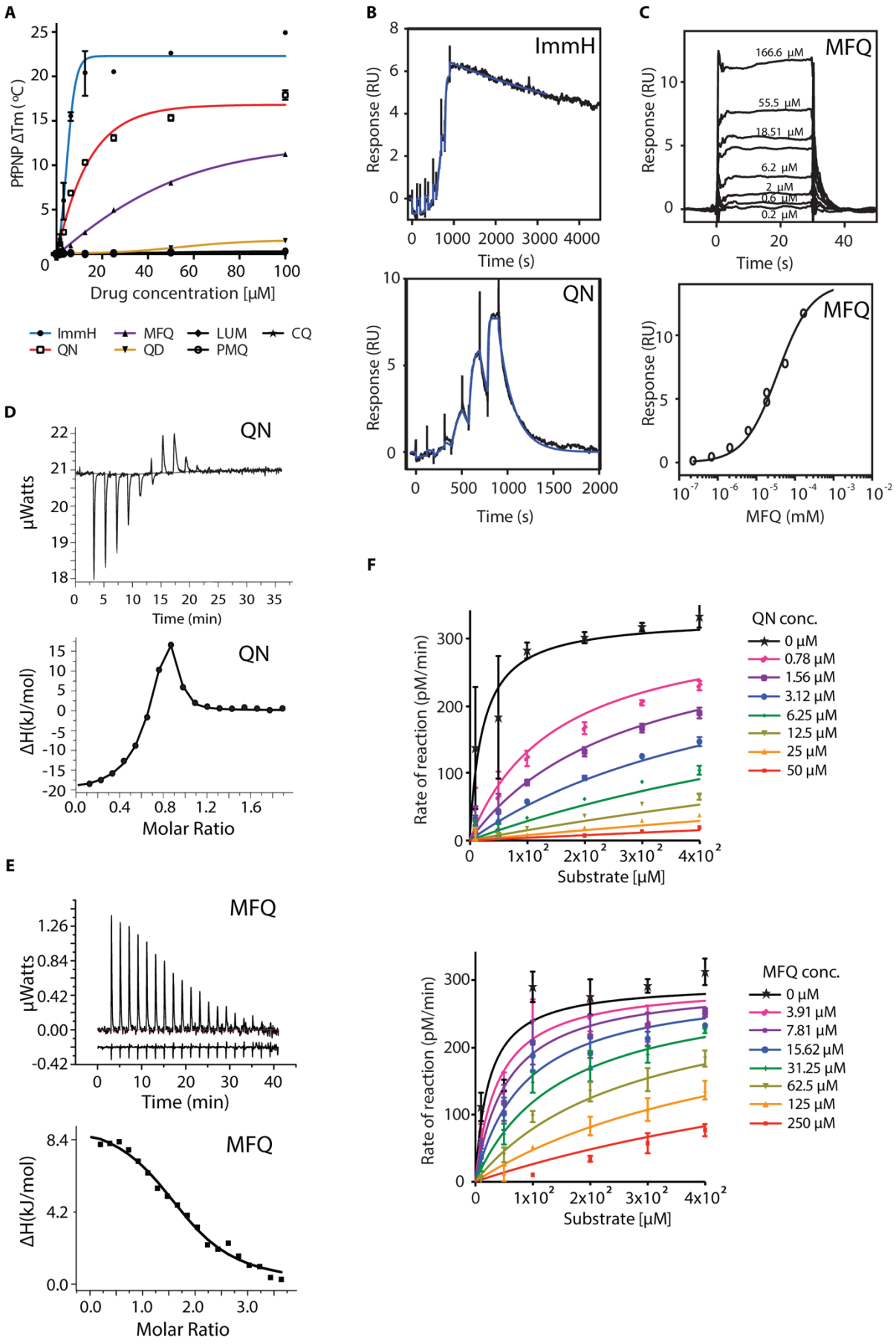

Figure 4.4 – Biochemical validation of PfPNP binding by QN and MFQ

(A) DSF analysis of PfPNP stabilisation by ImmH, MFQ, QN, QD, LM and PMQ in a concentration gradient (100-0μM). The change in PfPNP Tm under drug exposure relative to untreated sample is

represented on y axis in relation to drug concentration. (**B-C)** SPR Sensorgrams, double-referenced binding data (black traces) and fitted (blue traces) from SPR analysis of PfPNP binding affinity to three drugs. ImmH and QN (B) were analysed using single-cycle experiments and kinetic 1-to-1 model, whilst MFQ (C) was analysed in a multi-cycle experiment and fitted using a steady-state model. MFQ binding isotherm is represented below the sensogram. SPR experiments were conducted in collaboration with Dr. A. Larsson. Additional details on data acquisition and results are presented in Table S4.1 (**D-E**) ITC profiles for the binding of QN (D) and MFQ (E) titrated into recombinant PfPNP in an ITC cell. The area of each injection peak corresponds to the total heat released/absorbed from that injection. An additional control run performed for MFQ titration in the absence of PfPNP is included as a flat signature at ~ -0.21μWatts. Bottom panels represent binding isotherms for QN and MFQ data. ITC experiments were conducted in collaboration with Dr. Chen Dan. Additional details on data acquisition and results are presented in Table S4.2. (**F)** PfPNP enzymatic activity inhibition by QN and MFQ across 0-50μM and 0-250μM drug concentration gradients, respectively. The rate of reaction in the presence of different inhibitor concentrations indicates the formation of uric acid from the coupled assay with xanthine oxidase, measured over 1h period at 1min intervals as an increase in absorbance at 293nm wavelength.

4.2.2. Structural evidence for the drug interaction with PfPNP

To shed further light on the inhibition of PfPNP we determined co-crystal structures of the protein with QN and MFQ at 1.66Å and 2.30Å resolution, respectively (Table S4.5). The structures show that both compounds bind in the active site pocket of PfPNP, consistent with their suspected roles as enzyme inhibitors (Fig. 4.5A-B). The observed fold of co-crystallised PfPNP-QN·PO_4 and PfPNP-MFQ·PO_4 complexes is highly similar, with root mean square deviation (r.m.s.d.) equal 0.2Å for C alpha atoms. The overall structures also correspond to previously determined complexes of PfPNP-Inosine *(162)* [r.m.s.d. 0.34/0.41Å] and PfPNP-ImmH·SO_4 *(154)* [r.m.s.d. 0.24/0.28Å] (Fig. 4.6), except for the active site loop Trp212— Val222 of PfPNP which is not well-defined in the electron density of the PfPNP-MFQ·PO_4 complex. The steric hindrance with MFQ trifluoromethyl moiety likely destabilises the active site loop in the conformation presented in other complexes and displaces it.

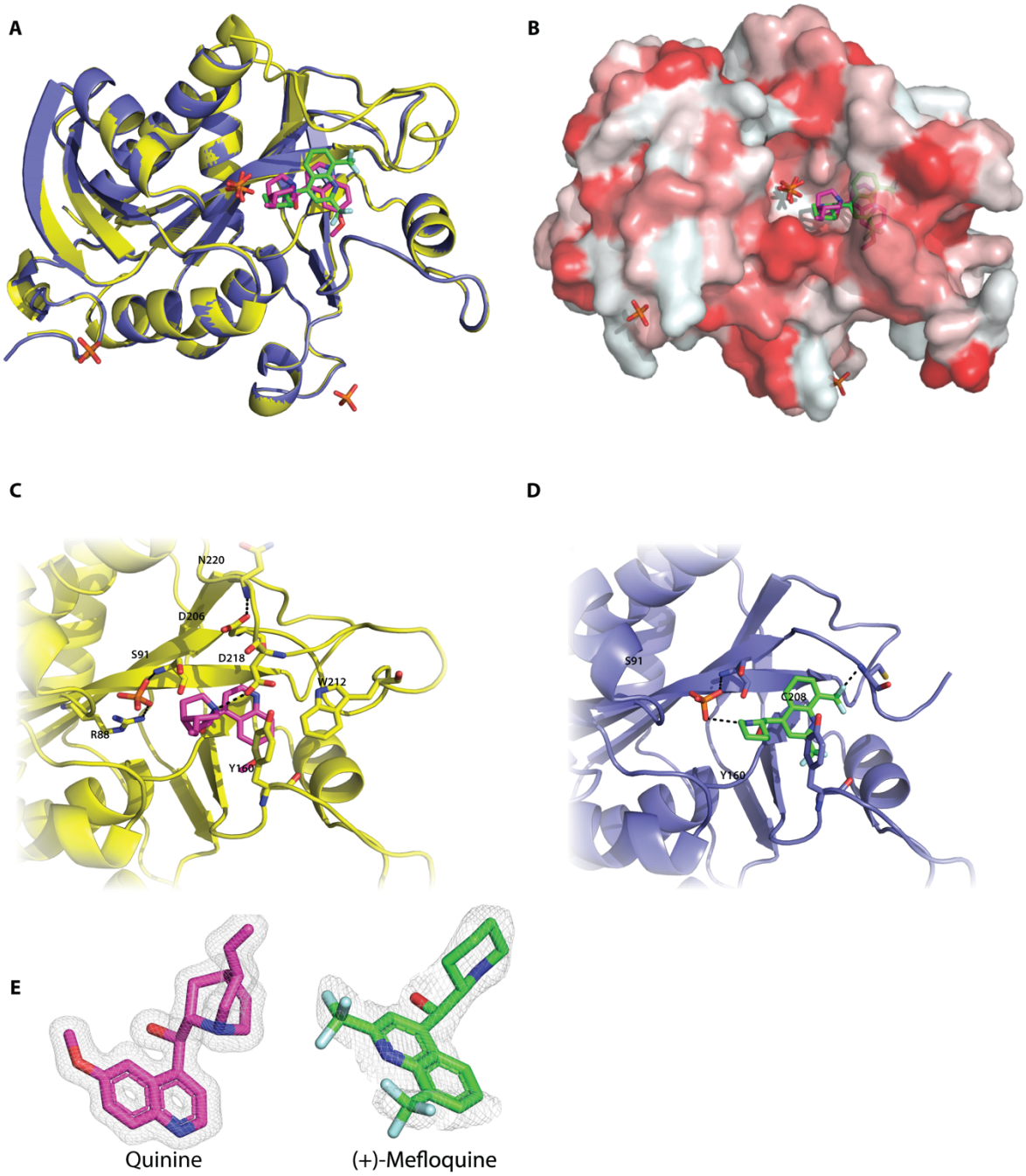

Figure 4.5 – Co-crystal structures of PfPNP with QN or MFQ

(A) An overlay of PFPNP-QN·PO_4 and PfPNP-MFQ·PO_4 co-crystal structures. QN is represented as pink sticks, MFQ as green sticks and the two corresponding protein structures in yellow and blue respectively. Oxygen (blue), phosphorus (orange), oxygen (red), fluorine (light cyan). (**B**) Surface representation of both structures, showing hydrophobic (red) regions and both ligands bound to PfPNP. (**C-D**) Magnified binding pockets of structures presented in (A), major interactions between ligands and binding pocket amino acids are represented by black dashed lines. (**E**) 2Fo-Fc electron density maps of QN and MFQ residing within binding pockets of the two co-crystal structures contoured at 1.0 sigma level. The co-crystal structures preparation was carried out by Dr. Chen Dan, followed by structure analysis by the author.

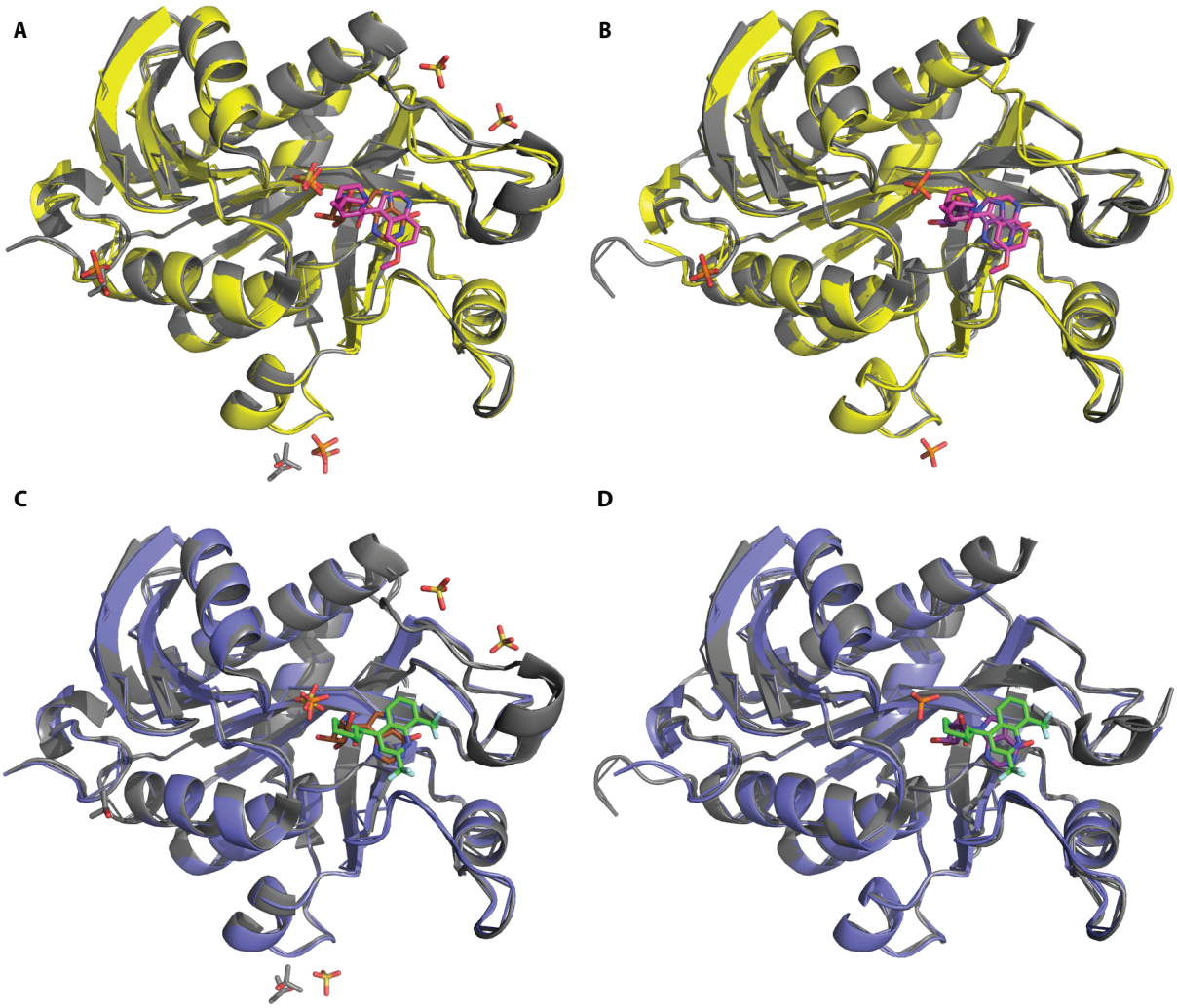

Figure 4.6 – Co-crystal structure overlay with 2bsx and 1nw4 reference PfPNP structures

Overlay of PfPNP-QN·PO_4 (**A,B**) and PFPNP-MFQ·PO_4 (**C,D**) co-crystal structures with PfPNP-Inosine (2bsx) (**B,D**) or PfPNP-ImmH·SO_4 (1nw4) (**A,C**) co-crystal structures *(154, 162)*. MFQ is represented as green sticks, QN as pink sticks, ImmH as brown sticks and Inosine as purple sticks. PfPNP protein structures with QN and MFQ are presented in yellow and blue, respectively, whilst reference 2bsx and 1nw4 structures in grey. Nitrogen (blue), phosphorus (orange), oxygen (red), fluorine (light cyan), sulphur (yellow), carbon (grey).

The binding of both compounds is mediated mainly through interactions with the hydrophobic environment of enzyme's active site (Fig. 4.5C-D). Both compounds are oriented by π-stacking and Van der Waals interactions with Tyr160. In the QN

structure, Trp212 constitutes an additional moiety with which π-stacking and Van der Waals interactions are formed. Ligand positioning is further mediated by hydrogen bond formation between the protonated nitrogen of QN quinuclidine ring and α-carboxylic group of Asp218 [2.6 Å]. In both the QN and MFQ structures, a phosphate ion is bound in the same region as the leaving phosphate ion of enzyme-inosine product complex. Its positioning is strikingly similar to that of an SO_4 ion in previously described PfPNP-ImmH·SO_4 structure, exhibiting central atom displacement by 0.4-0.5Å between two ions *(154)*. Therefore, this phosphate is likely essential for the binding of the two compounds when it shields the high positive charge of this region of the pocket. Despite similarities, few notable differences to previously described structures can be observed in the stereochemistry of the active site, most notably the orientation of the protonated side-chain carboxylate of Asp206. This catalytic residue interacts with a purine substrate during phosphorylysis and has been shown important for transition-state stabilisation of ImmH *(154, 162)*. In PfPNP-QN·PO_4 structure, Asp206 carboxylate appears to position itself at a distinct angle and likely forms hydrogen bond with Asn220 [2.9Å] stabilising the active site flexible loop. In PfPNP-MFQ·PO_4 complex, no interaction with that residue was identified. Interestingly, although MFQ is added to the crystal as a racemic mixture, only the (+)-mefloquine enantiomer binds to the active site of in the PfPNP (Fig. 4.5E). This is consistent with previous data supporting a stronger antiplasmodial activity of (+) enantiomer *(248–250)* and further supports that the PfPNP inhibition contributes to the antimalarial activity of MFQ.

4.2.3 The relevance of PfPNP inhibition for the antimalarial effect of QN and MFQ

It is therefore likely that inhibition of PfPNP is relevant for the MoA of QN. The relevance of PfPNP interaction with MFQ is uncertain due to high doses required for

the interaction to occur. The principal role of PfPNP is the catalysis of inosine-to-hypoxanthine conversion. Therefore, in standard *in vitro* culture conditions where the parasites are grown in excess of hypoxanthine, the need for the enzymatic activity of PfPNP is abolished. Consistently, the antimalarial activity of ImmH is also neutralised in the presence of high hypoxanthine levels *(251)*. Conversely, partial or complete limitation of purine availability renders ImmH gradually more potent, inducing purine-less parasite death. To examine the possibility that PfPNP inhibition contributes to the MoA QN and MFQ, we measured the extent of antimalarial activity of QN and MFQ in the presence of different purine concentrations and contrasted it with the effect of ImmH. To that end, we depleted RBCs of their endogenous purines and reconstituted hypoxanthine or inosine to physiological level (i.e. 10μM), excess level (i.e. 100μM) or retained them in purine-free media. Subsequently, we measured the extent of parasite growth inhibition each of these drugs induces in each of the conditions (Fig. 4.7A, Table S4.5). We reproduced previously reported gradual limitation of the antimalarial activity of ImmH relative to increasing hypoxanthine levels *(251)*, also demonstrating that similar but slightly more pronounced effect is obtained using inosine as a purine source. However, QN and MFQ exhibited identical killing profiles under all conditions, suggesting that other killing mechanisms might be masking the effect of PfPNP inhibition.

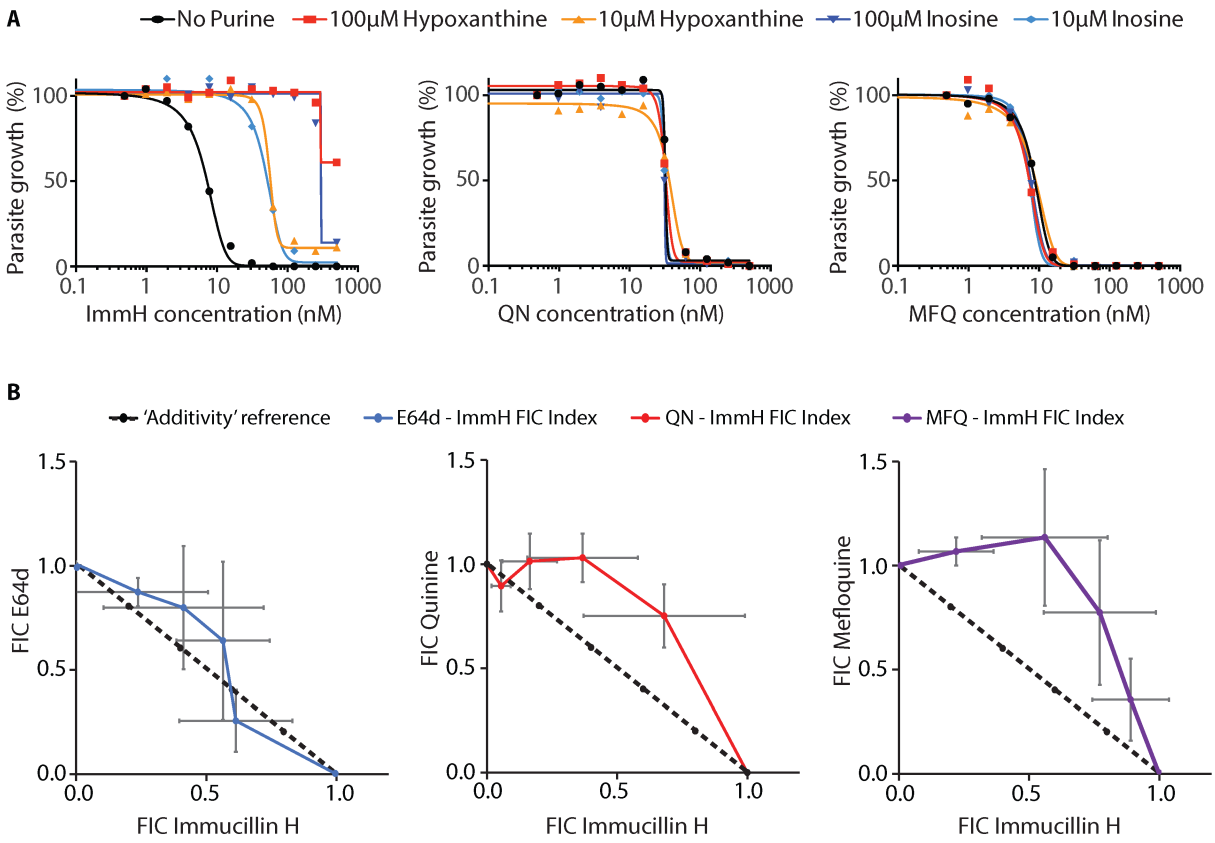

Figure 4.7 – Contribution of PfPNP inhibition to the MoA of QN/MFQ in cell culture *in vitro*

(**A**) *P. falciparum* 3D7 growth inhibition profiles determined in the presence of 0-500µM ImmH, QN or MFQ concentration gradients under variable purine availability conditions. Endogenous purine-depleted RBC were reconstituted in MCM containing no exogenous purines (black), 100µM Hypoxanthine (red), 10µM Hypoxanthine (yellow), 100µM Inosine (dark blue), 10µM Inosine (light blue) prior to the drug addition. Normalised level of parasite growth in the presence of inhibitor relative to the vesicle control is indicated on the x-axis. Data analysis and regression curve fitting were conducted using http://www.antimalarial-icestimator.net/ based on two technical replicates per condition. (See Table S4.5 for details on the determined inhibitory concentrations and 95% CI error margins obtained from the regression fit analysis). **(B)** Fractional Inhibitory concentration 50 (FIC) analysis for the combinations of ImmH with MFQ, QN and E64d. Isoboles representing FIC index of each drug in combination are plotted across a range of drug pair concentrations. Reference isobole indicating Loewe additivity model is presented as black dashed line. Drug synergy assays were conducted by Dr. Grennady Wirjanata.

Subsequently, we evaluated the antimalarial activity of both drugs in combination with ImmH in the absence of purines. The main rationale was to uncover synergistic and/or antagonistic effects, among the drug pairs that could signal their common target *(252)*. In assembled isobolograms of ImmH-QN and ImmH-MFQ combinations, both quinolines induced lower killing effect (QN $\sum FIC_{50} \leq 1.43$, MFQ $\sum FIC_{50} \leq 1.70$), than it would be expected from Loewe additivity model ($\sum FIC_{50}=1$) (Fig. 4.7B, Table S4.6). Essentially, a significant skewing of both isoboles can be observed across drug ratios tested, which is indicative of drug antagonism. Contrastingly, the isobologram of ImmH combination with E64d, which is not expected to interact with PfPNP, does not deviate significantly form a linear function, suggesting an additive effect and thus independent activities. Since PfPNP is the only known common target of ImmH and the two quinoline drugs, observed antagonistic effects are likely caused by the competition for PfPNP active site binding.

4.3 Discussion

An insufficient number of validated druggable targets in the *P. falciparum* proteome is one of the major bottlenecks for target-driven drug discovery approaches *(253)*. Diverse bioinformatic strategies have been undertaken to identify and prioritise potential drug targets for malaria *(254–257)*, however without extensive supporting experimental evidence; their output is purely theoretical. More conclusive evidence can be gained from diverse high-throughput studies employing compound libraries with antimalarial properties (e.g. MMV Malaria Box) *(129, 227, 258)*. However, their success in identifying novel drug targets was also limited. Furthermore, whenever a new drug-target pair is characterised, there remains a risk that the compound will interact with its human orthologs or other off-targets and exhibit non-mechanistic

toxicity *(259)*. Identification of specific molecular targets to existing and clinically used antimalarial drugs offers several advantages over candidate compounds. First of all, that knowledge can lead to formulation of more effective drug-combinations, providing direct therapeutic effect. Secondly, targets of the existing and clinically effective antimalarial drugs are highly druggable and their inhibition results in parasite death, while not posing extensive health risks to the host. Considering the apparent polypharmacology of many antimalarial drugs *(81, 99, 214, 215)*, their de-orphanisation could yield a number of novel druggable protein targets. Those can be subsequently exploited for fragment-based lead optimisation approaches to synthesise a new generation of inhibitors, which remain effective against resistant *P. falciparum* strains.

QN and MFQ likely have pleiotropic MoA, involving several targets. Based on MFQ's direct interaction with the ribosome, it has been proposed that the inhibition of parasite protein synthesis is a part of its MoA (81). Low-confidence engagement of several ribosomal subunits by MFQ observed in the lysate ITDR assay (Table 4.1) seems to corroborate these results. We did not observe the whole 80S ribosomal complex stabilization in our assay, which could be explained by the very low thermostability of the 40S and 60S ribosomal complexes in the lysate environment (Fig. 3.4C). This in turn results in their near complete denaturation under ITDR assay's thermal challenges. Additionally, an unknown integrity of the 80S complex in the lysate environment could have contributed to only low degree stabilization of ribosomal subunits observed under MFQ treatment. Optimized ITDR conditions with lower thermal challenge temperature in particular, may be necessary to validate the 80S Ribosome engagement by the MS-CETSA. Interestingly, the engagement of the 80S ribosome subunits was observed only in the lysate setting, similarly to PfPNP which did not exhibit stabilization in intact-cells. This apparent lack of MFQ interaction with these two targets in the intracellular environment could be a direct result of the

previously reported drug-induced endocytosis/membrane perturbations in treated parasites (77). Impaired vesicular transport and membrane dynamics could obstruct or slow down drug penetration inside the parasite over the 1h-long drug exposure in ITDR experiments. Alternatively, an intracellular presence of endogenous metabolites/ligands with higher affinities to these two targets might lead to out-competition of MFQ-binding in assay conditions at this particular stage of the parasite developmental cycle.

Nevertheless, our results demonstrating the inhibition of PfPNP by QN and MFQ (Fig. 4-5) suggest that both drugs possess an additional component to their MoA involving purine metabolism. PfPNP is a dual specificity enzyme important for purine salvage, as well as recycling of purines *(243, 245)*. Its relevance as an antimalarial target has been debated, as the human PNP homologue is present in the RBC in micromolar concentrations and the parasite is capable of scavenging its downstream metabolic products *(251, 260–262)*. Several genetic studies were previously undertaken to shed further light on this issue. PfPNP gene disruption increased parasite's requirement for purines and had proven lethal at physiological hypoxanthine levels in culture *in vitro (153)*. Further evidence in support of the critical importance of PNP for parasite's fitness, pathogenicity and sexual development were produced in *Plasmodium yoelli* mouse model *(263)*. PyPNP *knockout* parasites were viable but attenuated and instead of producing a lethal phenotype were efficiently cleared by infected mice *(263)*. Gene disruption also inhibited oocyst formation in mosquito midgut, preventing parasite transfer to a new host *(263)*. On the other hand, no significant effect of PNP gene knockout was found in *P. berghei* ANKA cerebral malaria model, as both WT and ΔPbPNP infected mice developed cerebral paralysis and haemorrhaging *(264)* suggesting some variability in PNP essentiality between species. Strong evidence in support of PNP importance as a drug-target was generated from a non-human primate *P. falciparum* infection model, demonstrating

clinical efficacy of orally administered DADMe-Immucillin-G, an inhibitor of both human and plasmodium PNPs *(265)*. Drug treatment provoked parasite clearance in otherwise lethal infection in *Aeotus* monkeys, although recrudescence was observed in two out of three subjects few days after the treatment was stopped *(265)*. More recently, it has also been shown that prolonged exposure of *P. falciparum* to sub-lethal concentrations of DADMe-Immucillin-G *in vitro* results in resistance, mediated by point mutations in the catalytic site of PfPNP and mutant gene copy number amplification *(266)*. This study provided conclusive evidence, supporting previous findings that inhibition of PfPNP is crucial for the antimalarial effect of immucillins *(154, 243, 251)*. Efforts to evaluate the effect of specific inhibition of PfPNP led to synthesis of MT-ImmH, an inhibitor with 100-fold higher affinity for parasite enzyme *(154)*. The drug displayed an antimalarial IC50 in *in vitro* assays within nanomolar range, however it did not completely attenuate parasite growth below micromolar concentrations *(154, 243)*, suggesting that inhibition of the host enzyme is also required to kill the parasite.

The antagonistic interactions observed for QN and MFQ in combination with ImmH supports the notion that PfPNP inhibition contributes to their antimalarial effect. Interestingly, while Immucillins appear to exert their antimalarial effect through simultaneous inhibition of host and parasite PNP enzymes, we found no evidence that QN and MFQ interact with human PNP. The composition of the binding pocket of two structures resolved in this study is very similar to previously described PfPNP structures *(154, 162)*. The co-crystal structure of PfPNP-ImmH determined by Cassera and colleagues revealed a large solvent-filled pocket within enzyme's active site located near 5'-hydroxyl group of ImmH *(265)*. This structural feature distinguishes the plasmodial enzyme from its human counterpart resulting in distinct substrate binding specificities between the two *(265)* and could be responsible for the interaction with quinoline compounds or the lack thereof. Overall, the data suggest that QN and MFQ might represent specific inhibitors of the *P. falciparum* PNP, however the lack of

interaction with the host enzyme needs to be further verified. The positioning of both quinoline drugs within the active site pocket of PfPNP is very similar to that of inosine and ImmH in the previously determined co-crystal structures *(154, 162)* and their binding is also mediated mainly through hydrophobic interactions. This is agreement with our data suggesting that both quinolines represent competitive reversible inhibitors of the enzyme, similarly to Immucillins *(267)*. Inhibition of PfPNP by the two quinolines, coinciding with retaining a fully functional hPNP in the host-cell, would explain observed invariable drug efficacy under different purine availability conditions. Nevertheless, we suggest that the described MFQ/QN-PfPNP interaction is additive rather than representing the dominant MoA of either drug. Other killing mechanisms might be more pronounced at concentrations required to kill the parasite in the *in vitro* assay conditions. However, in a clinical setting both quinoline methanols remain in circulation for substantially longer, either due to very long half-life (MFQ) or repetitive administration (QN) *(236)*, thus the potential impact of a prolonged PfPNP inhibition on parasite fitness is likely.

The identification of PfPNP as the target of QN and MFQ illustrates one of the main advantages of CETSA - its capacity to identify direct drug-targets without any prior knowledge about their mechanism or site of action *(142)*. The current gold standard traditional approach in *P. falciparum* relies on generating resistant mutants through prolonged *in vitro* parasite exposure to sublethal drug concentrations and identifying genetic mutations responsible for increased drug tolerance (227). However, this methodology poses the risk of identifying mechanisms of resistance to the drug, rather than their actual molecular targets. This was recently demonstrated by identification of PfCARL as the protein mediating resistance to KAF-156, rather than its direct protein target, it was originally believed to be *(268, 269)*. The majority of other studies (e.g. the recent identification of 80S ribosome as the target of MFQ *(81)*) rely

on initial data pointing to a specific target/MoA and are targeted at validating or rejecting that given interaction.

Nevertheless, CETSA possesses its limitations and may omit clinically relevant targets, similarly to other drug-target identification techniques and studies. QN and MFQ ITDR assays revealed a number of other proteins exhibiting apparent low significance stabilisations under drug exposure. A protein might not satisfy cut-off criteria in the ITDR analysis due to low abundance, poor solubility, particularly high/low Tm, sub-optimal assay conditions or other factors. Therefore, those could theoretically represent other direct protein targets, downstream effectors of the drug's MoA or other interacting proteins, such as transmembrane drug transporters. The Uncharacterised protein PF3D7_1456300, was the sole protein other than PfPNP responsive to both drugs. Furthermore, it showed a stabilisation profile similar to that of PfPNP and based on a structure-driven prediction of its function, similarly to PNP might be involved in nucleotide binding. Its predicted transmembrane nature suggests that it could represent an unknown transporter of QN/MFQ. If it is indeed involved in drug import of efflux from the cell and/or an organelle, mutations and copy number amplification to this gene might affect parasite susceptibility to those two quinoline drugs. However, prior to launching a full-scale target validation studies, the occurrence of observed stabilisations should be reproduced and demonstrated with a higher degree of confidence. Such follow-up studies, could for instance, involve ITDR assays with different thermal challenge temperatures or the melt curve CETSA assays in the presence or absence of physiologically relevant drug concentrations. In particular, the employment of an additional ITDR thermal challenge temperature or extending drug-exposure time could also allow validation of previously reported 80S Ribosome engagement *(81)* with a higher degree of confidence than the current study offers. Other experimental approaches could also be explored for the validation of potential drug-target interactions suggested by CETSA. Those, for instance, may involve the *in*

vitro biochemical studies using purified protein or genomic modifications of the parasite attempting to knock-out, knock-down or overexpress the protein in question. However, any identified and biochemically validated target of QN and MFQ, including the PfPNP should be subsequently evaluated for its clinical significance. Targeted genetic, proteomic and transcriptomic analysis of existing MFQ/QN-resistant clinical isolates and *in vitro* laboratory strains might reveal mutations, gene copy number variations, significant changes in gene/protein expression strongly associated with the resistance phenotype.

CHAPTER 5

Antimalarial drug discovery from Traditional Chinese Medicine (TCM)

The emergence of resistance to nearly all groups of antimalarial drugs has substantially decreased their usefulness in affected regions. The shrinking array of compounds, which still retain clinical effectiveness is stressing the need for the development of novel drugs, preferably representing radically different chemotypes and possessing distinct MoA *(17)*. Natural products are known for the unprecedented structural variability they offer, while retaining biological activity *(270)*. Unsurprisingly, the majority of pharmaceuticals currently in use are natural products themselves, their derivatives or have been inspired by natural products *(270, 271)*. Antimalarial drugs are not an exception, considering that the two most important compound families: quinolines and artemisinins are derived from natural products: quinine and artemisinin. TCM represents the largest and the most extensively documented body of knowledge on medicinal applications of plants, naturally occurring minerals and animal-derived products dating to ~2000BC *(114)*. Artemisinin, the active antimalarial compound isolated from a medicinal plant *Artemisia annua* in 1972, was discovered based on ancient records of TCM preparations for the treatment of malaria-like symptoms *(98)*. In this work, we explored TCM preparations in the search of new lead antimalarial compounds. For that purpose, we designed a pipeline for isolation and identification of natural products with antimalarial properties from raw TCM materials (Fig. 5.1). We provide the proof of principle for the pipeline, screening a batch of 15 selected TCM candidates, identifying the most potent antimalarial extracts and isolating bioactive compounds from one of them. Subsequently, we applied CETSA to identify potential molecular targets of the more potent of the two isolated compounds. Following

necessary validation of the candidate druggable target's relevance for the antimalarial effect of the isolated compounds, those targets could be used for subsequent target-based drug discovery approaches in order to identify novel more potent inhibitors through compound or fragment library screening.

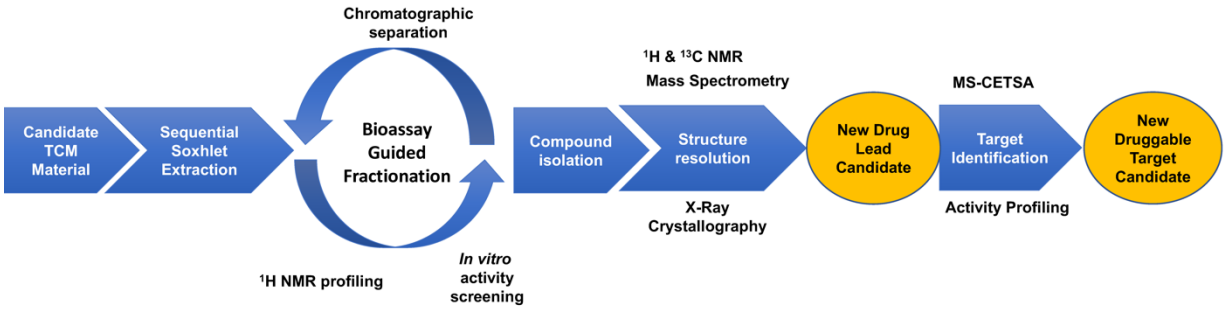

Figure 5.1 – Antimalarial drug-discovery from TCM pipeline overview

The initial prerequisite for a functional 'Drug discovery pipeline from TCM' was establishing a suitable method for extraction of bioactive phytochemicals from the crude biological material. Methods traditionally used in the medicinal preparations in TCM: infusion, maceration and decoction, although effective they tend to produce herbal extracts of high complexity *(272)*. This has proven a major obstacle for the identification of their biologically active components, primarily due to difficult sample clean-up and challenging separation of their component phytochemicals (results not shown). The implementation of a sequential Soxhlet extraction method partially resolved that problem, providing high extraction efficiency with an added benefit of pre-fractionation of plant's component phytochemicals, which decreased the crude sample complexity *(273)*. Preliminary extraction with hexane, permitted us to eliminate highly nonpolar compounds, such as oils and waxes, which tend to interfere with subsequent chromatographic separation *(274)*. Remaining 'defatted' plant powder was subjected to further 2-step extraction with additional solvents of increasing

polarity: dichloromethane (DCM) and methanol (MeOH), producing two extracts composed of phytochemicals of moderate and high polarity, respectively.

5.1 Preliminary screening of selected TCM materials for antimalarial activity

Fifteen TCM antimalarial candidates (Table 5.1), selected based on their proven activity against malaria or historical use for treatment of malaria-like symptoms *(163–165)* were pulverised and extracted. Consequently, each TCM candidate produced three independent extracts (Hex/DCM/MeOH) each composed of a distinct set of phytochemicals.

Abbreviation	Chinese name	Latin name	Type of material
AY	Ai Ye (*艾叶*)	*Artemisia argyi*	Leaves / stems
BJ	Bie Jia (鳖甲)	*Trionyx sinensis*	Bones
BL	Bing Lang (槟榔)	*Areca Catechu*	Nuts
CE	Cang Erzi (苍耳子)	*Xanthium sibiricum*	Nuts
CG	Cao Guo (草果)	*Ammomum Tsao-Ko*	Nuts
CH	Chai Hu (柴胡)	*Radix Bupleuri*	Stems
CX	Chuan Xiong (川芎)	*Ligusticum Rhizome*	Roots
CZ	Cang Zhu (苍术)	*Atractylodes lancea*	Bark
DGP	Di Gu Pi (地骨皮)	*Lycium chinense*	Stems
HQ	Huang Qin (黄芩)	*Scutellaria baicalensis*	Roots
HSW	He Shou Wu (何首乌)	*Polygonum multiflorum*	Bark
JH	Ju Hua (菊花)	*Chrysanthemum*	Flowers
LDC	Long Dan Cao (龙胆草)	*Gentiana manshurica*	Stems
XHC	Xian He Cao (仙鹤草)	*Herba Agrimoniae*	Leaves / stems
XXC	Xi Xian Cao (豨莶草)	*Siegesbeckia oritentalis*	Stems

Table 5.1 – Antimalarial Traditional Chinese Medicine candidates

Their antimalarial activity was determined based on a standardised growth inhibition assay in the presence of varying extract concentration against the T996 *P. falciparum* parasites, determining their respective $IC_{50,}$ IC_{90} and IC_{99} (Fig. 5.2). In brief, synchronised mid-ring parasites in culture *in vitro* were exposed to varying concentrations of isolated extracts and incubated for 48h (equivalent to an entire *P. falciparum* developmental cycle. Subsequently parasites were stained with DNA-binding fluorescent dye and the density of parasitized cells was measured in each

condition via flow cytometry and contrasted with that of vesicle- and death- controls. Regression analysis of resulting data allowed accurate quantification of extracts' inhibitory effect on parasite growth. A range of extracts (i.e. Hex: BL, HSW; DCM: BL, CE, CH and HSW; MeOH: CE, CH, CX, LDC, CZ) exhibited no apparent activity against *P. falciparum* at concentrations tested. The remaining extracts inhibited parasite growth to a varying extent, with IC_{50}s spanning from 3 to 366 μg/mL. Overall, DCM extracts exhibited the highest activity, whilst highly polar MeOH extracts required in general much higher concentrations to attenuate parasite growth (Fig. 5.2). Interestingly, despite their highly hydrophobic character, several Hex extracts also exhibited potent antimalarial activities suggesting they might contain active compounds. Partial (i.e. >50%; <90%) inhibition of parasite growth observed for Hex: CE, BJ, CH, CX and MeOH: XXC, JH extracts prohibited us from defining their respective IC_{90} and IC_{99}. Thus, the values were extrapolated from the regression fit analysis of available experimental data. Additionally, different degree of haemolysis in treated samples was observed at high concentrations of 14 extracts, which can be considered an indicator of general cytotoxicity *(275)*. The haemolytic effect, defined as >10% loss in the cell concentration of treated sample and quantified through Flow Cytometry, was observed at ≥125μg/mL for CH-DCM and XXC-DCM extracts, at ≥250μg/mL CG-Hex, CZ-Hex, XHC-Hex, CH-Hex, JH-Hex, DGP-DCM, CZ-DCM CH-MeOH and BL-MeOH extracts and at 500μg/mL for HQ-DCM and XHC-DCM extracts (Fig. 5.2).

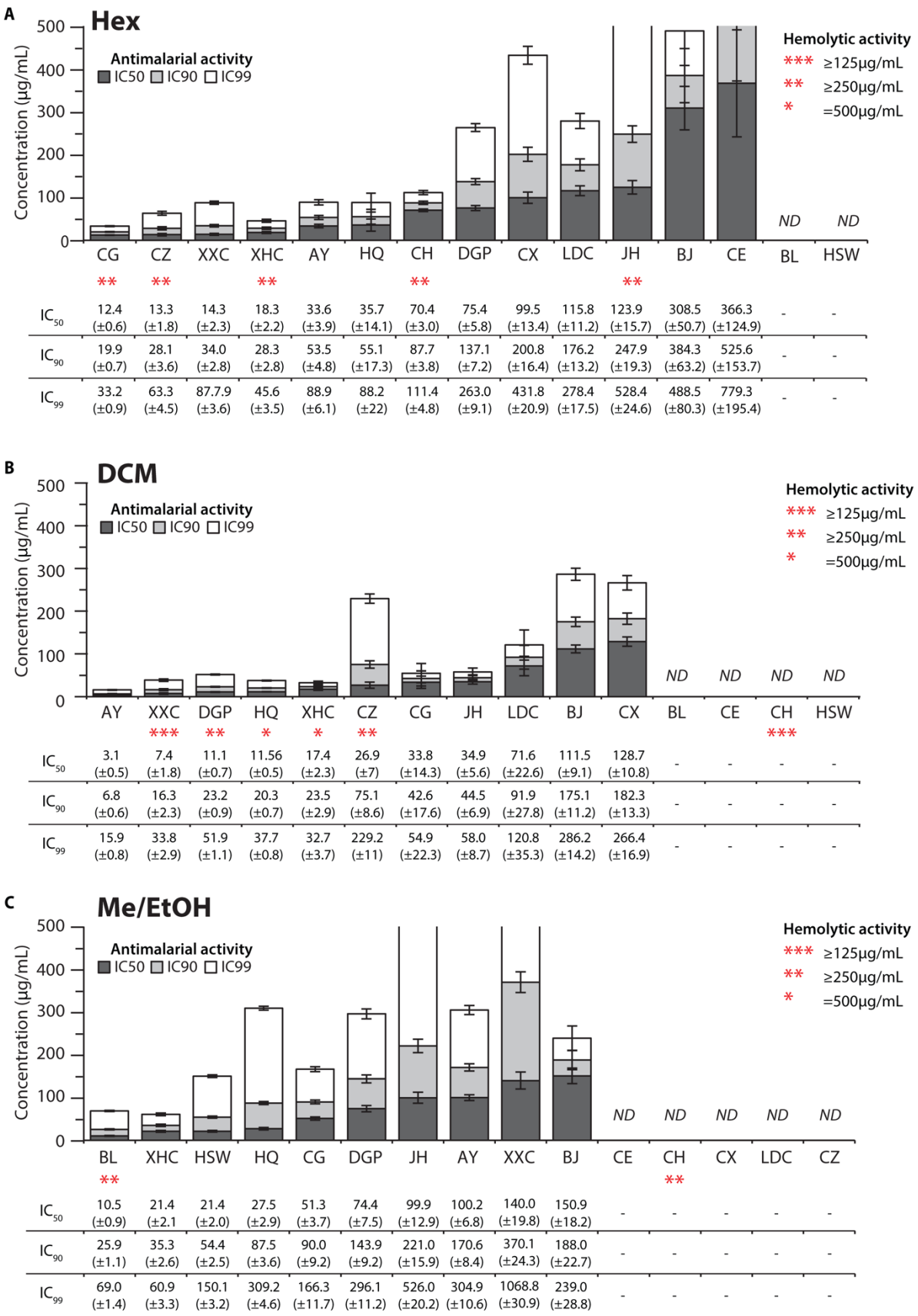

Figure 5.2 – Antimalarial activity of crude TCM extracts

Inhibitory concentration values [IC_{50} – dark grey; IC_{90} – light grey; IC_{99} – white (µg/mL)] calculated based on the regression fit analysis of T996 strain *P. falciparum in vitro* growth inhibition assays are represented as a bar chart for 15 extracts isolated with Hexane (**A**), DCM (**B**) and Methanol (**C**) from

selected TCM candidates (indicated on the x axis). The IC values are listed below each graph in a table. 'ND' refers to extracts which did not inhibit parasite growth by more than >50% in 500μg/mL concentration and their respective IC_{50} could not be determined. Error bars represent 95% confidence intervals. Additionally, the extent of haemolytic effect, observed during antimalarial growth inhibition assays and defined as the decrease in cell concentration by >10% in treated samples is indicated for each extract with red asterisks. Haemolytic effect was observed only at the 500μg/mL extract concentration (one asterisk), at 250μg/mL and higher conc. (two asterisks) and at 125μg/mL concentrations and higher (three asterisks).

The selection of extracts for further processing was based on three main characteristics: (i) relative antimalarial potency (i.e. IC_{50} values), (ii) ability to completely attenuate parasite growth represented by IC_{99} and (iii) the general cytotoxicity represented by the degree of extracts' haemolytic activity. Among the six most potent extracts (i.e. IC_{50}<20μg /mL and IC_{99}<50μg /mL), four were extracted with DCM (AY, XXC, HQ and XHC) and remaining two with Hex (CG and XHC). The highest relative antimalarial activity accompanied by the lack of haemolytic effect at the highest dose (i.e. ≤500μg/mL) was observed for AY-DCM extract suggesting that its antimalarial activity is likely specific. Conversely, the remaining five top candidates exhibited different degrees of haemolytic activity with HQ-DCM and XHC-DCM extracts being the least and XXC-DCM the most cytotoxic. Despite the extensive chromatographic separation of AY-DCM extracts, we did not succeed in isolating its component bioactive compounds in a purity high enough to allow structure resolution studies. Therefore, fractionation of HQ-DCM was conducted instead, aiming to isolate the compound(s) responsible for its potent antimalarial properties.

5.2 Bioassay-guided fractionation of *Scutellaria baicalensis* (HQ) DCM extract

The material isolated with DCM extraction of 'defatted' pulverised HQ was an equivalent to 0.88% of starting dry plant biomass. In order to de-complexify the phytochemical mixture present in the HQ-DCM extract, we conducted chromatography-based fractionation using a gradient of Hex and Ethyl Acetate, separating compounds based on polarity. Resulting fractions were subsequently tested for the extent of antimalarial activity they possess. Upon chromatographic separation of HQ-DCM, three fractions (i.e. F3, F4 and F5) with substantially improved antimalarial activity over the Crude HQ-DCM extract were isolated (Fig. 5.3). Their respective IC_{50} values were 70-80% lower and IC_{99} values 60-84% lower than the non-fractionated extract with higher relative potency observed in F3-F4. Mass spectrometry analysis revealed the same ion pattern in F3 and F4 with peaks at m/z 285, 179 and 157 and distinct signal present in F5 with m/z 375 (Fig, S5.1). The similarity of ^{1}H-NMR profiles position between F3/F4 (Fig. S5.2) suggested a similar chemical composition. The ^{1}H-NMR spectrum of F5 exhibited a distinct peak pattern from F3/F4, but some similarities were present suggesting potentially structurally related compounds. However, due to insufficient purity and low quantity of isolated material, structure resolution of their components or their further chromatographic separation could not be performed. De novo high-resolution separation of 1.1g of HQ-DCM was performed targeting the polarity region corresponding to the F3-5 elution range. All three compounds previously enriched in F3, F4 and F5 were successfully re-isolated in high purity in F9' [16.8mg], F12'-F13' [45mg] and F17' [31.3mg], respectively (Table 5.2, Fig. S5.3). Characteristic peaks were also observed in neighbouring fractions F10' and F18'-F19', however TLC and NMR analysis indicated a higher degree of contamination with other compounds.

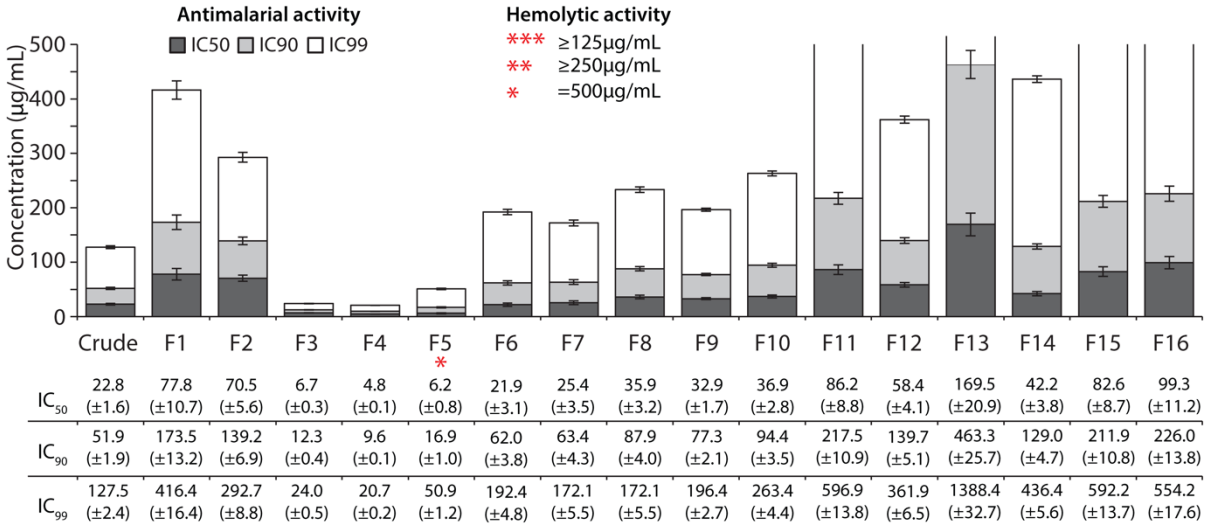

Figure 5.3 – Antimalarial activity of HQ DCM extract fractions

Inhibitory concentration values [IC_{50} – dark grey; IC_{90} – light grey; IC_{99} – white (µg/mL)] calculated based on the regression fit analysis of T996 strain *P. falciparum in vitro* growth inhibition assays are represented as a bar chart for 16 fractions isolated from initial chromatographic separation of HQ DCM extract (indicated on the x axis). The IC values are listed below each graph in a table. 'ND' refers to extracts which did not inhibit parasite growth by more than >50% in 500µg/mL concentration and their respective IC_{50} could not be determined. Error bars represent 95% confidence intervals. Additionally, the extent of haemolytic effect, observed during antimalarial growth inhibition assays and defined as the decrease in cell concentration by >10% in treated samples is indicated for each extract with red asterisks. Haemolytic effect was observed only at the 500µg/mL extract concentration (one asterisk), at 250µg/mL and higher conc. (two asterisks) and at 125µg/mL concentrations and higher (three asterisks).

F3	F4	F5	F9'	F13'	F17'
12.98 (s)	12.98 (s)	12.28 (s)	13.00 (1H, s, OH-5)	12.49 (1H, s, 5-OH),	12.28 (1H, s, OH),
12.49 (s)	12.49 (s)	7.89-7.93 (m)	7.87~7.89 (2H, d, H-2', 6')	7.91~7.93 (2H, d, H-2',6'),	7.28~7.32 (1H, t, J=8.36, H),
7.87~7.93 (m)	7.87~7.93 (m)	7.50-7.65 (m)	7.49~7.57 (3H, m, H- 3', 4', 5')	7.55~7.57 (3H, m, H-3',4',5')	6.65~6.67 (2H, d,s, H, H)
7.50~7.57 (m)	7.52~7.58 (m)	7.28~7.32 (m)	6.66 (1H, s, H-8)	6.69 (1H, s, H-3),	6.52~6.54 (1H, d, J=8.32, H),
6.69 (s)	6.69 (s)	6.65~6.68 (m)	6.61 (1H, s, H-3)	6.45 (1H, s, H-6)	4.1 (3H, s, OCH_3),
6.67 (s)	6.67 (s)	6.52~6.54 (d)	5.36 (1H, br s, OH-6)	6.3 (1H, br, 7-OH),	3.91~3.93 (6H, s, s, OCH_3, OCH_3),
6.61 (s)	6.61 (s)	5.29 (s)	4.05 (3H, s, OCH_3)	4.04 (3H, s, OCH_3)	3.81 (3H, s, OCH_3).
6.45 (s)	6.45 (s)	4.1 (s)			
5.35 (br)	5.29 (s)	3.94 (s)			
5.29 (s)	4.04 (s)	3.93 (s)			
4.05 (s)	3.94-3.98 (m)	3.91 (s)			
2.8-0.8 (m)	1.4 (s) 1.25	3.8 (s) 1.28 (s)			

Table 5.2 – ^{1}H-NMR evidence of a successful re-isolation of HQDCM F3-5

5.2.1 Structure determination of wogonin

Aiming to identify the structure of the antimalarial compound present in active fractions HQ-DCM F12' and F13' we employed a combination of available analytical chemistry techniques to characterise it. The compound isolated in HQ-DCM F12' and F13' was yellow and had a crystalline powder appearance. Upon TLC examination, the compound of interest has proven UV active, which suggests the presence of aromatic rings in its structure. It was also detected by Molybdate staining with trace amounts of one more polar compound. In order to further elucidate the compound's structure, F13' was analysed by ^{1}H-NMR and ^{13}C-NMR Spectroscopy. The ^{1}H-NMR spectrum (Fig. 5.4A) suggested the presence of 12 independent hydrogen atoms. The sharp singlet corresponding to 3H of identical character at ~4ppm was identified as typical for methoxy group and its location closer to 4ppm rather than 3ppm suggested its attachment to an aromatic moiety, rather than a non-aromatic moiety. Another very

sharp distinct peak at ~12.5ppm was identified as characteristic for hydrogen bonded enolic or phenolic proton, rather than carboxylic acid, which tends to produce broad peaks in this region. Several peaks in the aromatic region (7.9-6.3ppm) confirmed the aromatic character of the molecule with two independent H (s, 6.7ppm and s 6.4ppm), two very similar but non-identical H (two overlapping doublets, 7.9ppm) and a complex multiplet at 7.6ppm, which could correspond to 3H. Another variable (i.e. sometimes sharp, sometimes broad, sometimes absent) peak at 6.3ppm was identified as an exchangeable proton changing its character depending on the pH of the environment. Remaining peaks were classified as irrelevant: 5.3ppm-$CHCl_3$, 7.26ppm-$CDCl_3$, ~2ppm-H_2O/long hydrocarbon chains, ~0ppm-reference. Based on the ^{13}C-NMR spectrum (Fig. 5.4B) we determined that the molecule is likely composed of 16 independent carbon atoms. Two larger peaks at 129.2ppm and 126.1ppm each appeared to represent two carbons in a symmetrical aromatic system. The peak at 182ppm was characteristic for an acid, ester or a ketone, the peak at 61ppm was typical for C-O orientation in the methoxy group and peaks at 131-126ppm were identified as C=C in alkenes. Overall, the molecule profile suggested presence of one aryl group (6C), one methoxy group (1C) leaving 9C including a carbonyl group, which fit the flavonoid ring system. The sample was then analysed by COSY-NMR revealing only one cross-peak (results not shown) between 7.6ppm and 7.9ppm suggesting coupling of corresponding protons, which based on previous NMR experiments were most likely associated with the aryl group.

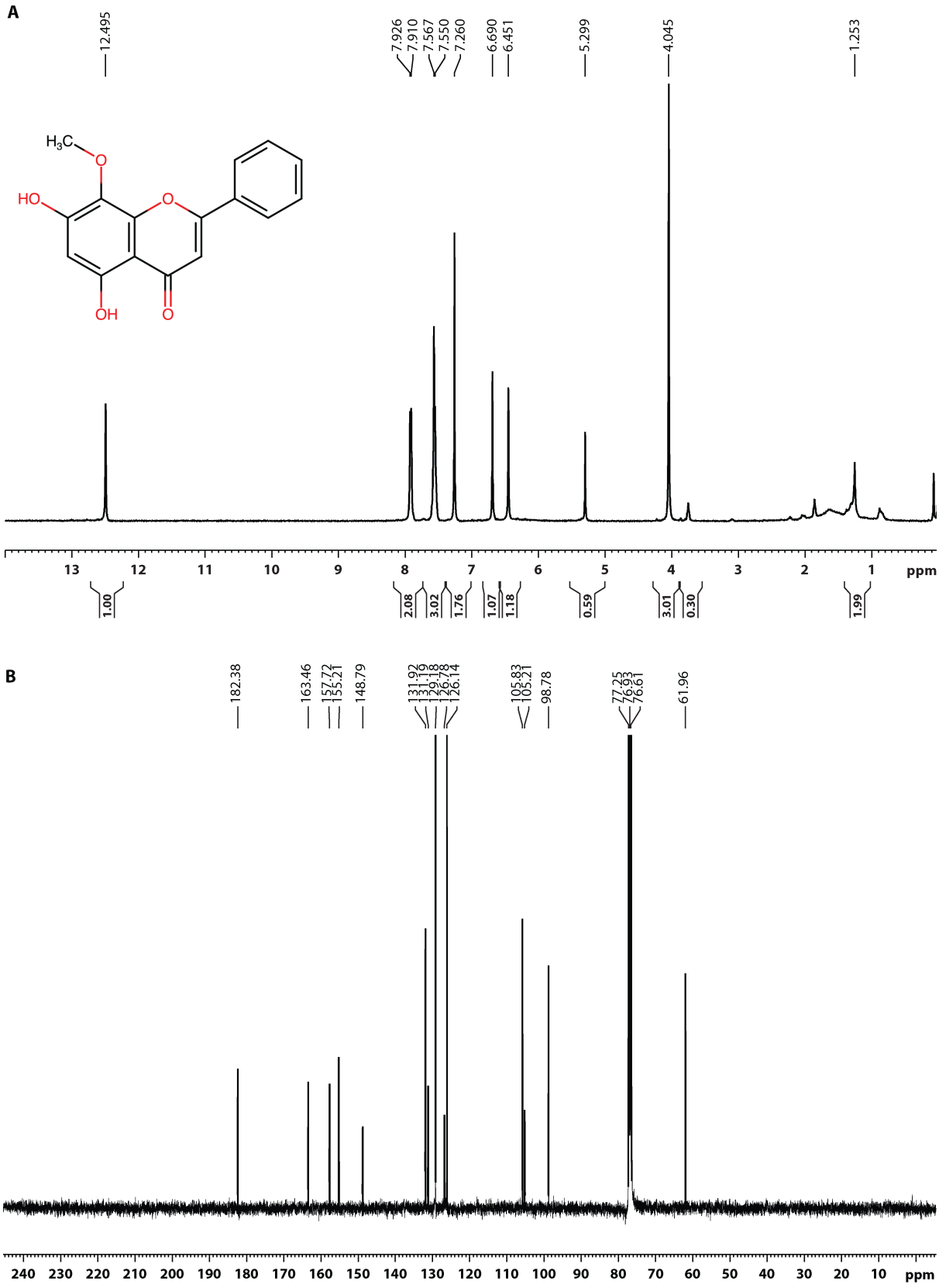

Figure 5.4 – HQ-DCM-F13' profiling by ^{1}H-NMR and ^{13}C-NMR Spectroscopy

Relative signal intensity (y-axis) is plotted against the chemical shift (ppm) (x-axis) of detected hydrogen (**A**) or carbon (**B**) atoms. The chemical shift of each atom is indicated on top of each peak and in case of the proton NMR the integration of each peak area is indicated below the x-axis. (**A**) ^{1}H NMR (400Hz, CDCl3) δ 12.49 (1H, s, 5-OH), 7.91~7.93 (2H, d, H-2,6), 7.55~7.57 (3H, m, H-3,4,5), 6.69 (1H, s, H-3),

6.45 (1H, s, H-6), 6.3 (1H, br, 7-OH), 4.04 (3H, s, OCH3). (**B**) ^{13}C-NMR (400Mhz, CDCl3) δ 182.38 (C-4), 163.46 (C-2), 157.72 (C-7), 155.21 (C-5), 148.79 (C-9), 131.92 (C-4'), 131.19 (C-2',6'), 129.18 (C-1'), 126.78 (C-3', 5'), 126.14 (C-8), 105.83 (C-3), 105.21 (C-10), 98.78 (C-6), 61.96 (OCH3).

Mass Spectrometry analysis of F12' and F13' revealed a dominant molecular ion peak of 285 m/z, identical minor peaks at 157m/z and 179m/z as in HQ-DCM F3 and F4 and a small ion at m/z, 363 or 622, presumably representing previously observed trace contaminants (Fig. S5.4). Based on the above evidence the m/z 285 peak could correspond to [C16H12O5] dihydroxy-methoxyflavone, whilst the m/z 179 and 157 peaks to its fragments produced during ionisation *(276, 277)*. The crystallised compound was analysed by X-Ray crystallography, which confirmed the presence of the previously assumed flavonoid ring system and allowed us to determine the exact regiochemistry (Fig. 5.5). The isolated compound was identified as 5,7 –Dihydroxy - 8 -Methoxyflavone (wogonin) and the obtained NMR spectra were matched to the previously reported profile (Table 5.3) *(278)*.

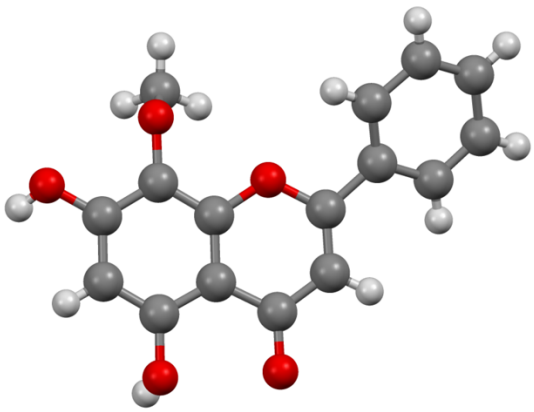

Figure 5.5 – X-ray spectroscopy crystal structure resolution of HQDCM-F13' compound

The x-ray diffraction analysis was performed at NTU SPMS X-ray crystallography facility. Carbon atoms are represented in grey, oxygen red and hydrogen white.

^{1}H NMR (400Hz, $CDCl_3$)	**Wogonin** ^{1}H-NMR (100MHz, $CDCl_3$)*(278)*	**^{13}C-NMR (400Mhz, $CDCl_3$)**	**Wogonin** ^{13}C-NMR (125 MHz, $CDCl_3$) *(278)*
12.49 (1H, s, 5-OH),	-	163.46 (C-2)	163.6 (C-2)
7.91~7.93 (2H, d, H-2',6'),	7.91~7.93 (2 H, m, 2',5'-H);	105.83 (C-3)	105.9 (C-3)
7.55~7.57 (3H, m, H-3',4',5')	7.54~7.58 (3 H, m, 3', 4', 5'-H)	182.38 (C-4)	182.5 (C-4)
6.69 (1H, s, H-3),	6.69 (1 H, s, 3-H),	155.21 (C-5)	155.4 (C-5)
6.45 (1H, s, H-6)	6.45 (1 H, s, 6-H),	98.78 (C-6)	98.9 (C-6)
6.3 (1H, br, 7-OH),	-	157.72 (C-7)	157.8(C-7)
4.04 (3H, s, OCH_3)	4.04 (3 H, s, OCH_3),	126.14 (C-8)	126.2 (C-8)
		148.79 (C-9)	148.9 (C-9)
		105.21 (C-10)	105.3 (C-10)
		129.18 (C-1')	129.3 (C-1')
		131.19 (C-2',6')	131.3 (C-2' ,6')
		126.78 (C-3', 5')	126.9 (C-3' ,5')
		131.92 (C-4')	132.0 (C-4')
		61.96 (OCH_3)	62.1 (OCH_3)

Table 5.3 – ^{1}H-NMR evidence for identification of HQDCM-F13' as wogonin

5.2.2 Structure determination of negletein

In order to define the structure of the antimalarial compound present in active fraction HQ-DCM F9' we employed NMR Spectroscopy and Mass Spectrometry. Similarly to wogonin, the compound isolated in F9' was a yellow crystalline powder. It was UV active and stained by Molybdate suggesting the presence of aromatic rings in its structure. The NMR spectroscopy analysis revealed ^{1}H/^{13}C NMR profiles very similar to wogonin suggesting that the F9' compound is likely a structurally related compound. The proton NMR spectrum (Fig. 5.6A) indicated the presence of 12H atoms including a single methoxy group (4.05ppm), an oxygen-bound enolic/phenolic proton (13ppm), an exchangeable likely hydroxy-proton (5.3ppm) and two uncoupled protons in the aromatic region (6.61ppm and 6.66ppm). The ^{13}C-NMR analysis revealed 16 independent carbon atoms fitting the profile of a flavonoid ring system observed in HQ-DCM F3 and F4 (Fig. 5.6B). Two larger peaks at 129ppm and 126ppm corresponding to two carbon atoms in a symmetrical aromatic system each were

determined a part of the aryl group. Furthermore, carbon atoms corresponding to a methoxy group (60.8ppm), a ketone (183ppm) and C=C alkenes were observed. COSY-NMR analysis revealed only one cross peak (results not shown) between 7.53ppm and 7.88ppm peaks. Therefore, the two corresponding proton pairs were deemed likely located on the aryl group. Mass spectrometry analysis of the corresponding fractions F9' and F10' revealed the same molecular ions previously identified in F3, F4, F12' and F13' **(**Fig. S5.4**)**. The comparison of HQDCMF3 compound's ^{1}H-NMR and ^{13}C-NMR spectra with published NMR profiles of possible compounds containing the flavone skeleton, a methoxy group and two hydroxy groups permitted identification of the molecule in 5,6-Dihydroxy-7-methoxyflavone (negletein) (Table 5.4) *(279)*, a compound never before isolated from *S. baicalensis* to our knowledge.

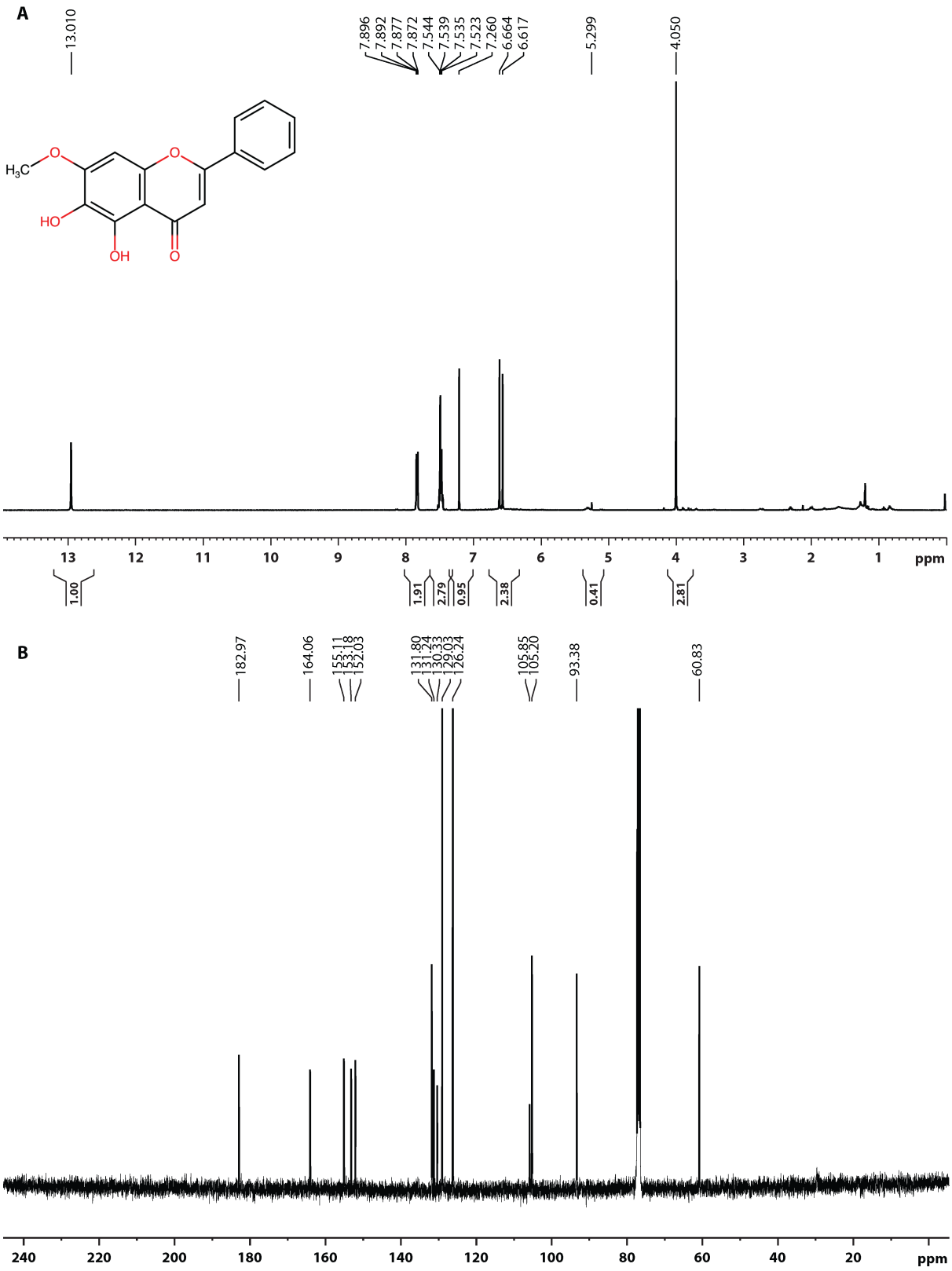

Figure 5.6 – HQDCM-F9' profiling by ^{1}H-NMR and ^{13}C-NMR Spectroscopy

Relative signal intensity (y-axis) is plotted against the chemical shift (ppm) (x-axis) of detected hydrogen (**A**) or carbon (**B**) atoms. The chemical shift of each atom is indicated on top of each peak and in case of the proton NMR the integration of each peak area is indicated below the x-axis. (**A**) ^{1}H NMR (400Hz, $CDCl_3$) δ 13.00 (1H, s, OH-5), 7.87~7.89 (2H, d, H-2', 6'), 7.49~7.57 (3H, m, H- 3', 4', 5'), 6.66 (1H, s, H-8), 6.61 (1H, s, H-3), 5.36 (1H, br s, OH-6), 4.05 (3H, s, OCH_3). (**B**) ^{13}C-NMR (400Mhz, $CDCl_3$) δ

182.97 (C-4), 164.06 (C-2), 155.11 (C-8), 153.18 (C-6), 152.03 (C-10), 131.80 (C-1'), 131.24 (C-7), 130.33 (C-4'), 129.03 (3', 5'), 126.24 (C-2', 6'), 105.85 (C-5), 105.20 (C-3), 93.38 (C-9), 60.82 (OCH_3)

^{1}H NMR (400Hz, $CDCl_3$)	**Negletein** ^{1}H-NMR (400 MHz, $CDCl_3$) *(279)*	**^{13}C-NMR (400Mhz, $CDCl_3$)**	**Negletein** ^{13}C-NMR (100 MHz, $CDCl_3$)*(279)*
4.05 (3H, s, OCH_3).	4.05 (3H, s, Ar-OCH3);	182.97 (C-4)	183.02 (C4)
5.36 (1H, br s, OH-6),	6.50 (1H, s, C6 -OH),	164.06 (C-2)	164.11 (C2)
6.61 (1H, s, H-3)	6.61 (1H, s, C3 -H)	155.11 (C-8)	155.34 (C7)
6.66 (1H, s, H-8)	6.66 (1H, s, C8 -H)	153.18 (C-6)	153.27 (C5)
7.49~7.57 (3H, m, H- 3', 4', 5')	7.54-7.52 (3H, m, C3′ -H, C4′ -H, C5′ - H)	152.03 (C-10)	152.19 (C8a)
7.87~7.89 (2H, d, H-2', 6')	7.89-7.87 (2H, m, C2′ -H, C6′ -H)	131.80 (C-1'),	131.84 (C1′)
13.00 (1H, s, OH-5)	13.01 (1H, s, C5 -OH)	131.24 (C-7)	131.35 (C6)
		130.33 (C-4'),	130.52 (C4′)
		129.03 (C-3', 5'),	129.09 (C3′ C6′)
		126.24 (C-2', 6'),	126.31 (C2′, C5′)
		105.85 (C-5)	105.89 (C4a)
		105.20 (C-3)	105.28 (C3)
		93.38 (C-9)	93.53 (C8)
		60.82 (OCH_3)a	60.87 (C 7 - OCH3)

Table 5.4 – ^{1}H-NMR evidence for identification of HQDCM-F9' as negletein

5.2.3 Structure determination of skullcapflavone II

The third active compound initially observed in the HQDCMF5 fraction and isolated in high purity at HQ-DCM F17' shared several characteristics with wogonin and negletein. The substance was a light-yellow powder, exhibited UV activity and was also stained by Molybdate. ^{1}H-NMR spectroscopic analysis of F17' suggested the presence of 19 hydrogen atoms, including four methoxy groups in an aromatic setting (3.8-4.1ppm) and a sharp peak in the 12.28ppm region, characteristic for an oxygen bonded enolic or phenolic proton (Fig. 5.7A). The remaining peaks within the 6.5-7.3ppm region suggested the presence of four single protons in the aromatic environment. ^{13}C-NMR spectroscopy analysis of HQDCM-F17' suggested the presence of 19 carbon atoms in its structure, including 4 methoxy groups (55-62ppm),

a ketone (183ppm) and remaining peaks within 103-162ppm range coherent with C=C profile in alkenes (Fig 5.7B). This would be in agreement with the flavonoid ring system with four methoxy groups. An unaccounted for hydrogen/group could be explained by the presence of an exchangeable proton in a hydroxy group, which tends to form ambiguous peaks or a different group (e.g. Cl, Br, F, NO_2) residing on its place. However, given known flavonoid natural products, the hydroxy group seemed most likely. Mass spectrometry analysis if F17' identified one major component with m/z 375 and a smaller peak 175 m/z, which likely represents fragmentation ions (Fig. S5.5). Overall, ^{1}H-NMR and MS profiles of F17' suggest that we successfully re-isolated enriched component of HQDCM-F5 and its profile fits dihydroxy-tetramethoxy-flavonoid. In order to determine the exact structure of this molecule, we investigated the coupling between ^{13}C and/or ^{1}H atoms through 2D NMR experiments. Homonuclear correlation spectroscopy (COSY) analysis (Fig. S5.6) revealed cross-peaks between 7.3ppm 'triplet' and two 6.5/6.7ppm 'doublet' protons, suggesting their adjacent localisation in the structure. Further information on short and long-distance heteronuclear coupling between ^{13}C and ^{1}H atoms was gained through Heteronuclear Multiple Bond Correlation (HMBC) (Fig. S5.7) and Heteronuclear Single Quantum Coherence (HSQC) (Fig. S5.8) 2D NMR experiments (Table 5.2). Based on the above we identified the compound isolated from HQ-DCM F17' as skullcapflavone II (SKF-II) and matched it to previously reported ^{1}H-NMR spectrum *(280)* in the absence of spectroscopic data provided by the authors.

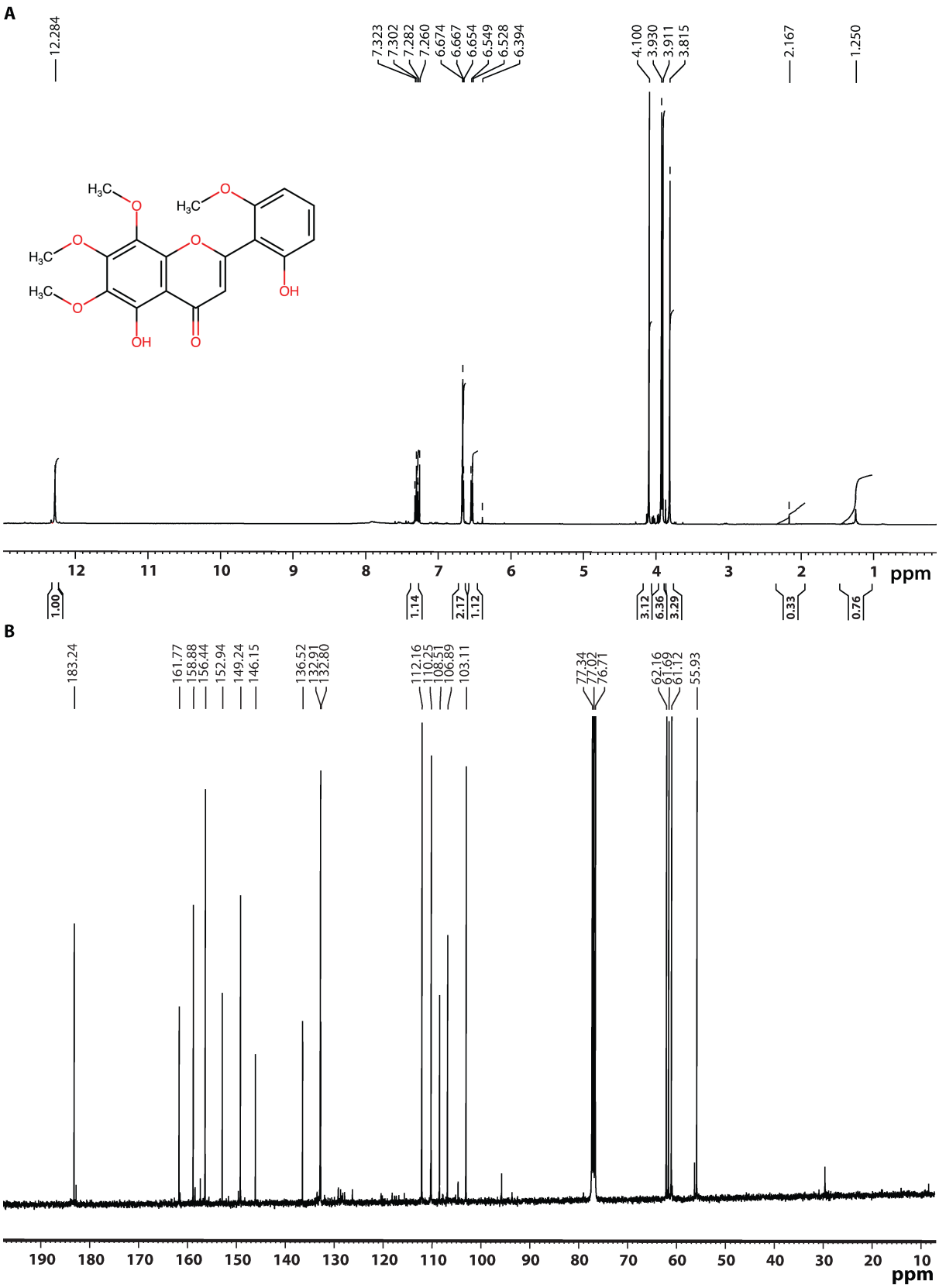

Figure 5.7 – HQDCM-F17' profiling by ^{1}H-NMR and ^{13}C-NMR Spectroscopy

Relative signal intensity (y-axis) is plotted against the chemical shift (ppm) (x-axis) of detected hydrogen (**A**) or carbon (**B**) atoms. The chemical shift of each atom is indicated on top of each peak and in case of the proton NMR the integration of each peak area is indicated below the x-axis. (**A**) ^{1}H NMR (400Hz, $CDCl_3$) δ 12.28 (1H, s, OH), 7.28~7.32 (1H, t, J=8.36, H), 6.65~6.67 (2H, d,s, H, H), 6.52~6.54 (1H, d,

J=8.32, H), 4.1 (3H, s, OCH_3), 3.91~3.93 (6H, s, s, OCH_3, OCH_3), 3.81 (3H, s, OCH_3). (**B**) ^{13}C-NMR (400Mhz, $CDCl_3$) δ 183.24 (C-4), 161.76 (C-2), 158.87 (C-2'), 156.43 (C-1'), 152.93 (C-8), 149.23 (C-10), 146.15 (C-5), 136.51 (C-7), 132.90 (C-9), 132.80 (C-4'), 112.15 (C-3), 110.24 (C-5'), 108.51 (C-6), 106.88 (C-6'), 103.10 (C-3'), 62.15 (C-9 OCH_3), 61.69 (C-8 OCH_3), 61.11 (C-7 OCH_3), 55.92 (C-2' OCH_3)

^{13}C atom	**HSQC ^{1}H cross-peak**	**HMBC ^{1}H cross-peak**
112.15	6.67 H	
161.76		6.67 H
106.88		6.67 H
183.23		
110.24	6.67 H	6.53 H
103.1	6.53 H	6.67 H
108.51		
156.43		
55.92	3.81 OCH3	
158.87		3.81 OCH3
132.80	7.3	
132.90		3.91 OCH3
62.15	3.91 OCH3	
61.11	3.93 OCH3	
136.51		3.93 OCH3
61.7	4.1 OCH3	
152.93		4.1 OCH3

Table 5.5 – Cross-peaks observed in HMBC and HSQC NMR spectroscopy analysis of HQDCM F17'

The less pure F18' fraction exhibited nearly identical ^{1}H NMR spectrum as F17' except for a small shift in the position of certain peaks, most noticeable with the change of the sharp single proton peak from 6.7ppm to 7.1ppm, no longer overlapping with the 6.7ppm doublet in F18' (Fig. S5.9). This could be suggestive of presence of close analogues in the two fractions. This is further supported by the MS analysis, which identified the same major peak m/z 375 with several minor peaks likely representing contaminants or fragmentation ions (Fig. S5.5).

5.3 Assessment of the antimalarial properties of wogonin, negletein and skullcapflavone II

Upon initial antimalarial activity screening of 19 HQDCM fractions obtained from the high-resolution extract separation, only three fractions containing ^{1}H-NMR signature peaks of SKF-II (i.e. F17'-19') exhibited activity substantially superior to that of the crude extract (Fig. 5.8A). Contrastingly, fractions containing negletein and wogonin (i.e. F9'-10' and F12'-13') displayed antimalarial activity comparable to or higher than the reference crude extract. In order to verify the obtained results, we carried out extensive antimalarial activity profiling of the isolated fractions against the reference *3D7 P. falciparum* strain in a triplicate biological assay. The parasiticidal activity was determined for fractions with highly purified compounds (i.e. F9' – negletein, F13' – wogonin and F-17' – SKF-II), those enriched in identified compounds (F10', F12', F18', F19') and in case of wogonin and negletein the synthesised molecules (Fig 5.8B). The fractions continuing SKF-II (F17') and its possible analogue (F18') exhibited antimalarial activity significantly superior to those previously observed for fractions F3-5, with IC_{50}s equal 2.8μg/mL and 4.1μg/mL, respectively. Both fractions were also able to completely attenuate parasite growth at 7.4μg/mL and 11μg/mL respectively. Furthermore, the F17' and F18' did not exhibit haemolytic activity previously observed in HQDCM-F5. Instead, the F19' induced more severe haemolysis than F5 in the prior test, suggesting that it contains the cytotoxic compound. Wogonin and negletein enriched fractions, as well as the synthesised compounds exhibited substantially lower activity than initially observed in corresponding fractions F3 and F4 with 24.6μg/mL and 19μg/mL for HQ-DCM F13' and F9', respectively. The less-pure neighbouring fractions (i.e. F10' and F12') displayed somewhat higher activity with IC_{50}s in 10-13μg/mL range, likely owing to the

additional antimalarial activity of unidentified impurities. The IC_{50} of synthesised wogonin was equal 32.6μM, whilst that of negletein 57μM (Fig.5.8B). Overall, validated highest antimalarial activity of F17' fraction supports the role of SKF-II as the principal compound responsible for the antimalarial activity of HQ-DCM extract, however moderate activity of wogonin is likely a contributing factor.

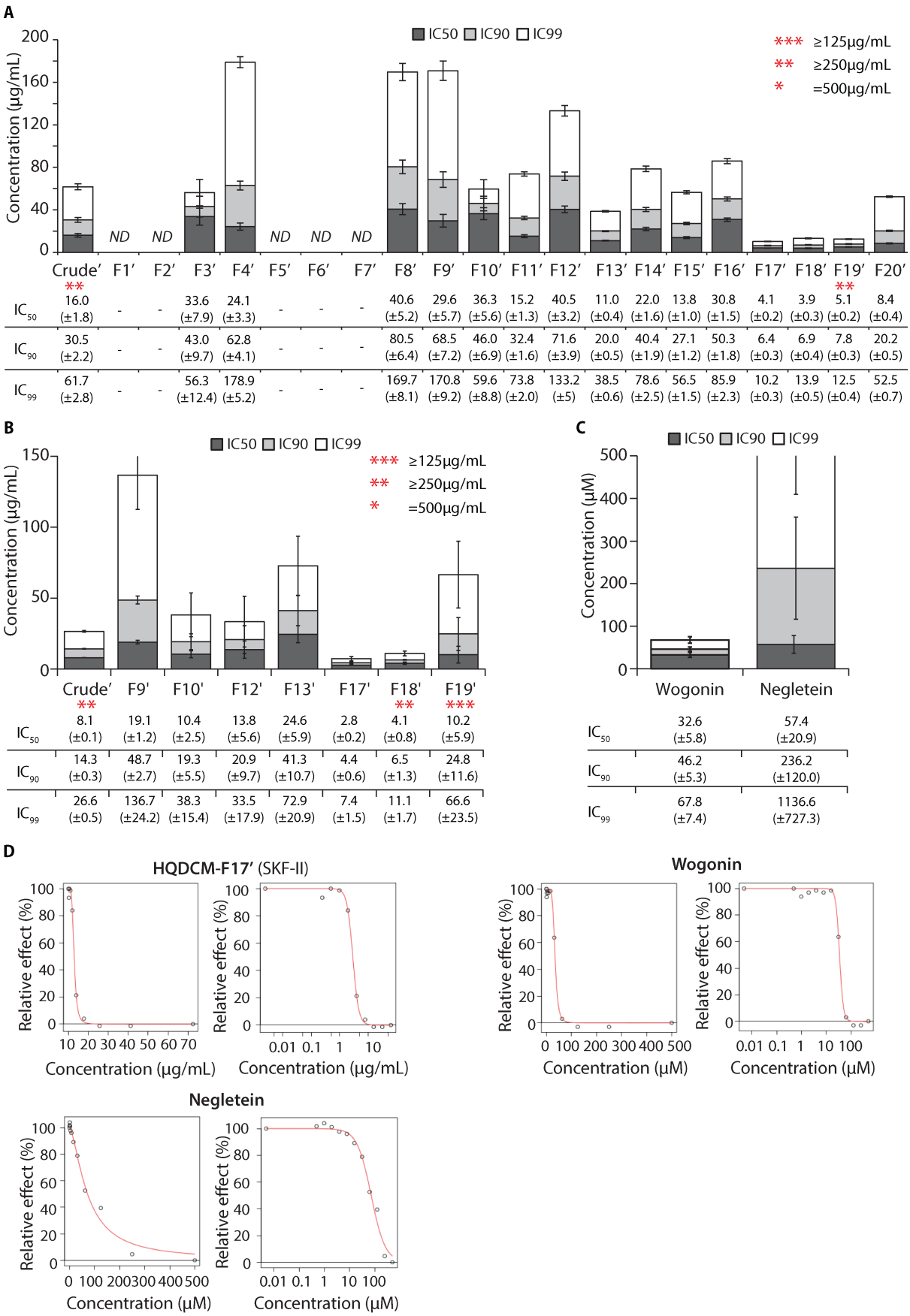

Figure 5.8 – Antimalarial activity profiling of wogonin, negletein and skullcapflavoneII

Inhibitory concentration values [IC_{50} – dark grey; IC_{90} – light grey; IC_{99} – white (µg/mL)] calculated based on the regression fit analysis of *P. falciparum in vitro* growth inhibition assays are represented

as a bar chart for fractions isolated from the targeted chromatographic separation of HQ DCM extract and (**A**) tested against the T996 parasite strain in one replicate, or (**B,C**) in biological triplicate against 3D7 strain together. 'Wogonin' and 'negletein' refer to pure synthesised commercially procured compounds. The IC values are listed below each graph in a table. 'ND' refers to extracts which did not inhibit parasite growth by more than >50% in 500ug/mL concentration and their respective IC_{50} could not be determined. Error bars represent (**A**) 95% confidence intervals for the regression curve fit (**B,C**) Standard deviation between three biological replicates. The extent of haemolytic effect, defined as decrease in cell concentration by >10%, is indicated for each extract with red asterisks, with one asterisk- haemolytic effect observed only at the 500ug/mL extract concentration, two at 250ug/mL and above and three asterisks at 125ug/mL and above. (**D**) The growth inhibition plot following curve fitting for three samples of interest based on experiments presented in panels B and C. The extent of parasite growth (y axis) is plotted against drug concentration (x axis). Left panel in each set represents linear and the right panel logarithmic plotting of extract concentration. While wogonin and negletein were purchased from a commercial supplier and represent pure chemical compounds, the data obtained for SKF-II are derived from a high purity compound isolated in-house (i.e. the fraction F17' of the HQ-DCM extract)

In order to shed more light on the plasmodiocidal mechanism of SKF-II, we assessed compound's effect on parasite's morphology following 12, 24, 36 and 48h incubation across a range of drug concentrations (i.e. 0-250μg/mL of HQDCM-F17') (Fig. 5.9). Compound concentrations <1.9μg/mL did not significantly affect parasite morphology and development. However, a dose-dependent developmental stalling effect was present at higher concentrations. Strong developmental inhibition can be observed at 7.8μg/mL dose for young trophozoites, which exhibit heavily perturbed morphology and do not reach schizont stage after 48h of drug administration. Higher doses of the drug completely attenuate parasite growth once it reaches early trophozoite stage (i.e. ~12h post drug administration) and further developmental stage progression is not observed, suggesting that the compound is active against trophozoite, but not ring parasite stages.

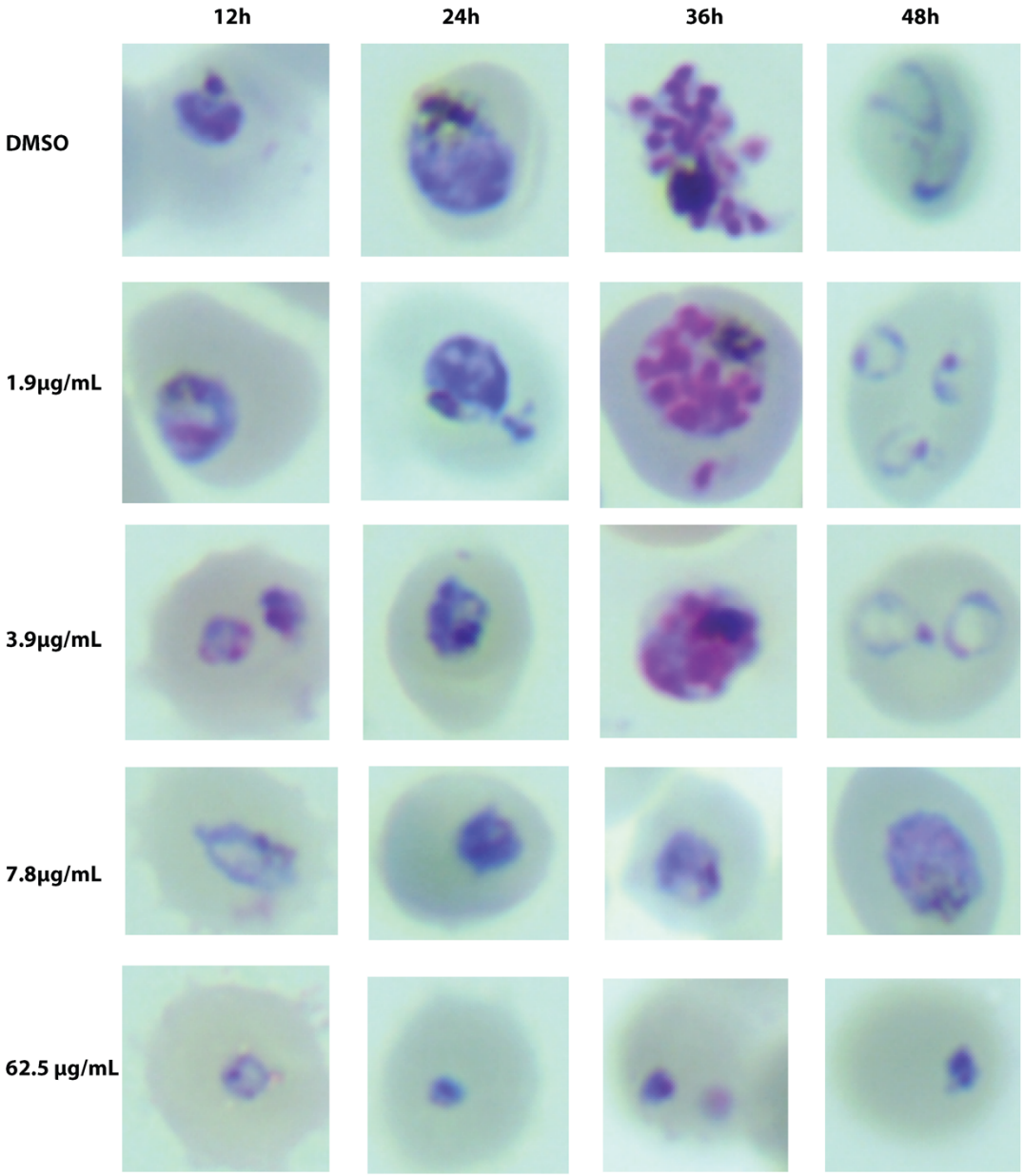

Figure 5.9 – The effect of skullcapflavone II on *P. falciparum* morphology *in vitro*

The morphology of parasites exposed to different concentrations of HQ-DCM-F17' in a standard *P. falciparum* 3D7 strain *in vitro* growth inhibition assay, visualised through Giemsa-stained malaria smear microscopy analysis. The addition of the extract was initiated at the mature ring-stage (i.e. 10-14hpi) followed by sampling and smear preparation 12h, 24h, 36h and 48h after assay initiation.

5.4 Identification of molecular targets of skullcapflavone II through MS-CETSA

Further elucidation of the MoA of SKF-II was conducted through Lysate ITDR experiments, aiming to identify its respective molecular targets. Whole-cell soluble protein lysate derived from *in vitro P. falciparum* 3D7 parasite culture was incubated with a range of HQDCM-F17' concentrations (i.e. 100-0μg/mL) for 3min, followed by 51°C thermal challenge or a 37°C control. Protein thermal stability under drug exposure was assessed relative to the vesicle-control treated sample and the non-denaturing 37°C condition. Among 1531 *P. falciparum* proteins detected in both 51°C and 37°C conditions only two exhibited a significant dose-dependent stabilisation: a conserved protein of unknown function (PF3D7_0217900) and kinesin−13, putative (KLP8, PF3D7_1245100) (Fig. 5.10A). Both proteins exhibited stabilisation in a similar concentration range corresponding to the *in vitro* antimalarial activity of HQDCM-F17' with MDTs of 0.56 μg/mL and 1.10 μg/mL for PF3D7_0217900 and KLP8 respectively (Fig. 5.10B). In order to identify the potential function of the PF3D7_0217900 protein, we carried out the extended similarity group Gene Ontology prediction by iterative PSI-Blast search (ESG) *(244)* based on protein's sequence. The structure analysis suggests a very high degree of confidence that the protein in question is an acyl-CoA hydrolase localised to the mitochondrion (Table 5.6). However, the further experimental evidence is required to validate this prediction.

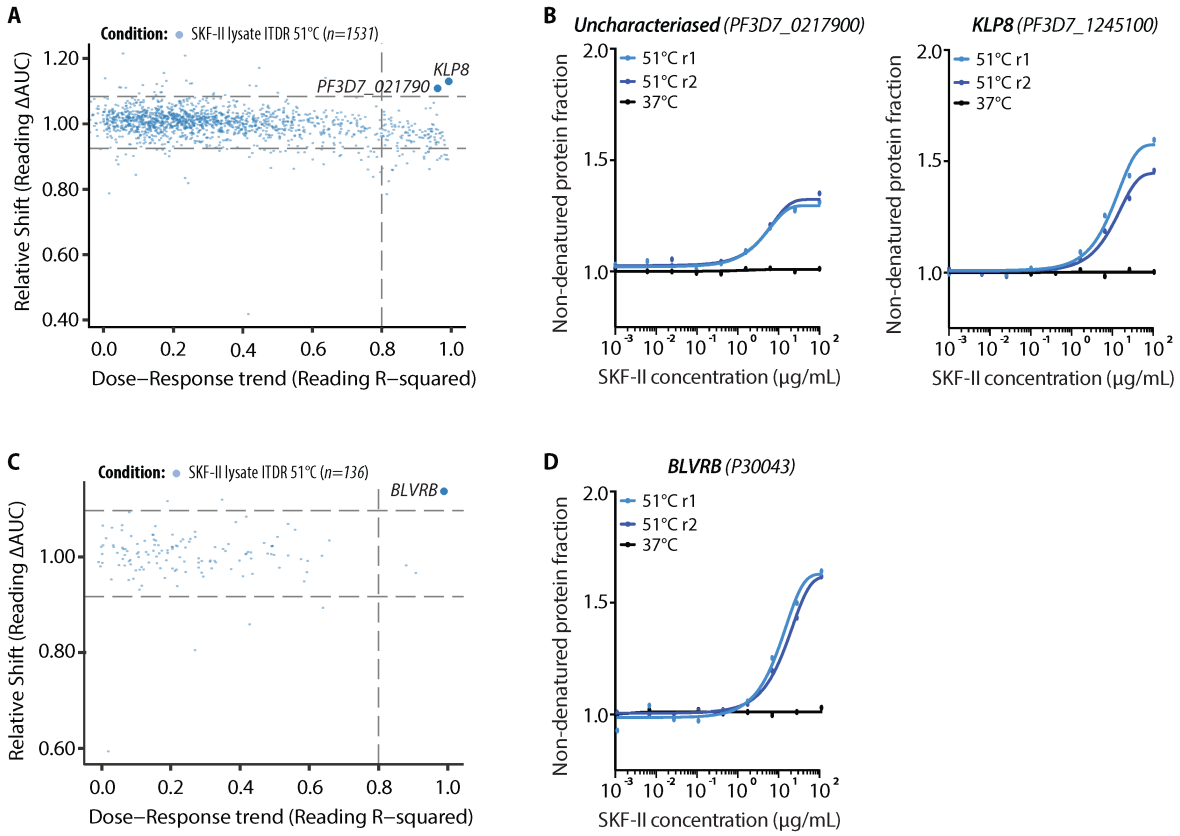

Figure 5.10 – MS-CETSA mediated identification of skullcapflavone II -binding protein targets

Whole proteome ITDR analysis performed with HQ-DCM-F17' in lysate with the thermal challenge at 51°C (blue dots) conducted for (**A**) *P. falciparum* and (**C**) human proteome. Distribution of protein stabilisation is plotted as a function of R against ΔAUC. MAD*3 of ΔAUC and R squared=0.8 cut-offs are indicated on the graph. Significantly stabilised proteins are highlighted. **(B,D)** Stabilisation curves of the proteins identified in the respective preceding panels, thus A->B, C->D. The extent of stabilisation depicted as remaining soluble protein level after thermal challenge: 51°C (blue) relative to the no-drug control is plotted along the drug gradient. Non-denaturing 37°C control condition is plotted in black.

Probability	Confidence level	Term	Description
100.0%	Very high	GO:0016787 [+]	hydrolase activity
97.7%	Very high	GO:0052689 [+]	carboxylic ester hydrolase activity
81.4%	Very high	GO:0047617 [+]	acyl-CoA hydrolase activity
74.6%	Very high	GO:0006637 [+]	acyl-CoA metabolic process
61.3%	High	GO:0005739 [+]	mitochondrion
48.7%	High	GO:0003986 [+]	acetyl-CoA hydrolase activity
39.6%	Moderate	GO:0005829 [+]	cytosol
39.0%	Moderate	GO:0005737 [+]	cytoplasm
30.4%	Moderate	GO:0006631 [+]	fatty acid metabolic process
30.1%	Moderate	GO:0035338 [+]	long-chain fatty-acyl-CoA biosynthetic process

Table 5.6 – ESG prediction model-based protein sequence analysis of PF3D7_0217900

An additional target engagement analysis conducted for 136 human proteins detected in the sample suggested that the HQ-DCM F17' also stabilizes Flavin reductase (BLVRB, P30043) with an MDT=1.99 μg/mL. BLVRB is a host-cell protein known to be actively imported and accumulated in parasite's cytoplasm *(127)* (Fig. 5.10C-D), thus its engagement by SKF-II could theoretically have therapeutic effects. However, similar mechanism has not been reported before for antimalarial drugs.

5.5 Discussion

The pressing need for new antimalarial drugs is not answered solely by phenotypical screening studies and identification of novel bioactive molecules. Only after resolution of their MoA and identification of their respective molecular targets can the follow-up optimisation and drug development studies take place. Identifying drug-target pairs gives not only mechanistic insights into the biological processes relevant to the disease or the pathogen, but also provides invaluable information on the structure-activity relationships *(281)*. Those can be exploited for the rational drug-design and further optimisation of the drug's molecular structure to increase its potency, specificity, half-life and avoid potential toxicity issues *(282)*. In this work, we provide a proof of principle for the preconceived antimalarial drug discovery pipeline, which allows identification of bioactive molecules from raw medicinal plant material, their isolation and characterisation of their candidate targets in the *P. falciparum* proteome. The pipeline therefore not only produces leads for new antimalarial drug candidates, but also identifies their associated and possibly novel druggable targets.

Here, we isolated two active antimalarial compounds from *Scutellaria baicalensis* (*a.k.a.* Baikal skullcap), one of the 50 fundamental herbs in TCM and a very common component of recipes for a wide range of illnesses *(283)*. Its' aqueous extract has previously been found to possess potent (4.2 μg/mL) antimalarial activity, however, no specific bioactive compounds were isolated nor characterised *(284)*. Low bioactivity of corresponding HQ-Hex and MeOH extracts, contrasted with substantial antimalarial activity displayed by the HQ-DCM extract suggests that HQDCM likely contains the bioactive compound isolated previously. While SKF-II and wogonin are known bioactive constituents of *S. baicalensis (285, 286)*, negletein has not been isolated from this plant to date. The three flavonoids had remained outside of the scope of antimalarial activity investigations until recently when Fernandez-Valdes and

colleagues reported antimalarial activity of wogonin against *P. berghei* malaria mouse model with an IC_{50}=15μM *(287)*. Our results indicate the similar extent of antimalarial activity of wogonin against *P. falciparum* culture *in vitro* with an IC_{50}=32.6μM. More interestingly, SKF-II was found to poses previously unreported antimalarial activity superior to wogonin with an IC_{50}=2.8μg/mL, which would be an equivalent of ~7.5μM for the pure compound. Whilst both compounds have not been pursued so far as candidate drugs for malaria, their anti-cancer and anti-metastatic activities have been well-established and demonstrated both *in vitro* and *in vivo* on multiple cancer lines and mouse tumour models *(288–292)*. Numerous studies have shown that wogonin preferentially kills tumour cells, evoking none or little toxicity to normal tissues *(293–296)* making it a good drug candidate. Furthermore, it possess neuroprotective *(297, 298)* anti-inflammatory *(299)* anti-viral *(300)* and antioxidant *(301)* properties. Regarding SKF-II, some anti-inflammatory properties in addition to its anti-cancer effect have been reported *(302, 303)*, but the compound has been studied to a lesser extent. Interestingly, several other structurally-related flavonoids displaying antimalarial properties have been described in the literature *(304–308)*, suggesting that the flavonoid ring backbone could represent an interesting antimalarial drug lead, and its structure can likely be further modified to increase its parasiticidal activity.

The two *P. falciparum* proteins identified as possible targets of SKF-II: the uncharacterised protein PF3D7_0217900 and KLP8 were both responsive within the same concentration range correlating with drug's antimalarial activity. The uncharacterised gene PF3D7_0217900 exhibits peak expression profile during the late trophozoite stage and is essential for *in vitro* asexual blood stage growth *(309, 310)*, supporting its role as a potential drug target. Its predicted function of an Acyl-CoA hydrolase needs to be further verified and its role in parasite's metabolism remains to be characterised. The KLP8 functions as the motor domain for microtubule depolymerisation essential for spindle assembly and chromosomal kinetochore

organisation in cell division *(311, 312)*. The insertional gene mutagenesis survey in *P. falciparum* found no significant deleterious effects of its disruption for the asexual blood stage parasite growth *in vitro*, suggesting its dispensability *(309)* and making it an unlikely drug-target. The concomitant stabilisation of a human protein: BLVRB, observed within similar concentration range of SKF-II is intriguing, as the protein has been shown to be imported by the parasite *(127)*. The BLVRB complements the haem Oxygenase in the haem catabolic pathway of the host cell, catalysing its second step and converting soluble biliverdin into insoluble pigment bilirubin. The bilirubin is a highly potent antioxidant for peroxyl radicals *(313, 314)* and the biliverdin-BLVRB pair serves as an important physiological cytoprotectant. It has been previously shown that low concentrations of bilirubin can protect mammalian cells from oxidative stress induced by 10,000-fold higher concentrations of H_2O_2 *(315)*. The presence of endogenous haem detoxification pathway in *P. falciparum* has been debated *(316)* and only the haem-Oxygenase enzyme has been identified in the *P. falciparum* genome *(317, 318)*. The parasite's reliance on the host's enzyme to complement its endogenous partial haem detoxification pathway is a rather controversial hypothesis, but would explain the accumulation of BLVRB in its cytoplasm. Similar mechanisms have been suggested for several other parasite pathways, but no conclusive proof was provided *(319–322)*. Although no host protein has been previously identified as a target of an antimalarial drug, if the parasite indeed relies on the enzymatic function of BLVRB, or at the very least, the enzyme has a supportive role for parasite's metabolism and redox management, its inhibition could have negative consequences for the cellular integrity of the parasite. Further investigation is required to examine the relevance of the observed interactions with the three proteins for the MoA of SKF-II and to validate them as actual molecular targets of this candidate compound.

Some small molecules can exert their biological activity in a manner independent of their interaction with protein targets. In respect to the antimalarial compounds, such MoAs have been suggested for instance for CQ – physical interference with hemozoin crystal formation *(63)*, MFQ – interference with parasite membrane integrity *(77)*, QN – intercalation with parasite DNA *(323)* or ART – oxidative damage *(97)*. The structures of wogonin, negletein and SKF-II feature planar aromatic ring system, characteristic for flavonoids and which has been shown capable to intercalate with DNA *(324, 325)*. Whether those compounds are capable of binding to parasite DNA and if this interaction is relevant for their antimalarial activity should be addressed in future research.

The antimalarial activity profiling of TCM herbs revealed several other extracts displaying comparable or even higher antimalarial activity than HQ-DCM. Bioactivity-driven separation of those candidate extracts could result in the identification of structurally diverse natural products with antimalarial properties. However, the haemolytic activity often coinciding with extracts' antimalarial activity suggests that they might contain phytochemicals with general cytotoxic properties, not specific to *P. falciparum*. Therefore, the priority should be given to those extracts which kill the malaria parasite without affecting the integrity of the host cell within a similar concentration range. Such specific antiparasitic effect was observed with AY DCM extract, which had no haemolytic properties while displaying the highest relative antimalarial activity among all tested extracts. The raw material AY-DCM was isolated from the leaves of *Artemisia argyi,* which is traditionally used in TCM to stop bleeding, promote contractions, dissipate cold, reduce pain, as well as for treating malaria, asthma, inflammation, hepatitis, bacterial and fungal infections *(326, 327)*. More recent studies reported that extracts derived from this plant possess potent antiheminthic. *(328)*, anti-HPV and antitumoral *(329, 330)* activity and are cytotoxic to multiple cancer cell lines *(331–333)*. Whilst, *A. argyi's* antimalarial activity has not been investigated

to our knowledge, several other *Artemisia* species have been reported to possess antimalarial properties *(334–336)* owing to the presence of artemisinin and/or other compounds including several flavonoids *(335, 337, 338)*. The significant antimalarial activity of AY-DCM extract determined in this study offers a chance to identify potentially novel antimalarial compounds structurally related or unrelated to artemisinin. The preliminary bioassay-guided fractionation attempted for the AYDCM extract yielded phytochemical fractions with improved antimalarial activity (results not shown), but the identification and purification its active molecules was not achieved due to low yields, insufficient chromatographic separation and the project's time constraints. Overall, this pilot implementation of the drug discovery pipeline allowed us to identify its weaknesses and areas with the potential for improvement.

Sequential Soxhlet extraction has proven to be a highly reliable and reproducible technique for isolation and pre-fractionation of phytochemicals present in TCM materials. Extracts obtained from different batches of the same herb exhibited comparable yields and exhibited corresponding ^{1}H-NMR profiles suggesting that their general composition was consistent, at least in regard to the main constituents. However, some variability was observed in the antimalarial activity between different batches of crude extracts. Despite quality control and stringent standards required by the TCM clinics from their suppliers, a degree of variability in the presence and quantity of phytochemicals in plants from different shipments is expected and unavoidable due to variable conditions and fluctuating environmental factors during growth in various locations *(339–341)*. Nonetheless, the major challenge encountered in the pipeline development was achieving sufficient separation of extracts' constituent phytochemicals to isolate their active components in high purity. Silica-gel column chromatography with elution profiling through TLC is a low-cost method offering good level fractionation and detection of a wide range of diverse compounds, but has limited sensitivity and resolution capacity *(342)*. The method was successfully used in this

study to isolate two bioactive compounds from *S. baicalensis* in a purity sufficient for their structural identification. However, unsuccessful attempts to isolate active antimalarial compounds devoid of contaminants during pilot fractionations of several other extracts (including AY, XXC and CG-DCM) demonstrated its limits. Implementation of a more robust separation technique should be considered in the interest of increasing the throughput and the analysis depth of the pipeline. High Pressure Liquid Chromatography (HPLC) offers several advantages over the traditional column chromatography, including capacity for full automatisation, fractionation reproducibility and significantly higher resolution *(343, 344)*. In order to take the full advantage of the HPLC, it could be coupled with two independent detectors, such as the diode array detector and the GC-MS, what would allow real-time profiling of eluting compounds and in-turn a more accurate fractionation *(345, 346)*. Overall, incorporation of HPLC into the pipeline could substantially accelerate the process of extract fractionation and provide better profiling of their component phytochemicals. The second principal area for protocol improvement concerns the biological testing of extracts'/fractions' antimalarial activity. Although current protocol is functional and delivers expected results, introduction of an additional pre-screening step could be advantageous. Activity testing of a single extract concentration, deemed the minimal activity threshold expected from extract/fraction to be considered for further processing, would allow removal of the 'non-active' substances from the processing pipeline in an early stage. Consequently, it would increase the throughput of the pipeline through a decrease in the necessary workload and sample processing cost.

Future iterations of the drug discovery pipeline could also involve more extensive safety/toxicity screening protocol. While the information on the RBC-haemolytic effect induced by TCM fractions gained from standard antimalarial drug activity assays is valuable, it cannot account for all potential cytotoxic effects the

phytochemicals might have on other cell types. Current protocol efficiently identifies compound mixtures with lytic properties, but will not indicate which phytochemicals interfere with normal physiological processes of eukaryotic cells, such as transcription and translation absent from RBC. Implementation of a standardised in vitro cytotoxicity screening involving one of the commonly used cell types (e.g. Caco-2, HaCaT, CaLu, HeLa, 3 T3 or HEK293) would allow more extensive toxicity screening. Such approach should include assessment of cell morphology and activities of metabolic biomarkers attributable to cell survival and maintenance (e.g. Lactate dehydrogenase, ATP reductase, mitochondrial reductase or different homeostatic enzymes) *(347)*.

Altogether, the identification of wogonin and SKFII along with candidate molecular targets of the latter demonstrates the functionality of the designed natural products drug discovery pipeline. Moreover, it illustrates that TCM still represents an attractive source of previously unidentified antimalarial compounds, despite past and present studies conducted in this field. The implementation of suggested improvements to the current pipeline should further increase its robustness and throughput. Further deconvolution of the MoA of SKF-II should be carried out, initially validating target engagement in the intact-cell setting and followed by more in-depth characterisation of the downstream molecular effects through transcriptomic and metabolomic studies.

CHAPER 6
Conclusions and future prospects

6.1 Summary and conclusions

The development of MS-CETSA for identification of antimalarial drug targets in the *P. falciparum* proteome represents one of the very first translational medicine applications of this technique extending beyond cancer cells. We provided a comprehensive characterisation of method's performance through the analysis of parasite's trophozoite stage, both in the lysate setting, as well as in the intraerythrocytic 'intact-cell' condition. This work represents the very first proteome-wide melting curve characterisation of *P. falciparum* and RBC proteins and the generated data can be used in the future to structural and functional studies on *P. falciparum* protein properties. More importantly, we demonstrated that MS-CETSA protocol constitutes a novel promising platform for drug-target identification in *P. falciparum*. We have proven the method's functionality to unambiguously identify known interacting protein-partners of well-characterised antimalarial compounds: PM and E64d. Subsequently, we deployed it to identify the molecular targets of two clinically used antimalarial drugs with poorly-understood MoA: QN and MFQ, leading to the identification of PfPNP, a previously unknown common putative target of both drugs. Binding of the two compounds to PfPNP was validated and extensively characterised, but the degree of the clinical relevance of this interaction remains uncertain for both drugs. Our results warrant further studies to investigate how the PfPNP inhibition contributes to the therapeutic effect of QN and MFQ. Considering that CETSA might not identify all relevant targets of a drug and that not all of the identified drug-protein interactions might be relevant for its principal MoA, the results of the CETSA analysis should be analysed with caution. This is illustrated for instance by only partial (and low confidence) detection of the ribosomal subunit as a plausible

target of MFQ in the lysate ITDR assays. The interaction between the drug and the 80S Ribosomal complex was previously characterised and validated *(81)*, but was not confidently identified in this study due to inadequate thermal challenge temperatures chosen for the ITDR assays, relative to low thermal stability of the Ribosome. Additionally, there always remains the need for additional experimental evidence to validate or refute the occurrence and clinical relevance of the protein-engagement observed in CETSA. Nevertheless, the method represents a novel and previously largely unexplored approach to identify antimalarial drug targets. This might be particularly relevant for compounds for which the identity of their molecular targets have remained elusive for decades, despite a significant scientific effort to deconvolute their MoA. We demonstrated this through identification of PfPNP as a previously unreported target of QN and MFQ. Even though, we were unable to prove the clinical relevance of PfPNP for the MoA of QN and MFQ, it shows how CETSA might be used to uncover direct molecular partners of antimalarial drugs, providing a starting point for subsequent comprehensive characterisation of their MoA.

Furthermore, we designed a drug-discovery pipeline from TCM and identified two compounds with previously unknown antimalarial properties from *S. baicalensis*: wogonin and SKF-II. We demonstrated how CETSA could complement drug discovery efforts, using it to identify candidate molecular targets of SKF-II, the more potent of the two compounds. Drug-protein interactions identified for SKF-II: Uncharacterised protein PF3D7_0217900, KLP8 and BLVRB need be further validated and their clinical relevance needs to be investigated before pursuing SKF-II as a novel drug candidate. Overall, the work presented here supports the notion that CETSA represents a valuable novel tool for drug-target identification studies in *P. falciparum*, complementing existing techniques and assisting research efforts to characterise the MoAs of known and candidate antimalarial drugs. Even the information concerning drug interactions unrelated to drug's intended MoA may be valuable. In the context of

antimalarial drugs, these might include drug-engagement of RBC proteins, which may be responsible for treatment's side-effects. Information on drug's predisposition for off-target engagement is invaluable particularly during the early stages of the drug development process *(348)*. An MS-CETSA-mediated assessment of off-target engagement by candidate antimalarial drugs could be conducted for a variety of human cell-lines beyond the RBC to signal potential toxicity risks before the compound reaches human trials.

6.2 Existing limitations of MS-CETSA and how to overcome them

Despite the proven functionality of the drug-target identification CETSA protocol in *P. falciparum*, current methodology contains several key limitations. On a side of previously discussed modifications of the sample preparation protocol, which could help increase the depth of the *P. falciparum* proteome coverage; there remain more global conceptual changes to the experimental design, which can be implemented in future to further CETSA's robustness. Firstly, all CETSA-mediated drug target discovery efforts presented in this work were focused on the mature trophozoite parasite stage, due to its proven high metabolic activity and susceptibility to the majority of antimalarial drugs *(349)*. However, it is likely that different molecular targets are relevant for the MoA of tested compounds at different stages of parasite's IDC *(349, 350)*. Considering that the gene expression *(351)* and proteomic *(352)* analyses of the *P. falciparum* IDC demonstrate temporal gene/protein expression patterns, only a proportion of parasite proteome was included in our analysis and others might have been missed. Additionally, the predominantly insoluble nature of membrane proteins *(353)* results in their near absence in the soluble protein fraction analysed by CETSA, resulting in limited coverage of the membrane proteome *(144)*. Membrane proteins may be vital to antimalarial drug's MoA, as illustrated by the example of atovaquone

targeting the bc1 complex located on the mitochondrial membrane *(95)*. Consequently, drug-target identification experiments presented in this work encompasses only ~20-25% of the entire parasite proteome *(309)*. It is therefore likely, that some clinically relevant protein targets of tested compounds were not identified due to their absence in the analysed sample.

The coverage of the parasite proteome in future implementations of *P. falciparum* MS-CETSA can be increased through two protocol modifications. In order to ensure a more comprehensive characterisation of drug's MoA throughout the IDC, additional corresponding CETSA experiments with schizont and ring parasite forms should be performed. Although, analysing the ring-stages will necessitate the development of a parasite enrichment strategy alternative to MACS. An improved membrane proteome coverage in *P. falciparum* CETSA analysis can be potentially achieved, through modification of the lysis protocol. Addition of low concentration of a mild detergent, such as NP-40, to the lysis buffer has been recently demonstrated to be compatible with CETSA, increasing membrane protein solubility, without significantly affecting their temperature-induced unfolding patterns *(354)*. A combination of those approaches may significantly increase the proportion of the *P. falciparum* proteome included in the CETSA analysis and render the method more widely-applicable.

The second drawback of the ITDR analysis presented in this study is its limited scope resulting from a relatively low number of conditions tested. Among those, the thermal challenge temperature and the length of the drug treatment step being most relevant. A non-optimal thermal challenge temperature could result in a lack of an observable protein stabilisation response *(147)*. While an overly low temperature will not provoke sufficient degree of protein unfolding, thus a significant stabilising effect cannot be observed; an overly high temperature might induce irrevocable precipitation

of the target protein, making stabilization of the protein, if possible, unachievable. In an attempt to include proteins with diverse thermostability profiles in this study, we implemented 51°C and 57°C challenge temperatures for the ITDR analysis. However, it is possible that the selected thermal challenge temperatures were still inadequate to detect certain stabilising events taking place upon binding of tested compounds. Similarly, the time required for the drug to penetrate to its intended intracellular localisation, accumulate to required levels and engage the target will differ for different compounds. Therefore, an hour-long exposure time in intact-cell ITDR assays might be insufficient for some drugs and be overly long for others, with a considerable number of downstream events taking place.

An ITDR experimental set-up involving additional diverse (i.e. lower and higher) thermal challenge temperatures, analogous to the 2D-TPP experiments conducted in cancer cells *(355)* would ensure that even proteins with particularly low/high melting temperatures or a non-canonical melting profile (e.g. PfDHFR-TS) would be included in the analysis. An assessment of drug's stabilising effect under more diverse denaturing conditions would therefore lead to identification of a higher number of direct molecular partners and provide more conclusive data on the low significance stabilisations, such as those observed in the MFQ ITDR experiments. The intact-cell ITDR experiments can identify possible downstream effectors of drug's MoA *(144)*. However, the characterisation of a contextual relationship between observed stabilisations and drug's MoA may be challenging, especially when a large number of proteins are involved. Further multiplexing of the experimental setup to include different exposure time (e.g. 1min, 5min, 10min, 30min, 1h, 2h and 5h) in addition to the drug concentration gradient and the thermal challenge temperature variable, would provide invaluable information on the sequence of events following drug binding. Such 3D experiments would allow distinction between direct-drug engagement and the

downstream effects, as well as could enable complete characterisation of drug's MoA including the resulting downstream perturbations and parasite's response to them.

The successful identification of drug-targets through MS-CETSA, or the lack thereof might be additionally influenced by integral properties and the nature of a given drug-target pair. For instance, not all proteins will exhibit canonical stabilisation in response to drug binding, thus might not be detected. Additionally, the MoA of a drug might not be dependent on binding to a protein, but rather rely for instance on a non-specific oxidative damage, disruption of structural integrity of parasite membranes, DNA-damage or physical inhibition of haemozoin crystal growth, as has been suggested for some clinically used antimalarial compounds *(7, 63, 71, 77, 91)*. In such cases, CETSA would not be able to identify the drug targets, nor directly help the MoA deconvolution efforts.

6.3 Future prospects

MS-CETSA has the potential to extend beyond its applied use and serve to address more fundamental questions about the parasite biology (Fig. 6.1). The molecular mechanisms responsible for diverse phenomena observed in malaria are still not fully comprehended. Parasite's metabolism is distinct to that of eukaryotic organisms and plants, sharing characteristics of both systems. Consequently, the relevant components and the sequence of events in many metabolic pathways remains only partially characterised. Diverse *in silico* metabolic network models for *P. falciparum* try to reconstruct the associations and roles of different proteins in the parasite's metabolic cascades *(356–359)*. However, our limited understanding of the cellular role of a substantial number of *P. falciparum* proteins severely hampers those efforts. CETSA could be used to gather additional information on the protein binding properties to an array of important metabolites, helping to predict their molecular

functions *(200)*. The perturbations of proteins, metabolites under parasite exposure to ROS, heat or starvation could help to profile how the parasite responds to stress. Furthermore, the variation in protein stability and solubility in response to different post-translational modifications could provide additional information regarding enzymatic activity and metabolic pathway regulation *(198, 200)*. CETSA data can also be used to predict protein-protein interactions and identify unknown protein complexes, exploiting the fact that independent complex components exhibit co-aggregation behaviour and homogeneity in their melting profiles *(152)*. Such an approach might help to discover interactions central to various cellular processes. Together, this data combined with available genomic, transcriptomic, and proteomic information would help to construct more reliable and complete regulatory and metabolic networks giving us a holistic insight into the lifestyle of this peculiar parasite.

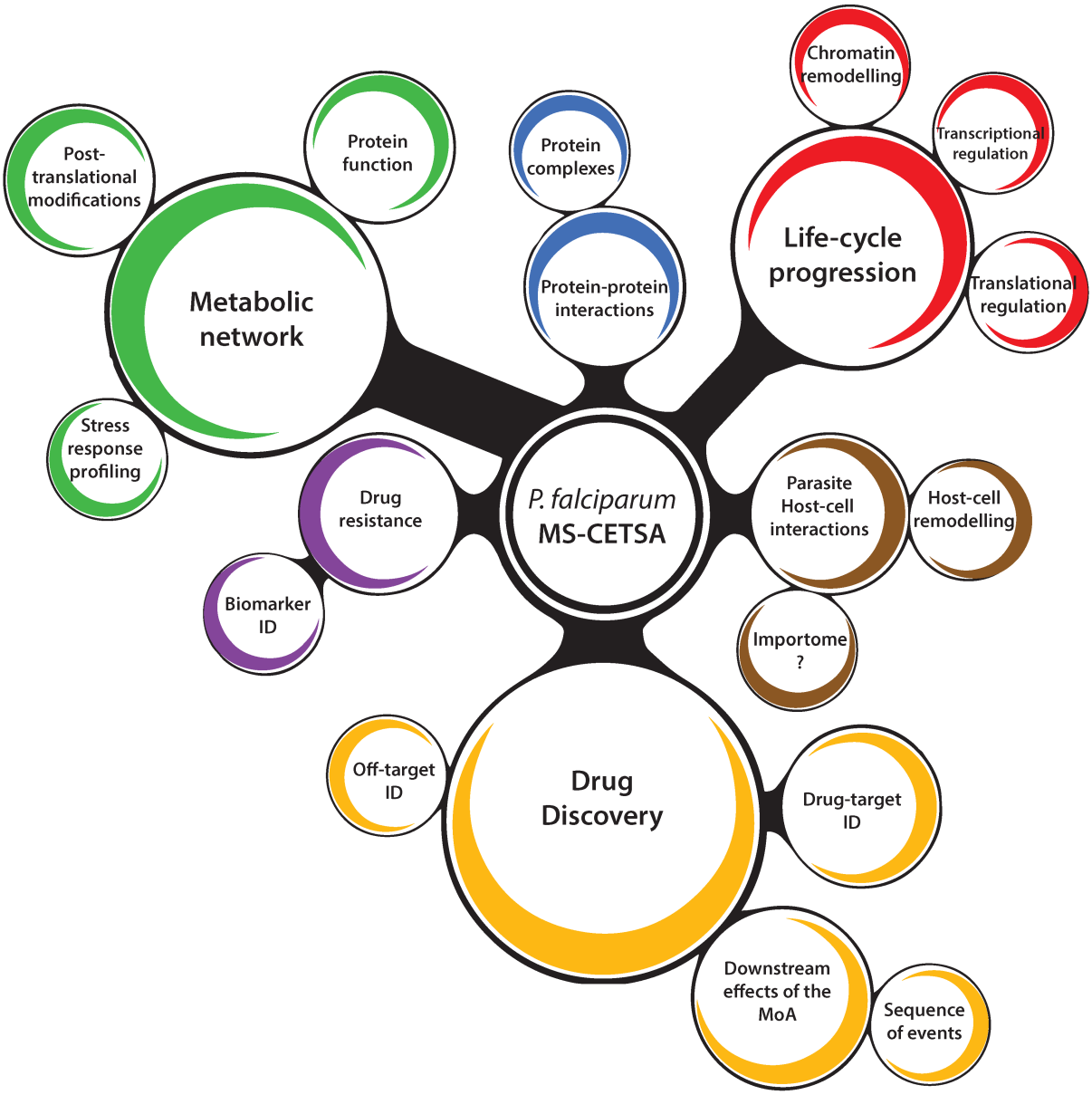

Figure 6.1 – Possible applications of MS-CETSA in the *P. falciparum* research

Early transcriptomic studies in *P. falciparum* revealed hard-wired gene expression patterns governing parasite's life-cycle progression *(351, 360)*. Beyond transcriptional regulation, the involvement of genomic *(361)*, translational *(362)*, epigenetic *(363, 364)* and phosphoregulatory *(365, 366)* factors in this complex regulatory network driving parasite development has been demonstrated to date. Nevertheless, the exact mechanisms governing the cell division and parasite development remain not fully understood. Recent work in cancer cells demonstrated

that the protein thermal stability profiling approaches could be used to study cell-cycle progression *(367, 368)*. The changes in protein thermal stability and solubility can signal varying enzyme activity, interactions with other proteins or DNA or complex formation and can be correlated with protein roles in transcription, translation and chromatin remodelling across the cell cycle stages *(367, 368)*. A melt curve CETSA assessment of protein thermostability across the IDC would reveal which proteins exhibit a change in Tm in relation to each other and the parasite development, which could signal protein complex assembly, protein-protein association, chromatin association, post-translational modifications, etc. Therefore, the MS-CETSA in *P. falciparum* could offer new insights into the mechanisms governing the intraerythrocytic developmental cycle progression.

Additionally, a comparison of host-cell protein melting curves in parasite-infected and -uninfected RBCs, could help to identify specific parasite-driven changes occurring during the host-cell remodelling *(208–210)*. It could also help determine if the host-proteins, which seemingly are imported by the parasite *(127)* undergo post-translational or other modifications. The technique might also be used to better characterise emerging antimalarial drug resistance. Comparative characterisation of global protein melting curves between drug-susceptible and drug-resistant clinical isolates might help to identify which specific changes in the parasite proteome mediate increased drug tolerance. Similarly, the corresponding comparison conducted for different *P. falciparum* clinical isolates could help to narrow down which proteins are directly involved in determining parasite virulence or the severity-onset of the disease it causes.

In conclusion, MS-CETSA represents a valuable addition to already existing methods for the identification of antimalarial drug targets. Though, more importantly, it has the potential to become a novel tool for the analysis of parasite biology with widely diverse applications. It offers a highly comprehensive global assessment of the parasite proteome and its fluctuations in response to chemical, physical, physiological or genetic variables. It can help identify drug-protein, protein-protein, protein-metabolite, and protein-DNA interactions and the differences in those between parasite lines. Overall, the development of CETSA for *P. falciparum* can complement existing techniques and help achieve a more complete understanding of this protozoan parasite's biology.

Appendix

Supplementary Figures and Tables

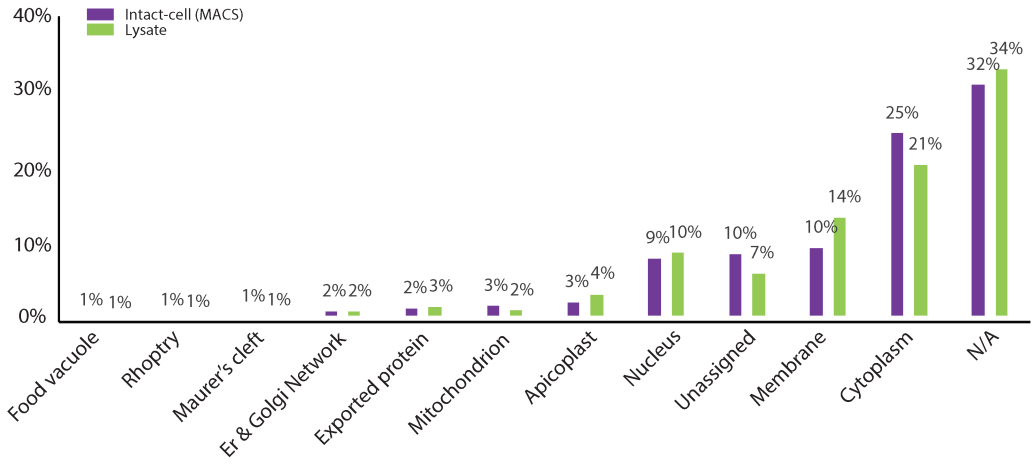

Figure S3.1. Comparison of proteome coverage in Lysate and Intact-cell CETSA method variants

Sub-cellular localisation of proteins in Lysate melt curve CETSA and Intact-cell melt curve CETSA experimental sets. Only proteins with ≥3 PSMs were included in the analysis. Reported values reflect the percentage of total number of detected proteins falling within a given category. Protein assignment to subcellular localisation was conducted manually based on Gene Ontology (GO) terms. “Unassigned” refers to proteins with ambiguous localisation profile and “NA” to proteins with no GO information.

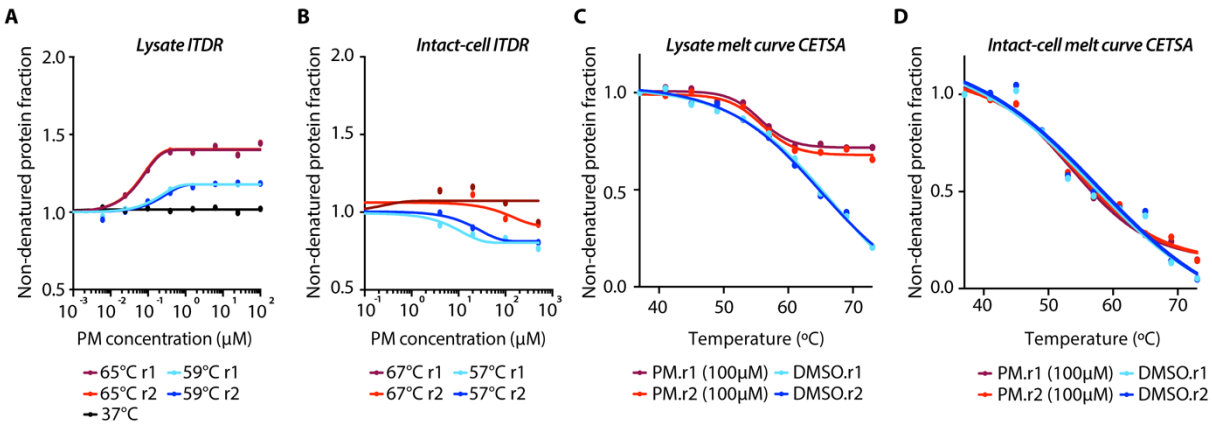

Figure S3.2 – PfDHFR-TS engagement by pyrimethamine across four CETSA variants

DHFR-TS stability under pyrimethamine treatment in lysate 100-0µM (**A**) or intact-cells 250-0µM (**C**). Protein relative abundance in soluble protein fraction (y axis) is represented for each drug concentration point relative to 0µM (i.e. DMSO control). The behaviour of DHFR-TS in melt curve CETSA experiments in lysate (**B**) and intact-cells (**D**) conditions upon exposure to DMSO or 100µM of pyrimethamine. Non-denatured soluble protein fraction (y axis) remaining after thermal challenge (x axis) is plotted in two replicates as fold change relative to 37ºC non-denaturing condition.

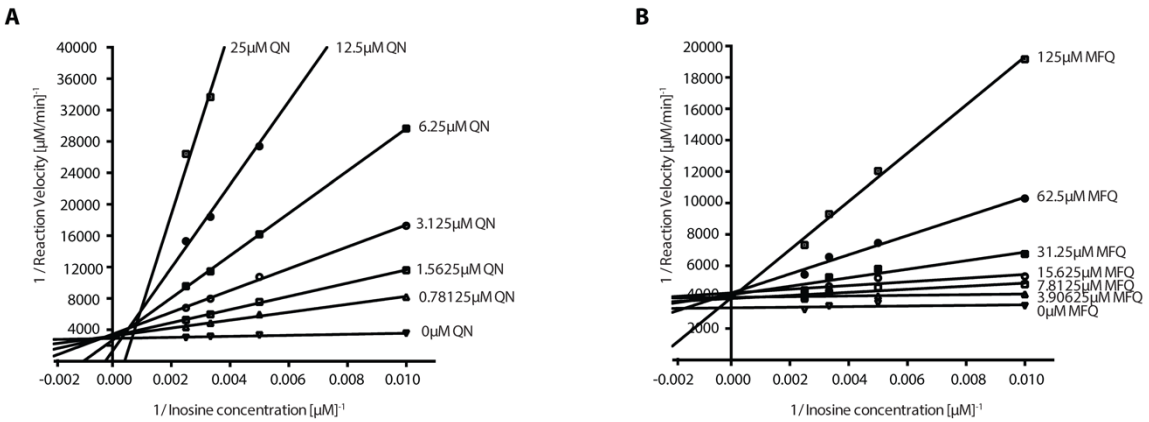

Figure S4.1 – Lineweaver-Burk plot analysis of PfPNP inhibition by QN/MFQ

Inosine-to-hypoxanthine conversion assay coupled with Xanthine Oxidase mediated hypoxanthine-to-uric acid reaction, conducted with recombinant PfPNP in the presence of varying concentration of substrate (inosine) and an inhibitor: (**A**) Quinine (QN) or (**B**) Mefloquine (MFQ), as described and plotted on figure 4.4F. In brief, Lineweaver Burk plots were generated by linear regression of the reciprocal data of triplicate assays of PfPNP enzymatic activity across 400-50µM Inosine concentration gradient and in the presence of 0-25µM QN or 0-125µM MFQ concentration gradients.

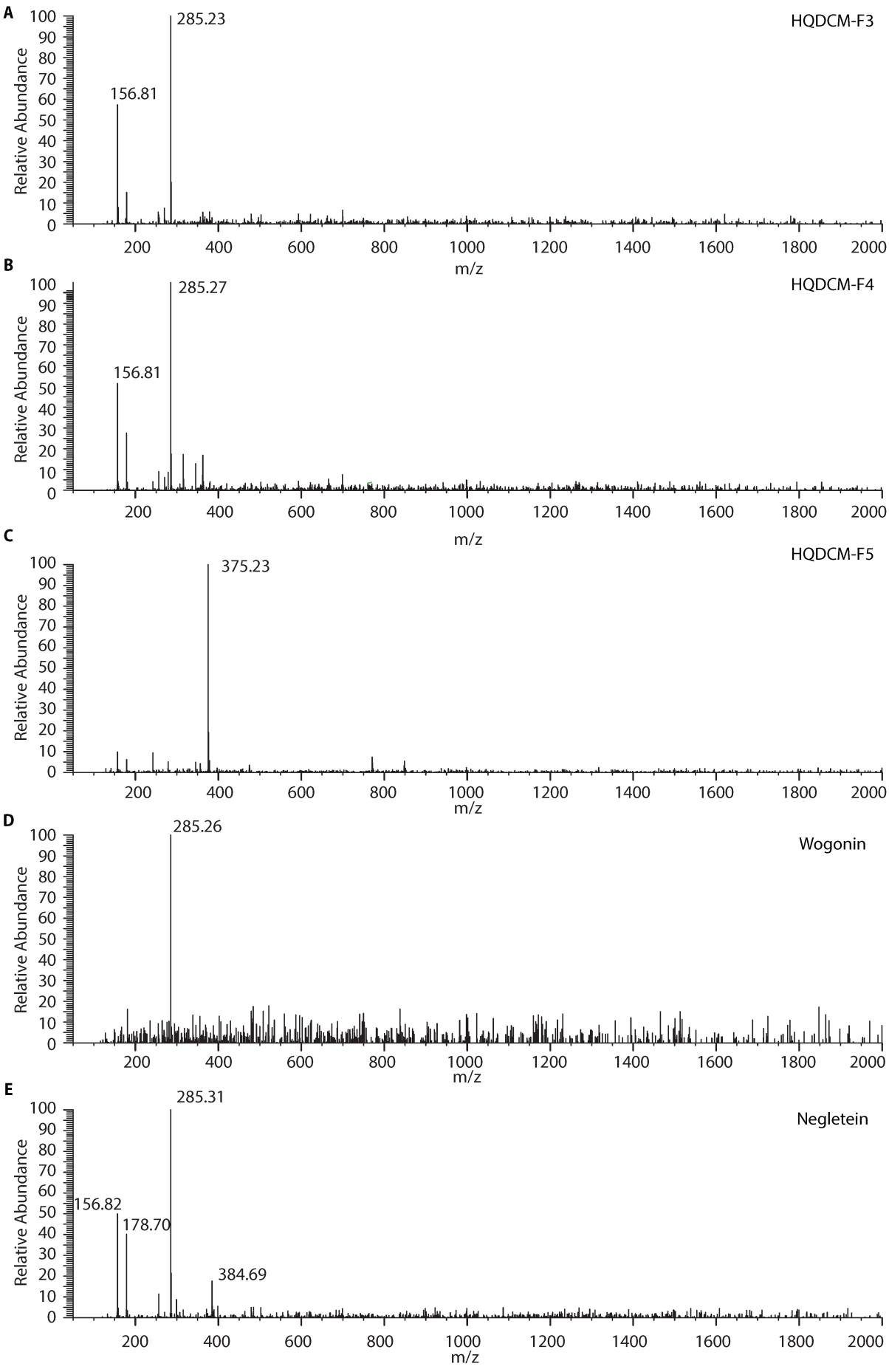

Figure S5.1 – Mass Spectrometry analysis of HQDCM F3-5, wogonin and negletein

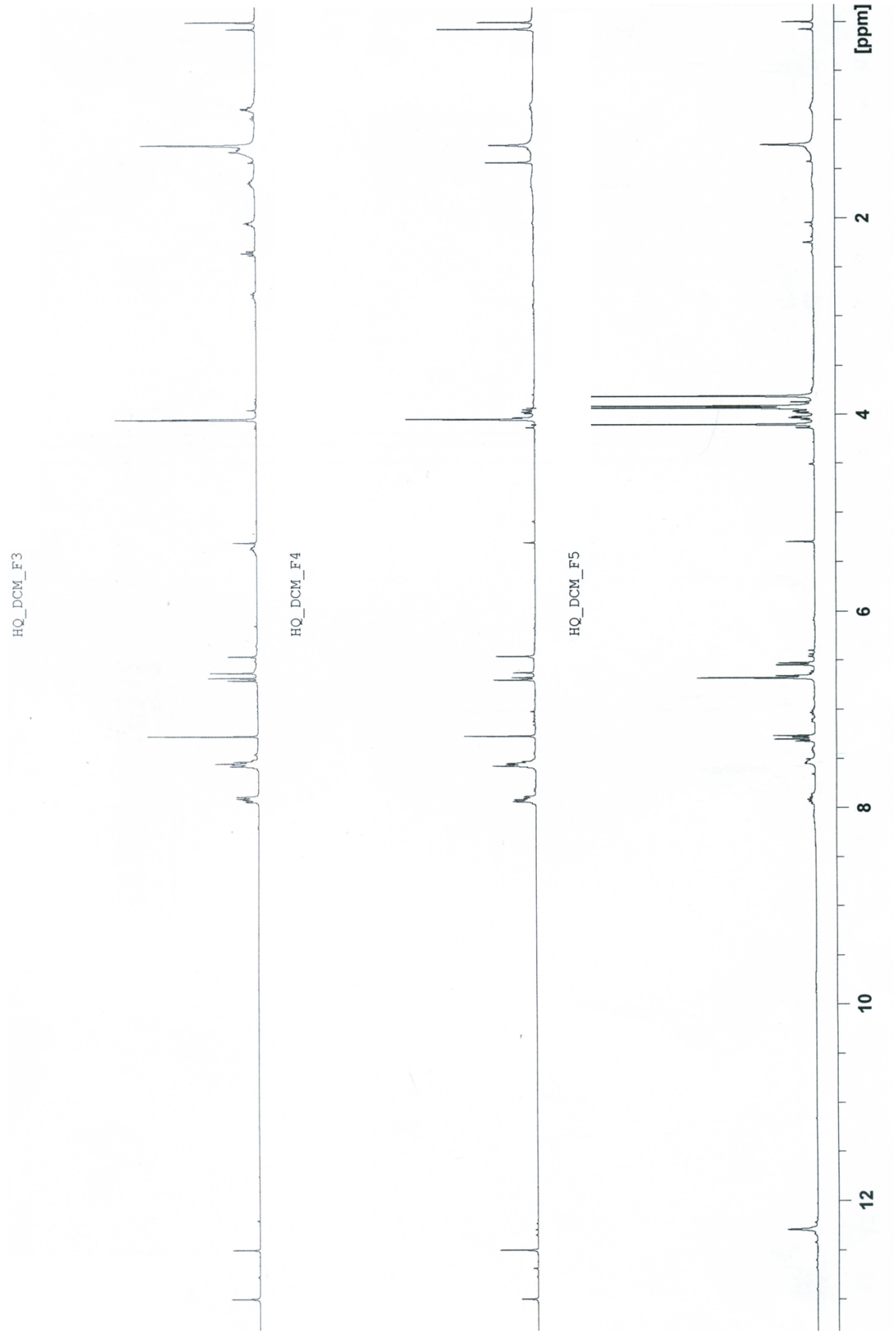

Figure S5.2 – ^{1}H-NMR spectroscopy analysis of HQDCM F3-5

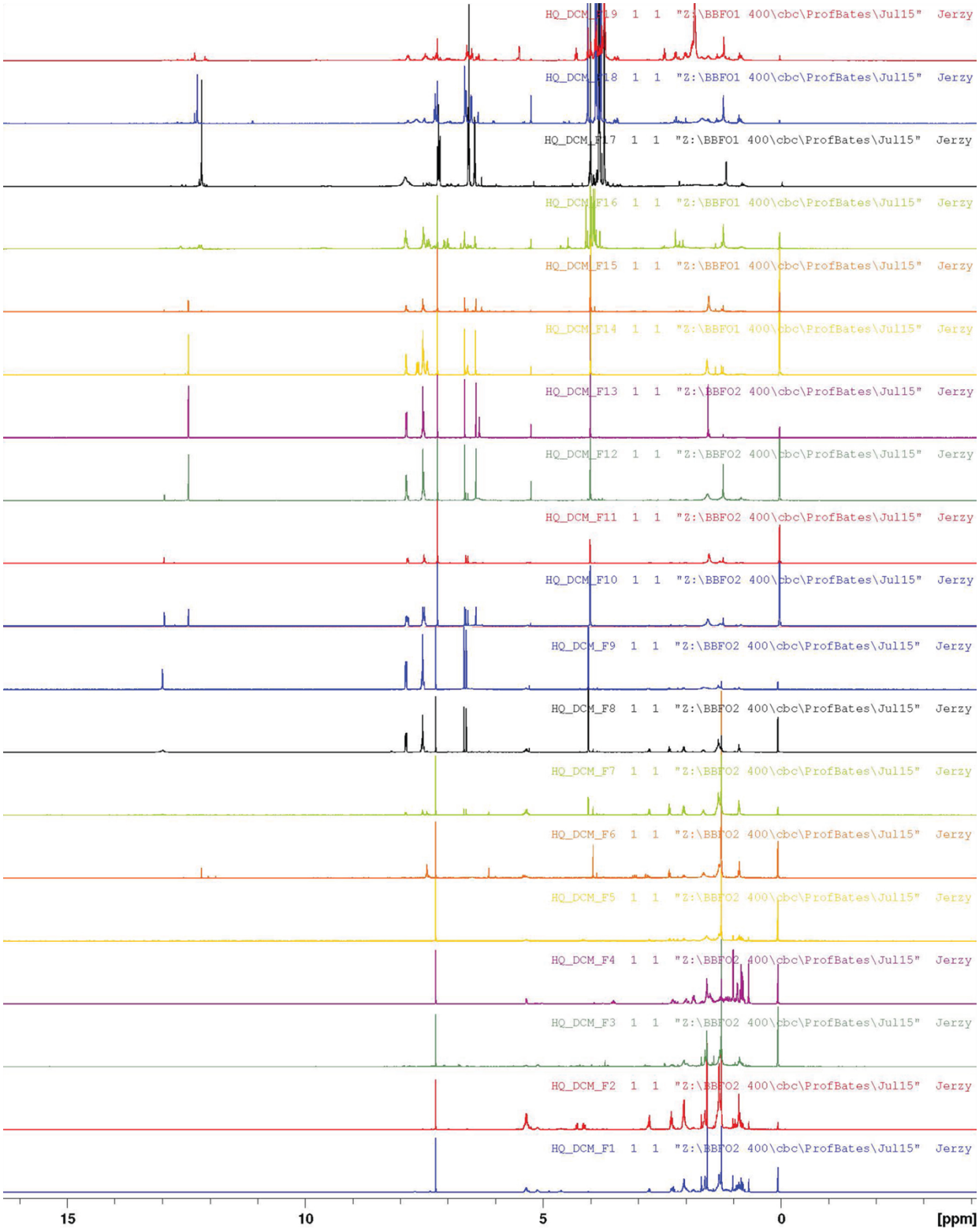

Figure S5.3 – ^{1}H-NMR spectroscopy profiling of targeted separation of HQDCM extract

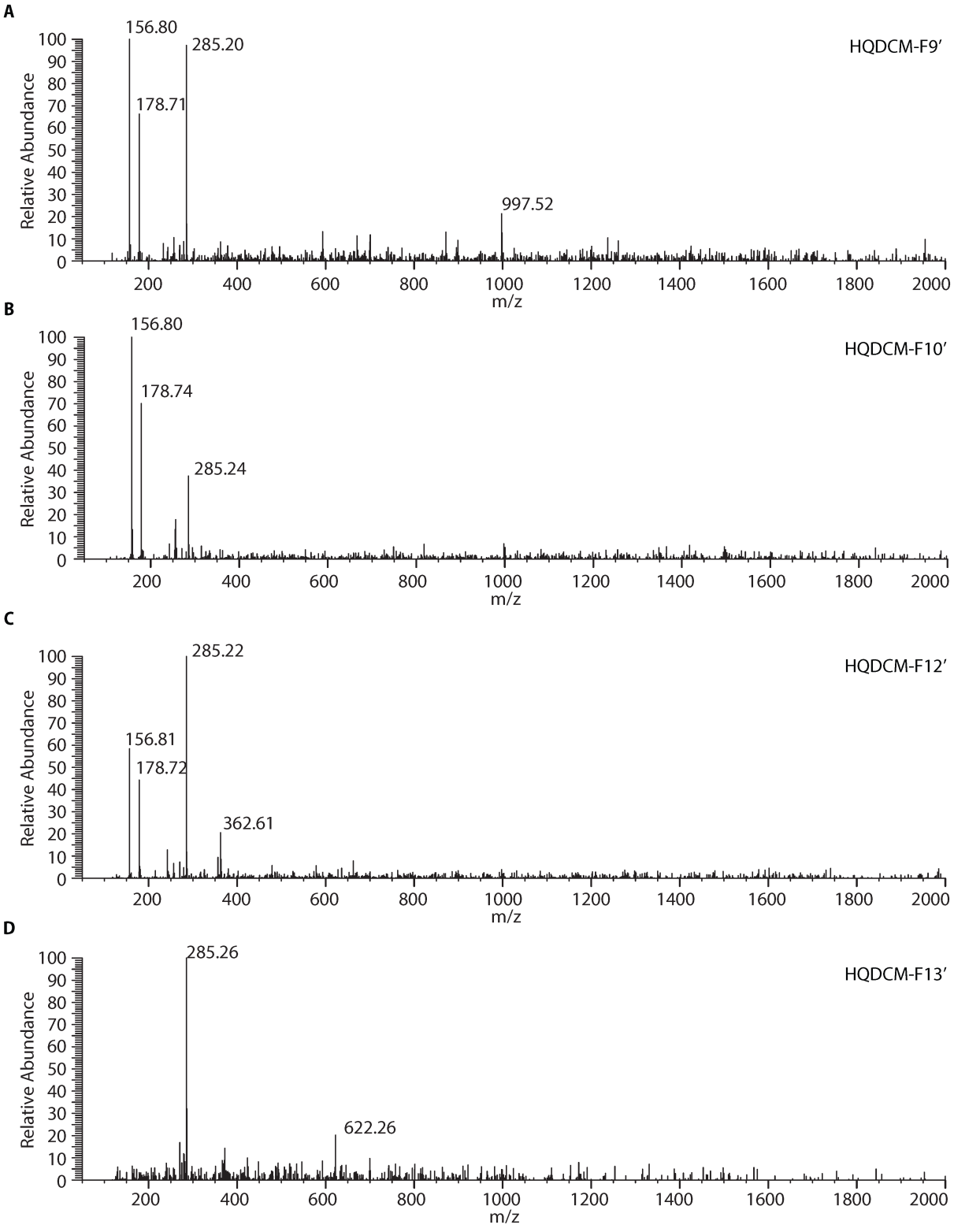

Figure S5.4 – Mass Spectrometry analysis of HQDCM F9', F10', F12' and F13'

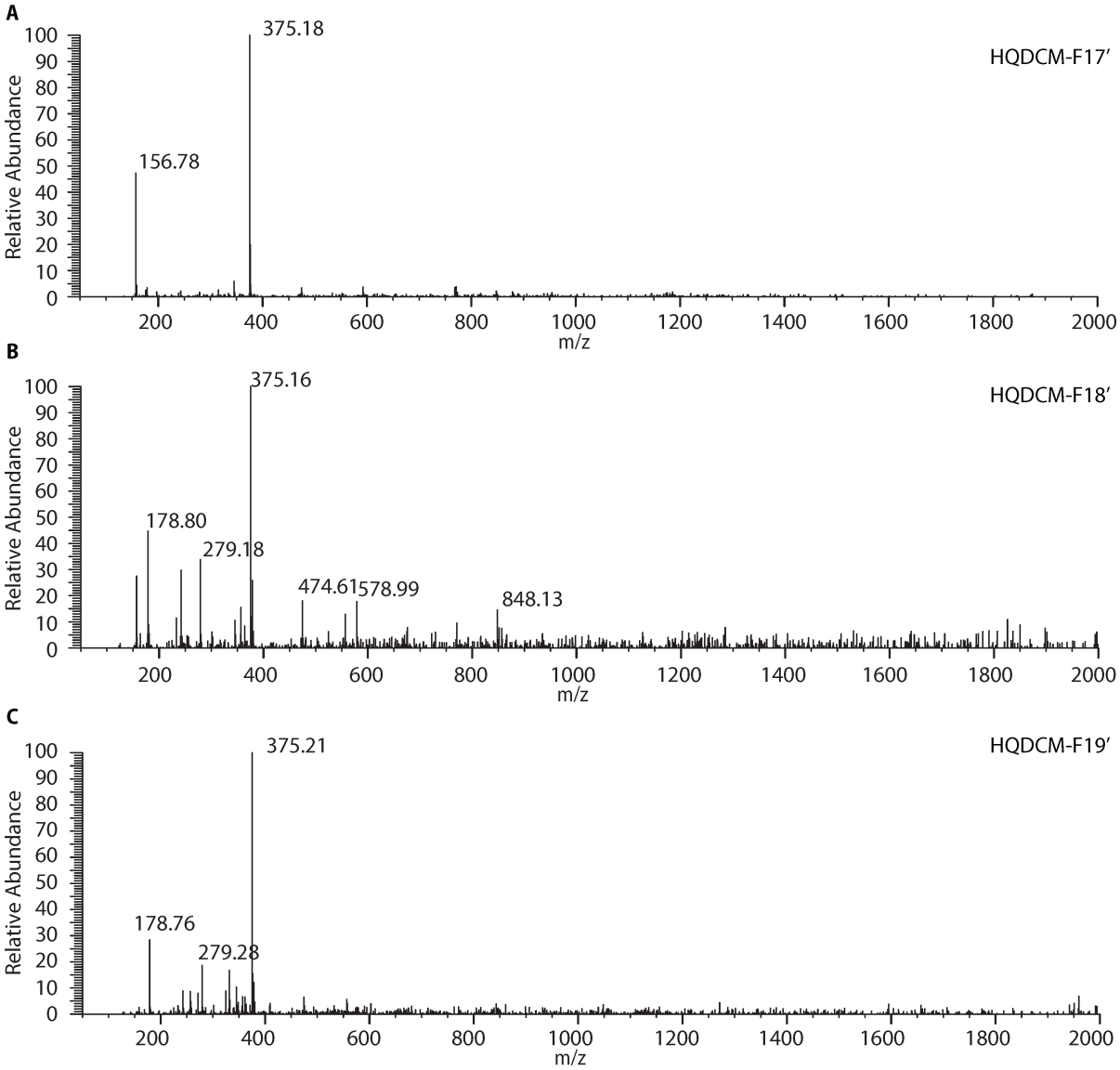

Figure S5.5 – Mass Spectrometry analysis of HQDCM F17', F18', F19'

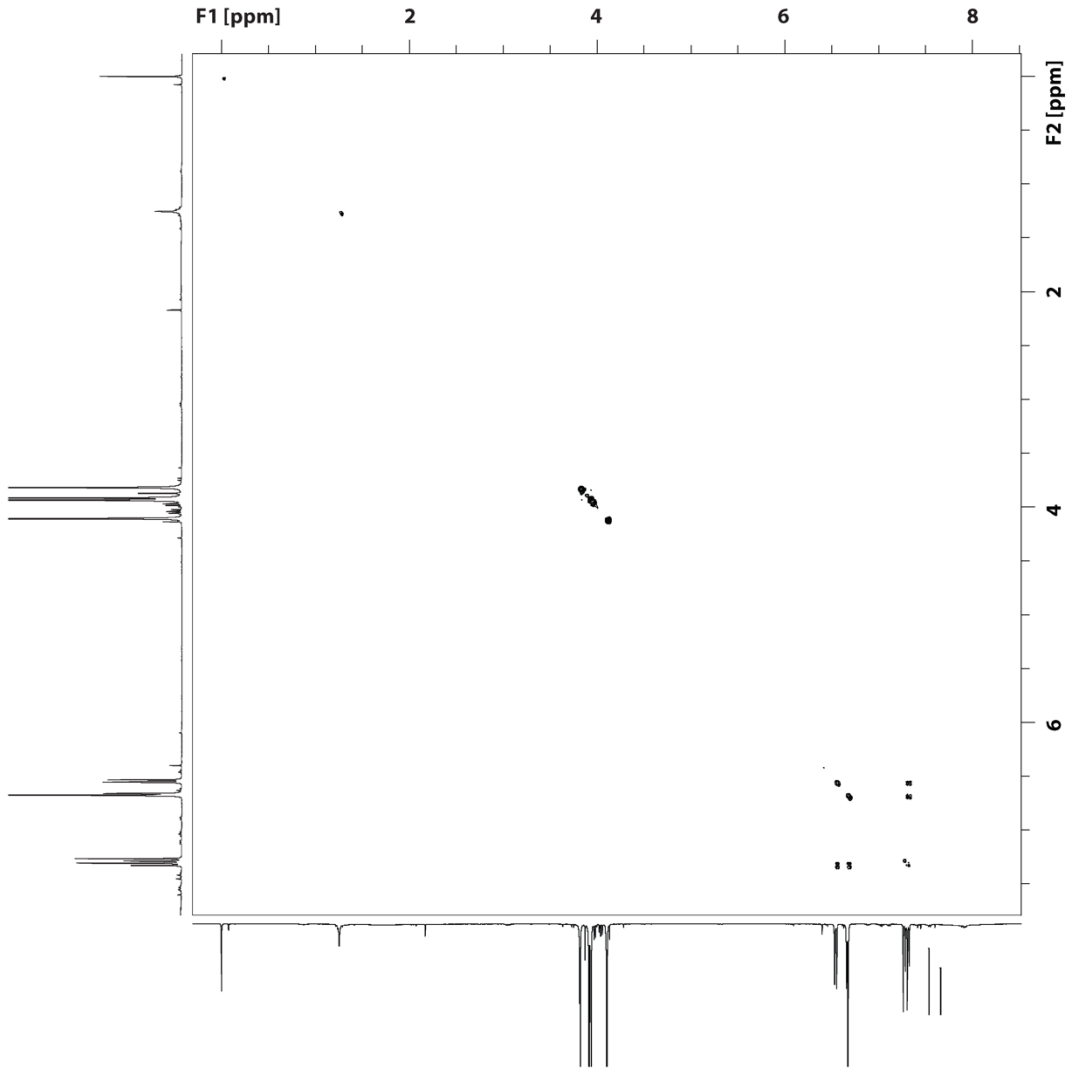

Figure S5.6 – Homonuclear correlation spectroscopy (COSY) analysis of HQDCM F17'

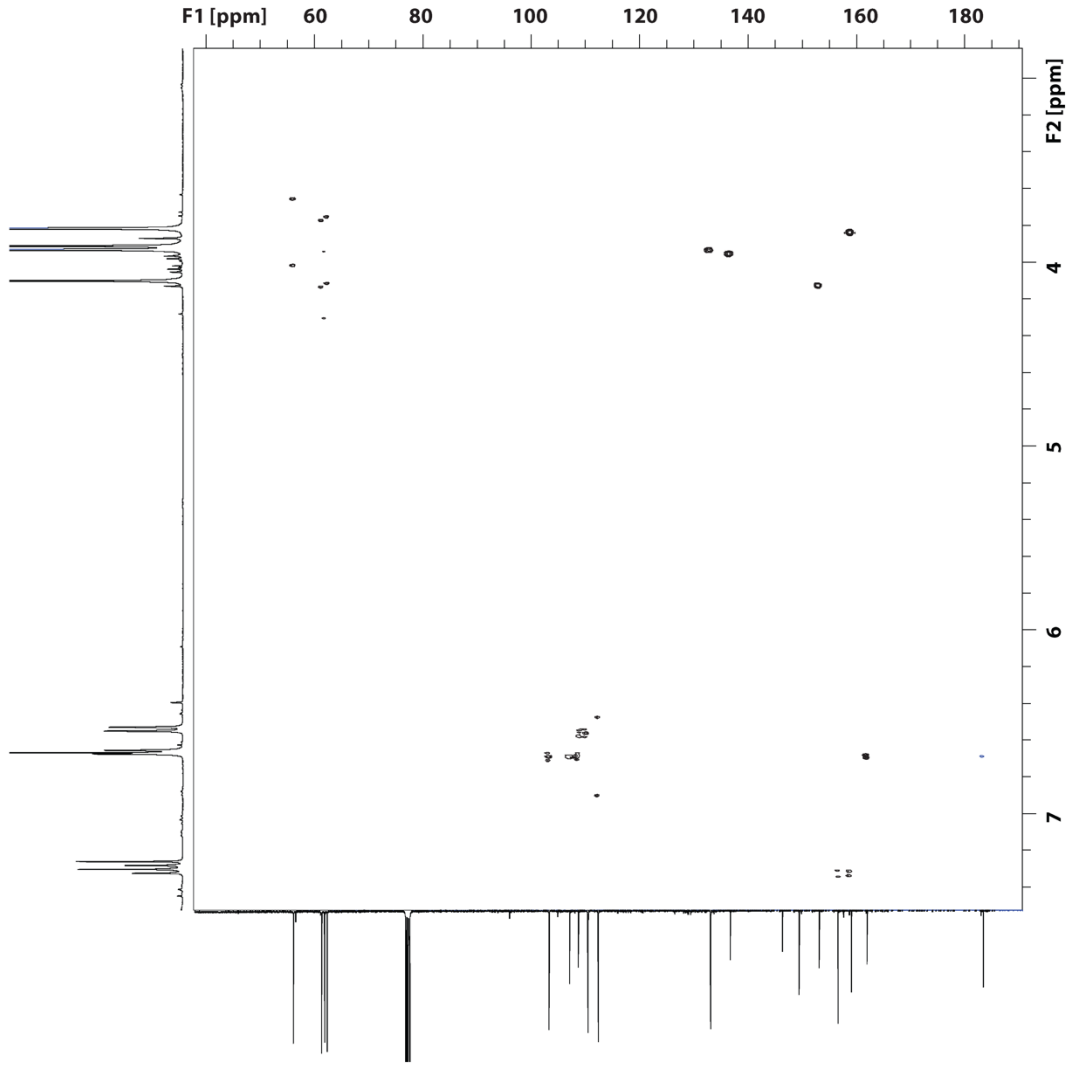

Figure S5.7 – Heteronuclear Multiple Bond Correlation spectroscopy analysis of HQDCM F17'

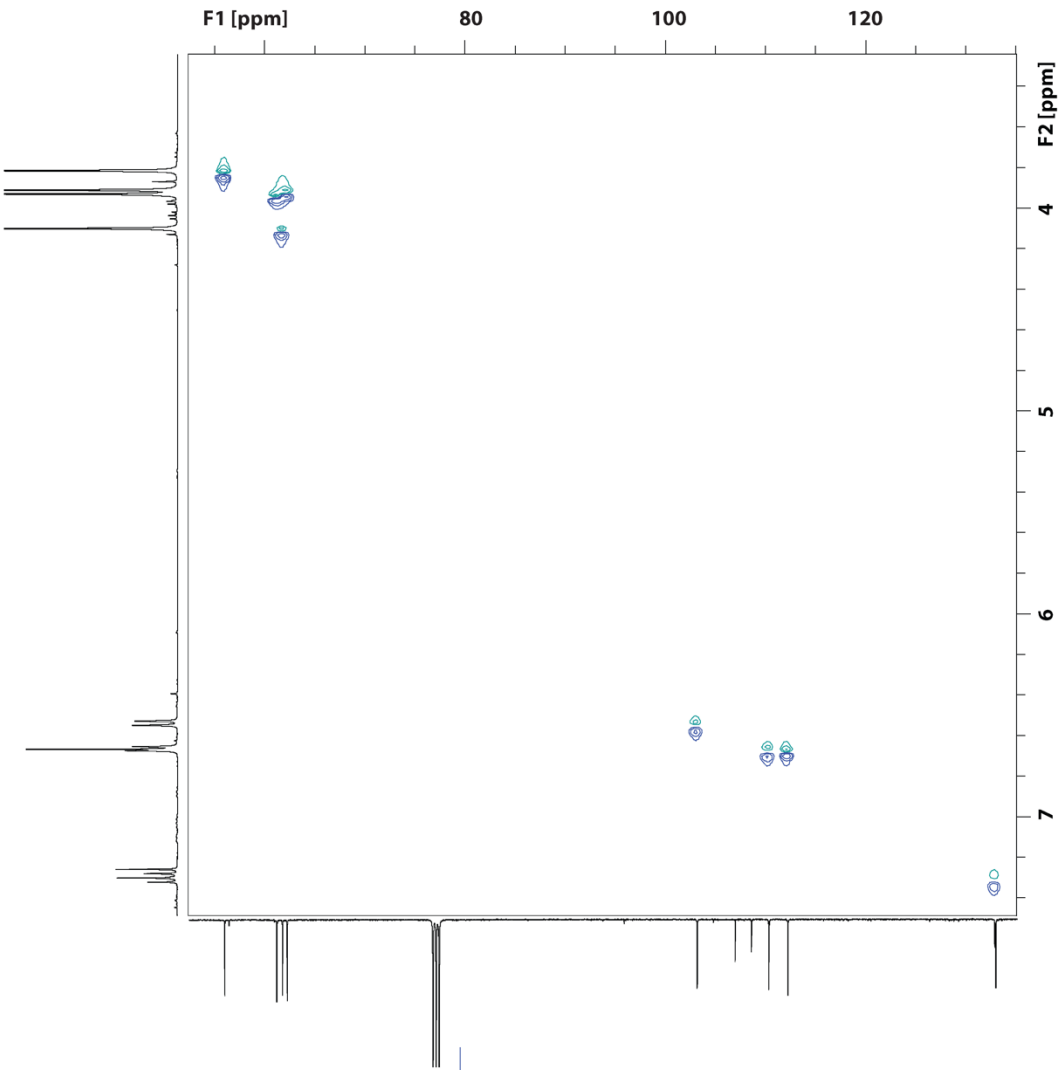

Figure S5.8 – Heteronuclear Single Quantum Coherence spectroscopy analysis of HQDCM F17'

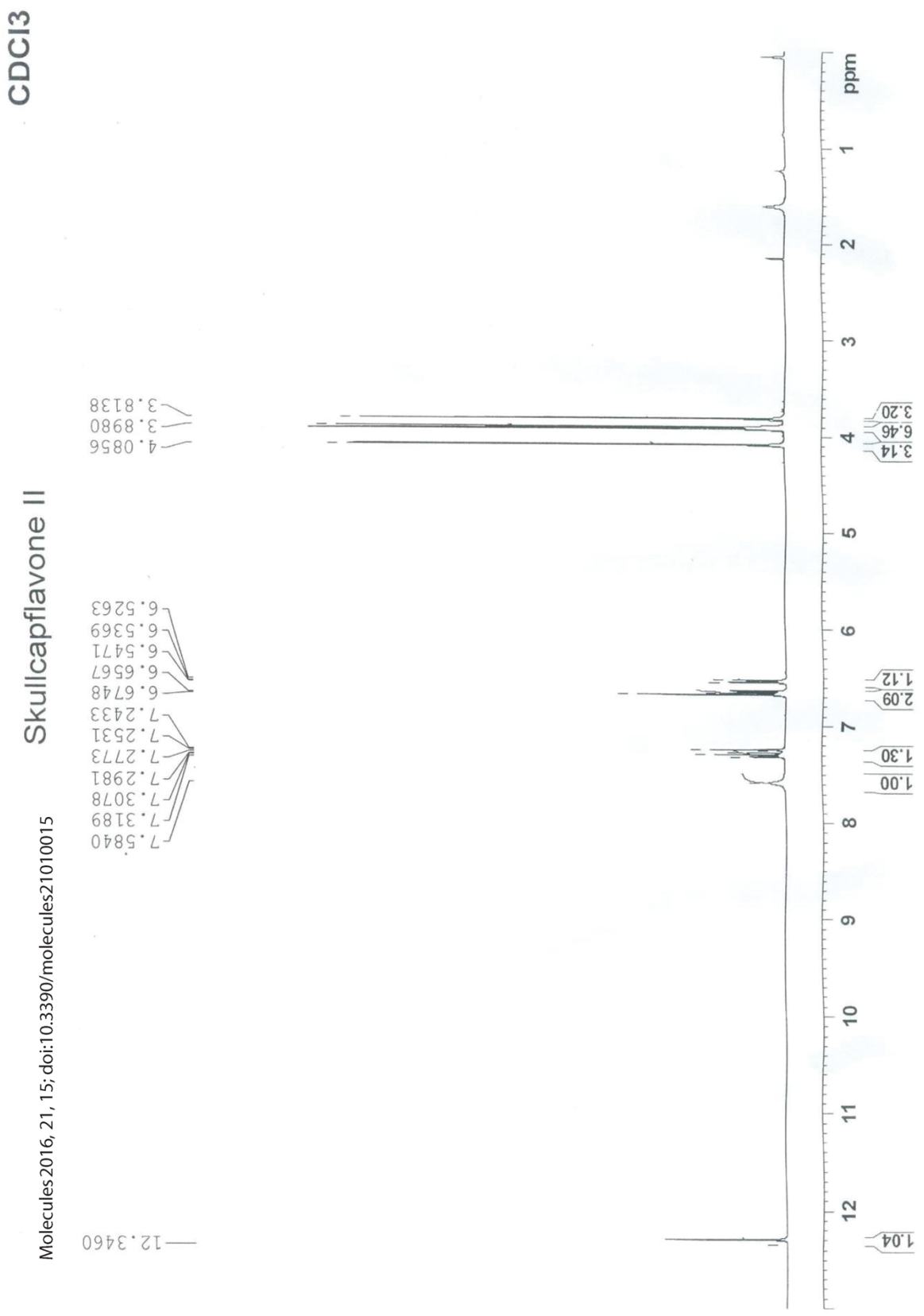

Figure S5.9 – Reference ^{1}H-NMR Spectrum of skullcapflavone II (Tsai et al., 2015)*(280)*

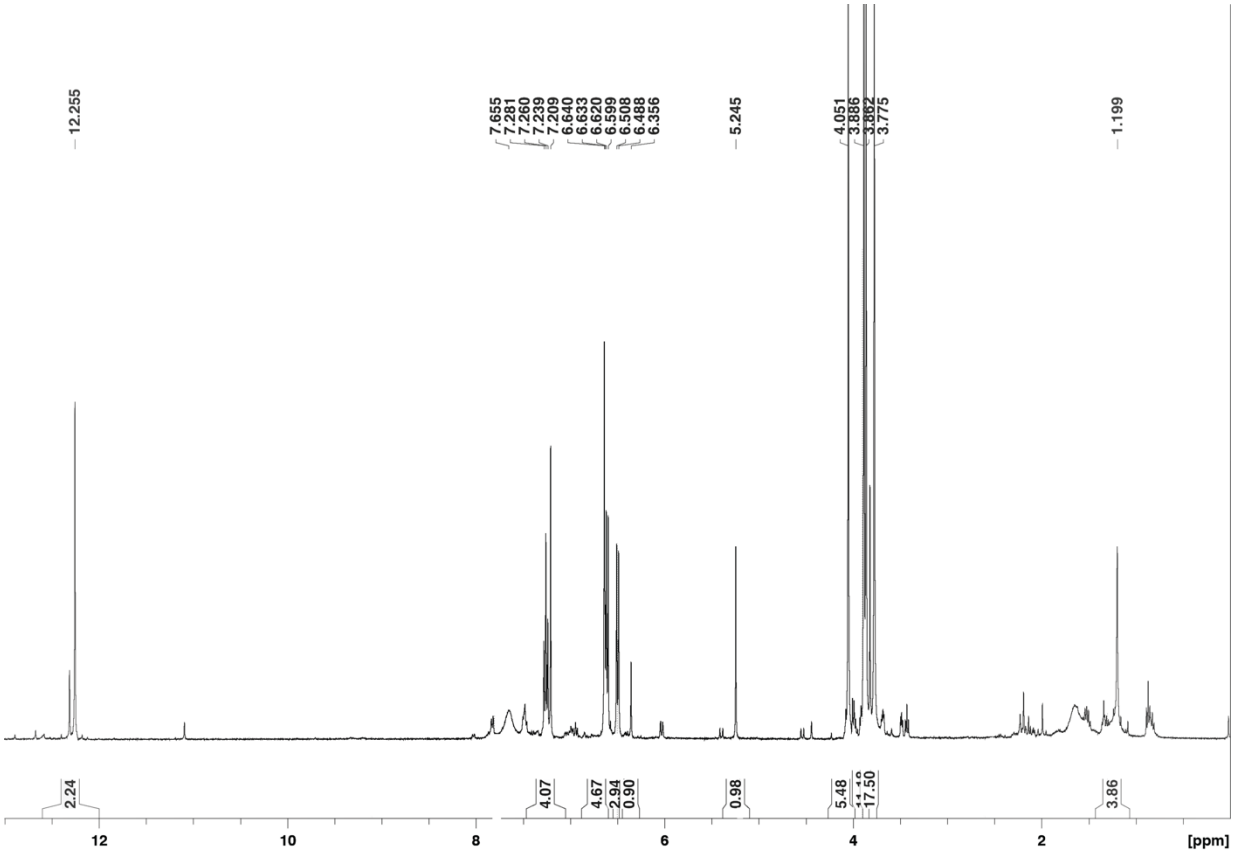

Figure S5.10 – ^{1}H-NMR Spectroscopy analysis of HQDCM F18'

Supplementary Tables

Rank	GO ID	Term	Count	%	p-value	Fold Enrichment
1	GO:0005829	cytosol	89	7.04	6E-21	2.43
2	GO:0005737	cytoplasm	153	12.09	7E-18	1.81
3	GO:0005634	nucleus	146	11.54	8E-16	1.77
4	GO:0022625	cytosolic large ribosomal subunit	42	3.32	7E-14	2.90
5	GO:0006511	ubiquitin-dependent protein catabolic process	40	3.16	5E-10	2.26
6	GO:0005838	proteasome regulatory particle	14	1.11	3E-07	3.80
7	GO:0022627	cytosolic small ribosomal subunit	23	1.82	1E-06	2.65
8	GO:0004175	endopeptidase activity	22	1.74	4E-06	2.33
9	GO:0005839	proteasome core complex	13	1.03	5E-06	3.52
10	GO:0008540	proteasome regulatory particle, base subcomplex	10	0.79	4E-05	3.80
11	GO:0004298	threonine-type endopeptidase activity	14	1.11	8E-05	2.57
12	GO:0003743	translation initiation factor activity	29	2.29	1E-04	1.86
13	GO:0016282	eukaryotic 43S preinitiation complex	10	0.79	2E-04	3.45
14	GO:0033290	eukaryotic 48S preinitiation complex	10	0.79	2E-04	3.45
15	GO:0005665	DNA-directed RNA polymerase II, core complex	11	0.87	2E-04	3.21
16	GO:0006457	protein folding	37	2.92	4E-04	1.64
17	GO:0006446	regulation of translational initiation	13	1.03	5E-04	2.45
18	GO:0005852	eukaryotic translation initiation factor 3 complex	9	0.71	6E-04	3.42
19	GO:0003723	RNA binding	72	5.69	6E-04	1.38
20	GO:0020020	food vacuole	21	1.66	7E-04	2.04
21	GO:0001731	formation of translation preinitiation complex	11	0.87	9E-04	2.60
22	GO:0051082	unfolded protein binding	21	1.66	0.0012	1.87
23	GO:0002181	cytoplasmic translation	13	1.03	0.0014	2.30
24	GO:0006888	ER to Golgi vesicle-mediated transport	17	1.34	0.0016	2.01
25	GO:0031595	nuclear proteasome complex	7	0.55	0.0018	3.80
26	GO:0019773	proteasome core complex, alpha-subunit complex	7	0.55	0.0018	3.80
27	GO:0006412	translation	77	6.09	0.0020	1.32
28	GO:0006260	DNA replication	19	1.50	0.0028	1.85
29	GO:0005643	nuclear pore	8	0.63	0.0047	3.04
30	GO:0005832	chaperonin-containing T-complex	7	0.55	0.0055	3.32
31	GO:0031597	cytosolic proteasome complex	6	0.47	0.0059	3.80
32	GO:0042555	MCM complex	6	0.47	0.0059	3.80
33	GO:0003746	translation elongation factor activity	16	1.26	0.0076	1.84
34	GO:0007264	small GTPase mediated signal transduction	14	1.11	0.0113	1.89
35	GO:0005681	spliceosomal complex	15	1.19	0.0127	1.90
36	GO:0000502	proteasome complex	7	0.55	0.0129	2.95
37	GO:0005794	Golgi apparatus	13	1.03	0.0159	1.97

38	GO:0008541	proteasome regulatory particle, lid subcomplex	5	0.40	0.0189	3.80
39	GO:0051603	proteolysis involved in cellular protein catabolic process	12	0.95	0.0222	1.89
40	GO:0045899	positive regulation of RNA polymerase II transcriptional preinitiation complex assembly	6	0.47	0.0230	2.83
41	GO:0006606	protein import into nucleus	6	0.47	0.0230	2.83
42	GO:0006414	translational elongation	11	0.87	0.0238	1.95
43	GO:0017025	TBP-class protein binding	6	0.47	0.0260	2.76
44	GO:0036402	proteasome-activating ATPase activity	6	0.47	0.0260	2.76
45	GO:0043248	proteasome assembly	7	0.55	0.0262	2.48
46	GO:0008565	protein transporter activity	17	1.34	0.0280	1.62
47	GO:0005759	mitochondrial matrix	11	0.87	0.0288	1.99
48	GO:0000166	nucleotide binding	49	3.87	0.0311	1.27
49	GO:0005732	small nucleolar ribonucleoprotein complex	8	0.63	0.0317	2.34
50	GO:0000398	mRNA splicing, via spliceosome	25	1.98	0.0321	1.44
51	GO:0003735	structural constituent of ribosome	69	5.45	0.0349	1.21
52	GO:0031201	SNARE complex	10	0.79	0.0389	2.00
53	GO:0005525	GTP binding	40	3.16	0.0396	1.30
54	GO:0019013	viral nucleocapsid	11	0.87	0.0407	1.90
55	GO:0006366	transcription from RNA polymerase II promoter	10	0.79	0.0438	1.89
56	GO:0008380	RNA splicing	14	1.11	0.0441	1.65
57	GO:0005622	intracellular	24	1.90	0.0469	1.45
58	GO:0006334	nucleosome assembly	9	0.71	0.0479	1.96
59	GO:0005515	protein binding	31	2.45	0.0495	1.34

Table S3.1 – Functional enrichment of GO terms in lysate melt curve CETSA datasets

Rank	GO ID	Term	Count	%	p-value	Fold Enrichment
1	GO:0005829	cytosol	88	6.49	1E-18	2.28
2	GO:0005634	nucleus	147	10.84	4E-14	1.69
3	GO:0005737	cytoplasm	149	10.99	9E-14	1.67
4	GO:0022625	cytosolic large ribosomal subunit	42	3.10	5E-13	2.75
5	GO:0006511	ubiquitin-dependent protein catabolic process	42	3.10	2E-11	2.35
6	GO:0022627	cytosolic small ribosomal subunit	27	1.99	1E-09	2.95
7	GO:0006457	protein folding	45	3.32	5E-08	1.96
8	GO:0005838	proteasome regulatory particle	14	1.03	6E-07	3.60
9	GO:0004175	endopeptidase activity	23	1.70	9E-07	2.36
10	GO:0005839	proteasome core complex	13	0.96	1E-05	3.35
11	GO:0003743	translation initiation factor activity	31	2.29	1E-05	1.92
12	GO:0051082	unfolded protein binding	24	1.77	3E-05	2.07
13	GO:0008540	proteasome regulatory particle, base subcomplex	10	0.74	7E-05	3.60
14	GO:0004298	threonine-type endopeptidase activity	14	1.03	1E-04	2.49
15	GO:0020020	food vacuole	23	1.70	1E-04	2.13
16	GO:0033290	eukaryotic 48S preinitiation complex	10	0.74	3E-04	3.28
17	GO:0016282	eukaryotic 43S preinitiation complex	10	0.74	3E-04	3.28
18	GO:0006446	regulation of translational initiation	13	0.96	6E-04	2.42
19	GO:0006412	translation	80	5.90	6E-04	1.35

20	GO:0005515	protein binding	38	2.80	6E-04	1.58
21	GO:0005852	eukaryotic translation initiation factor 3 complex	9	0.66	9E-04	3.24
22	GO:0005643	nuclear pore	9	0.66	9E-04	3.24
23	GO:0001731	formation of translation preinitiation complex	11	0.81	0.0010	2.56
24	GO:0002181	cytoplasmic translation	13	0.96	0.0016	2.27
25	GO:0050776	regulation of immune response	9	0.66	0.0016	2.79
26	GO:0005665	DNA-directed RNA polymerase II, core complex	10	0.74	0.0022	2.77
27	GO:0031595	nuclear proteasome complex	7	0.52	0.0024	3.60
28	GO:0019773	proteasome core complex, alpha-subunit complex	7	0.52	0.0024	3.60
29	GO:0000502	proteasome complex	8	0.59	0.0026	3.20
30	GO:0003746	translation elongation factor activity	17	1.25	0.0033	1.89
31	GO:0002377	immunoglobulin production	8	0.59	0.0041	2.79
32	GO:0005759	mitochondrial matrix	13	0.96	0.0042	2.23
33	GO:0008234	cysteine-type peptidase activity	11	0.81	0.0044	2.26
34	GO:0005615	extracellular space	11	0.81	0.0068	2.33
35	GO:0006099	tricarboxylic acid cycle	12	0.88	0.0073	2.09
36	GO:0051603	proteolysis involved in cellular protein catabolic process	13	0.96	0.0073	2.02
37	GO:0005832	chaperonin-containing T-complex	7	0.52	0.0073	3.15
38	GO:0031597	cytosolic proteasome complex	6	0.44	0.0075	3.60
39	GO:0042555	MCM complex	6	0.44	0.0075	3.60
40	GO:0005764	lysosome	9	0.66	0.0109	2.50
41	GO:0007264	small GTPase mediated signal transduction	14	1.03	0.0128	1.86
42	GO:0006413	translational initiation	14	1.03	0.0128	1.86
43	GO:0009408	response to heat	13	0.96	0.0135	1.91
44	GO:0006986	response to unfolded protein	11	0.81	0.0144	2.05
45	GO:0006334	nucleosome assembly	10	0.74	0.0144	2.15
46	GO:0030126	COPI vesicle coat	6	0.44	0.0202	3.09
47	GO:0000166	nucleotide binding	51	3.76	0.0228	1.28
48	GO:0008541	proteasome regulatory particle, lid subcomplex	5	0.37	0.0229	3.60
49	GO:0006606	protein import into nucleus	6	0.44	0.0245	2.79
50	GO:0045899	positive regulation of RNA polymerase II transcriptional preinitiation complex assembly	6	0.44	0.0245	2.79
51	GO:0006414	translational elongation	11	0.81	0.0263	1.92
52	GO:0006890	retrograde vesicle-mediated transport, Golgi to ER	7	0.52	0.0280	2.44
53	GO:0036402	proteasome-activating ATPase activity	6	0.44	0.0301	2.67
54	GO:0017025	TBP-class protein binding	6	0.44	0.0301	2.67
55	GO:0003723	RNA binding	66	4.87	0.0307	1.22
56	GO:0003735	structural constituent of ribosome	71	5.24	0.0343	1.21
57	GO:0004722	protein serine/threonine phosphatase activity	10	0.74	0.0376	1.91
58	GO:0005623	cell	8	0.59	0.0415	2.22
59	GO:1990225	rhoptry neck	6	0.44	0.0418	2.70
60	GO:0000786	nucleosome	6	0.44	0.0418	2.70
61	GO:0020008	rhoptry	13	0.96	0.0457	1.74
62	GO:0006096	glycolytic process	10	0.74	0.0477	1.86
63	GO:0006888	ER to Golgi vesicle-mediated transport	14	1.03	0.0491	1.63

Table S3.2 – Functional enrichment of GO terms in intact-cell melt curve CETSA datasets

Rank	ID	Term	Count	%	p-value	Fold Enrichment
1	GO:0005730	nucleolus	25	2.33	4E-06	2.60
2	GO:0005634	nucleus	87	8.11	1E-05	1.53
3	GO:0003700	transcription factor activity, sequence-specific DNA binding	20	1.86	1E-05	2.75
4	GO:0071013	catalytic step 2 spliceosome	18	1.68	3E-05	2.84
5	GO:0008270	zinc ion binding	45	4.19	5E-05	1.78
6	GO:0003676	nucleic acid binding	42	3.91	8E-05	1.78
7	GO:0046540	U4/U6 x U5 tri-snRNP complex	10	0.93	0.0012	3.24
8	GO:0000398	mRNA splicing, via spliceosome	19	1.77	0.0012	2.16
9	GO:0032040	small-subunit processome	13	1.21	0.0014	2.66
10	GO:0006355	regulation of transcription, DNA-templated	18	1.68	0.0015	2.18
11	GO:0000387	spliceosomal snRNP assembly	7	0.65	0.0016	4.33
12	GO:0010501	RNA secondary structure unwinding	15	1.40	0.0017	2.39
13	GO:0005686	U2 snRNP	10	0.93	0.0020	3.06
14	GO:0005682	U5 snRNP	8	0.75	0.0021	3.68
15	GO:0004004	ATP-dependent RNA helicase activity	19	1.77	0.0028	2.02
16	GO:1990225	rhoptry neck	6	0.56	0.0066	4.14
17	GO:0000375	RNA splicing, via transesterification reactions	11	1.03	0.0077	2.45
18	GO:0006364	rRNA processing	13	1.21	0.0087	2.20
19	GO:0019013	viral nucleocapsid	10	0.93	0.0104	2.51
20	GO:0005681	spliceosomal complex	12	1.12	0.0122	2.21
21	GO:0071011	precatalytic spliceosome	10	0.93	0.0144	2.40
22	GO:0017070	U6 snRNA binding	5	0.47	0.0156	4.24
23	GO:0000166	nucleotide binding	31	2.89	0.0174	1.49
24	GO:0030490	maturation of SSU-rRNA	5	0.47	0.0225	3.98
25	GO:0034399	nuclear periphery	9	0.84	0.0246	2.36
26	GO:0003688	DNA replication origin binding	4	0.37	0.0256	5.09
27	GO:0006468	protein phosphorylation	17	1.58	0.0317	1.69
28	GO:0004386	helicase activity	8	0.75	0.0336	2.40
29	GO:0005664	nuclear origin of replication recognition complex	4	0.37	0.0442	4.41
30	GO:0003677	DNA binding	35	3.26	0.0459	1.35
31	GO:0042787	protein ubiquitination involved in ubiquitin-dependent protein catabolic process	6	0.56	0.0475	2.79
32	GO:0046872	metal ion binding	30	2.80	0.0475	1.39
33	GO:0071004	U2-type prespliceosome	6	0.56	0.0497	2.76

Table S3.3 – Functional enrichment of GO terms in the non-melting protein subset of lysate melt curve CETSA

Compound	*N*	Model	p*KD* ± SD	*KD* (M)
MFQ	3	1:1 Steady-state	4.395 ± 0.192	4.03E-05
QN	3	1:1 Kinetic	7.524 ± 0.204	2.99E-08
ImmH	3	1:1 Kinetic	9.618 ± 0.129	2.41E-10

Table S4.1 – Surface Plasmon resonance measurements of PfPNP-MFQ/QN/ImmH KD

	MFQ	**QN**
Model	One site	Two sets of sites
K_D 1 (M)	11.6 e-6	65.8 e-9
ΔH1 (kcal/mol)	2.286 ± 0.88	-5.12 ± 9.0
K_D 2 (M)	-	534e-9
ΔH2 (kcal/mol)	-	14.0 ± 0.762

Table S4.2 – Isothermal Titration Calorimetry binding affinities for PfPNP-MFQ/QN interaction

	QN	MFQ
Km (μM)	22.77	23.68
Ki (μM)	0.1380	5.869
Vmax (pM/min)	331.9	296.4
Std. Error Km	3.573	3.479
Std. Error Ki	0.01975	0.8828
Std. Error Vmax	9.211	6.850
95% CI Km	15.71 to 29.84	16.80 to 30.56
95% CI Ki	0.09901 to 0.1771	4.124 to 7.614
95% CI Vmax	313.7 to 350.1	282.9 to 309.9
R squared	0.9443	0.9363
Absolute Sum of Squares	68813	80585

Table S4.3 – PfPNP *in vitro* enzymatic activity inhibition by MFQ and QN

	PfPNP-MFQ	PfPNP-QN
Crystallisation condition	0.2 M magnesium formate	0.1 M sodium citrate tribasic pH 5.6 and 1.0 M ammonium phosphate monobasic
Data collection		
Wave length (Å)	1.000	1.000
Space group	H32	P321
Cell dimension (Å)	95.59, 95.59, 136.57	95.12, 95.12, 47.14
Resolution (Å)	25.94 – 2.30	47.14 – 1.66
(outer shell)	(2.38 – 2.30)	(1.69 – 1.66)
Rmerge, %	4.6 (8.3)	5.0 (19.2)
<I>/σI	21.6 (10.5)	27.7 (7.9)
Completeness (%)	99.6 (100.0)	99.3 (89.3)
Redundancy	5.5 (5.6)	10.7 (9.7)
No. of observed reflections	59 291	313 554
No. of unique reflections	10 842	29 272
Model refinement		
Resolution (Å)	25.94 – 2.30	47.14 – 1.66
No. of protein molecules/AU	1	1
*R*work/*R*free, %	19.3/25.4	17.2/20.5
Number of atoms		
Protein	1762	1913
Ligands	26 (mefloquine) and 5 (one phosphate ions)	24 (quinine) and 15 (three phosphate ions)
Water	82	212
Average *B* factor (Å2)	28.0	19.0
r.m.s. deviations		
Bond length (Å)	0.0144	0.0226
Bond angle (°)	1.7459	2.1969
Ramachandran plot (%)		
Favoured region	96.9	97.1
Allowed region	3.1	2.9
Outlier region	0.0	0.0
PDB entry	5ZNI	5ZNC

Table S4.4 – Data collection and refinement statistics of PfPNP-MFQ and PfPNP-QN co-crystals

		Hypoxanthine 100 µM	Hypoxanthine 10 µM	Inosine 100 µM	Inosine 10 µM	No Purine
ImmH (nM)	**IC_{50}**	N/A	53.95 ±4.37	289.09 ±13.75	51.32 ±8.01	7.1 ±0.39
	IC_{90}	N/A	74.76 ±5.36	360.12 ±17.12	98.62 ±9.83	16.67 ±0.48
	IC_{99}	N/A	106.72 ±6.81	457.71 ±21.77	201.15 ±12.49	42.29 ±0.61
QN (nM)	**IC_{50}**	34.26 ±3.94	35.5 ±4.73	31.31 ±1.11	33.36 ±1.75	38.21 ±4.27
	IC_{90}	53.97 ±4.84	60.56 ±5.8	39.01 ±1.39	54.26 ±2.15	57.61 ±5.24
	IC_{99}	88.61 ±6.14	108.48 ±7.38	49.58 ±1.76	92.26 ±2.74	90.18 ±6.67
MFQ (nM)	**IC_{50}**	7.18 ±0.63	8.4 ±1.24	7.51 ±0.36	7.24 ±0.71	8.39 ±0.73
	IC_{90}	13.86 ±0.77	18.66 ±1.52	14.07 ±0.44	12.64 ±0.88	15.5 ±0.9
	IC_{99}	28.42 ±0.98	44.56 ±1.93	27.93 ±0.56	23.21 ±1.12	30.3 ±1.14

Table S4.5 – The influence of purine availability on the antimalarial drug efficacy in vitro

Drug Combination	ΣFIC_{50} 4:1	3:2	2:3	1:4	Mean ΣFIC_{50}	Interaction
MFQ + ImmH	1.24	1.54	1.69	1.28	1.44	Antagonism
QN + ImmH	1.43	1.40	1.18	0.95	1.24	Antagonism
E64d + ImmH	0.87	1.20	1.21	1.10	1.09	Additivity

Table S4.6 – Combinatory effect of fixed-ratio drug combinations against *P. falciparum* 3D7 strain

References

1. WHO, Geneva, World Malaria Report (2013).

2. WHO, Geneva, World Malaria Report (2017).

3. A. Kiszewski, A. Mellinger, A. Spielman, P. Malaney, S. E. Sachs, J. Sachs, A GLOBAL INDEX REPRESENTING THE STABILITY OF MALARIA TRANSMISSION, *Am. J. Trop. Med. Hyg.* 70, 486–498 (2004).

4. A. Bartoloni, L. Zammarchi, Clinical Aspects of Uncomplicated and Severe Malaria, *Mediterr. J. Hematol. Infect. Dis.* 4 (2012), doi:10.4084/MJHID.2012.026.

5. W. Hofheinz, B. Merkli, in *Antimalarial Drug II*, Handbook of Experimental Pharmacology. (Springer, Berlin, Heidelberg, 1984), pp. 61–81.

6. Loeb FF, Clark WM, Coatney GR, et al, Activity of a new antimalarial agent, chloroquine (sn 7618): Statement approved by the board for coordination of malarial studies, *J. Am. Med. Assoc.* 130, 1069–1070 (1946).

7. T. J. Egan, Quinoline antimalarials, *Expert Opin. Ther. Pat.* 11, 185–209 (2001).

8. L. J. Bruce-Chwatt, R. H. Black, C. J. Canfield, D. F. Clyde, W. Peters, W. H. Wernsdorfer, W. H. Organization, Chemotherapy of malaria, (1986) (available at http://apps.who.int/iris/handle/10665/38605).

9. R. Ferone, *Antimalarial Drug II: Current Antimalarial and New Drug Developments; Chapter V Dihydrofolate reductase Inhibitors* (Springer-Verlag, Berlin Heidelberg, 1984; //www.springer.com/gp/book/9783642692567).

10. A. Gregson, C. V. Plowe, Mechanisms of Resistance of Malaria Parasites to Antifolates, *Pharmacol. Rev.* 57, 117–145 (2005).

11. U. S. Neill, From branch to bedside: Youyou Tu is awarded the 2011 Lasker~DeBakey Clinical Medical Research Award for discovering artemisinin as a treatment for malaria, *J. Clin. Invest.* 121, 3768–3773 (2011).

12. E. Hsu, Reflections on the 'discovery' of the antimalarial qinghao, *Br. J. Clin. Pharmacol.* 61, 666–670 (2006).

13. S. Looareesuwan, C. Viravan, H. K. Webster, D. E. Kyle, D. B. Hutchinson, C. J. Canfield, Clinical Studies of Atovaquone, Alone or in Combination with other Antimalarial Drugs, for Treatment of Acute Uncomplicated Malaria in Thailand, *Am. J. Trop. Med. Hyg.* 54, 62–66 (1996).

14. I. K. Srivastava, A. B. Vaidya, A Mechanism for the Synergistic Antimalarial Action of Atovaquone and Proguanil, *Antimicrob. Agents Chemother.* 43, 1334–1339 (1999).

15. T. Gaillard, M. Madamet, B. Pradines, Tetracyclines in malaria, *Malar. J.* 14, 445 (2015).

16. P. B. Bloland, WHO, Geneva, Drug resistance in malaria, *World Health Organisation* , 32 (2001).

17. T. N. C. Wells, R. H. van Huijsduijnen, W. C. V. Voorhis, Malaria medicines: a glass half full?, *Nat. Rev. Drug Discov.* 14, 424–442 (2015).

18. E. L. Flannery, A. K. Chatterjee, E. A. Winzeler, Antimalarial Drug Discovery: Approaches and Progress towards New Medicines, *Nat. Rev. Microbiol.* 11, 849–862 (2013).

19. WHO, Geneva, Implications of insecticide resistance for malaria vector control (2016).

20. E. A. Ashley, M. Dhorda, R. M. Fairhurst, C. Amaratunga, P. Lim, S. Suon, S. Sreng, J. M. Anderson, S. Mao, B. Sam, C. Sopha, C. M. Chuor, C. Nguon, S. Sovannaroth, S. Pukrittayakamee,

P. Jittamala, K. Chotivanich, K. Chutasmit, C. Suchatsoonthorn, R. Runcharoen, T. T. Hien, N. T. Thuy-Nhien, N. V. Thanh, N. H. Phu, Y. Htut, K.-T. Han, K. H. Aye, O. A. Mokuolu, R. R. Olaosebikan, O. O. Folaranmi, M. Mayxay, M. Khanthavong, B. Hongvanthong, P. N. Newton, M. A. Onyamboko, C. I. Fanello, A. K. Tshefu, N. Mishra, N. Valecha, A. P. Phyo, F. Nosten, P. Yi, R. Tripura, S. Borrmann, M. Bashraheil, J. Peshu, M. A. Faiz, A. Ghose, M. A. Hossain, R. Samad, M. R. Rahman, M. M. Hasan, A. Islam, O. Miotto, R. Amato, B. MacInnis, J. Stalker, D. P. Kwiatkowski, Z. Bozdech, A. Jeeyapant, P. Y. Cheah, T. Sakulthaew, J. Chalk, B. Intharabut, K. Silamut, S. J. Lee, B. Vihokhern, C. Kunasol, M. Imwong, J. Tarning, W. J. Taylor, S. Yeung, C. J. Woodrow, J. A. Flegg, D. Das, J. Smith, M. Venkatesan, C. V. Plowe, K. Stepniewska, P. J. Guerin, A. M. Dondorp, N. P. Day, N. J. White, Spread of Artemisinin Resistance in Plasmodium falciparum Malaria, *N. Engl. J. Med.* 371, 411–423 (2014).

21. A. M. Dondorp, F. Nosten, P. Yi, D. Das, A. P. Phyo, J. Tarning, K. M. Lwin, F. Ariey, W. Hanpithakpong, S. J. Lee, P. Ringwald, K. Silamut, M. Imwong, K. Chotivanich, P. Lim, T. Herdman, S. S. An, S. Yeung, P. Singhasivanon, N. P. J. Day, N. Lindegardh, D. Socheat, N. J. White, Artemisinin Resistance in Plasmodium falciparum Malaria, *N. Engl. J. Med.* 361, 455–467 (2009).

22. N. J. White, Antimalarial drug resistance, *J. Clin. Invest.* 113, 1084–1092 (2004).

23. A. M. Croft, A lesson learnt: the rise and fall of Lariam and Halfan, *J. R. Soc. Med.* 100, 170–174 (2007).

24. F. P. Mockenhaupt, Mefloquine resistance in Plasmodium falciparum, *Parasitol. Today Pers. Ed* 11, 248–253 (1995).

25. D. Menard, A. Dondorp, Antimalarial Drug Resistance: A Threat to Malaria Elimination, *Cold Spring Harb. Perspect. Med.* 7, a025619 (2017).

26. P. Olliaro, Mode of action and mechanisms of resistance for antimalarial drugs, *Pharmacol. Ther.* 89, 207–219 (2001).

27. K. H. Rieckmann, D. R. Davis, D. C. Hutton, Plasmodium vivax resistance to chloroquine?, *Lancet Lond. Engl.* 2, 1183–1184 (1989).

28. A. Ecker, A. M. Lehane, J. Clain, D. A. Fidock, PfCRT and its role in antimalarial drug resistance, *Trends Parasitol.* 28, 504–514 (2012).

29. A. F. Cowman, D. Galatis, J. K. Thompson, Selection for mefloquine resistance in Plasmodium falciparum is linked to amplification of the pfmdr1 gene and cross-resistance to halofantrine and quinine, *Proc. Natl. Acad. Sci. U. S. A.* 91, 1143–1147 (1994).

30. A. B. S. Sidhu, A.-C. Uhlemann, S. G. Valderramos, J.-C. Valderramos, S. Krishna, D. A. Fidock, Decreasing pfmdr1 copy number in plasmodium falciparum malaria heightens susceptibility to mefloquine, lumefantrine, halofantrine, quinine, and artemisinin, *J. Infect. Dis.* 194, 528–535 (2006).

31. J. Verdrager, Epidemiology of the emergence and spread of drug-resistant falciparum malaria in South-East Asia and Australasia, *J. Trop. Med. Hyg.* 89, 277–289 (1986).

32. S. Vinayak, M. T. Alam, T. Mixson-Hayden, A. M. McCollum, R. Sem, N. K. Shah, P. Lim, S. Muth, W. O. Rogers, T. Fandeur, J. W. Barnwell, A. A. Escalante, C. Wongsrichanalai, F. Ariey, S. R. Meshnick, V. Udhayakumar, Origin and Evolution of Sulfadoxine Resistant Plasmodium falciparum, *PLoS Pathog* 6, e1000830 (2010).

33. D. S. Peterson, D. Walliker, T. E. Wellems, Evidence that a point mutation in dihydrofolate reductase-thymidylate synthase confers resistance to pyrimethamine in falciparum malaria., *Proc. Natl. Acad. Sci. U. S. A.* 85, 9114–9118 (1988).

34. J. Yuvaniyama, P. Chitnumsub, S. Kamchonwongpaisan, J. Vanichtanankul, W. Sirawaraporn, P. Taylor, M. D. Walkinshaw, Y. Yuthavong, Insights into antifolate resistance from malarial DHFR-TS structures, *Nat. Struct. Biol.* 10, 357 (2003).

35. L. M. Fohl, D. S. Roos, Fitness effects of DHFR-TS mutations associated with pyrimethamine resistance in apicomplexan parasites, *Mol. Microbiol.* 50, 1319–1327 (2003).

36. P. Maitarad, P. Saparpakorn, S. Hannongbua, S. Kamchonwongpaisan, B. Tarnchompoo, Y. Yuthavong, Particular interaction between pyrimethamine derivatives and quadruple mutant type dihydrofolate reductase of Plasmodium falciparum: CoMFA and quantum chemical calculations studies, *J. Enzyme Inhib. Med. Chem.* 24, 471–479 (2009).

37. J. G. Kublin, F. K. Dzinjalamala, D. D. Kamwendo, E. M. Malkin, J. F. Cortese, L. M. Martino, R. A. G. Mukadam, S. J. Rogerson, A. G. Lescano, M. E. Molyneux, P. A. Winstanley, P. Chimpeni, T. E. Taylor, C. V. Plowe, Molecular markers for failure of sulfadoxine-pyrimethamine and chlorproguanil-dapsone treatment of Plasmodium falciparum malaria, *J. Infect. Dis.* 185, 380–388 (2002).

38. M. Korsinczky, K. Fischer, N. Chen, J. Baker, K. Rieckmann, Q. Cheng, Sulfadoxine Resistance in Plasmodium vivax Is Associated with a Specific Amino Acid in Dihydropteroate Synthase at the Putative Sulfadoxine-Binding Site, *Antimicrob. Agents Chemother.* 48, 2214–2222 (2004).

39. D. R. Brooks, P. Wang, M. Read, W. M. Watkins, P. F. G. Sims, J. E. Hyde, Sequence Variation of the Hydroxymethyldihydropterin Pyrophosphokinase: Dihydropteroate Synthase Gene in Lines of the Human Malaria Parasite, Plasmodium falciparum, with Differing Resistance to Sulfadoxine, *Eur. J. Biochem.* 224, 397–405 (1994).

40. P. Wang, M. Read, P. F. G. Sims, J. E. Hyde, Sulfadoxine resistance in the human malaria parasite Plasmodium falciparum is determined by mutations in dihydropteroate synthetase and an additional factor associated with folate utilization, *Mol. Microbiol.* 23, 979–986 (2003).

41. WHO, Geneva, Status report on artemisinin and ACT resistance (April 2017)*WHO* (2017) (available at http://www.who.int/malaria/publications/atoz/artemisinin-resistance-april2017/en/).

42. M. D. Bustos, C. Wongsrichanalai, C. Delacollette, B. Burkholder, Monitoring antimalarial drug efficacy in the Greater Mekong Subregion: an overview of in vivo results from 2008 to 2010., *Southeast Asian J. Trop. Med. Public Health* 44 Suppl 1, 201–30; discussion 306-7 (2013).

43. V. I. Carrara, K. M. Lwin, A. P. Phyo, E. Ashley, J. Wiladphaingern, K. Sriprawat, M. Rijken, M. Boel, R. McGready, S. Proux, C. Chu, P. Singhasivanon, N. White, F. Nosten, Malaria Burden and Artemisinin Resistance in the Mobile and Migrant Population on the Thai–Myanmar Border, 1999–2011: An Observational Study, *PLOS Med.* 10, e1001398 (2013).

44. M. B. Denis, R. Tsuyuoka, P. Lim, N. Lindegardh, P. Yi, S. N. Top, D. Socheat, T. Fandeur, A. Annerberg, E. M. Christophel, P. Ringwald, Efficacy of artemether-lumefantrine for the treatment of uncomplicated falciparum malaria in northwest Cambodia, *Trop. Med. Int. Health TM IH* 11, 1800–1807 (2006).

45. R. Leang, A. Barrette, D. M. Bouth, D. Menard, R. Abdur, S. Duong, P. Ringwald, Efficacy of Dihydroartemisinin-Piperaquine for Treatment of Uncomplicated Plasmodium falciparum and Plasmodium vivax in Cambodia, 2008 to 2010, *Antimicrob. Agents Chemother.* 57, 818–826 (2013).

46. W. O. Rogers, R. Sem, T. Tero, P. Chim, P. Lim, S. Muth, D. Socheat, F. Ariey, C. Wongsrichanalai, Failure of artesunate-mefloquine combination therapy for uncomplicated Plasmodium falciparum malaria in southern Cambodia, *Malar. J.* 8, 10 (2009).

47. D. L. Saunders, P. Vanachayangkul, C. Lon, Dihydroartemisinin–Piperaquine Failure in Cambodia, *N. Engl. J. Med.* 371, 484–485 (2014).

48. S. Vijaykadga, C. Rojanawatsirivej, S. Cholpol, D. Phoungmanee, A. Nakavej, C. Wongsrichanalai, In vivo sensitivity monitoring of mefloquine monotherapy and artesunate-mefloquine combinations for the treatment of uncomplicated falciparum malaria in Thailand in 2003, *Trop. Med. Int. Health TM IH* 11, 211–219 (2006).

49. S. Mok, E. A. Ashley, P. E. Ferreira, L. Zhu, Z. Lin, T. Yeo, K. Chotivanich, M. Imwong, S. Pukrittayakamee, M. Dhorda, C. Nguon, P. Lim, C. Amaratunga, S. Suon, T. T. Hien, Y. Htut, M. A. Faiz, M. A. Onyamboko, M. Mayxay, P. N. Newton, R. Tripura, C. J. Woodrow, O. Miotto, D. P. Kwiatkowski, F. Nosten, N. P. J. Day, P. R. Preiser, N. J. White, A. M. Dondorp, R. M. Fairhurst, Z. Bozdech, Population transcriptomics of human malaria parasites reveals the mechanism of artemisinin resistance, *Science* 347, 431–435 (2015).

50. S. Mok, M. Imwong, M. J. Mackinnon, J. Sim, R. Ramadoss, P. Yi, M. Mayxay, K. Chotivanich, K.-Y. Liong, B. Russell, D. Socheat, P. N. Newton, N. P. Day, N. J. White, P. R. Preiser, F. Nosten, A. M. Dondorp, Z. Bozdech, Artemisinin resistance in Plasmodium falciparum is associated with an altered temporal pattern of transcription, *BMC Genomics* 12, 391 (2011).

51. A. Hott, D. Casandra, K. N. Sparks, L. C. Morton, G.-G. Castanares, A. Rutter, D. E. Kyle, Artemisinin-resistant Plasmodium falciparum parasites exhibit altered patterns of development in infected erythrocytes, *Antimicrob. Agents Chemother.* 59, 3156–3167 (2015).

52. T. Mita, S.-I. Tachibana, M. Hashimoto, M. Hirai, Plasmodium falciparum kelch 13: a potential molecular marker for tackling artemisinin-resistant malaria parasites, *Expert Rev. Anti Infect. Ther.* 14, 125–135 (2016).

53. F. M. C. Rocamora, thesis, Nanyang Technological University, Singapore (2017).

54. F. Rocamora, L. Zhu, K. Y. Liong, A. Dondorp, O. Miotto, S. Mok, Z. Bozdech, Oxidative stress and protein damage responses mediate artemisinin resistance in malaria parasites, *PLOS Pathog.* 14, e1006930 (2018).

55. M. Chugh, C. Scheurer, S. Sax, E. Bilsland, D. A. van Schalkwyk, K. J. Wicht, N. Hofmann, A. Sharma, S. Bashyam, S. Singh, S. G. Oliver, T. J. Egan, P. Malhotra, C. J. Sutherland, H.-P. Beck, S. Wittlin, T. Spangenberg, X. C. Ding, Identification and Deconvolution of Cross-Resistance Signals from Antimalarial Compounds Using Multidrug-Resistant Plasmodium falciparum Strains, *Antimicrob. Agents Chemother.* 59, 1110–1118 (2015).

56. D. F. Echeverry, G. Holmgren, C. Murillo, J. C. Higuita, A. Björkman, J. P. Gil, L. Osorio, Short report: polymorphisms in the pfcrt and pfmdr1 genes of Plasmodium falciparum and in vitro susceptibility to amodiaquine and desethylamodiaquine, *Am. J. Trop. Med. Hyg.* 77, 1034–1038 (2007).

57. D. Menard, F. Yapou, A. Manirakiza, D. Djalle, M. D. Matsika-Claquin, A. Talarmin, Polymorphisms in pfcrt, pfmdr1, dhfr genes and in vitro responses to antimalarials in Plasmodium falciparum isolates from Bangui, Central African Republic, *Am. J. Trop. Med. Hyg.* 75, 381–387 (2006).

58. S. Pelleau, E. L. Moss, S. K. Dhingra, B. Volney, J. Casteras, S. J. Gabryszewski, S. K. Volkman, D. F. Wirth, E. Legrand, D. A. Fidock, D. E. Neafsey, L. Musset, Adaptive evolution of malaria parasites in French Guiana: Reversal of chloroquine resistance by acquisition of a mutation in pfcrt, *Proc. Natl. Acad. Sci. U. S. A.* 112, 11672–11677 (2015).

59. C. A. Homewood, D. C. Warhurst, W. Peters, V. C. Baggaley, Lysosomes, pH and the Anti-malarial Action of Chloroquine, *Nature* 235, 50–52 (1972).

60. P. Olliaro, F. Castelli, S. Caligaris, P. Druilhe, G. Carosi, Ultrastructure of Plasmodium falciparum “in vitro”. II. Morphological patterns of different quinolines effects, *Microbiologica* 12, 15–28 (1989).

61. A. F. G. Slater, A. Cerami, Inhibition by chloroquine of a novel haem polymerase enzyme activity in malaria trophozoites, *Nature* 355, 167 (1992).

62. A. C. Chou, R. Chevli, C. D. Fitch, Ferriprotoporphyrin IX fulfills the criteria for identification as the chloroquine receptor of malaria parasites., *Biochemistry* 19, 1543–1549 (1980).

63. K. N. Olafson, M. A. Ketchum, J. D. Rimer, P. G. Vekilov, Mechanisms of hematin crystallization and inhibition by the antimalarial drug chloroquine, *Proc. Natl. Acad. Sci.* 112, 4946–4951 (2015).

64. D. J. Sullivan, I. Y. Gluzman, D. G. Russell, D. E. Goldberg, On the molecular mechanism of chloroquine’s antimalarial action, *Proc. Natl. Acad. Sci. U. S. A.* 93, 11865–11870 (1996).

65. D. J. Sullivan, Theories on malarial pigment formation and quinoline action, *Int. J. Parasitol.* 32, 1645–1653 (2002).

66. M. Mungthin, P. G. Bray, R. G. Ridley, S. A. Ward, Central Role of Hemoglobin Degradation in Mechanisms of Action of 4-Aminoquinolines, Quinoline Methanols, and Phenanthrene Methanols, *Antimicrob. Agents Chemother.* 42, 2973–2977 (1998).

67. F. Kwakye-Berko, S. R. Meshnick, Binding of chloroquine to DNA, *Mol. Biochem. Parasitol.* 35, 51–55 (1989).

68. N. Surolia, G. Padmanaban, Chloroquine inhibits heme-dependent protein synthesis in Plasmodium falciparum, *Proc. Natl. Acad. Sci. U. S. A.* 88, 4786–4790 (1991).

69. E. Königk, S. Mirtsch, B. Putfarken, S. Abdel-Rasoul, Plasmodium chabaudi-infection of mice: effects of chloroquine and mefloquine. Inhibition of ornithine decarboxylase activity, *Tropenmed. Parasitol.* 32, 73–76 (1981).

70. U. S. N. L. of M. 8600 R. Pike, 20894 Usa, *Pharmacology of antimalarial drugs* (World Health Organization, 2015; http://www.ncbi.nlm.nih.gov/books/NBK294433/).

71. P. G. Bray, S. A. Ward, P. M. O'Neill, Quinolines and artemisinin: chemistry, biology and history, *Curr. Top. Microbiol. Immunol.* 295, 3–38 (2005).

72. A. C. C. Aguiar, R. de M. Santos, F. J. B. Figueiredo, W. A. Cortopassi, A. S. Pimentel, T. C. C. França, M. R. Meneghetti, A. U. Krettli, Antimalarial Activity and Mechanisms of Action of Two Novel 4-Aminoquinolines against Chloroquine-Resistant Parasites, *PLOS ONE* 7, e37259 (2012).

73. T. J. Egan, W. W. Mavuso, D. C. Ross, H. M. Marques, Thermodynamic factors controlling the interaction of quinoline antimalarial drugs with ferriprotoporphyrin IX, *J. Inorg. Biochem.* 68, 137–145 (1997).

74. T. J. Egan, D. C. Ross, P. A. Adams, Quinoline anti-malarial drugs inhibit spontaneous formation of beta-haematin (malaria pigment), *FEBS Lett.* 352, 54–57 (1994).

75. K. A. de Villiers, J. Gildenhuys, T. le Roex, Iron(III) protoporphyrin IX complexes of the antimalarial Cinchona alkaloids quinine and quinidine, *ACS Chem. Biol.* 7, 666–671 (2012).

76. G. H. Jacobs, M. Aikawa, W. K. Milhous, J. R. Rabbege, An ultrastructural study of the effects of mefloquine on malaria parasites, *Am. J. Trop. Med. Hyg.* 36, 9–14 (1987).

77. O. Famin, H. Ginsburg, Differential effects of 4-aminoquinoline-containing antimalarial drugs on hemoglobin digestion in Plasmodium falciparum-infected erythrocytes, *Biochem. Pharmacol.* 63, 393–398 (2002).

78. A. P. Phyo, E. A. Ashley, T. J. C. Anderson, Z. Bozdech, V. I. Carrara, K. Sriprawat, S. Nair, M. M. White, J. Dziekan, C. Ling, S. Proux, K. Konghahong, A. Jeeyapant, C. J. Woodrow, M. Imwong, R. McGready, K. M. Lwin, N. P. J. Day, N. J. White, F. Nosten, Declining Efficacy of Artemisinin Combination Therapy Against P. Falciparum Malaria on the Thai-Myanmar Border (2003-2013): The Role of Parasite Genetic Factors, *Clin. Infect. Dis. Off. Publ. Infect. Dis. Soc. Am.* 63, 784–791 (2016).

79. M. B. Reed, K. J. Saliba, S. R. Caruana, K. Kirk, A. F. Cowman, Pgh1 modulates sensitivity and resistance to multiple antimalarials in Plasmodium falciparum, *Nature* 403, 906–909 (2000).

80. S. R. Karcz, D. Galatis, A. F. Cowman, Nucleotide binding properties of a P-glycoprotein homologue from Plasmodium falciparum, *Mol. Biochem. Parasitol.* 58, 269–276 (1993).

81. W. Wong, X.-C. Bai, B. E. Sleebs, T. Triglia, A. Brown, J. K. Thompson, K. E. Jackson, E. Hanssen, D. S. Marapana, I. S. Fernandez, S. A. Ralph, A. F. Cowman, S. H. W. Scheres, J. Baum, Mefloquine targets the Plasmodium falciparum 80S ribosome to inhibit protein synthesis, *Nat. Microbiol.* 2, nmicrobiol201731 (2017).

82. K. A. Schellenberg, G. R. Coatney, The influence of antimalarial drugs on nucleic acid synthesis in Plasmodium gallinaceum and Plasmodium berghei, *Biochem. Pharmacol.* 6, 143–152 (1961).

83. J. M. Combrinck, T. E. Mabotha, K. K. Ncokazi, M. A. Ambele, D. Taylor, P. J. Smith, H. C. Hoppe, T. J. Egan, Insights into the role of heme in the mechanism of action of antimalarials, *ACS Chem. Biol.* 8, 133–137 (2013).

84. R. Friedman, A. Caflisch, Discovery of Plasmepsin Inhibitors by Fragment-Based Docking and Consensus Scoring, *ChemMedChem* 4, 1317–1326.

85. L. J. C. Bolchoz, A. K. Gelasco, D. J. Jollow, D. C. McMillan, Primaquine-induced hemolytic anemia: formation of free radicals in rat erythrocytes exposed to 6-methoxy-8-hydroxylaminoquinoline, *J. Pharmacol. Exp. Ther.* 303, 1121–1129 (2002).

86. S. R. Marcsisin, J. C. Sousa, G. A. Reichard, D. Caridha, Q. Zeng, N. Roncal, R. McNulty, J. Careagabarja, R. J. Sciotti, J. W. Bennett, V. E. Zottig, G. Deye, Q. Li, L. Read, M. Hickman, N. P. Dhammika Nanayakkara, L. A. Walker, B. Smith, V. Melendez, B. S. Pybus, Tafenoquine and NPC-1161B require CYP 2D metabolism for anti-malarial activity: implications for the 8-aminoquinoline class of anti-malarial compounds, *Malar. J.* 13, 2 (2014).

87. J. L. Vennerstrom, E. O. Nuzum, R. E. Miller, A. Dorn, L. Gerena, P. A. Dande, W. Y. Ellis, R. G. Ridley, W. K. Milhous, 8-Aminoquinolines active against blood stage Plasmodium falciparum in vitro inhibit hematin polymerization, *Antimicrob. Agents Chemother.* 43, 598–602 (1999).

88. S. R. Hawley, P. G. Bray, M. Mungthin, J. D. Atkinson, P. M. O'Neill, S. A. Ward, Relationship between Antimalarial Drug Activity, Accumulation, and Inhibition of Heme Polymerization in Plasmodium falciparum In Vitro, *Antimicrob. Agents Chemother.* 42, 682–686 (1998).

89. Y. A. Ebstie, S. M. Abay, W. T. Tadesse, D. A. Ejigu, Tafenoquine and its potential in the treatment and relapse prevention of Plasmodium vivax malaria: the evidence to date, *Drug Des. Devel. Ther.* 10, 2387–2399 (2016).

90. F. Giovanella, G. K. Ferreira, S. D. T. de Prá, M. Carvalho-Silva, L. M. Gomes, G. Scaini, R. C. Gonçalves, M. Michels, L. S. Galant, L. M. Longaretti, A. L. Dajori, V. M. Andrade, F. Dal-Pizzol, E. L. Streck, R. P. de Souza, Effects of primaquine and chloroquine on oxidative stress parameters in rats, *An. Acad. Bras. Cienc.* 87, 1487–1496 (2015).

91. J. K. Baird, K. H. Rieckmann, Can primaquine therapy for vivax malaria be improved?, *Trends Parasitol.* 19, 115–120 (2003).

92. A. F. Cowman, M. J. Morry, B. A. Biggs, G. A. Cross, S. J. Foote, Amino acid changes linked to pyrimethamine resistance in the dihydrofolate reductase-thymidylate synthase gene of Plasmodium falciparum, *Proc. Natl. Acad. Sci. U. S. A.* 85, 9109–9113 (1988).

93. J. Vanichtanankul, S. Taweechai, C. Uttamapinant, P. Chitnumsub, T. Vilaivan, Y. Yuthavong, S. Kamchonwongpaisan, Combined spatial limitation around residues 16 and 108 of Plasmodium falciparum dihydrofolate reductase explains resistance to cycloguanil, *Antimicrob. Agents Chemother.* 56, 3928–3935 (2012).

94. A. Nzila, Inhibitors of de novo folate enzymes in Plasmodium falciparum, *Drug Discov. Today* 11, 939–944 (2006).

95. M. Fry, M. Pudney, Site of action of the antimalarial hydroxynaphthoquinone, 2-[trans-4-(4'-chlorophenyl) cyclohexyl]-3- hydroxy-1,4-naphthoquinone (566C80), *Biochem. Pharmacol.* 43, 1545–1553 (1992).

96. J. Wang, C.-J. Zhang, W. N. Chia, C. C. Y. Loh, Z. Li, Y. M. Lee, Y. He, L.-X. Yuan, T. K. Lim, M. Liu, C. X. Liew, Y. Q. Lee, J. Zhang, N. Lu, C. T. Lim, Z.-C. Hua, B. Liu, H.-M. Shen, K. S. W. Tan, Q. Lin, Haem-activated promiscuous targeting of artemisinin in Plasmodium falciparum, *Nat. Commun.* 6 (2015), doi:10.1038/ncomms10111.

97. P. M. O'Neill, V. E. Barton, S. A. Ward, The molecular mechanism of action of artemisinin--the debate continues, *Mol. Basel Switz.* 15, 1705–1721 (2010).

98. S. R. Meshnick, T. E. Taylor, S. Kamchonwongpaisan, Artemisinin and the antimalarial endoperoxides: from herbal remedy to targeted chemotherapy., *Microbiol. Rev.* 60, 301–315 (1996).

99. H. M. Ismail, V. Barton, M. Phanchana, S. Charoensutthivarakul, M. H. L. Wong, J. Hemingway, G. A. Biagini, P. M. O'Neill, S. A. Ward, Artemisinin activity-based probes identify multiple molecular targets within the asexual stage of the malaria parasites Plasmodium falciparum 3D7, *Proc. Natl. Acad. Sci.* 113, 2080–2085 (2016).

100. E. A. Ashley, A. P. Phyo, Drugs in Development for Malaria, *Drugs* 78, 861–879 (2018).

101. P. L. Alonso, G. Brown, M. Arevalo-Herrera, F. Binka, C. Chitnis, F. Collins, O. K. Doumbo, B. Greenwood, B. F. Hall, M. M. Levine, K. Mendis, R. D. Newman, C. V. Plowe, M. H. Rodríguez, R. Sinden, L. Slutsker, M. Tanner, A Research Agenda to Underpin Malaria Eradication, *PLOS Med.* 8, e1000406 (2011).

102. J. N. Burrows, E. Burlot, B. Campo, S. Cherbuin, S. Jeanneret, D. Leroy, T. Spangenberg, D. Waterson, T. N. Wells, P. Willis, Antimalarial drug discovery – the path towards eradication, *Parasitology* 141, 128–139 (2014).

103. D. A. Fidock, P. J. Rosenthal, S. L. Croft, R. Brun, S. Nwaka, Antimalarial drug discovery: efficacy models for compound screening, *Nat. Rev. Drug Discov.* 3, 509–520 (2004).

104. M. A. Phillips, J. Lotharius, K. Marsh, J. White, A. Dayan, K. L. White, J. W. Njoroge, F. El Mazouni, Y. Lao, S. Kokkonda, D. R. Tomchick, X. Deng, T. Laird, S. N. Bhatia, S. March, C. L. Ng, D. A. Fidock, S. Wittlin, M. Lafuente-Monasterio, F. J. G. Benito, L. M. S. Alonso, M. S. Martinez, M. B. Jimenez-Diaz, S. F. Bazaga, I. Angulo-Barturen, J. N. Haselden, J. Louttit, Y. Cui, A. Sridhar, A.-M. Zeeman, C. Kocken, R. Sauerwein, K. Dechering, V. M. Avery, S. Duffy, M. Delves, R. Sinden, A. Ruecker, K. S. Wickham, R. Rochford, J. Gahagen, L. Iyer, E. Riccio, J. Mirsalis, I. Bathhurst, T. Rueckle, X. Ding, B. Campo, D. Leroy, M. J. Rogers, P. K. Rathod, J. N. Burrows, S. A. Charman, A long-duration dihydroorotate dehydrogenase inhibitor (DSM265) for prevention and treatment of malaria, *Sci. Transl. Med.* 7, 296ra111 (2015).

105. S. Abbat, V. Jain, P. V. Bharatam, Origins of the specificity of inhibitor P218 toward wild-type and mutant PfDHFR: a molecular dynamics analysis, *J. Biomol. Struct. Dyn.* 33, 1913–1928 (2015).

106. M. Lahlou, The Success of Natural Products in Drug Discovery, *Pharmacol. Amp Pharm.* 04, 17–31 (2013).

107. H.-F. Ji, X.-J. Li, H.-Y. Zhang, Natural products and drug discovery. Can thousands of years of ancient medical knowledge lead us to new and powerful drug combinations in the fight against cancer and dementia?, *EMBO Rep.* 10, 194–200 (2009).

108. J. D. Phillipson, Phytochemistry and medicinal plants, *Phytochemistry* 56, 237–243 (2001).

109. A. U. Krettli, V. F. Andrade-Neto, M. das G. L. Brandão, W. M. Ferrari, The search for new antimalarial drugs from plants used to treat fever and malaria or plants ramdomly selected: a review, *Mem. Inst. Oswaldo Cruz* 96, 1033–1042 (2001).

110. S. Schwikkard, F. R. van Heerden, Antimalarial activity of plant metabolites, *Nat. Prod. Rep.* 19, 675–692 (2002).

111. Y.-J. Xu, L. Pieters, Recent Developments in Antimalarial Natural Products Isolated from Medicinal Plants, *Mini-Rev. Med. Chem.* 13, 1056–1072 (2013).

112. J. Bero, M. Frédérich, J. Quetin-Leclercq, Antimalarial compounds isolated from plants used in traditional medicine, *J. Pharm. Pharmacol.* 61, 1401–1433 (2009).

113. W.-F. Li, J.-G. Jiang, J. Chen, Chinese medicine and its modernization demands, *Arch. Med. Res.* 39, 246–251 (2008).

114. R. Graziose, M. A. Lila, I. Raskin, Merging Traditional Chinese Medicine with Modern Drug Discovery Technologies to Find Novel Drugs and Functional Foods, *Curr. Drug Discov. Technol.* 7, 2–12 (2010).

115. V. M. Avery, S. Bashyam, J. N. Burrows, S. Duffy, G. Papadatos, S. Puthukkuti, Y. Sambandan, S. Singh, T. Spangenberg, D. Waterson, P. Willis, Screening and hit evaluation of a chemical library against blood-stage Plasmodium falciparum, *Malar. J.* 13, 190 (2014).

116. F.-J. Gamo, L. M. Sanz, J. Vidal, C. de Cozar, E. Alvarez, J.-L. Lavandera, D. E. Vanderwall, D. V. S. Green, V. Kumar, S. Hasan, J. R. Brown, C. E. Peishoff, L. R. Cardon, J. F. Garcia-Bustos, Thousands of chemical starting points for antimalarial lead identification, *Nature* 465, 305–310 (2010).

117. W. A. Guiguemde, A. A. Shelat, D. Bouck, S. Duffy, G. J. Crowther, P. H. Davis, D. C. Smithson, M. Connelly, J. Clark, F. Zhu, M. B. Jiménez-Díaz, M. S. Martinez, E. B. Wilson, A. K. Tripathi, J. Gut,

E. R. Sharlow, I. Bathurst, F. El Mazouni, J. W. Fowble, I. Forquer, P. L. McGinley, S. Castro, I. Angulo-Barturen, S. Ferrer, P. J. Rosenthal, J. L. DeRisi, D. J. Sullivan, J. S. Lazo, D. S. Roos, M. K. Riscoe, M. A. Phillips, P. K. Rathod, W. C. Van Voorhis, V. M. Avery, R. K. Guy, Chemical genetics of Plasmodium falciparum, *Nature* 465, 311–315 (2010).

118. S. Meister, D. M. Plouffe, K. L. Kuhen, G. M. C. Bonamy, T. Wu, S. W. Barnes, S. E. Bopp, R. Borboa, A. T. Bright, J. Che, S. Cohen, N. V. Dharia, K. Gagaring, M. Gettayacamin, P. Gordon, T. Groessl, N. Kato, M. C. S. Lee, C. W. McNamara, D. A. Fidock, A. Nagle, T. Nam, W. Richmond, J. Roland, M. Rottmann, B. Zhou, P. Froissard, R. J. Glynne, D. Mazier, J. Sattabongkot, P. G. Schultz, T. Tuntland, J. R. Walker, Y. Zhou, A. Chatterjee, T. T. Diagana, E. A. Winzeler, Imaging of Plasmodium liver stages to drive next-generation antimalarial drug discovery, *Science* 334, 1372–1377 (2011).

119. D. Plouffe, A. Brinker, C. McNamara, K. Henson, N. Kato, K. Kuhen, A. Nagle, F. Adrián, J. T. Matzen, P. Anderson, T. Nam, N. S. Gray, A. Chatterjee, J. Janes, S. F. Yan, R. Trager, J. S. Caldwell, P. G. Schultz, Y. Zhou, E. A. Winzeler, In silico activity profiling reveals the mechanism of action of antimalarials discovered in a high-throughput screen, *Proc. Natl. Acad. Sci. U. S. A.* 105, 9059–9064 (2008).

120. D. M. Plouffe, M. Wree, A. Y. Du, S. Meister, F. Li, K. Patra, A. Lubar, S. L. Okitsu, E. L. Flannery, N. Kato, O. Tanaseichuk, E. Comer, B. Zhou, K. Kuhen, Y. Zhou, D. Leroy, S. L. Schreiber, C. A. Scherer, J. Vinetz, E. A. Winzeler, High-Throughput Assay and Discovery of Small Molecules that Interrupt Malaria Transmission, *Cell Host Microbe* 19, 114–126 (2016).

121. T. Spangenberg, J. N. Burrows, P. Kowalczyk, S. McDonald, T. N. C. Wells, P. Willis, The Open Access Malaria Box: A Drug Discovery Catalyst for Neglected Diseases, *PLOS ONE* 8, e62906 (2013).

122. J. Swann, N. Jamshidi, N. E. Lewis, E. A. Winzeler, Systems analysis of host–parasite interactions, *Wiley Interdiscip. Rev. Syst. Biol. Med.* 7, 381–400 (2015).

123. M. W. Vos, W. J. R. Stone, K. M. Koolen, G.-J. van Gemert, B. van Schaijk, D. Leroy, R. W. Sauerwein, T. Bousema, K. J. Dechering, A semi-automated luminescence based standard membrane feeding assay identifies novel small molecules that inhibit transmission of malaria parasites by mosquitoes, *Sci. Rep.* 5 (2015), doi:10.1038/srep18704.

124. A.-M. Zeeman, S. M. van Amsterdam, C. W. McNamara, A. Voorberg-van der Wel, E. J. Klooster, A. van den Berg, E. J. Remarque, D. M. Plouffe, G.-J. van Gemert, A. Luty, R. Sauerwein, K. Gagaring, R. Borboa, Z. Chen, K. Kuhen, R. J. Glynne, A. K. Chatterjee, A. Nagle, J. Roland, E. A. Winzeler, D. Leroy, B. Campo, T. T. Diagana, B. K. S. Yeung, A. W. Thomas, C. H. M. Kocken, KAI407, a Potent Non-8-Aminoquinoline Compound That Kills Plasmodium cynomolgi Early Dormant Liver Stage Parasites In Vitro, *Antimicrob. Agents Chemother.* 58, 1586–1595 (2014).

125. R. L. Edwards, A. R. Odom John, Muddled mechanisms: recent progress towards antimalarial target identification, *F1000Research* 5 (2016), doi:10.12688/f1000research.9477.1.

126. C. McNamara, E. A. Winzeler, Target identification and validation of novel antimalarials, *Future Microbiol.* 6, 693–704 (2011).

127. B. J. Foth, N. Zhang, B. K. Chaal, S. K. Sze, P. R. Preiser, Z. Bozdech, Quantitative Time-course Profiling of Parasite and Host Cell Proteins in the Human Malaria Parasite Plasmodium falciparum, *Mol. Cell. Proteomics* 10, M110.006411 (2011).

128. S. H. Adjalley, D. Scanfeld, E. Kozlowski, M. Llinás, D. A. Fidock, Genome-wide transcriptome profiling reveals functional networks involving the Plasmodium falciparum drug resistance transporters PfCRT and PfMDR1, *BMC Genomics* 16 (2015), doi:10.1186/s12864-015-2320-8.

129. E. L. Allman, H. J. Painter, J. Samra, M. Carrasquilla, M. Llinás, Metabolomic Profiling of the Malaria Box Reveals Antimalarial Target Pathways, *Antimicrob. Agents Chemother.* 60, 6635–6649 (2016).

130. B. Blasco, D. Leroy, D. A. Fidock, Antimalarial drug resistance: linking Plasmodium falciparum parasite biology to the clinic, *Nat. Med.* 23, 917–928 (2017).

131. M. A. Carey, J. A. Papin, J. L. Guler, Novel Plasmodium falciparum metabolic network reconstruction identifies shifts associated with clinical antimalarial resistance, *BMC Genomics* 18, 543 (2017).

132. P. R. Graves, J. J. Kwiek, P. Fadden, R. Ray, K. Hardeman, A. M. Coley, M. Foley, T. A. J. Haystead, Discovery of Novel Targets of Quinoline Drugs in the Human Purine Binding Proteome, *Mol. Pharmacol.* 62, 1364–1372 (2002).

133. T. Paquet, C. L. Manach, D. G. Cabrera, Y. Younis, P. P. Henrich, T. S. Abraham, M. C. S. Lee, R. Basak, S. Ghidelli-Disse, M. J. Lafuente-Monasterio, M. Bantscheff, A. Ruecker, A. M. Blagborough, S. E. Zakutansky, A.-M. Zeeman, K. L. White, D. M. Shackleford, J. Mannila, J. Morizzi, C. Scheurer, I. Angulo-Barturen, M. S. Martínez, S. Ferrer, L. M. Sanz, F. J. Gamo, J. Reader, M. Botha, K. J. Dechering, R. W. Sauerwein, A. Tungtaeng, P. Vanachayangkul, C. S. Lim, J. Burrows, M. J. Witty, K. C. Marsh, C. Bodenreider, R. Rochford, S. M. Solapure, M. B. Jiménez-Díaz, S. Wittlin, S. A. Charman, C. Donini, B. Campo, L.-M. Birkholtz, K. K. Hanson, G. Drewes, C. H. M. Kocken, M. J. Delves, D. Leroy, D. A. Fidock, D. Waterson, L. J. Street, K. Chibale, Antimalarial efficacy of MMV390048, an inhibitor of Plasmodium phosphatidylinositol 4-kinase, *Sci. Transl. Med.* 9, eaad9735 (2017).

134. E. Deu, Proteases as antimalarial targets: strategies for genetic, chemical, and therapeutic validation, *Febs J.* 284, 2604–2628 (2017).

135. M. Ghorbal, M. Gorman, C. R. Macpherson, R. M. Martins, A. Scherf, J.-J. Lopez-Rubio, Genome editing in the human malaria parasite *Plasmodium falciparum* using the CRISPR-Cas9 system, *Nat. Biotechnol.* 32, 819–821 (2014).

136. A. Aroonsri, O. Akinola, N. Posayapisit, W. Songsungthong, C. Uthaipibull, S. Kamchonwongpaisan, G. O. Gbotosho, Y. Yuthavong, P. J. Shaw, Identifying antimalarial compounds targeting dihydrofolate reductase-thymidylate synthase (DHFR-TS) by chemogenomic profiling, *Int. J. Parasitol.* 46, 527–535 (2016).

137. A. Pradhan, G. H. Siwo, N. Singh, B. Martens, B. Balu, K. A. Button-Simons, A. Tan, M. Zhang, K. O. Udenze, R. H. Y. Jiang, M. T. Ferdig, J. H. Adams, D. E. Kyle, Chemogenomic profiling of Plasmodium falciparum as a tool to aid antimalarial drug discovery, *Sci. Rep.* 5, 15930 (2015).

138. G. H. Siwo, R. S. Smith, A. Tan, K. A. Button-Simons, L. A. Checkley, M. T. Ferdig, An integrative analysis of small molecule transcriptional responses in the human malaria parasite Plasmodium falciparum, *BMC Genomics* 16, 1030 (2015).

139. D. M. Penarete-Vargas, A. Boisson, S. Urbach, H. Chantelauze, S. Peyrottes, L. Fraisse, H. J. Vial, A chemical proteomics approach for the search of pharmacological targets of the antimalarial clinical candidate albitiazolium in Plasmodium falciparum using photocrosslinking and click chemistry, *PloS One* 9, e113918 (2014).

140. W. Sun, T. Q. Tanaka, C. T. Magle, W. Huang, N. Southall, R. Huang, S. J. Dehdashti, J. C. McKew, K. C. Williamson, W. Zheng, Chemical signatures and new drug targets for gametocytocidal drug development, *Sci. Rep.* 4, 3743 (2014).

141. K. A. Meissner, S. Lunev, Y.-Z. Wang, M. Linzke, F. de Assis Batista, C. Wrenger, M. R. Groves, Drug Target Validation Methods in Malaria - Protein Interference Assay (PIA) as a Tool for Highly Specific Drug Target Validation, *Curr. Drug Targets* 18, 1069–1085 (2017).

142. D. M. Molina, P. Nordlund, The Cellular Thermal Shift Assay: A Novel Biophysical Assay for In Situ Drug Target Engagement and Mechanistic Biomarker Studies, *Annu. Rev. Pharmacol. Toxicol.* 56, null (2016).

143. D. M. Molina, R. Jafari, M. Ignatushchenko, T. Seki, E. A. Larsson, C. Dan, L. Sreekumar, Y. Cao, P. Nordlund, Monitoring Drug Target Engagement in Cells and Tissues Using the Cellular Thermal Shift Assay, *Science* 341, 84–87 (2013).

144. M. M. Savitski, F. B. M. Reinhard, H. Franken, T. Werner, M. F. Savitski, D. Eberhard, D. M. Molina, R. Jafari, R. B. Dovega, S. Klaeger, B. Kuster, P. Nordlund, M. Bantscheff, G. Drewes, Tracking cancer drugs in living cells by thermal profiling of the proteome, *Science* 346, 1255784 (2014).

145. U. B. Ericsson, B. M. Hallberg, G. T. Detitta, N. Dekker, P. Nordlund, Thermofluor-based high-throughput stability optimization of proteins for structural studies, *Anal. Biochem.* 357, 289–298 (2006).

146. M.-C. Lo, A. Aulabaugh, G. Jin, R. Cowling, J. Bard, M. Malamas, G. Ellestad, Evaluation of fluorescence-based thermal shift assays for hit identification in drug discovery, *Anal. Biochem.* 332, 153–159 (2004).

147. R. Jafari, H. Almqvist, H. Axelsson, M. Ignatushchenko, T. Lundbäck, P. Nordlund, D. Martinez Molina, The cellular thermal shift assay for evaluating drug target interactions in cells, *Nat. Protoc.* 9, 2100–2122 (2014).

148. J. Chang, Y. Kim, H. J. Kwon, Advances in identification and validation of protein targets of natural products without chemical modification, *Nat. Prod. Rep.* 33, 719–730 (2016).

149. C. Lambros, J. P. Vanderberg, Synchronization of Plasmodium falciparum erythrocytic stages in culture, *J. Parasitol.* 65, 418–420 (1979).

150. K. Silamut, N. H. Phu, C. Whitty, G. D. H. Turner, K. Louwrier, N. T. H. Mai, J. A. Simpson, T. T. Hien, N. J. White, A Quantitative Analysis of the Microvascular Sequestration of Malaria Parasites in the Human Brain, *Am. J. Pathol.* 155, 395–410 (1999).

151. M. Wahlgren, K. Berzins, P. Perlmann, A. Björkman, Characterization of the humoral immune response in Plasmodium falciparum malaria. I. Estimation of antibodies to P. falciparum or human erythrocytes by means of microELISA, *Clin. Exp. Immunol.* 54, 127–134 (1983).

152. C. S. H. Tan, K. D. Go, X. Bisteau, L. Dai, C. H. Yong, N. Prabhu, M. B. Ozturk, Y. T. Lim, L. Sreekumar, J. Lengqvist, V. Tergaonkar, P. Kaldis, R. M. Sobota, P. Nordlund, Thermal proximity coaggregation for system-wide profiling of protein complex dynamics in cells, *Science* 359, 1170–1177 (2018).

153. D. C. Madrid, L.-M. Ting, K. L. Waller, V. L. Schramm, K. Kim, Plasmodium falciparum purine nucleoside phosphorylase is critical for viability of malaria parasites, *J. Biol. Chem.* 283, 35899–35907 (2008).

154. W. Shi, L.-M. Ting, G. A. Kicska, A. Lewandowicz, P. C. Tyler, G. B. Evans, R. H. Furneaux, K. Kim, S. C. Almo, V. L. Schramm, Plasmodium falciparum Purine Nucleoside Phosphorylase CRYSTAL STRUCTURES, IMMUCILLIN INHIBITORS, AND DUAL CATALYTIC FUNCTION, *J. Biol. Chem.* 279, 18103–18106 (2004).

155. S. Gräslund, Structural Genomics Consortium, China Structural Genomics Consortium, Northeast Structural Genomics Consortium, P. Nordlund, J. Weigelt, B. M. Hallberg, J. Bray, O. Gileadi, S. Knapp, U. Oppermann, C. Arrowsmith, R. Hui, J. Ming, S. dhe-Paganon, H. Park, A. Savchenko, A. Yee, A. Edwards, R. Vincentelli, C. Cambillau, R. Kim, S.-H. Kim, Z. Rao, Y. Shi, T. C. Terwilliger, C.-Y. Kim, L.-W. Hung, G. S. Waldo, Y. Peleg, S. Albeck, T. Unger, O. Dym, J. Prilusky, J. L. Sussman, R. C. Stevens, S. A. Lesley, I. A. Wilson, A. Joachimiak, F. Collart, I. Dementieva, M. I. Donnelly, W. H. Eschenfeldt, Y. Kim, L. Stols, R. Wu, M. Zhou, S. K. Burley, J. S. Emtage, J. M. Sauder, D. Thompson, K. Bain, J. Luz, T. Gheyi, F. Zhang, S. Atwell, S. C. Almo, J. B. Bonanno, A. Fiser, S. Swaminathan, F. W. Studier, M. R. Chance, A. Sali, T. B. Acton, R. Xiao, L. Zhao, L. C. Ma, J. F. Hunt, L. Tong, K. Cunningham, M. Inouye, S. Anderson, H. Janjua, R. Shastry, C. K. Ho, D. Wang, H. Wang, M. Jiang, G. T. Montelione, D. I. Stuart, R. J. Owens, S. Daenke, A. Schütz, U. Heinemann, S. Yokoyama, K. Büssow, K. C. Gunsalus, Protein production and purification, *Nat. Methods* 5, 135–146 (2008).

156. W. Kabsch, XDS, *Acta Crystallogr. D Biol. Crystallogr.* 66, 125–132 (2010).

157. A. J. McCoy, R. W. Grosse-Kunstleve, P. D. Adams, M. D. Winn, L. C. Storoni, R. J. Read, Phaser crystallographic software, *J. Appl. Crystallogr.* 40, 658–674 (2007).

158. G. N. Murshudov, P. Skubák, A. A. Lebedev, N. S. Pannu, R. A. Steiner, R. A. Nicholls, M. D. Winn, F. Long, A. A. Vagin, REFMAC5 for the refinement of macromolecular crystal structures, *Acta Crystallogr. D Biol. Crystallogr.* 67, 355–367 (2011).

159. P. Emsley, K. Cowtan, Coot: model-building tools for molecular graphics, *Acta Crystallogr. D Biol. Crystallogr.* 60, 2126–2132 (2004).

160. G. N. Ramachandran, C. Ramakrishnan, V. Sasisekharan, Stereochemistry of polypeptide chain configurations, *J. Mol. Biol.* 7, 95–99 (1963).

161. N. W. Moriarty, R. W. Grosse-Kunstleve, P. D. Adams, electronic Ligand Builder and Optimization Workbench (eLBOW): a tool for ligand coordinate and restraint generation, *Acta Crystallogr. D Biol. Crystallogr.* 65, 1074–1080 (2009).

162. C. Schnick, M. A. Robien, A. M. Brzozowski, E. J. Dodson, G. N. Murshudov, L. Anderson, J. R. Luft, C. Mehlin, W. G. J. Hol, J. A. Brannigan, A. J. Wilkinson, Structures of Plasmodium falciparum purine nucleoside phosphorylase complexed with sulfate and its natural substrate inosine, *Acta Crystallogr. D Biol. Crystallogr.* 61, 1245–1254 (2005).

163. Z. Q. Chia, B. Kua, X. Chai, Amomum tsao-ko & Areca catechu show effectiveness in decreasing ring formation of Plasmodium parasite while Chrysanthemum flower is effective in delaying parasite life cycle (2012).

164. Zhong F., *Zhong yao xue tu jie biao 中药学图解表* (People's Medical Publishing House, Beijing, China, 2004).

165. Gao, X., *Zhong yao xue 中药学* (China: Zhong guo zhong yi yao chu ban she 中国中医药出版社., Beijing, China, ed. 2nd, 2009).

166. A. J. Harborne, *Phytochemical Methods A Guide to Modern Techniques of Plant Analysis* (Springer Netherlands, ed. 3, 1998; //www.springer.com/gp/book/9780412572609).

167. H. Le Nagard, C. Vincent, F. Mentré, J. Le Bras, Online analysis of in vitro resistance to antimalarial drugs through nonlinear regression, *Comput. Methods Programs Biomed.* 104, 10–18 (2011).

168. H. Kaddouri, S. Nakache, S. Houzé, F. Mentré, J. Le Bras, Assessment of the Drug Susceptibility of Plasmodium falciparum Clinical Isolates from Africa by Using a Plasmodium Lactate Dehydrogenase Immunodetection Assay and an Inhibitory Maximum Effect Model for Precise Measurement of the 50-Percent Inhibitory Concentration, *Antimicrob. Agents Chemother.* 50, 3343 (2006).

169. J. H. Ringrose, W. W. van Solinge, S. Mohammed, M. C. O'Flaherty, R. van Wijk, A. J. R. Heck, M. Slijper, Highly efficient depletion strategy for the two most abundant erythrocyte soluble proteins improves proteome coverage dramatically, *J. Proteome Res.* 7, 3060–3063 (2008).

170. E. M. Pasini, M. Kirkegaard, P. Mortensen, H. U. Lutz, A. W. Thomas, M. Mann, In-depth analysis of the membrane and cytosolic proteome of red blood cells, *Blood* 108, 791–801 (2006).

171. R. Siqueira-Batista, A. P. Gomes, E. G. de Mendonça, R. R. Vitorino, S. F. M. de Azevedo, R. de B. Freitas, L. A. Santana, M. G. de A. Oliveira, Plasmodium falciparum malaria: proteomic studies, *Rev. Bras. Ter. Intensiva* 24, 394–400 (2012).

172. S. S. R. Christophers, J. D. Fulton, Experiments with Isolated Malaria Parasites (Plasmodium Knowlesi) Free from Red Cells, *Ann. Trop. Med. Parasitol.* 33, 161–170 (1939).

173. C. Simó, A. Bachi, A. Cattaneo, L. Guerrier, F. Fortis, E. Boschetti, A. Podtelejnikov, P. G. Righetti, Performance of combinatorial peptide libraries in capturing the low-abundance proteome of red blood cells. 1. Behavior of mono- to hexapeptides, *Anal. Chem.* 80, 3547–3556 (2008).

174. P. F. Lange, P. F. Huesgen, K. Nguyen, C. M. Overall, Annotating N termini for the human proteome project: N termini and Nα-acetylation status differentiate stable cleaved protein species from degradation remnants in the human erythrocyte proteome, *J. Proteome Res.* 13, 2028–2044 (2014).

175. E. N. Pesciotta, S. Sriswasdi, H.-Y. Tang, D. W. Speicher, P. J. Mason, M. Bessler, Dysferlin and Other Non-Red Cell Proteins Accumulate in the Red Cell Membrane of Diamond-Blackfan Anemia Patients, *PLOS ONE* 9, e85504 (2014).

176. A. H. Bryk, J. R. Wiśniewski, Quantitative Analysis of Human Red Blood Cell Proteome, *J. Proteome Res.* 16, 2752–2761 (2017).

177. B. Barasa, M. Slijper, Challenges for red blood cell biomarker discovery through proteomics, *Biochim. Biophys. Acta* 1844, 1003–1010 (2014).

178. G. Alvarez-Llamas, F. de la Cuesta, M. G. Barderas, V. M. Darde, I. Zubiri, C. Caramelo, F. Vivanco, A novel methodology for the analysis of membrane and cytosolic sub-proteomes of erythrocytes by 2-DE, *Electrophoresis* 30, 4095–4108 (2009).

179. K. Walpurgis, M. Kohler, A. Thomas, F. Wenzel, H. Geyer, W. Schänzer, M. Thevis, Validated hemoglobin-depletion approach for red blood cell lysate proteome analysis by means of 2D PAGE and Orbitrap MS, *ELECTROPHORESIS* 33, 2537–2545.

180. R. M. Tubaon, P. R. Haddad, J. P. Quirino, Sample Clean-up Strategies for ESI Mass Spectrometry Applications in Bottom-up Proteomics: Trends from 2012 to 2016, *PROTEOMICS* 17, 1700011.

181. L. Mata-Cantero, M. J. Lafuente, L. Sanz, M. S. Rodriguez, Magnetic isolation of Plasmodium falciparum schizonts iRBCs to generate a high parasitaemia and synchronized in vitro culture, *Malar. J.* 13, 112 (2014).

182. A. Sardarian, K. T. Douglas, M. Read, P. F. G. Sims, J. E. Hyde, P. Chitnumsub, R. Sirawaraporn, W. Sirawaraporn, Pyrimethamine analogs as strong inhibitors of double and quadruple mutants of dihydrofolate reductase in human malaria parasites, *Org. Biomol. Chem.* 1, 960–964 (2003).

183. L. Vivas, L. Rattray, L. B. Stewart, B. L. Robinson, B. Fugmann, R. K. Haynes, W. Peters, S. L. Croft, Antimalarial efficacy and drug interactions of the novel semi-synthetic endoperoxide artemisone in vitro and in vivo, *J. Antimicrob. Chemother.* 59, 658–665 (2007).

184. Y. Yuthavong, B. Tarnchompoo, T. Vilaivan, P. Chitnumsub, S. Kamchonwongpaisan, S. A. Charman, D. N. McLennan, K. L. White, L. Vivas, E. Bongard, C. Thongphanchang, S. Taweechai, J. Vanichtanankul, R. Rattanajak, U. Arwon, P. Fantauzzi, J. Yuvaniyama, W. N. Charman, D. Matthews, Malarial dihydrofolate reductase as a paradigm for drug development against a resistance-compromised target, *Proc. Natl. Acad. Sci. U. S. A.* 109, 16823–16828 (2012).

185. I. D. Kerr, J. H. Lee, K. C. Pandey, A. Harrison, M. Sajid, P. J. Rosenthal, L. S. Brinen, Structures of Falcipain-2 and Falcipain-3 Bound to Small Molecule Inhibitors: Implications for Substrate Specificity, *J. Med. Chem.* 52, 852–857 (2009).

186. B. R. Shenai, P. S. Sijwali, A. Singh, P. J. Rosenthal, Characterization of Native and Recombinant Falcipain-2, a Principal Trophozoite Cysteine Protease and Essential Hemoglobinase ofPlasmodium falciparum, *J. Biol. Chem.* 275, 29000–29010 (2000).

187. S. C. Xie, C. Dogovski, E. Hanssen, F. Chiu, T. Yang, M. P. Crespo, C. Stafford, S. Batinovic, S. Teguh, S. Charman, N. Klonis, L. Tilley, Haemoglobin degradation underpins the sensitivity of early ring stage Plasmodium falciparum to artemisinins, *J Cell Sci* 129, 406–416 (2016).

188. P. S. Sijwali, K. Kato, K. B. Seydel, J. Gut, J. Lehman, M. Klemba, D. E. Goldberg, L. H. Miller, P. J. Rosenthal, Plasmodium falciparum cysteine protease falcipain-1 is not essential in erythrocytic stage malaria parasites, *Proc. Natl. Acad. Sci.* 101, 8721–8726 (2004).

189. J. M. Carlton, S. L. Perkins, K. W. Deitsch, *Malaria Parasites: Comparative Genomics, Evolution and Molecular Biology* (Horizon Scientific Press, 2013).

190. J. M. Carlton, J. H. Adams, J. C. Silva, S. L. Bidwell, H. Lorenzi, E. Caler, J. Crabtree, S. V. Angiuoli, E. F. Merino, P. Amedeo, Q. Cheng, R. M. R. Coulson, B. S. Crabb, H. A. del Portillo, K. Essien, T. V. Feldblyum, C. Fernandez-Becerra, P. R. Gilson, A. H. Gueye, X. Guo, S. Kang'a, T. W. A. Kooij, M. Korsinczky, E. V.-S. Meyer, V. Nene, I. Paulsen, O. White, S. A. Ralph, Q. Ren, T. J. Sargeant, S. L. Salzberg, C. J. Stoeckert, S. A. Sullivan, M. M. Yamamoto, S. L. Hoffman, J. R. Wortman, M. J. Gardner, M. R. Galinski, J. W. Barnwell, C. M. Fraser-Liggett, Comparative genomics of the neglected human malaria parasite *Plasmodium vivax*, *Nature* 455, 757–763 (2008).

191. O. Reamtong, K. Srimuang, N. Saralamba, P. Sangvanich, N. P. J. Day, N. J. White, M. Imwong, Protein profiling of mefloquine resistant Plasmodium falciparum using mass spectrometry-based proteomics, *Int. J. Mass Spectrom.* 391, 82–92 (2015).

192. P. J. Shaw, S. Chaotheing, P. Kaewprommal, J. Piriyapongsa, C. Wongsombat, N. Suwannakitti, P. Koonyosying, C. Uthaipibull, Y. Yuthavong, S. Kamchonwongpaisan, Plasmodium parasites mount an arrest response to dihydroartemisinin, as revealed by whole transcriptome shotgun sequencing (RNA-seq) and microarray study, *BMC Genomics* 16 (2015), doi:10.1186/s12864-015-2040-0.

193. E. Lasonder, Y. Ishihama, J. S. Andersen, A. M. W. Vermunt, A. Pain, R. W. Sauerwein, W. M. C. Eling, N. Hall, A. P. Waters, H. G. Stunnenberg, M. Mann, Analysis of the Plasmodium falciparum proteome by high-accuracy mass spectrometry, *Nature* 419, 537–542 (2002).

194. E. Lasonder, S. R. Rijpma, B. C. L. van Schaijk, W. A. M. Hoeijmakers, P. R. Kensche, M. S. Gresnigt, A. Italiaander, M. W. Vos, R. Woestenenk, T. Bousema, G. R. Mair, S. M. Khan, C. J. Janse, R. Bártfai, R. W. Sauerwein, Integrated transcriptomic and proteomic analyses of P. falciparum gametocytes: molecular insight into sex-specific processes and translational repression, *Nucleic Acids Res.* 44, 6087–6101 (2016).

195. C. Segura, Y. Cuesta-Astroz, C. Nunes-Batista, M. Zalis, W. M. de A. von Krüger, P. Mascarello Bisch, Partial characterization of Plasmodium falciparum trophozoite proteome under treatment with quinine, mefloquine and the natural antiplasmodial diosgenone, *Biomed. Rev. Inst. Nac. Salud* 34, 237–249 (2014).

196. I. Papatheodorou, A. Oellrich, D. Smedley, Linking gene expression to phenotypes via pathway information, *J. Biomed. Semant.* 6, 17 (2015).

197. V. Vu, A. J. Verster, M. Schertzberg, T. Chuluunbaatar, M. Spensley, D. Pajkic, G. T. Hart, J. Moffat, A. G. Fraser, Natural Variation in Gene Expression Modulates the Severity of Mutant Phenotypes, *Cell* 162, 391–402 (2015).

198. E. Shakhnovich, Protein Folding Thermodynamics and Dynamics: Where Physics, Chemistry, and Biology Meet, *Chem. Rev.* 106, 1559–1588 (2006).

199. C. J. Layton, H. W. Hellinga, Thermodynamic Analysis of Ligand-Induced Changes in Protein Thermal Unfolding Applied to High-Throughput Determination of Ligand Affinities with Extrinsic Fluorescent Dyes, *Biochemistry* 49, 10831–10841 (2010).

200. A. Mateus, T. A. Määttä, M. M. Savitski, Thermal proteome profiling: unbiased assessment of protein state through heat-induced stability changes, *Proteome Sci.* 15 (2017), doi:10.1186/s12953-017-0122-4.

201. P. Leuenberger, S. Ganscha, A. Kahraman, V. Cappelletti, P. J. Boersema, C. von Mering, M. Claassen, P. Picotti, Cell-wide analysis of protein thermal unfolding reveals determinants of thermostability, *Science* 355, eaai7825 (2017).

202. S. R. McGuffee, A. H. Elcock, Diffusion, crowding & protein stability in a dynamic molecular model of the bacterial cytoplasm, *PLoS Comput. Biol.* 6, e1000694 (2010).

203. J. Danielsson, X. Mu, L. Lang, H. Wang, A. Binolfi, F.-X. Theillet, B. Bekei, D. T. Logan, P. Selenko, H. Wennerström, M. Oliveberg, Thermodynamics of protein destabilization in live cells, *Proc. Natl. Acad. Sci.* 112, 12402–12407 (2015).

204. A. Gershenson, L. M. Gierasch, Protein folding in the cell: challenges and progress, *Curr. Opin. Struct. Biol.* 21, 32–41 (2011).

205. S. A. Wagner, P. Beli, B. T. Weinert, M. L. Nielsen, J. Cox, M. Mann, C. Choudhary, A proteome-wide, quantitative survey of in vivo ubiquitylation sites reveals widespread regulatory roles, *Mol. Cell. Proteomics* , mcp.M111.013284 (2011).

206. C. Choudhary, C. Kumar, F. Gnad, M. L. Nielsen, M. Rehman, T. C. Walther, J. V. Olsen, M. Mann, Lysine Acetylation Targets Protein Complexes and Co-Regulates Major Cellular Functions, *Science* 325, 834–840 (2009).

207. B. Christensen, C. C. Kazanecki, T. E. Petersen, S. R. Rittling, D. T. Denhardt, E. S. Sørensen, Cell Type-specific Post-translational Modifications of Mouse Osteopontin Are Associated with Different Adhesive Properties, *J. Biol. Chem.* 282, 19463–19472 (2007).

208. S. B. Reiff, B. Striepen, Malaria: The gatekeeper revealed, *Nature* 459, 918–919 (2009).

209. A. Mbengue, X. Y. Yam, C. Braun-Breton, Human erythrocyte remodelling during Plasmodium falciparum malaria parasite growth and egress, *Br. J. Haematol.* 157, 171–179 (2012).

210. K. Haldar, N. Mohandas, Erythrocyte remodeling by malaria parasites, *Curr. Opin. Hematol.* 14, 203–209 (2007).

211. M. J. Kluger, Fever in Ectotherms: Evolutionary Implications, *Integr. Comp. Biol.* 19, 295–304 (1979).

212. P. M. Small, M. G. Täuber, C. J. Hackbarth, M. A. Sande, Influence of body temperature on bacterial growth rates in experimental pneumococcal meningitis in rabbits, *Infect. Immun.* 52, 484–487 (1986).

213. D. Kwiatkowski, B. M. Greenwood, Why is malaria fever periodic? A hypothesis, *Parasitol. Today Pers. Ed* 5, 264–266 (1989).

214. M. Foley, L. Tilley, Quinoline Antimalarials, *Pharmacol. Ther.* 79, 55–87 (1998).

215. F. W. Muregi, Antimalarial drugs and their useful therapeutic lives: rational drug design lessons from pleiotropic action of quinolines and artemisinins, *Curr. Drug Discov. Technol.* 7, 280–316 (2010).

216. J. Desneves, G. Thorn, A. Berman, D. Galatis, N. La Greca, J. Sinding, M. Foley, L. W. Deady, A. F. Cowman, L. Tilley, Photoaffinity labeling of mefloquine-binding proteins in human serum, uninfected erythrocytes and Plasmodium falciparum-infected erythrocytes, *Mol. Biochem. Parasitol.* 82, 181–194 (1996).

217. J. A. Read, K. W. Wilkinson, R. Tranter, R. B. Sessions, R. L. Brady, Chloroquine Binds in the Cofactor Binding Site ofPlasmodium falciparum Lactate Dehydrogenase, *J. Biol. Chem.* 274, 10213–10218 (1999).

218. H. Franken, T. Mathieson, D. Childs, G. M. A. Sweetman, T. Werner, I. Tögel, C. Doce, S. Gade, M. Bantscheff, G. Drewes, F. B. M. Reinhard, W. Huber, M. M. Savitski, Thermal proteome profiling for unbiased identification of direct and indirect drug targets using multiplexed quantitative mass spectrometry, *Nat. Protoc.* 10, 1567 (2015).

219. A. Alshareef, H.-F. Zhang, Y.-H. Huang, C. Wu, J. D. Zhang, P. Wang, A. El-Sehemy, M. Fares, R. Lai, The use of cellular thermal shift assay (CETSA) to study Crizotinib resistance in ALK-expressing human cancers, *Sci. Rep.* 6, 33710 (2016).

220. H. Almqvist, H. Axelsson, R. Jafari, C. Dan, A. Mateus, M. Haraldsson, A. Larsson, D. M. Molina, P. Artursson, T. Lundbäck, P. Nordlund, CETSA screening identifies known and novel thymidylate synthase inhibitors and slow intracellular activation of 5-fluorouracil, *Nat. Commun.* 7, 11040 (2016).

221. A. J. Barrett, A. A. Kembhavi, M. A. Brown, H. Kirschke, C. G. Knight, M. Tamai, K. Hanada, L-trans-Epoxysuccinyl-leucylamido(4-guanidino)butane (E-64) and its analogues as inhibitors of cysteine proteinases including cathepsins B, H and L., *Biochem. J.* 201, 189–198 (1982).

222. K. Matsumoto, K. Mizoue, K. Kitamura, W.-C. Tse, C. P. Huber, T. Ishida, Structural basis of inhibition of cysteine proteases by E-64 and its derivatives, *Pept. Sci.* 51, 99–107 (1999).

223. H.-H. Otto, T. Schirmeister, Cysteine Proteases and Their Inhibitors, *Chem. Rev.* 97, 133–172 (1997).

224. J. C. Powers, J. L. Asgian, Ö. D. Ekici, K. E. James, Irreversible Inhibitors of Serine, Cysteine, and Threonine Proteases, *Chem. Rev.* 102, 4639–4750 (2002).

225. P. J. Rosenthal, Cysteine proteases of malaria parasites, *Int. J. Parasitol.* 34, 1489–1499 (2004).

226. F. Wang, P. Krai, E. Deu, B. Bibb, C. Lauritzen, J. Pedersen, M. Bogyo, M. Klemba, Biochemical characterization of Plasmodium falciparum dipeptidyl aminopeptidase 1, *Mol. Biochem. Parasitol.* 175, 10–20 (2011).

227. A. N. Cowell, E. S. Istvan, A. K. Lukens, M. G. Gomez-Lorenzo, M. Vanaerschot, T. Sakata-Kato, E. L. Flannery, P. Magistrado, E. Owen, M. Abraham, G. LaMonte, H. J. Painter, R. M. Williams, V. Franco, M. Linares, I. Arriaga, S. Bopp, V. C. Corey, N. F. Gnädig, O. Coburn-Flynn, C. Reimer, P. Gupta, J. M. Murithi, P. A. Moura, O. Fuchs, E. Sasaki, S. W. Kim, C. H. Teng, L. T. Wang, A. Akidil, S. Adjalley, P. A. Willis, D. Siegel, O. Tanaseichuk, Y. Zhong, Y. Zhou, M. Llinás, S. Ottilie, F.-J. Gamo, M. C. S. Lee, D. E. Goldberg, D. A. Fidock, D. F. Wirth, E. A. Winzeler, Mapping the malaria parasite druggable genome by using in vitro evolution and chemogenomics, *Science* 359, 191–199 (2018).

228. N. Méthot, J. Rubin, D. Guay, C. Beaulieu, D. Ethier, T. J. Reddy, D. Riendeau, M. D. Percival, Inhibition of the Activation of Multiple Serine Proteases with a Cathepsin C Inhibitor Requires Sustained Exposure to Prevent Pro-enzyme Processing, *J. Biol. Chem.* 282, 20836–20846 (2007).

229. H. Richly, M. Rape, S. Braun, S. Rumpf, C. Hoege, S. Jentsch, A Series of Ubiquitin Binding Factors Connects CDC48/p97 to Substrate Multiubiquitylation and Proteasomal Targeting, *Cell* 120, 73–84 (2005).

230. L. Wang, C. Delahunty, K. Fritz-Wolf, S. Rahlfs, J. H. Prieto, J. R. Yates, K. Becker, Characterization of the 26S proteasome network in *Plasmodium falciparum*, *Sci. Rep.* 5, 17818 (2015).

231. N. Ponts, J. Yang, D.-W. D. Chung, J. Prudhomme, T. Girke, P. Horrocks, K. G. L. Roch, Deciphering the Ubiquitin-Mediated Pathway in Apicomplexan Parasites: A Potential Strategy to Interfere with Parasite Virulence, *PLOS ONE* 3, e2386 (2008).

232. D. Shi, S. R. Grossman, Ubiquitin becomes ubiquitous in cancer, *Cancer Biol. Ther.* 10, 737–747 (2010).

233. R. L. Welchman, C. Gordon, R. J. Mayer, Ubiquitin and ubiquitin-like proteins as multifunctional signals, *Nat. Rev. Mol. Cell Biol.* 6, 599 (2005).

234. A. M. Thu, A. P. Phyo, J. Landier, D. M. Parker, F. H. Nosten, Combating multidrug-resistant Plasmodium falciparum malaria, *Febs J.* 284, 2569–2578 (2017).

235. P. E. Meissner, G. Mandi, B. Coulibaly, S. Witte, T. Tapsoba, U. Mansmann, J. Rengelshausen, W. Schiek, A. Jahn, I. Walter-Sack, G. Mikus, J. Burhenne, K.-D. Riedel, R. H. Schirmer, B. Kouyaté, O. Müller, Methylene blue for malaria in Africa: results from a dose-finding study in combination with chloroquine, *Malar. J.* 5, 84 (2006).

236. WHO, Geneva, Guidelines for the treatment of malaria - 3rd edition (2015) (available at http://apps.who.int/iris/bitstream/10665/162441/1/9789241549127_eng.pdf).

237. L. W. Kitchen, D. W. Vaughn, D. R. Skillman, Role of US Military Research Programs in the Development of US Food and Drug Administration–Approved Antimalarial Drugs, *Clin. Infect. Dis.* 43, 67–71 (2006).

238. P. Schlagenhauf, M. Adamcova, L. Regep, M. T. Schaerer, H.-G. Rhein, The position of mefloquine as a 21st century malaria chemoprophylaxis, *Malar. J.* 9, 357 (2010).

239. M. Chan, D. S. H. Tan, T. S. Sim, Plasmodium falciparum pyruvate kinase as a novel target for antimalarial drug-screening, *Travel Med. Infect. Dis.* 5, 125–131 (2007).

240. T. Maeda, T. Saito, O. S. Harb, D. S. Roos, S. Takeo, H. Suzuki, T. Tsuboi, T. Takeuchi, T. Asai, Pyruvate kinase type-II isozyme in Plasmodium falciparum localizes to the apicoplast, *Parasitol. Int.* 58, 101–105 (2009).

241. J. M. Njunge, M. H. Ludewig, A. Boshoff, E.-R. Pesce, G. L. Blatch, Hsp70s and J proteins of Plasmodium parasites infecting rodents and primates: structure, function, clinical relevance, and drug targets, *Curr. Pharm. Des.* 19, 387–403 (2013).

242. P. E. Daddona, W. P. Wiesmann, W. Milhouse, J. W. Chern, L. B. Townsend, M. S. Hershfield, H. K. Webster, Expression of human malaria parasite purine nucleoside phosphorylase in host enzyme-deficient erythrocyte culture. Enzyme characterization and identification of novel inhibitors, *J. Biol. Chem.* 261, 11667–11673 (1986).

243. L.-M. Ting, W. Shi, A. Lewandowicz, V. Singh, A. Mwakingwe, M. R. Birck, E. A. T. Ringia, G. Bench, D. C. Madrid, P. C. Tyler, G. B. Evans, R. H. Furneaux, V. L. Schramm, K. Kim, Targeting a Novel Plasmodium falciparum Purine Recycling Pathway with Specific Immucillins, *J. Biol. Chem.* 280, 9547–9554 (2005).

244. M. Chitale, T. Hawkins, C. Park, D. Kihara, ESG: extended similarity group method for automated protein function prediction, *Bioinformatics* 25, 1739–1745 (2009).

245. G. A. Kicska, P. C. Tyler, G. B. Evans, R. H. Furneaux, K. Kim, V. L. Schramm, Transition State Analogue Inhibitors of Purine Nucleoside Phosphorylase from Plasmodium falciparum, *J. Biol. Chem.* 277, 3219–3225 (2002).

246. R. W. Miles, P. C. Tyler, R. H. Furneaux, C. K. Bagdassarian, V. L. Schramm, One-Third-the-Sites Transition-State Inhibitors for Purine Nucleoside Phosphorylase, *Biochemistry* 37, 8615–8621 (1998).

247. R. Sharma, Enzyme Inhibition: Mechanisms and Scope, *Enzyme Inhib. Bioapplications* (2012), doi:10.5772/39273.

248. A. Dassonville-Klimpt, C. Cézard, C. Mullié, P. Agnamey, A. Jonet, S. Da Nascimento, M. Marchivie, J. Guillon, P. Sonnet, Absolute Configuration and Antimalarial Activity of erythro-Mefloquine Enantiomers, *ChemPlusChem* 78, 642–646 (2013).

249. J. M. Karle, R. Olmeda, L. Gerena, W. K. Milhous, Plasmodium falciparum: role of absolute stereochemistry in the antimalarial activity of synthetic amino alcohol antimalarial agents, *Exp. Parasitol.* 76, 345–351 (1993).

250. M. Schmidt, H. Sun, P. Rogne, G. K. E. Scriba, C. Griesinger, L. T. Kuhn, U. M. Reinscheid, Determining the Absolute Configuration of (+)-Mefloquine HCl, the Side-Effect-Reducing Enantiomer of the Antimalaria Drug Lariam, *J. Am. Chem. Soc.* 134, 3080–3083 (2012).

251. G. A. Kicska, P. C. Tyler, G. B. Evans, R. H. Furneaux, V. L. Schramm, K. Kim, Purine-less Death in Plasmodium falciparumInduced by Immucillin-H, a Transition State Analogue of Purine Nucleoside Phosphorylase, *J. Biol. Chem.* 277, 3226–3231 (2002).

252. A. Bell, Antimalarial drug synergism and antagonism: Mechanistic and clinical significance, *FEMS Microbiol. Lett.* 253, 171–184 (2005).

253. P. Ludin, B. Woodcroft, S. A. Ralph, P. Mäser, In silico prediction of antimalarial drug target candidates, *Int. J. Parasitol. Drugs Drug Resist.* 2, 191–199 (2012).

254. M. P. Magariños, S. J. Carmona, G. J. Crowther, S. A. Ralph, D. S. Roos, D. Shanmugam, W. C. Van Voorhis, F. Agüero, TDR Targets: a chemogenomics resource for neglected diseases, *Nucleic Acids Res.* 40, D1118–D1127 (2012).

255. I. Yeh, T. Hanekamp, S. Tsoka, P. D. Karp, R. B. Altman, Computational analysis of Plasmodium falciparum metabolism: organizing genomic information to facilitate drug discovery, *Genome Res.* 14, 917–924 (2004).

256. G. Plata, T.-L. Hsiao, K. L. Olszewski, M. Llinás, D. Vitkup, Reconstruction and flux-balance analysis of the Plasmodium falciparum metabolic network, *Mol. Syst. Biol.* 6, 408 (2010).

257. F. Joubert, C. M. Harrison, R. J. Koegelenberg, C. J. Odendaal, T. A. P. de Beer, Discovery: an interactive resource for the rational selection and comparison of putative drug target proteins in malaria, *Malar. J.* 8, 178 (2009).

258. W. C. V. Voorhis, J. H. Adams, R. Adelfio, V. Ahyong, M. H. Akabas, P. Alano, A. Alday, Y. A. Resto, A. Alsibaee, A. Alzualde, K. T. Andrews, S. V. Avery, V. M. Avery, L. Ayong, M. Baker, S. Baker, C. B. Mamoun, S. Bhatia, Q. Bickle, L. Bounaadja, T. Bowling, J. Bosch, L. E. Boucher, F. F.

Boyom, J. Brea, M. Brennan, A. Burton, C. R. Caffrey, G. Camarda, M. Carrasquilla, D. Carter, M. B. Cassera, K. C.-C. Cheng, W. Chindaudomsate, A. Chubb, B. L. Colon, D. D. Colón-López, Y. Corbett, G. J. Crowther, N. Cowan, S. D'Alessandro, N. L. Dang, M. Delves, J. L. DeRisi, A. Y. Du, S. Duffy, S. A. E.-S. El-Sayed, M. T. Ferdig, J. A. F. Robledo, D. A. Fidock, I. Florent, P. V. T. Fokou, A. Galstian, F. J. Gamo, S. Gokool, B. Gold, T. Golub, G. M. Goldgof, R. Guha, W. A. Guiguemde, N. Gural, R. K. Guy, M. A. E. Hansen, K. K. Hanson, A. Hemphill, R. H. van Huijsduijnen, T. Horii, P. Horrocks, T. B. Hughes, C. Huston, I. Igarashi, K. Ingram-Sieber, M. A. Itoe, A. Jadhav, A. N. Jensen, L. T. Jensen, R. H. Y. Jiang, A. Kaiser, J. Keiser, T. Ketas, S. Kicka, S. Kim, K. Kirk, V. P. Kumar, D. E. Kyle, M. J. Lafuente, S. Landfear, N. Lee, S. Lee, A. M. Lehane, F. Li, D. Little, L. Liu, M. Llinás, M. I. Loza, A. Lubar, L. Lucantoni, I. Lucet, L. Maes, D. Mancama, N. R. Mansour, S. March, S. McGowan, I. M. Vera, S. Meister, L. Mercer, J. Mestres, A. N. Mfopa, R. N. Misra, S. Moon, J. P. Moore, F. M. R. da Costa, J. Müller, A. Muriana, S. N. Hewitt, B. Nare, C. Nathan, N. Narraidoo, S. Nawaratna, K. K. Ojo, D. Ortiz, G. Panic, G. Papadatos, S. Parapini, K. Patra, N. Pham, S. Prats, D. M. Plouffe, S.-A. Poulsen, A. Pradhan, C. Quevedo, R. J. Quinn, C. A. Rice, M. A. Rizk, A. Ruecker, R. S. Onge, R. S. Ferreira, J. Samra, N. G. Robinett, U. Schlecht, M. Schmitt, F. S. Villela, F. Silvestrini, R. Sinden, D. A. Smith, T. Soldati, A. Spitzmüller, S. M. Stamm, D. J. Sullivan, W. Sullivan, S. Suresh, B. M. Suzuki, Y. Suzuki, S. J. Swamidass, D. Taramelli, L. R. Y. Tchokouaha, A. Theron, D. Thomas, K. F. Tonissen, S. Townson, A. K. Tripathi, V. Trofimov, K. O. Udenze, I. Ullah, C. Vallieres, E. Vigil, J. M. Vinetz, P. V. Vinh, H. Vu, N. Watanabe, K. Weatherby, P. M. White, A. F. Wilks, E. A. Winzeler, E. Wojcik, M. Wree, W. Wu, N. Yokoyama, P. H. A. Zollo, N. Abla, B. Blasco, J. Burrows, B. Laleu, D. Leroy, T. Spangenberg, T. Wells, P. A. Willis, Open Source Drug Discovery with the Malaria Box Compound Collection for Neglected Diseases and Beyond, *PLOS Pathog.* 12, e1005763 (2016).

259. J. Hughes, S. Rees, S. Kalindjian, K. Philpott, Principles of early drug discovery, *Br. J. Pharmacol.* 162, 1239–1249 (2011).

260. M. J. Downie, K. Kirk, C. B. Mamoun, Purine Salvage Pathways in the Intraerythrocytic Malaria Parasite Plasmodium falciparum, *Eukaryot. Cell* 7, 1231–1237 (2008).

261. N. B. Quashie, D. Dorin-Semblat, P. G. Bray, G. A. Biagini, C. Doerig, L. C. Ranford-Cartwright, H. P. De Koning, A comprehensive model of purine uptake by the malaria parasite Plasmodium falciparum: identification of four purine transport activities in intraerythrocytic parasites, *Biochem. J.* 411, 287–295 (2008).

262. N. B. Quashie, L. C. Ranford-Cartwright, H. P. de Koning, Uptake of purines in Plasmodium falciparum-infected human erythrocytes is mostly mediated by the human Equilibrative Nucleoside Transporter and the human Facilitative Nucleobase Transporter, *Malar. J.* 9, 36 (2010).

263. L.-M. Ting, M. Gissot, A. Coppi, P. Sinnis, K. Kim, Attenuated Plasmodium yoelii lacking purine nucleoside phosphorylase confer protective immunity, *Nat. Med.* 14, 954–958 (2008).

264. M. Niikura, S.-I. Inoue, S. Mineo, Y. Yamada, I. Kaneko, S. Iwanaga, M. Yuda, F. Kobayashi, Experimental cerebral malaria is suppressed by disruption of nucleoside transporter 1 but not purine nucleoside phosphorylase, *Biochem. Biophys. Res. Commun.* 432, 504–508 (2013).

265. M. B. Cassera, K. Z. Hazleton, E. F. Merino, N. O. Iii, M.-C. Ho, A. S. Murkin, R. DePinto, J. A. Gutierrez, S. C. Almo, G. B. Evans, Y. S. Babu, V. L. Schramm, Plasmodium falciparum Parasites Are Killed by a Transition State Analogue of Purine Nucleoside Phosphorylase in a Primate Animal Model, *PLOS ONE* 6, e26916 (2011).

266. R. G. Ducati, H. A. Namanja-Magliano, R. K. Harijan, J. E. Fajardo, A. Fiser, J. P. Daily, V. L. Schramm, Genetic resistance to purine nucleoside phosphorylase inhibition in Plasmodium falciparum, *Proc. Natl. Acad. Sci.* 115, 2114–2119 (2018).

267. V. L. Schramm, Development of transition state analogues of purine nucleoside phosphorylase as anti-T-cell agents, *Biochim. Biophys. Acta BBA - Mol. Basis Dis.* 1587, 107–117 (2002).

268. G. LaMonte, M. Y.-X. Lim, M. Wree, C. Reimer, M. Nachon, V. Corey, P. Gedeck, D. Plouffe, A. Du, N. Figueroa, B. Yeung, P. Bifani, E. A. Winzeler, Mutations in the Plasmodium falciparum Cyclic Amine Resistance Locus (PfCARL) Confer Multidrug Resistance, *mBio* 7 (2016), doi:10.1128/mBio.00696-16.

269. P. A. Magistrado, V. C. Corey, A. K. Lukens, G. LaMonte, E. Sasaki, S. Meister, M. Wree, E. Winzeler, D. F. Wirth, Plasmodium falciparum Cyclic Amine Resistance Locus (PfCARL), a Resistance Mechanism for Two Distinct Compound Classes, *ACS Infect. Dis.* 2, 816–826 (2016).

270. D. J. Newman, G. M. Cragg, Natural Products as Sources of New Drugs from 1981 to 2014, *J. Nat. Prod.* 79, 629–661 (2016).

271. B. David, J.-L. Wolfender, D. A. Dias, The pharmaceutical industry and natural products: historical status and new trends, *Phytochem. Rev.* 14, 299–315 (2015).

272. A. Nn, A Review on the Extraction Methods Use in Medicinal Plants, Principle, Strength and Limitation, *Med. Aromat. Plants* 4, 1–6 (2015).

273. J. Schwager, M. H. Mohajeri, A. Fowler, P. Weber, Challenges in discovering bioactives for the food industry, *Curr. Opin. Biotechnol.* 19, 66–72 (2008).

274. D. A. Vattem, V. Maitin, *Functional Foods, Nutraceuticals and Natural Products: Concepts and Applications* (DEStech Publications, Inc, 2015).

275. E. Da Silva, P. Shahgaldian, A. W. Coleman, Haemolytic properties of some water-soluble para-sulphonato-calix-[n]-arenes, *Int. J. Pharm.* 273, 57–62 (2004).

276. M. Pikulski, J. S. Brodbelt, Differentiation of flavonoid glycoside isomers by using metal complexation and electrospray ionization mass spectrometry, *J. Am. Soc. Mass Spectrom.* 14, 1437–1453 (2003).

277. N. Fabre, I. Rustan, E. de Hoffmann, J. Quetin-Leclercq, Determination of flavone, flavonol, and flavanone aglycones by negative ion liquid chromatography electrospray ion trap mass spectrometry, *J. Am. Soc. Mass Spectrom.* 12, 707–715 (2001).

278. X.-D. Cao, Z.-S. Ding, F.-S. Jiang, X.-H. Ding, J.-Z. Chen, S.-H. Chen, G.-Y. Lv, Antitumor constituents from the leaves of Carya cathayensis, *Nat. Prod. Res.* 26, 2089–2094 (2012).

279. B. Singh, T. Sidiq, P. Joshi, S. K. Jain, Y. Lawaniya, S. Kichlu, A. Khajuria, R. A. Vishwakarma, S. B. Bharate, Anti-inflammatory and immunomodulatory flavones from Actinocarya tibetica Benth, *Nat. Prod. Res.* 27, 2227–2230 (2013).

280. P.-J. Tsai, W.-C. Huang, M.-C. Hsieh, P.-J. Sung, Y.-H. Kuo, W.-H. Wu, Flavones Isolated from Scutellariae radix Suppress Propionibacterium Acnes-Induced Cytokine Production In Vitro and In Vivo, *Molecules* 21, 15 (2015).

281. G. C. Terstappen, C. Schlüpen, R. Raggiaschi, G. Gaviraghi, Target deconvolution strategies in drug discovery, *Nat. Rev. Drug Discov.* 6, 891–903 (2007).

282. G. M. Keserű, G. M. Makara, Hit discovery and hit-to-lead approaches, *Drug Discov. Today* 11, 741–748 (2006).

283. S. M. Jung, H. R. Schumacher, H. Kim, M. Kim, S. H. Lee, F. Pessler, Reduction of urate crystal-induced inflammation by root extracts from traditional oriental medicinal plants: elevation of prostaglandin D2 levels, *Arthritis Res. Ther.* 9, R64 (2007).

284. Park Hyun, Kim MyungSoo, Jeon ByungHun, Kim TaeKyun, Kim YongMan, Ahnn Joohong, Kwon DongYeul, Y. Takaya, Y. Wataya, Kim HyeSook, Antimalarial activity of herbal extracts used in traditional medicine in Korea, *Biol. Pharm. Bull.* 26, 1623–1624 (2003).

285. N. Sekiya, N. Shibahara, I. Sakakibara, N. Hattori, H. Goto, K. Terasawa, Inhibitory effects of Oren-Gedoku-To (Huanglian-Jie-Du-Tang) on free radical-induced lysis of human red blood cells, *Phytother. Res.* 17, 147–151 (2003).

286. S. Chandra, H. Lata, A. Varma, *Biotechnology for Medicinal Plants: Micropropagation and Improvement* (Springer Science & Business Media, 2012).

287. A. F.-C. Valdés, L. M. Fidalgo, I. S. Ramos, D. M. Delange, C. L. M. Rico, J. M. Martínez, A. C. Cuéllar, Antiprotozoal screening of the Cuban native plant Scutellaria havanensis, *Pharm. Biol.* 54, 3197–3202 (2016).

288. J.-H. Won, K.-K. Park, W.-Y. Chung, P23. Inhibitory effects of baicalein, baicalin and wogonin on osteolytic bone metastasis of breast cancer, *Cancer Treat. Rev.* 34, Supplement 1, 21–22 (2008).

289. M. Li-Weber, New therapeutic aspects of flavones: The anticancer properties of Scutellaria and its main active constituents Wogonin, Baicalein and Baicalin, *Cancer Treat. Rev.* 35, 57–68 (2009).

290. S.-T. Huang, C.-Y. Wang, R.-C. Yang, C.-J. Chu, H.-T. Wu, J.-H. S. Pang, Wogonin, an active compound in Scutellaria baicalensis, induces apoptosis and reduces telomerase activity in the HL-60 leukemia cells, *Phytomedicine* 17, 47–54 (2010).

291. Y. Kimura, M. Sumiyoshi, Anti-tumor and anti-metastatic actions of wogonin isolated from Scutellaria baicalensis roots through anti-lymphangiogenesis, *Phytomedicine* 20, 328–336 (2013).

292. M. Boozari, A. Mohammadi, J. Asili, S. A. Emami, Z. Tayarani-Najaran, Growth inhibition and apoptosis induction by Scutellaria pinnatifida A. Ham. on HL-60 and K562 leukemic cell lines, *Environ. Toxicol. Pharmacol.* 39, 307–312 (2015).

293. W. Wang, Q.-L. Guo, Q.-D. You, K. Zhang, Y. Yang, J. Yu, W. Liu, L. Zhao, H.-Y. Gu, Y. Hu, Z. Tan, X.-T. Wang, The anticancer activities of wogonin in murine sarcoma S180 both in vitro and in vivo, *Biol. Pharm. Bull.* 29, 1132–1137 (2006).

294. S. Baumann, S. C. Fas, M. Giaisi, W. W. Müller, A. Merling, K. Gülow, L. Edler, P. H. Krammer, M. Li-Weber, Wogonin preferentially kills malignant lymphocytes and suppresses T-cell tumor growth by inducing PLCgamma1- and Ca2+-dependent apoptosis, *Blood* 111, 2354–2363 (2008).

295. H. Chung, Y. Jung, D.-H. Shin, J.-Y. Lee, M.-Y. Oh, H.-J. Kim, K. S. Jang, S. J. Jeon, K. H. Son, G. Kong, Anticancer effects of wogonin in both estrogen receptor-positive and -negative human breast cancer cell lines in vitro and in nude mice xenografts, *Int. J. Cancer J. Int. Cancer* 122, 816–822 (2008).

296. N. Lu, Y. Gao, Y. Ling, Y. Chen, Y. Yang, H.-Y. Gu, Q. Qi, W. Liu, X.-T. Wang, Q.-D. You, Q.-L. Guo, Wogonin suppresses tumor growth in vivo and VEGF-induced angiogenesis through inhibiting tyrosine phosphorylation of VEGFR2, *Life Sci.* 82, 956–963 (2008).

297. D. H. Kim, S. Kim, S. J. Jeon, K. H. Son, S. Lee, B. H. Yoon, J. H. Cheong, K. H. Ko, J. H. Ryu, The effects of acute and repeated oroxylin A treatments on Abeta(25-35)-induced memory impairment in mice, *Neuropharmacology* 55, 639–647 (2008).

298. Y. Cheng, G. He, X. Mu, T. Zhang, X. Li, J. Hu, B. Xu, G. Du, Neuroprotective effect of baicalein against MPTP neurotoxicity: behavioral, biochemical and immunohistochemical profile, *Neurosci. Lett.* 441, 16–20 (2008).

299. L. Li, H. Bao, J. Wu, X. Duan, B. Liu, J. Sun, W. Gong, Y. Lv, H. Zhang, Q. Luo, X. Wu, J. Dong, Baicalin is anti-inflammatory in cigarette smoke-induced inflammatory models in vivo and in vitro: A possible role for HDAC2 activity, *Int. Immunopharmacol.* 13, 15–22 (2012).

300. E.-J. Choi, C.-H. Lee, Y.-C. Kim, O. S. Shin, Wogonin inhibits Varicella-Zoster (shingles) virus replication via modulation of type I interferon signaling and adenosine monophosphate-activated protein kinase activity, *J. Funct. Foods* 17, 399–409 (2015).

301. H. K. Kim, B. S. Cheon, Y. H. Kim, S. Y. Kim, H. P. Kim, Effects of naturally occurring flavonoids on nitric oxide production in the macrophage cell line RAW 264.7 and their structure–activity relationships, *Biochem. Pharmacol.* 58, 759–765 (1999).

302. H.-Y. Jang, K.-S. Ahn, M.-J. Park, O.-K. Kwon, H.-K. Lee, S.-R. Oh, Skullcapflavone II inhibits ovalbumin-induced airway inflammation in a mouse model of asthma, *Int. Immunopharmacol.* 12, 666–674 (2012).

303. N. M. Khan, A. Haseeb, M. Y. Ansari, T. M. Haqqi, A wogonin-rich-fraction of Scutellaria baicalensis root extract exerts chondroprotective effects by suppressing IL-1β-induced activation of AP-1 in human OA chondrocytes, *Sci. Rep.* 7 (2017), doi:10.1038/srep43789.

304. Merlin Willcox, Philippe Rasoanaivo, Gerard Bodeker, *Traditional Medicinal Plants and Malaria* (CRC Press, 2004; http://www.crcnetbase.com.ezlibproxy1.ntu.edu.sg/doi/book/10.1201/9780203502327).

305. F. de Monbrison, M. Maitrejean, C. Latour, F. Bugnazet, F. Peyron, D. Barron, S. Picot, In vitro antimalarial activity of flavonoid derivatives dehydrosilybin and 8-(1;1)-DMA-kaempferide, *Acta Trop.* 97, 102–107 (2006).

306. F. Ntie-Kang, P. A. Onguéné, L. L. Lifongo, J. C. Ndom, W. Sippl, L. M. Mbaze, The potential of anti-malarial compounds derived from African medicinal plants, part II: a pharmacological evaluation of non-alkaloids and non-terpenoids, *Malar. J.* 13, 81 (2014).

307. A. M. Lehane, K. J. Saliba, Common dietary flavonoids inhibit the growth of the intraerythrocytic malaria parasite, *BMC Res. Notes* 1, 26 (2008).

308. P. Khaomek, C. Ichino, A. Ishiyama, H. Sekiguchi, M. Namatame, N. Ruangrungsi, E. Saifah, H. Kiyohara, K. Otoguro, S. Omura, H. Yamada, In vitro antimalarial activity of prenylated flavonoids from Erythrina fusca, *J. Nat. Med.* 62, 217–220 (2008).

309. M. Zhang, C. Wang, T. D. Otto, J. Oberstaller, X. Liao, S. R. Adapa, K. Udenze, I. F. Bronner, D. Casandra, M. Mayho, J. Brown, S. Li, J. Swanson, J. C. Rayner, R. H. Y. Jiang, J. H. Adams, Uncovering the essential genes of the human malaria parasite Plasmodium falciparum by saturation mutagenesis, *Science* 360, eaap7847 (2018).

310. M. J. López-Barragán, J. Lemieux, M. Quiñones, K. C. Williamson, A. Molina-Cruz, K. Cui, C. Barillas-Mury, K. Zhao, X. Su, Directional gene expression and antisense transcripts in sexual and asexual stages of Plasmodium falciparum, *BMC Genomics* 12, 587 (2011).

311. C. A. Moores, M. Yu, J. Guo, C. Beraud, R. Sakowicz, R. A. Milligan, A Mechanism for Microtubule Depolymerization by KinI Kinesins, *Mol. Cell* 9, 903–909 (2002).

312. C. A. Moores, J. Cooper, M. Wagenbach, Y. Ovechkina, L. Wordeman, R. A. Milligan, The role of the kinesin-13 neck in microtubule depolymerization, *Cell Cycle Georget. Tex* 5, 1812–1815 (2006).

313. V. Gopinathan, N. J. Miller, A. D. Milner, C. A. Rice-Evans, Bilirubin and ascorbate antioxidant activity in neonatal plasma, *FEBS Lett.* 349, 197–200 (1994).

314. R. Stocker, Y. Yamamoto, A. F. McDonagh, A. N. Glazer, B. N. Ames, Bilirubin is an antioxidant of possible physiological importance, *Science* 235, 1043–1046 (1987).

315. D. E. Barañano, M. Rao, C. D. Ferris, S. H. Snyder, Biliverdin reductase: A major physiologic cytoprotectant, *Proc. Natl. Acad. Sci.* 99, 16093–16098 (2002).

316. P. A. Sigala, J. R. Crowley, S. Hsieh, J. P. Henderson, D. E. Goldberg, Direct Tests of Enzymatic Heme Degradation by the Malaria Parasite Plasmodium falciparum, *J. Biol. Chem.* 287, 37793–37807 (2012).

317. K. Okada, The novel heme oxygenase-like protein from Plasmodiumfalciparum converts heme to bilirubin IXα in the apicoplast, *FEBS Lett.* 583, 313–319 (2009).

318. R. Sartorello, A. Budu, P. Bagnaresi, C. A. H. Fernandes, P. M. Sato, V. B. Bueno, M. R. M. Fontes, P. L. Oliveira, G. O. Paiva-Silva, S. V. Alves, L. E. S. Netto, L. H. Catalani, C. R. S. Garcia, In vivo uptake of a haem analogue Zn protoporphyrin IX by the human malaria parasite P. falciparum-infected red blood cells, *Cell Biol. Int.* 34, 859–865 (2010).

319. E. Yeh, J. L. DeRisi, Chemical Rescue of Malaria Parasites Lacking an Apicoplast Defines Organelle Function in Blood-Stage Plasmodium falciparum, *PLoS Biol.* 9 (2011), doi:10.1371/journal.pbio.1001138.

320. V. A. Nagaraj, B. Sundaram, N. M. Varadarajan, P. A. Subramani, D. M. Kalappa, S. K. Ghosh, G. Padmanaban, Malaria Parasite-Synthesized Heme Is Essential in the Mosquito and Liver Stages and Complements Host Heme in the Blood Stages of Infection, *PLoS Pathog.* 9 (2013), doi:10.1371/journal.ppat.1003522.

321. C. M. Smith, A. Jerkovic, H. Puy, I. Winship, J.-C. Deybach, L. Gouya, G. van Dooren, C. D. Goodman, A. Sturm, H. Manceau, G. I. McFadden, P. David, O. Mercereau-Puijalon, G. Burgio, B. J. McMorran, S. J. Foote, Red cells from ferrochelatase-deficient erythropoietic protoporphyria patients are resistant to growth of malarial parasites, *Blood* 125, 534–541 (2015).

322. P. M. Lelliott, B. J. McMorran, S. J. Foote, G. Burgio, The influence of host genetics on erythrocytes and malaria infection: is there therapeutic potential?, *Malar. J.* 14, 289 (2015).

323. M. W. Davidson, B. G. Griggs, D. W. Boykin, W. D. Wilson, Molecular structural effects involved in the interaction of quinolinemethanolamines with DNA. Implications for antimalarial action, *J. Med. Chem.* 20, 1117–1122 (1977).

324. M. R. Webb, S. E. Ebeler, Comparative analysis of topoisomerase IB inhibition and DNA intercalation by flavonoids and similar compounds: structural determinates of activity, *Biochem. J.* 384, 527–541 (2004).

325. Z. Wang, M. Cui, F. Song, L. Lu, Z. Liu, S. Liu, Evaluation of Flavonoids Binding to DNA Duplexes by Electrospray Ionization Mass Spectrometry, *J. Am. Soc. Mass Spectrom.* 19, 914–922 (2008).

326. X. Li, *Chinese Materia Medica: Combinations and Applications* (Elsevier Health Sciences, 2002).

327. X. Zheng, C. Deng, G. Song, Y. Hu, Comparison of Essential Oil Composition of Artemisia argyi Leaves at Different Collection Times by Headspace Solid-Phase Microextraction and Gas Chromatography-Mass Spectrometry, *Chromatographia* 59, 729–732 (2004).

328. A.-G. Huang, Y.-L. Yi, F. Ling, L. Lu, Q.-Z. Zhang, G.-X. Wang, Screening of plant extracts for anthelmintic activity against Dactylogyrus intermedius (Monogenea) in goldfish (Carassius auratus), *Parasitol. Res.* 112, 4065–4072 (2013).

329. X. Bao, H. Yuan, C. Wang, J. Liu, M. Lan, Antitumor and immunomodulatory activities of a polysaccharide from Artemisia argyi, *Carbohydr. Polym.* 98, 1236–1243 (2013).

330. J.-M. Seo, H.-M. Kang, K.-H. Son, J. H. Kim, C. W. Lee, H. M. Kim, S.-I. Chang, B.-M. Kwon, Antitumor activity of flavones isolated from Artemisia argyi, *Planta Med.* 69, 218–222 (2003).

331. M. Shoemaker, B. Hamilton, S. H. Dairkee, I. Cohen, M. J. Campbell, In vitro anticancer activity of twelve Chinese medicinal herbs, *Phytother. Res.* 19, 649–651 (2005).

332. E. Choi, G. Kim, Effect of Artemisia species on cellular proliferation and apoptosis in human breast cancer cells via estrogen receptor-related pathway, *J. Tradit. Chin. Med.* 33, 658–663 (2013).

333. H.-J. K. Jeung-Min Lee, H.-R. Park, Anticancer Activity of Artemisia argyi Extracts on HT-29 Human Colon Cancer Cells, *Cancer prevention research* 15, 76–82 (2010).

334. A. Ramazani, S. Sardari, S. Zakeri, B. Vaziri, In vitro antiplasmodial and phytochemical study of five Artemisia species from Iran and in vivo activity of two species, *Parasitol. Res.* 107, 593–599 (2010).

335. M. Willcox, Artemisia species: From traditional medicines to modern antimalarials--and back again, *J. Altern. Complement. Med. N. Y. N* 15, 101–109 (2009).

336. M. Mojarrab, R. Naderi, F. Heshmati Afshar, Screening of Different Extracts from Artemisia Species for Their Potential Antimalarial Activity, *Iran. J. Pharm. Res. IJPR* 14, 603–608 (2015).

337. A. Rustaiyan, S. Masoudi, Chemical constituents and biological activities of Iranian Artemisia species, *Phytochem. Lett.* 4, 440–447 (2011).

338. R. X. Tan, W. F. Zheng, H. Q. Tang, Biologically active substances from the genus Artemisia, *Planta Med.* 64, 295–302 (1998).

339. J.-Y. Li, X.-B. Wang, J.-G. Luo, L.-Y. Kong, Seasonal Variation of Alkaloid Contents and Anti-Inflammatory Activity of Rhizoma coptidis Based on Fingerprints Combined with Chemometrics Methods, *J. Chromatogr. Sci.* 53, 1131–1139 (2015).

340. S. Y. Wang, W. Zheng, Effect of Plant Growth Temperature on Antioxidant Capacity in Strawberry, *J. Agric. Food Chem.* 49, 4977–4982 (2001).

341. W. Liu, D. Yin, N. Li, X. Hou, D. Wang, D. Li, J. Liu, Influence of Environmental Factors on the Active Substance Production and Antioxidant Activity in Potentilla fruticosa L. and Its Quality Assessment, *Sci. Rep.* 6, 28591 (2016).

342. C. L. F. Meyers, D. J. Meyers, Thin-Layer Chromatography, *Curr. Protoc. Nucleic Acid Chem.* 34, A.3D.1-A.3D.13.

343. K. Sprogøe, D. Stærk, A. K. Jäger, A. Adsersen, S. H. Hansen, M. Witt, A.-K. R. Landbo, A. S. Meyer, J. W. Jaroszewski, Targeted Natural Product Isolation Guided by HPLC–SPE–NMR: Constituents of Hubertia Species, *J. Nat. Prod.* 70, 1472–1477 (2007).

344. T. Wennberg, K. Kreander, M. Lähdevuori, H. Vuorela, P. Vuorela, Primary Screening of Natural Products Using Micro Fractionation Combined with a Bioassay, *J. Liq. Chromatogr. Relat. Technol.* 27, 2573–2592 (2004).

345. Y. Tu, C. Jeffries, H. Ruan, C. Nelson, D. Smithson, A. A. Shelat, K. M. Brown, X.-C. Li, J. P. Hester, T. Smillie, I. A. Khan, L. Walker, K. Guy, B. Yan, An Automated High-Throughput System to Fractionate Plant Natural Products for Drug Discovery, *J. Nat. Prod.* 73, 751–754 (2010).

346. Y. Tu, B. Yan, High-throughput fractionation of natural products for drug discovery, *Methods Mol. Biol. Clifton NJ* 918, 117–126 (2012).

347. I. Bácskay, D. Nemes, F. Fenyvesi, J. Váradi, G. Vasvári, P. Fehér, M. Vecsernyés, Z. Ujhelyi, Role of Cytotoxicity Experiments in Pharmaceutical Development, *Cytotoxicity* (2017), doi:10.5772/intechopen.72539.

348. S. I. Berger, R. Iyengar, Role of systems pharmacology in understanding drug adverse events, *Wiley Interdiscip. Rev. Syst. Biol. Med.* 3, 129–135.

349. D. W. Wilson, C. Langer, C. D. Goodman, G. I. McFadden, J. G. Beeson, Defining the Timing of Action of Antimalarial Drugs against Plasmodium falciparum, *Antimicrob. Agents Chemother.* 57, 1455–1467 (2013).

350. M. Delves, D. Plouffe, C. Scheurer, S. Meister, S. Wittlin, E. A. Winzeler, R. E. Sinden, D. Leroy, The Activities of Current Antimalarial Drugs on the Life Cycle Stages of Plasmodium : A Comparative Study with Human and Rodent Parasites, *PLOS Med* 9, e1001169 (2012).

351. Z. Bozdech, M. Llinás, B. L. Pulliam, E. D. Wong, J. Zhu, J. L. DeRisi, The Transcriptome of the Intraerythrocytic Developmental Cycle of Plasmodium falciparum, *PLoS Biol* 1, e5 (2003).

352. L. Florens, M. P. Washburn, J. D. Raine, R. M. Anthony, M. Grainger, J. D. Haynes, J. K. Moch, N. Muster, J. B. Sacci, D. L. Tabb, A. A. Witney, D. Wolters, Y. Wu, M. J. Gardner, A. A. Holder, R. E. Sinden, J. R. Yates, D. J. Carucci, A proteomic view of the Plasmodium falciparum life cycle, *Nature* 419, 520–526 (2002).

353. A. E. Rawlings, Membrane proteins: always an insoluble problem?, *Biochem. Soc. Trans.* 44, 790–795 (2016).

354. F. B. M. Reinhard, D. Eberhard, T. Werner, H. Franken, D. Childs, C. Doce, M. F. Savitski, W. Huber, M. Bantscheff, M. M. Savitski, G. Drewes, Thermal proteome profiling monitors ligand interactions with cellular membrane proteins, *Nat. Methods* 12, 1129–1131 (2015).

355. I. Becher, T. Werner, C. Doce, E. A. Zaal, I. Tögel, C. A. Khan, A. Rueger, M. Muelbaier, E. Salzer, C. R. Berkers, P. F. Fitzpatrick, M. Bantscheff, M. M. Savitski, Thermal profiling reveals phenylalanine hydroxylase as an off-target of panobinostat, *Nat. Chem. Biol.* 12, 908–910 (2016).

356. A. Chiappino-Pepe, S. Tymoshenko, M. Ataman, D. Soldati-Favre, V. Hatzimanikatis, Bioenergetics-based modeling of Plasmodium falciparum metabolism reveals its essential genes, nutritional requirements, and thermodynamic bottlenecks, *PLOS Comput. Biol.* 13, e1005397 (2017).

357. J. Oyelade, I. Isewon, E. Uwoghiren, O. Aromolaran, O. Oladipupo, In Silico Knockout Screening of Plasmodium falciparum Reactions and Prediction of Novel Essential Reactions by Analysing the Metabolic Network*BioMed Res. Int.* (2018), doi:10.1155/2018/8985718.

358. S. G. Tewari, S. T. Prigge, J. Reifman, A. Wallqvist, Using a genome-scale metabolic network model to elucidate the mechanism of chloroquine action in Plasmodium falciparum, *Int. J. Parasitol. Drugs Drug Resist.* 7, 138–146 (2017).

359. S. Tymoshenko, R. D. Oppenheim, D. Soldati-Favre, V. Hatzimanikatis, Functional genomics of Plasmodium falciparum using metabolic modelling and analysis, *Brief. Funct. Genomics* 12, 316–327 (2013).

360. M. Llinás, Z. Bozdech, E. D. Wong, A. T. Adai, J. L. DeRisi, Comparative whole genome transcriptome analysis of three Plasmodium falciparum strains, *Nucleic Acids Res.* 34, 1166–1173 (2006).

361. S. H. Adjalley, C. D. Chabbert, B. Klaus, V. Pelechano, L. M. Steinmetz, Landscape and Dynamics of Transcription Initiation in the Malaria Parasite Plasmodium falciparum, *Cell Rep.* 14, 2463–2475 (2016).

362. L. Cui, S. Lindner, J. Miao, Translational regulation during stage transitions in malaria parasites, *Ann. N. Y. Acad. Sci.* 1342, 1–9 (2015).

363. F. Ay, E. M. Bunnik, N. Varoquaux, J.-P. Vert, W. S. Noble, K. G. Le Roch, Multiple dimensions of epigenetic gene regulation in the malaria parasite Plasmodium falciparum: gene regulation via histone modifications, nucleosome positioning and nuclear architecture in P. falciparum, *BioEssays News Rev. Mol. Cell. Dev. Biol.* 37, 182–194 (2015).

364. A. P. Gupta, W. H. Chin, L. Zhu, S. Mok, Y.-H. Luah, E.-H. Lim, Z. Bozdech, Dynamic Epigenetic Regulation of Gene Expression during the Life Cycle of Malaria Parasite Plasmodium falciparum, *PLOS Pathog.* 9, e1003170 (2013).

365. B. M. Invergo, M. Brochet, L. Yu, J. Choudhary, P. Beltrao, O. Billker, Sub-minute Phosphoregulation of Cell Cycle Systems during Plasmodium Gamete Formation, *Cell Rep.* 21, 2017–2029 (2017).

366. F. C. Koyama, D. Chakrabarti, C. R. S. Garcia, Molecular machinery of signal transduction and cell cycle regulation in Plasmodium, *Mol. Biochem. Parasitol.* 165, 1–7 (2009).

367. I. Becher, A. Andrés-Pons, N. Romanov, F. Stein, M. Schramm, F. Baudin, D. Helm, N. Kurzawa, A. Mateus, M.-T. Mackmull, A. Typas, C. W. Müller, P. Bork, M. Beck, M. M. Savitski, Pervasive Protein Thermal Stability Variation during the Cell Cycle, *Cell* 173, 1495-1507.e18 (2018).

368. L. Dai, T. Zhao, X. Bisteau, W. Sun, N. Prabhu, Y. T. Lim, R. M. Sobota, P. Kaldis, P. Nordlund, Modulation of Protein-Interaction States through the Cell Cycle, *Cell* 173, 1481-1494.e13 (2018).